EVALUATING THE ROLES SPINAL PLASTICITY AND AN ACCESSORY

INSPIRATORY MUSCLE HAVE IN A RODENT MODEL OF RESPIRATORY

MOTOR NEURON DEATH

_____

A Dissertation

presented to

the Faculty of the Graduate School

at the University of Missouri-Columbia

_____

In Partial Fulfillment

Of the Requirements for the Degree

Doctor of Philosophy

_____

by

LAUREN F. BORKOWSKI

Dr. Nicole L. Nichols, Dissertation Supervisor

July, 2021

The undersigned, appointed by the Dean of the Graduate School, have examined the dissertation entitled:

EVALUATING THE ROLES SPINAL PLASTICITY AND AN ACCESSORY MUSCLE HAVE IN A RODENT MODEL OF RESPIRATORY MOTOR NEURON DEATH

Presented by Lauren F. Borkowski,

a candidate for the degree of Doctor of Philosophy in Biomedical Sciences,

and hereby certify that in their opinion is worthy of acceptance.

_____

Nicole L. Nichols

_____

Eileen M. Hasser

_____

Kevin J. Cummings

_____

Dawn D. Cornelison

_____

David J. Schulz

Dedication

For my family, friends, and colleagues who have cheered me on throughout my journey

and challenged me to become a successful researcher.

ACKNOWLEDGEMENTS

I am deeply grateful to my dissertation chair, Dr. Nicole L. Nichols, who has supported my ideas and challenged me to critically think about an area of research I previously did not have experience in. She constantly encouraged me to participate in environments that promoted academic discussion in respiratory physiology, apply for various awards, collaborate with other researchers in our area of interest, and pursue new techniques to answer our questions. She was always there to help me through times when research techniques failed or handle challenges that come with *in vivo* research. I appreciate the support, guidance, and encouragement she has provided me, and I know that she has been crucial in my publication and award success, as well as in successfully completing this degree.

I sincerely thank my committee members, Dr. Eileen Hasser, Dr. Kevin Cummings, Dr. David Schulz, and Dr. Dawn Cornelison for providing advice and direction throughout my journey. I was lucky to have a flexible, diverse committee who challenged me to think about respiratory physiology from many different angles.

I also thank the past and present members of our lab. They provided me with constructive feedback for my dissertation work and have assisted me in troubleshooting new ideas. Amy Keilholz and Catherine Smith played a pivotal role in creating the CTB-SAP model and were always willing to assist me with plethysmography, perfusions, and immunohistochemical techniques.

I greatly appreciate my family and friends who supported me through the tears and through the moments when celebration was in order. My fellow PhD students supported and encouraged me through this process and were always willing to listen to me reason through my research observations. I specifically want to thank Nathan Kerr and Shannon Kelly for sharing an office space with me and being an incredible support system. I also greatly appreciate the support from

TABLE OF CONTENTS

LIST OF TABLES

LIST OF FIGURES

LIST OF NOMENCLATURE

AIH: acute-intermittent hypoxia

ALS: amyotrophic lateral sclerosis

BDNF: brain-derived neurotrophic factor

BötC: Bötzinger complex

CNS: central nervous system

CO_2: carbon dioxide

CTB: cholera toxin B

CTB-AF488: cholera toxin B conjugated to AlexaFluor488

CTB-AF647: cholera toxin B conjugated to AlexaFluro647

CTB-SAP: cholera toxin B conjugated to saporin

CVLM/RVLM: caudal and rostral ventrolateral medulla

EMG: electromyography

$FiCO_2$: fictive carbon dioxide

FiO_2: fictive oxygen

GABA: γ-Aminobutyric acid

Glut: glutamate

HO: heme oxigenase

i.p: intraperitoneal

i.t.: intrathecal

i.v.: intravenous

IH: intermittent hypoxia

IM: intramuscular

IPL: intrapleural

keto: ketoprofen

LTF: long-term facilitation

LPS: lipopolysaccaride

MAP: mean arterial pressure

MAPK: mitogen-activated protein kinase

NADPH: nicotinamide adenine dinucleotide phosphate

NMDA: N -methyl-D-aspartate

NO: nitrous oxide

NOS: nitric oxide synthase (endothelial: eNOS; neuronal: nNOS; inducible: iNOS)

NREM: non-rapid eye movement sleep

NTS: nucleus of the solitary tract

O_2: Oxygen

$PaCO_2$: partial pressure of carbon dioxide

PaO_2: partial pressure of oxygen

pLTF: phrenic long-term facilitation

pMF: phrenic motor facilitation

PMN: phrenic motor nucleus

pre-BötC: pre-Bötzinger complex

REM: rapid eye movement sleep

RR: respiratory rate

RTN: retrotrapezoid nucleus

SAP: saporin

TrkB: tyrosine kinase B

V_E: minute ventilation

V_T: tidal volume

ABSTRACT

Death by ventilatory failure most frequently occurs in patients with neuromuscular diseases in which there is a loss of respiratory motor neurons. There are currently no significant treatments to prolong or correct for these respiratory deficits. Genetic rodent models of motor neuron loss develop many phenotypes (*e.g.,* dysphagia, limb paralysis, etc.), so in order to study how motor neuron death only impacts respiration and to develop therapeutic interventions, we have developed an inducible model of respiratory motor neuron death. Briefly, rats are intrapleurally injected with cholera toxin B conjugated to saporin (CTB-SAP), which selectively eliminates respiratory motor neurons. Surprisingly, this model displays considerable respiratory plasticity that functions over time to preserve eupneic ventilation. Thus, the fundamental goal of this dissertation is to determine potential strategies that preserve eupneic ventilation following respiratory motor neuron loss. Our data suggest that respiratory plasticity requires different G-protein-coupled receptors and downstream signaling and that the exhibited plasticity is differentially affected by COX1/2-induced inflammation over the course of CTB-SAP induced neuropathology, which may collectively represent one way eupnea is maintained. Additional pilot data indicate diaphragmatic amplitude is decreased in CTB-SAP treated rats, which suggests that extradiaphragmatic muscles (*e.g*., accessory inspiratory muscles such as the pectoralis minor muscles that can be utilized in disease/injury) are also utilized to maintain eupneic ventilation. Our data suggest that pectoralis minor activity is increased in CTB-SAP rats *vs*. controls and is further increased in 28d *vs*. 7d CTB-SAP rats. The overall hypotheses of this dissertation are that following CTB-SAP treatment: 1) respiratory plasticity requires differential activation of G-protein-coupled receptor pathways; 2) respiratory plasticity is differentially impacted by COX1/2-induced inflammation; and 3) pectoralis minor muscle amplitude is increased to maintain eupnea. This project will advance our understanding of potential targets (*i.e*., receptors, inflammatory markers, or muscles) that could be harnessed or stimulated to further preserve and/or improve ventilatory function and quality of life in patients with neuromuscular diseases that are suffering from respiratory motor neuron loss.

CHAPTER 1: INTRODUCTION

1.1 - Dissertation Overview

Homeostasis of the respiratory system is maintained through the integration of chemosensory afferent inputs and alterations in efferent motor neuron signaling to respiratory effector muscles (*e.g.,* diaphragm and external intercostals) to maintain appropriate ventilation. In instances of neuromuscular disease and injury, the efferent projections (*e.g.,* respiratory motor neurons) are lost resulting in ventilatory failure, and, ultimately, death. The purpose of this dissertation is to examine the role of underlying mechanisms of acute intermittent hypoxia (AIH)-induced respiratory plasticity and the recruitment of a group of accessory inspiratory muscles, specifically, the pectoralis minor muscles, in the maintenance of ventilation following CTB-saporin-induced respiratory motor neuron death. Three studies (Chapters 2-4) were performed to investigate the overall hypothesis that following CTB-SAP-induced respiratory motor neuron loss: 1.) differential G-coupled protein receptors and their downstream signaling mechanisms are utilized for eliciting respiratory plasticity at 7d and 28d post-CTB-SAP; and 2.) accessory inspiratory muscles (*e.g.,* pectoralis minor muscles) become recruited to assist with eupnea.

1.2 - Overview of the Neural Control of Respiration

The Chemical Drive to Breathe and Chemoreflexes

The cardiopulmonary system is innervated by sensory afferent nerves that respond to mechanical and chemical changes to then affect autonomic output. Sensory reflexes occur in response to short term blood gas changes in order to maintain homeostasis by tightly regulating heart rate, blood pressure, and ventilation (Nattie, 1999). Eupnea, or normal

respiration, is driven by $PaCO_2$ and acidity in the blood and cerebrospinal fluid that is detected in the brain by chemosensitive receptors. All cellular metabolic functions produce CO_2, and consequently H^+, which leads to a rise in $PaCO_2$ and a decrease in blood pH. This change is detected in the brain by central chemoreceptors in the brainstem, cerebellum, hypothalamus and midbrain. The continual chemoreception and regulation of CO_2/H^+ provides a tonic stimulus to breath (Guyenet and Bayliss, 2015; Kumar and Prabhakar, 2011; Nattie and Li, 2012). The purpose of these chemoreceptors and chemoreceptor reflexes are to minimize $PaCO_2$ fluctuations by changing lung ventilation to eliminate CO_2 and to regulate pH. The process by which ventilation is changed to return CO_2/H^+, or pH, to homeostatic ranges is known as central chemoreception (Guyenet and Bayliss, 2015; Kumar and Prabhakar, 2011; Nattie and Li, 2012). Tight pH regulation is required for cellular functions, organ function, and overall life. Therefore, reflexes that regulate alterations in pH need to be highly sensitive. For example, activation of the central chemoreflex doubles alveolar ventilation when pH is dropped from 7.30 to 7.25 (Guyenet and Bayliss, 2015). The neural circuit and reflexes responsible for changing ventilation are located in the medulla.

There are also peripheral chemosensors that adjust ventilation to maintain acid-base homeostasis. Peripheral chemoreceptors are chemosensors that are activated in a pH-dependent manner by arterial hypoxemia and hypercapnia and relay sensory information to respiratory centers in the medulla oblongata to change respiratory patterns (Smith et al., 2007). Peripheral chemoreceptors are located in aortic bodies on the aortic arch, and in carotid bodies located in the bifurcation of the carotid arteries(Smith et al., 2007). Hypoxemia is sensed by glomus cells (type I cells) of the carotid body. These glomus cells

depolarize and dump neurotransmitters onto sensory afferents of the carotid sinus nerve (CSN). The glomus cells and CSN fire in a graded fashion (increasing discharge) as PaO_2 decreases. However, in cases of extreme hypoxia (1-3% O_2), PaO_2 drops below 20-30 mmHg, and CSN discharge decreases. Chemoreceptor afferents of the aorta and carotid bodies travel to the brain *via* the vagus and glossopharyngeal nerves to the integrative center of the medulla oblongata, the nucleus tractus solitarius (NTS). Pulmonary afferent stretch receptors also travel with the vagus and terminate on the NTS (Grassino et al., 1978; Hruska Jr, 1997; Loring and De Troyer, 1985). This signal is then integrated and ventilation is adjusted.

When chemoafferents terminate in the NTS, the NTS sends projections to the respiratory central pattern generator (CPG). Projections from the CPG terminate onto the ventral respiratory group (VRG), which contains the Pre-Bötzinger (Pre-BötC) and Bötzinger Complex (BötC), to regulate respiratory rhythm (Hruska Jr, 1997). There are four phases of the respiratory cycle (pre-inspiratory, inspiratory, post-inspiratory, and expiratory) that are affiliated with different brainstem regions and motor neuron discharge. During the pre-inspiratory phase, the inspiratory neurons of the Pre-BötC fire onto the hypoglossal nucleus, which leads to the opening of the upper airway. The inspiratory neurons also terminate on the rostral VRG (rVRG), and neurons of the rVRG project to and activate the phrenic and intercostal motor neurons (Hruska Jr, 1997; Nattie and Li, 2012). Activation of these motor neurons leads to contraction of the diaphragm and intercostal muscles to increase the space inside the chest cavity. This results in a pressure gradient in which the pressure in the lungs is lower than the pressure outside of the body. Inspiratory neurons then continue to fire as air enters the lungs, moving from a higher

pressure outside of the body to a lower pressure in the lungs. In the post-inspiratory phase, the lungs are inflated and the pressure outside of the body is nearly in equilibrium with the pressure in the lungs. The pulmonary stretch receptors are activated by lung inflation, and stretch-activated afferents relay to the NTS that inspiration can cease (Bianchi et al., 1995; Hruska Jr, 1997; Nattie and Li, 2012). Expiratory neurons from the BötC inhibit inspiratory neurons from the Pre-BötC, causing the muscles of inspiration (discussed further in section 1.3) to relax, and expiration occurs passively. The back and forth inhibition of expiratory and inspiratory neurons determines the duration in each phase, which is shortened during exposure to hypoxia and/or hypercapnia to increase ventilation (Bianchi et al., 1995; Dale-Nagle et al., 2010; Mitchell et al., 2001; Nattie, 1999; Nattie and Li, 2012). These neural networks responsible for making necessary adjustments in ventilation depend on highly sensitive chemoreceptors.

Mechanisms of O_2-sensing

The mechanism(s) by which carotid body glomus cells (type I cells) detect O_2 is highly debated. There is also evidence that multiple mechanisms by which O_2 is detected in glomus cells converge, leading to redundancy in O_2 sensing. First, glomus cell membranes have been shown to contain several classes of O_2-sensitive K^+ channels. During hypoxia, the opening probability of these O_2-sensitive K^+ channels decreases (Conforti et al., 2000; Hayashi et al., 2003; Montoro et al., 1996). This prevents inward K^+ currents and results in glomus cell depolarization and increases the firing frequency of these cells (Conforti et al., 2000; Montoro et al., 1996). When depolarization occurs, voltage-gated calcium channels open and the calcium influx into the glomus cell results in neurosecretion of many

neurotransmitters including catecholamines such as dopamine (Benot and Lopez-Barneo, 1990; Gonzalez et al., 1994; Lopez-Barneo et al., 1999; Nurse, 2010; Weir et al., 2005).

Another proposed mechanism by which O_2 is detected by glomus cells involves the mitochondria. The mitochondria convert O_2 into reactive oxygen species (ROS) and the redox state of the cell is altered. Nicotinamide adenine dinucleotide phosphate (NADPH) oxidase (NOX) is an enzyme that converts O_2 to superoxide anions (Dröge, 2002). The rate of enzymatic activity of NOX has been proposed as a mechanism by which O_2 levels are sensed in glomus cells. For example, when O_2 levels are low, the conversion of O_2 to superoxide anions and then hydrogen peroxide is increased. Additionally, inhibitors of the electron transport chain (ETC) or mitochondrial uncouplers have been shown to increase activity of glomus cells and the CSN (Chang, 2017; López-Barneo et al., 2016; López-Barneo et al., 2008; Waypa et al., 2016). Blocking complexes of the ETC and uncoupling of mitochondrial proteins have been shown to increase intracellular Ca^{2+} and neurotransmitter release (Bianchi et al., 1995; Feldman et al., 2003). Research has shown that hypoxia also inhibits specific complexes of the ETC and uncouples mitochondrial proteins leading to an increase in ROS and a decrease in ATP production (López-Barneo et al., 2008).

It has been postulated that mechanisms of mitochondrial dysfunction alter ion channel activity on the plasmalemma in response to hypoxia. Altering the redox state of the cell is thought to alter signaling molecules and ion channel function. Oxidation of K^+ channels by mitochondrial ROS production may be the mechanism by which K^+ channels are inhibited during hypoxia, leading to the depolarization of glomus cells (López-Barneo et al., 2008; López-López et al., 1997). Mitochondria uncoupling also results in a decrease

in ATP generation. It has been proposed that ATP-regulated background K^+ channels on the glomus cell membrane close during hypoxia when there is a decrease in ATP (López-Barneo et al., 2008; Nurse and Piskuric, 2013). These findings highlight a few mechanisms that may be involved in O_2-sensing. There are additional factors (hypoxia-inducible factors and heme-oxygenase) that are O_2-sensitive and may contribute to the increase in carotid body discharge observed with hypoxia. Understanding these mechanisms of O_2-sensing by the carotid body and the changes in the excitability of these cells in the context of respiratory homeostasis provides insight as to how hypoxia exposure impacts phrenic nerve output which will be discussed in the following sections as it pertains to the neural control of breathing.

1.3 – Primary and Accessory Muscles of Respiration

Under eupneic breathing conditions, the diaphragm, which is innervated by the phrenic motor nerve, is responsible for 70-80% of the inspiratory tidal volume (Benditt, 2006) making it the primary muscle of inspiration. All other muscles involved with inspiration are then considered accessory muscles of inspiration. When inspiratory requirement increases (*e.g.,* exercise, chronic obstructive pulmonary disease, etc.) or in cases of functional reduction of the primary inspiratory muscle (*e.g.,* spinal cord injury, ALS, etc.), the accessory muscles (internal and external intercostals, sternocleidomastoid, scalenes, pectoralis major and minor, serrati and trapezii) can operate to actively elevate the ribs upward and outward to move the chest wall (Grassino et al., 1978). Studies have shown that the recruitment of the accessory inspiratory muscles is graded and differ based on physiological states. When evaluating the recruitment time and duration of five inspiratory

muscles during eupneic breathing, Saboisky et al. found that the motor units of the diaphragm were recruited first and fired throughout inspiration. The third space dorsal external intercostal muscles, scalene muscles and parasternal intercostal muscles were then recruited in that order, while the fifth space dorsal external intercostal muscles were recruited significantly later in inspiration and to a lesser extent (Saboisky et al., 2007). Another study found that the scalenes and parasternal intercostals were always active during eupneic breathing. Using EMG, it was found that not only was their pattern of activation identical to each other, but both muscle groups had an identical increase in EMG activity as inspiration persisted (De Troyer and Estenne, 1984). The coordination, recruitment, and distribution of these various muscle groups are thought to be necessary for compensation when diaphragmatic output is compromised (Saboisky et al., 2007).

Pectoralis Minor Muscle

The accessory muscles of inspiration have also been studied in disease/injury states during wakefulness and sleep when the diaphragm is dysfunctional. During respiratory distress and diaphragmatic loss, it has been suggested that breathing switches from 'thoracic breathing' to 'chest breathing' (Schleifer et al., 2002). In humans, the pectoralis minor muscles are deep muscles within the chest that are inserted on the medial border and superior surface of the coracoid process of the scapula. These muscles cross the 3rd through the 5th rib creating a fan-shape across the anterior chest wall and are innervated by the medial and lateral pectoral nerves, which originate from the C5/C6 region of the cervical spinal cord (Aszmann et al., 2000; Moosman, 1980). This muscle's role in breathing is to lift the top of the rib cage upward and outward (Bartley, 2011). Hypoplasia, aplasia, loss

of muscle tone and dysfunction can potentially result in herniation of the lung (Aznar et al., 1996) and inadequate chest wall movement. The pectoralis minor muscles are not usually recruited during eupnea, and only have minimal activity late in deep inspiration (Campbell, 1955). However, the pectoralis minor muscles get recruited during forced inspiration and increased inspiratory demand such as in exercise or disease/injury states, which will be explored in this dissertation.

1.4 – Breathing Impairment in Neuromuscular Injury and Disease

Amyotrophic Lateral Sclerosis

In patients with amyotrophic lateral sclerosis (ALS), progressive loss of respiratory motor neurons results in reduced maximal inspiratory and expiratory pressures, transdiaphragmatic pressure, and capacity to produce sniff nasal pressure due to respiratory muscle weakness. In pre-symptomatic stages of the disease, no deficits in resting ventilation are observed because only innervation to muscles involved in max force are affected (*e.g.*, sneeze and cough)(Seven and Mitchell, 2019). As respiratory muscle strength decreases, PCO_2 increases (Harrison et al., 1971; Kreitzer et al., 1978b; Stone and Keltz, 1963). Before the disease becomes severe, patients hyperventilate to correct for changes in PCO_2. However, when these patients sleep, particularly during REM sleep, skeletal muscle activity, including the accessory muscles of respiration, is reduced. This reduction in combination with reduced diaphragm strength, can lead to significant hypoventilation (Bye et al., 1990). ALS patients can have normal daytime blood gases but experience hypoxia and hypercapnia during sleep. In patients with bilateral diaphragm

8

paralysis (BDP), extradiaphragmatic inspiratory muscles are recruited during wakefulness and tonic and phasic REM (Bennett et al., 2004).

In a model of ALS in which rodents overexpress copper/zinc superoxidedismutase-1 (SOD-1) gene, the SOD1 enzyme has a toxic gain of function and produces free radicals (Vucic and Kiernan, 2009). In the mouse model (hSOD1^{G93A}), ventilation is maintained until late in disease much like in human patients. In fact, ventilatory failure occurs over two days and the mouse quickly dies (Tankersley et al., 2007). Similarly, in hSOD1^{G93A} rats that have lost ~ 60-80% of their phrenic and ~65% of their intercostal motor neurons, breathing capacity is maintained during maximal chemosensory stimulation (exposure to hypoxia + hypercapnia). This preservation may be due to the fact that spontaneous activation of the diaphragm remains (Seven et al., 2018) when challenged with maximal chemosensory stimulation even when spontaneous phrenic nerve activity and diaphragm action potentials are blunted at disease end-stage in this rat model (Lladó et al., 2006; Nichols et al., 2014). These models recapitulate the ventilatory preservation observed in human patients until late in disease and therefore have been used to examine how breathing function is maintained.

Spinal Cord Injury

Similar studies to evaluate breathing and respiratory muscle weakness have been conducted in spinal cord injury (SCI) patients, however, breathing deficits greatly vary depending on the cervical location of the injury and the amount of impairment to respiratory motor neurons. For example, high cervical spinal cord injury most often results in respiratory failure (Frankel et al., 1998) and the need for mechanical ventilation due to the dramatic

loss of phrenic motor neurons. When cervical spinal cord injuries occur at C5 and above, peak cough flow and maximal inspiratory and expiratory pressures are reduced. As seen with ALS patients, SCI patients also experience a greater inability to maintain appropriate ventilation to regulate blood gases when transitioning from wakefulness to sleep. During this transition, SCI patients exhibit a significant reduction in tidal volume, which causes end-tidal CO_2 to be high and O_2 to be low (Bascom et al., 2015). SCI patients have a high prevalence of central sleep apnea, as well as obstructive sleep apnea due to the loss of upper airway tone depending on the level of the injury (Berlowitz et al., 2005; Sajkov et al., 1998). The recruitment of accessory muscles is also highly dependent on the location of the injury (above or below the cervical spinal cord segments 3-6) (Zimmer et al., 2007). Luckily, most SCIs in human patients are incomplete and therefore the neurons and descending pathways that are spared can undergo plasticity to compensate for function (Goshgarian, 2003; Goshgarian, 2009; Khurram et al., 2019; Lane et al., 2009; Lee, 2019; Lee and Hsu, 2017; Lee and Kuo, 2017; Mansel and Norman, 1990; Mantilla et al., 2013; Wen and Lee, 2018).

In models of cervical spinal cord injury, a hemisection of the C2 segment of the spinal cord is performed resulting in paralysis of the ipsilateral hemidiaphragm. This model is an incomplete injury in which the contralateral neurons and descending pathways are spared, and represents the most common spinal cord injury observed in humans. In both anesthetized and unanesthetized, spontaneously breathing rats with a C2-hemisection injury, tidal volume was significantly reduced, while breathing frequency was significantly increased. Although these breathing patterns are altered, there is no overall change in total minute ventilation (Fuller et al., 2006; Golder et al., 2001). Cervical contusions in rodent

models also recapitulate human SCIs because the affected neurons at the epicenter of the contusion experience demyelination and degeneration, resulting in ~50% loss of phrenic motor neurons and diaphragmatic motor end plat denervation (Nicaise et al., 2013; Nicaise et al., 2012a; Nicaise et al., 2012b; Rana et al., 2017). When this happens, there is a reduction in phrenic nerve activity and evoked compound action potentials of the diaphragm which causes abnormal patterns in ventilation (Golder et al., 2011; Nicaise et al., 2012a; Warren et al., 2018; Wen and Lee, 2018).

1.5 – Mechanisms of Respiratory Plasticity

Naïve animals

Research suggests that respiratory compensation following motor neuron loss is due to increased phrenic motor output by neighboring surviving motor neurons. The long-lasting increase in phrenic motor output is known as phrenic motor facilitation (pMF). pMF can be elicited by pharmacological activation of a number of receptors or physiologically *via* acute intermittent hypoxia (AIH) in naïve animals. When phrenic plasticity is induced pharmacologically, we refer to the change in phrenic motor output as pMF. However, when phrenic plasticity is induced by AIH, we specifically refer to this as pLTF (*i.e.,* pLTF is a form of pMF) (Bach and Mitchell, 1996; Dale-Nagle et al., 2010; Feldman et al., 2003; Hayashi et al., 2003; Mitchell et al., 2001). During AIH, pLTF occurs through the activation of Gq (5-HT$_{2A/B}$) (Bach and Mitchell, 1996; MacFarlane et al., 2011) or Gs (A$_{2A}$)-coupled receptor-dependent pathways (Golder et al., 2008). When naïve adult rats are exposed to *moderate* AIH (45-55 mmHg PaO$_2$) with isocapnia, pLTF is induced through activation of medullary raphe serotonergic neurons that release serotonin (5-HT)

in the phrenic motor nucleus. 5-HT2 receptors on or near phrenic motor neurons within the C3-6 sections of the spinal cord then become activated (Bach and Mitchell, 1996). When 5-HT2 receptors become activated, protein kinase C theta (PKCθ) is activated (Devinney et al., 2015; Liu et al., 2011) and leads to the new synthesis of brain-derived neurotrophic factor (BDNF) (Agosto-Marlin and Mitchell, 2017; Baker-Herman et al., 2004). BDNF then binds to the mTrkB receptor (Baker-Herman et al., 2004), activating MEK and the phosphorylation of ERK, ultimately resulting in pLTF (Hoffman et al., 2012). pLTF also requires reactive oxygen species (ROS) formation *via* NADPH oxidase activity since ROS disinhibits phosphatase action on PKC (*i.e.,* ROS formation allows pLTF to be evoked) (MacFarlane and Mitchell, 2007; MacFarlane et al., 2011). Pharmacological activation of 5-HT2A and 5-HT2B receptors also leads to pMF in naïve adult rats (MacFarlane and Mitchell, 2009; MacFarlane et al., 2011). Furthermore, pMF *via* 5-HT2A activation is NADPH oxidase-independent, while 5-HT2B induced pMF is NADPH oxidase-dependent (MacFarlane et al., 2011). Studies have also shown that pre-treatment with ketanserin (5-HT2A antagonist) blocks pLTF, whereas giving ketanserin after AIH does not. This suggests that 5-HT2A receptors are required for the initiation, but not the maintenance, of AIH-induced pLTF (Fuller et al., 2001).

Activation of spinal metabotropic receptors coupled to Gs proteins, such as the adenosine 2A (A2A) receptor can also result in pMF (Golder et al., 2008). pMF induced pharmacologically by an A2A receptor agonist requires the new synthesis of an immature TrkB isoform that is thought to signal from within phrenic motor neurons through auto-activation (Baker-Herman et al., 2004; Golder et al., 2008). This mechanism of pMF occurs independently from 5-HT receptor activation. When naïve rats are exposed to more severe

AIH (*i.e.,* 25–35 mmHg PaO2) adenosine is released into the extracellular space and activates adenosinergic mechanisms of pLTF (Devinney et al., 2013; Devinney et al., 2012; Nichols et al., 2012) leading to the activation of protein kinase B (pAkt) *via* phosphatidylinositol 3-kinases (PI3K) (Agosto-Marlin et al., 2017; Devinney et al., 2013; Golder et al., 2008; Hoffman and Mitchell, 2011; Nichols et al., 2012; Nichols and Mitchell, 2021). This severe protocol of AIH elicits pLTF that is enhanced from those rats exposed to the moderate AIH protocol (Nichols et al., 2012). Using the CTB-SAP model of respiratory motor neuron death, which will be further discussed in section 1.6, we aim to understand underlying mechanisms of pLTF and how they could be used as therapeutic targets to maintain breathing following instances of neuromuscular disease or injury that result in respiratory motor neuron loss. A schematic of the Gq and Gs-dependent signaling pathways is shown in Figure 1.1.

Mechanisms of pLTF in Disease

Pre-symptomatic and end-stage SOD1^{G93A} rats exhibit both pLTF and XII LTF. At end-stage, pLTF was actually enhanced in this model (Nichols et al., 2015a). Furthermore, it was found that AIH-induced pLTF in pre-symptomatic SOD1^{G93A} rats is NADPH oxidase-dependent, but end-stage SOD1^{G93A} rats exhibit NADPH oxidase-independent pLTF (Nichols et al., 2015a). Additionally, siRNA against BDNF and inhibition of MEK/ERK signaling attenuated the enhanced pLTF observed in end-stage SOD1^{G93A} rats, while siRNA against TrkB and inhibition of PI3K/Akt signaling had no effect on pLTF (Nichols et al., 2017). This indicates that enhanced pLTF in end-stage SOD1^{G93A} rats is elicited through Gq signaling. These findings assisted in the work expressed in the current
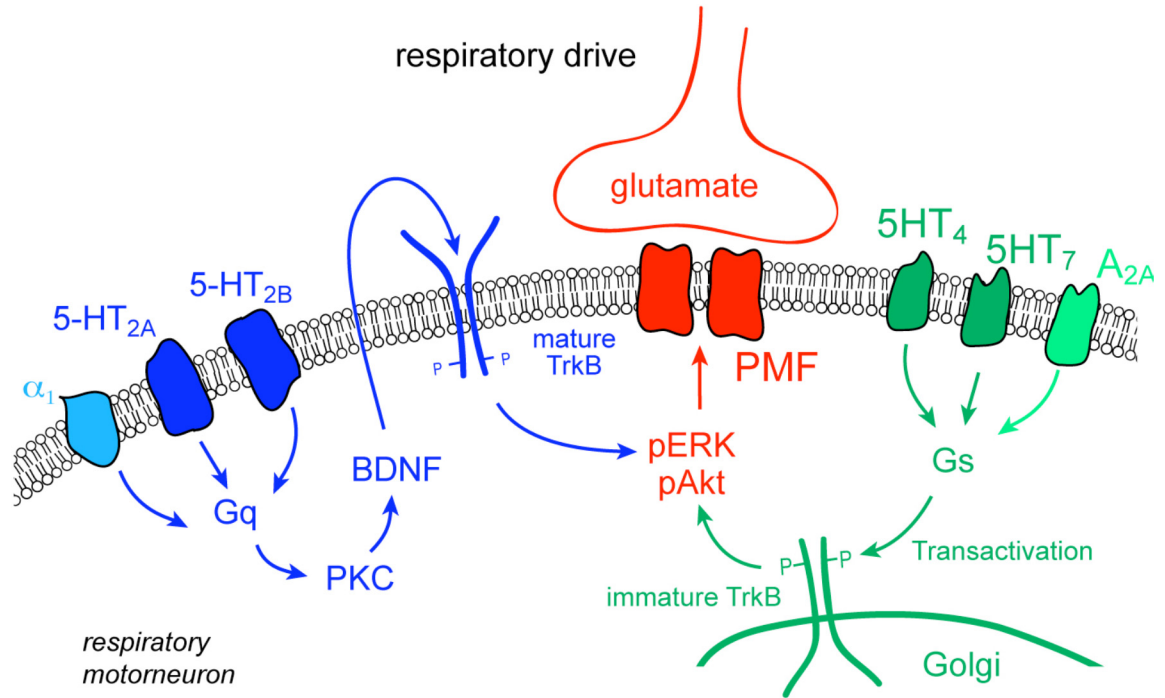
Figure 1.1: A schematic of the known Gq and Gs mechanisms of phrenic motor facilitation. The left-hand side of the figure shows how activation of the 5-HT2A/B receptor or the alpha-1 (α1) adrenergic receptor leads to Gq signaling through the activation of protein kinase C, the new synthesis of BDNF, and the phosphorylation of ERK to lead to pMF. Note, α1 receptor activation is sufficient to cause pMF, but is not necessary for pLTF (Huxtable et al., 2014). On the right-hand side of the figure are the receptors that activate Gs signaling (5-HT4/7 and adenosine 2A (A2A)). Once activated, the new synthesis of TrkB leads to the phosphorylation of Akt and leads to pMF. Note, 5-HT4/7 receptors are sufficient to cause pMF, but are not necessary for pLTF (Hoffman and Mitchell, 2011; Hoffman and Mitchell, 2013).

dissertation when trying to delineate mechanisms of pLTF in our model of respiratory motor neuron death, which is described in the next section.

1.6 – Model and Overview of Techniques utilized in this Dissertation

To control for the rate and amount of respiratory motor neuron death in order to study the underlying mechanisms of plasticity and recruitment of accessory inspiratory muscles explored by the current research presented in this dissertation, an inducible model of respiratory motor neuron death is used for these studies. Cholera toxin B (CTB) is a retrograde motor neuron tracer that has been shown to label phrenic motor neurons when injected into the intrapleural space (Mantilla et al., 2009). Through endocytosis (Lian and Ho, 1997), CTB is then taken into resident phrenic and intercostal motor neurons where it is retrogradely transported to the phrenic motor nucleus in the cervical spinal cord (C3-6). When CTB is conjugated to saporin (CTB-SAP), a plant toxin, by disulfide bonds and injected intrapleurally, the CTB component then binds to GM1 (Galactosyl-N-Acetylgalactosaminyl) receptors on the cell membrane of motor neurons (Lian and Ho, 1997). This allows for the entire CTB–SAP construct to enter the cell (Lencer and Tsai, 2003), where CTB and SAP will then dissociate (Llewellyn-Smith et al., 2000). Saporin is a ribosomal inactivating protein (RIP) that binds to the large (28S) subunit on the ribosome and disables protein synthesis by interfering with protein translation. Once the protein synthetic machinery is disabled, cell death occurs over a matter of hours to days via apoptosis (Llewellyn-Smith et al., 1999; Lujan et al., 2010). These intrapleural injections induce targeted phrenic and intercostal motor neuron death *only* when CTB is conjugated

to saporin (CTB–SAP) (Llewellyn-Smith et al., 2000; Llewellyn-Smith et al., 1999; Lujan et al., 2010).

Nichols et al., found that rats that received an intrapleural injection of CTB–SAP (25µg or 50 µg) experienced a dose-dependent effect on respiratory motor neuron survival where rats that received 25µg of CTB–SAP had a significant decrease in phrenic and intercostal motor neuron survival at 7 days post injection compared to control animals that received the unconjugated CTB + SAP injection (phrenic = ~40% survival and intercostal = ~60% survival; $p < 0.05$) (Nichols et al., 2015b). Phrenic motor neuron death was similar to 7d treated rats at 28d (~25% survival), but intercostal motor neuron death was significantly increased in 28d CTB-SAP rats (~15% survival) compared to 7d CTB-SAP rats (Nichols et al., 2015b). Most importantly, intrapleural CTB–SAP injection did not have significant off-target effects (lack of cell death in the brainstem or in other spinal cord regions). Similar to what is observed in $SOD1^{G93A}$ rats, CTB-SAP treatment, also significantly decreased phrenic motor output (~50% less than controls) (Nichols et al., 2015b). Interestingly, despite phrenic motor loss and a decrease in phrenic output, CTB-SAP rats were able to maintain eupneic ventilation (Fig. 1.2) (Nichols et al., 2015b). When pLTF was evaluated following CTB-SAP-induced respiratory motor neuron death, Nichols et al., found that following moderate AIH exposure, pLTF is enhanced in 7d CTB-SAP rats while pLTF is similar to control or naïve rats in 28d CTB-SAP rats (Fig 1.3) (Nichols et al., 2015b). This indicates that respiratory compensation is occurring, that differential underlying mechanisms of respiratory plasticity elicited by CTB-SAP-induced respiratory motor neuron death contribute to the difference in magnitude of the pLTF elicited, and that these mechanisms potentially assist in maintaining eupneic ventilation in this model.
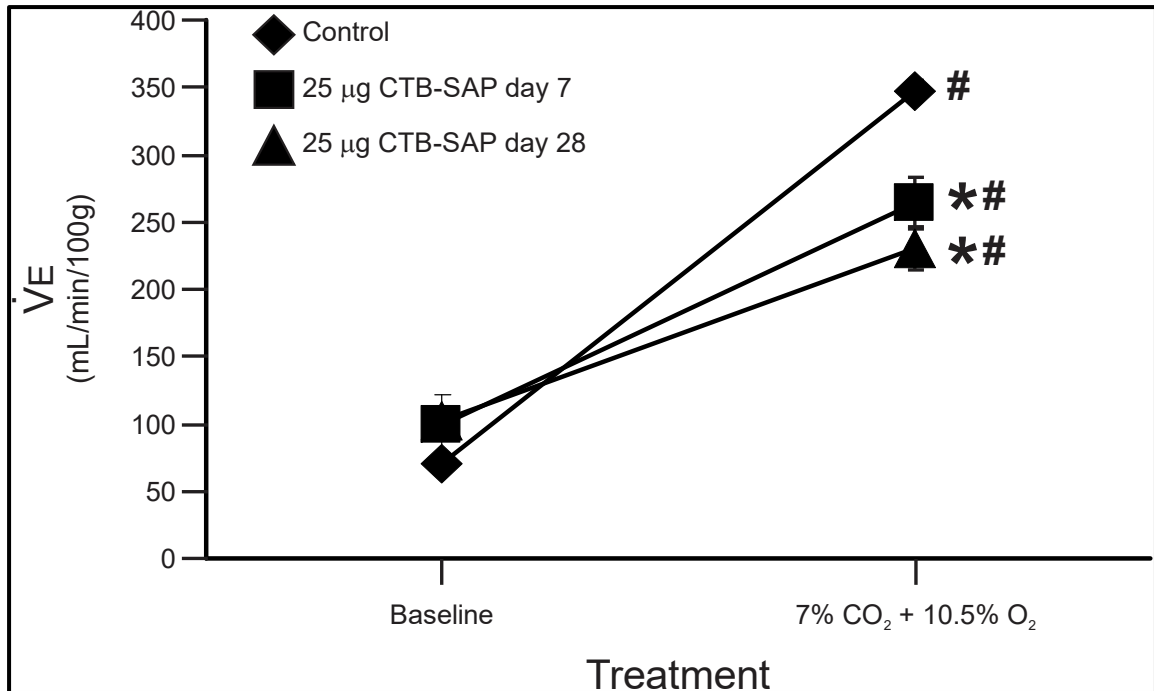
Figure 1.2: Minute ventilation normalized to body mass at baseline and during hypercapnia + hypoxia (7% CO$_2$ + 10.5% O$_2$) in rats treated with CTB+SAP (control) or 25 µg CTB-SAP at 7d and 28d. Minute ventilation was unaffected at baseline in CTB-SAP rats, but was decreased from controls during hypercapnia + hypoxia (*; p<0.05). Minute ventilation was also increased from baseline in all groups with exposure to hypercapnia + hypoxia (#; p<0.05). Adapted from Nichols et al., 2015 (Nichols et al., 2015b).
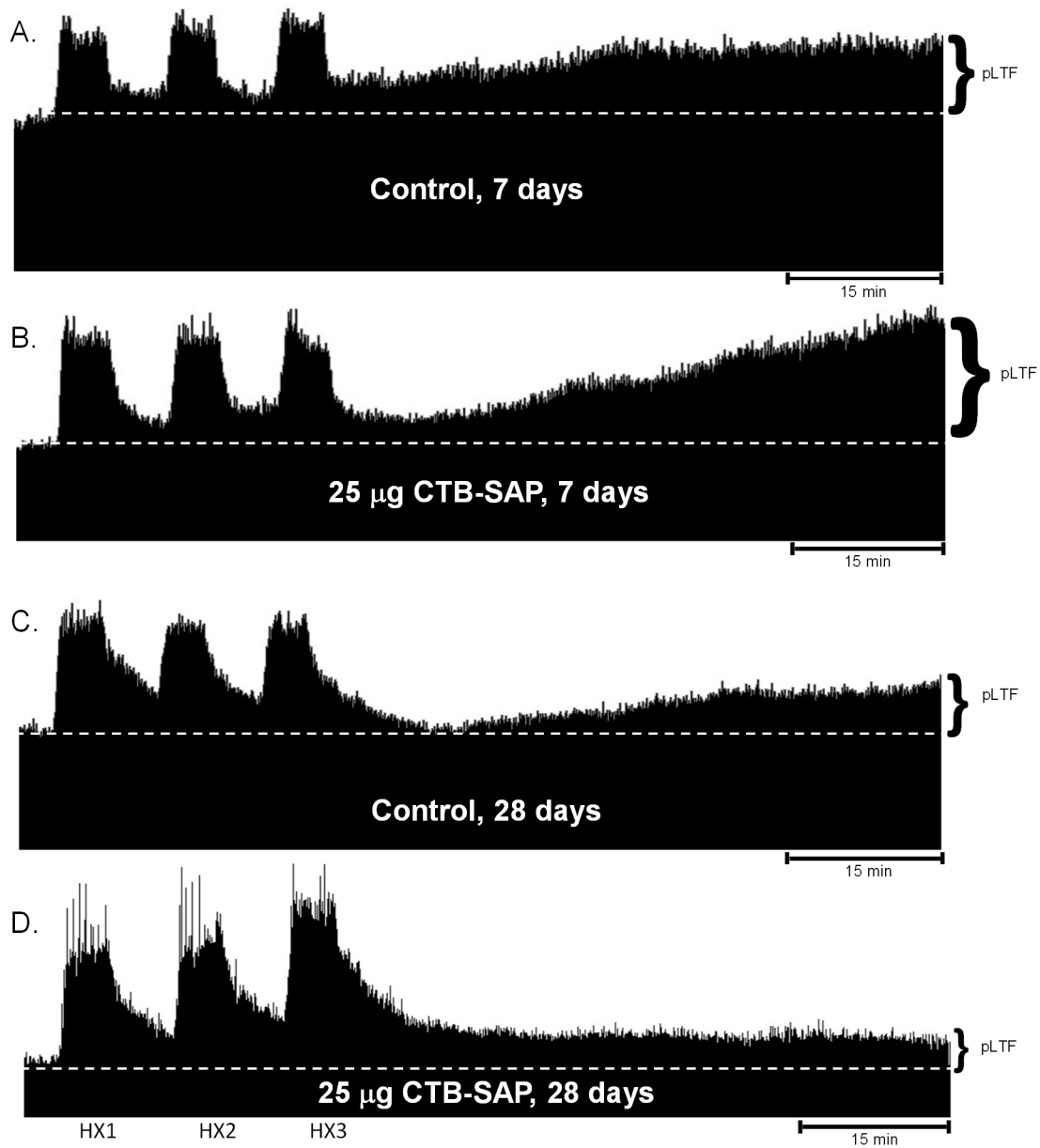
Figure 1.3: pLTF in 7d and 28d control and CTB-SAP treated rats. A-D. Representative compressed neurograms recorded from the phrenic nerve in 7d and 28d control (A, C) and CTB-SAP (B, D) treated rats that were urethane anesthetized, vagotomized, pump-ventilated, and paralyzed. The white dotted line indicates baseline nerve output before acute intermittent hypoxia (AIH; 3, 5 min bouts of 10.5% O_2) exposure (HX1, HX2, HX3). After the final bout of hypoxia, rats were returned to baseline conditions and phrenic nerve output was recorded for the next 60 minutes. The change from baseline is known as phrenic long-term facilitation (pLTF). It can be appreciated that pLTF is enhanced in the 7d CTB-SAP treated rat *vs*. the 7d control rat and 28d CTB-SAP treated rat, whereas pLTF in the 28d CTB-SAP rat is not different from the 28d control rat.

Techniques to Assess Mechanisms of pLTF

Male Sprague-Dawley rats (300-400g) received an intrapleural injection of either: 1) CTB–SAP (25 µg), or 2) unconjugated CTB and SAP (*i.e.,* control; (CTB + SAP). *In vivo* neurophysiology experiments were conducted on rats either 7- or 28-days post-injection. In brief, the phrenic nerve output was recorded in rats that were urethane anesthetized, vagotomized, pump-ventilated, and paralyzed. An intrathecal catheter was inserted subdurally over the phrenic motor nucleus in the C4 section of the spinal cord for the delivery of siRNAs or inhibitors of proteins or receptors involved in Gs or Gq-receptor pathways. To assess the necessity of Gq and Gs-dependent mechanisms, small interfering RNA that targeted BDNF or TrkB mRNA, UO126 (MEK/ERK inhibitor), PI828 (PI3K/Akt inhibitor), MSX-3 (A_{2A} receptor antagonist), or methysergide (broad-spectrum 5-HT receptor antagonist) were administered. Baseline phrenic nerve output was recorded before rats were exposed to the AIH with isocapnia protocol (3, 5-minute bouts 35-45 mmHg PaO_2), and then phrenic nerve output was recorded over the following hour. The percent change in phrenic nerve output (pLTF) from baseline to 60-minute post-AIH exposure will be quantified.

Techniques to Assess 5-$HT_{2A/B}$ receptor expression

Spinal cord tissue was taken from the C4 spinal cord of 7d and 28d control and CTB-SAP rats to assess the expression of 5-$HT_{2A/B}$ receptors within the phrenic motor nucleus and in the non-phrenic ventral horn. Rats were first perfused with 4% paraformaldehyde, and then the C4 spinal cord was isolated, preserved, and sectioned. C4 sections were then stained for CTB(+) phrenic motor neurons and 5-$HT_{2A/B}$ receptors, and receptor

expression within the phrenic motor nucleus and in the non-phrenic ventral horn was subsequently analyzed using an Olympus BX51 microscope (Ludl Electronic Products, Hawthorne, NY), Neurolucida software (version 10, MicroBrightField, Willston, VT), and ImageJ.

Techniques to Assess the Impact of COX1/2-induced inflammation on pLTF

Male Sprague-Dawley rats (300-400g) received an intrapleural injection of either: 1) CTB–SAP (25 µg), or 2) unconjugated CTB and SAP (*i.e.,* control; (CTB + SAP). *In vivo* neurophysiology experiments were conducted on rats either 7- or 28-days post-injection. As described above, the phrenic nerve output was recorded in rats that were urethane anesthetized, vagotomized, pump-ventilated, and paralyzed 3 hours after receiving an intraperitoneal injection of either ketoprofen or the vehicle. Baseline phrenic nerve output was recorded before rats were exposed to the AIH with isocapnia protocol (3, 5-minute bouts 35-45 mmHg PaO_2), and then phrenic nerve output was recorded over the following hour. The percent change in phrenic nerve output (pLTF) from baseline to 60-minute post-AIH exposure will be quantified.

Techniques to Assess Inflammatory-Associated Marker Expression and Microglial Morphology

To begin to characterize the inflammatory response following CTB-SAP-induced respiratory motor neuron loss, cervical (C_{3-5}, which encompasses the phrenic motor nucleus) expression of inflammatory-associated markers was evaluated in control and CTB-SAP rats that did not receive ketoprofen. Specifically, qRT-PCR was used to

determine TNF-α, BDNF, iNOS, IL-10, IL-6, and Arg-1 gene expression in homogenate tissue. In addition, microglial morphology was studied within the phrenic motor nucleus of 7d and 28d control and CTB-SAP rats. In brief, Z-stack images of C4 sections stained for CTB(+) phrenic motor neurons and microglia (Cd11b) were taken and opened in the IMARIS software program. An ROI was set for the phrenic motor nucleus through the stack, and the CD11b(+) cells were analyzed for changes in microglial morphological parameters within the phrenic motor nucleus.

Whole-body plethysmography

Whole-body plethysmography was performed in awake, freely-moving rats to evaluate quantitative breathing measurements with altered inspired gas concentrations. Rats were placed in a whole-body flow-through plethysmograph (Data Sciences International, St. Paul, MN) 7d or 28d post- intrapleural and intramuscular (pectoralis minor muscle) injection of control or CTB-SAP. The rats acclimated to the chamber while breathing room air (21% O_2, balance N_2; flushed at ~ 3 L/min) for 15 minutes before ventilatory measurements were recorded for baseline conditions for an additional 15 minutes. Rats were then exposed to a hypoxic + hypercapnic gas mixture (10.5% O_2/7% CO_2; 5 min). A pressure calibration signal, ambient and chamber pressures, and rat body mass were used to calculate breath-by-breath tidal volume (V_T; Drorbaugh and Fenn, 1955, Jacky, 1978), respiratory frequency, mean inspiratory flow (V_T/TI), minute ventilation ($\dot{V}_E$), peak inspiratory flow (PIF), peak expiratory flow (PEF), inspiratory time (Ti), and expiratory time (Te). V_T, $\dot{V}_E$, and V_T/TI are reported normalized to body mass (per 100 g). Data were rejected if there was evidence of pressure fluctuations caused by gross body movements or

sniffing behavior. At the conclusion of the study, rats were removed from the chambers and were prepared for surgery for electromyographical experiments.

Techniques to Assess Pectoralis Minor Output and Pectoralis Minor Motor Neuron Survival in CTB-SAP rats

Male Sprague-Dawley rats (300-400g) received intrapleural injection of either: 1) CTB–SAP (25 µg), or 2) unconjugated CTB and SAP (*i.e.,* control; (CTB + SAP). Electromyographical recordings of the pectoralis minor muscle were performed in urethane anesthetized, spontaneously breathing rats at 7d or 28d post intrapleural injection. The rats were exposed to normoxia for 20 minutes ($PaO_2 > 85$ mmHg), followed by maximum chemoreceptor stimulation where rats breathed combined hypercapnia (10.5% $FiCO_2$) and hypoxia (10.5% FiO_2) (~65 mmHg $PaCO_2$ and ~45 mmHg PaO_2) for 5 min (Seven et al., 2017). In a subset group of rats, simultaneous recordings from the pectoralis minor muscle and phrenic nerve were performed to ensure that the pectoralis minor muscle contraction occurred at the same times as phrenic nerve bursting to coincide with breathing. Baseline pectoralis minor amplitude was compared to that elicited by hypercapnia + hypoxia (max) within and across treatment groups.

Furthermore, we wanted to determine the extent to which the pectoralis minor muscles were utilized for the maintenance of eupnea. In order to do so, rats were given bilateral intrapleural injections of the control or CTB-SAP, as described above, and were bilaterally injected with the control or CTB-SAP (5µl per side) into the pectoralis minor muscle (intramuscular; IM). The intrapleural and IM injections also contained retrograde tracers to enable quantification of phrenic motor neuron (CTB-AlexaFluor647) and

pectoralis minor motor neuron (CTB-AlexaFluor488) survival. The combination of the intrapleural and IM injections allowed us to determine the utilization of the pectoralis minor muscle in urethane anesthetized, spontaneously breathing rats and compare it to the muscle's involvement in breathing when rats were awake and freely-moving during whole-body plethysmography.

1.7 – Specific Aims and Hypotheses

AIM 1:

Determine the requirement of A2A and 5-HT receptors for pLTF in CTB-SAP treated rats.

Rationale: As discussed above, respiratory plasticity can be induced pharmacologically through Gq (5-HT2A/B) or Gs (A2A) protein-coupled metabotropic receptors. Respiratory plasticity can also be induced physiologically by exposure to AIH, known as phrenic long-term facilitation (pLTF). In naïve rats, moderate AIH-induced pLTF requires 5-HT2 receptors (Gq) (Fuller et al., 2001), while exposure to severe AIH induces enhanced pLTF through activation of the A2A receptor (Gs). Studies have suggested that A2A receptors actually constrain pLTF during moderate AIH exposure by inhibiting downstream activators in the Gq pathway. However, the receptor(s) and mechanisms required for triggering AIH-induced pLTF following CTB-SAP-induced respiratory motor neuron death have yet to be understood. Following CTB-SAP, 7d rats exhibit an enhanced pLTF, suggesting 7d CTB-SAP rats utilize the A2A-dependent mechanism for the enhanced pLTF observed. We found in 7d CTB-SAP rats that pLTF is blocked by the A2A antagonist (MSX-3), not the broad-spectrum 5-HT antagonist (methysergide), again suggesting that

pLTF is exhibited by an A2A receptor-dependent mechanism. We also have preliminary data that shows that A2A receptor expression (data not shown) is increased while 5-HT terminal density (data not shown) is unchanged. In contrast, we have observed that the amount of pLTF exhibited by 28d CTB-SAP treated rats is similar to that of 28d control and naïve rats, suggesting that the underlying pathways used to elicit pLTF is through 5-HT2 receptor activation and downstream signaling pathways (Nichols et al., 2018).

Hypotheses: A2A receptors are required for pLTF in 7d (but not 28d) rats, and 5-HT receptors are required for pLTF in 28d (but not 7d) rats. As assessed by in vivo neurophysiology, pLTF will be abolished in: 1) 7d rats following intrathecal delivery of the A2A receptor antagonist (MSX-3), and will not be affected by the antagonism of the 5-HT receptor (methysergide); and 2) 28d rats with 5-HT receptor antagonism, but will not be affected by antagonism of the A2A receptor.

AIM 2:

Determine the requirement of downstream Gs and Gq-dependent signaling pathways that contribute to the differential magnitude in pLTF elicited in 7d and 28d CTB-SAP rats following moderate AIH.

Rationale: We know that exposure to moderate AIH leads to the activation of 5-HT2 receptors on or near phrenic motor neurons (Bach and Mitchell, 1996), followed by the activation of protein kinase C theta (PKCθ) (Devinney et al., 2015; Devinney et al., 2013)

which leads to the new synthesis of brain-derived neurotrophic factor (BDNF) (Baker-Herman et al., 2004; McGuire and Ling, 2004). BDNF then binds to the mature TrkB receptor (Baker-Herman et al., 2004) and causes MEK/ERK activation/phosphorylation (Hoffman et al., 2012) to ultimately result in moderate pLTF. Because moderate pLTF is elicited in 28d CTB-SAP rats, we speculate the new synthesis of BDNF and MEK/ERK signaling are required. Conversely, pLTF occurs at a greater magnitude when naïve adult rats are exposed to severe bouts of AIH (25–35 mmHg PaO_2) and requires a Gs-adenosine (A_{2A}) receptor-dependent pathway. This severe AIH exposure causes adenosine to be released into the extracellular space and activates A_{2A} receptors, which leads to the activation of protein kinase B (pAkt) *via* phosphatidylinositol 3-kinases (PI3K), and ultimately results in enhanced pLTF (Agosto-Marlin et al., 2017; Devinney et al., 2013; Golder et al., 2008; Hoffman and Mitchell, 2011; Nichols et al., 2012; Nichols and Mitchell, 2021). We observe enhanced pLTF in 7d CTB-SAP rats, therefore, we speculate the necessity of TrkB synthesis and subsequent PI3K/Akt signaling in eliciting enhanced pLTF at this time point.

Hypotheses: pLTF following CTB-SAP is iTrkB and PI3K/Akt, not BDNF and MEK/ERK, dependent at 7d, while pLTF is BDNF and MEK/ERK, not iTrkB and PI3K/Akt, dependent at 28d. As assessed by in vivo neurophysiology, pLTF will be abolished in: 1) 7d CTB-SAP rats following intrathecal delivery of siRNA against the new synthesis of TrkB and inhibitors of PI3K/Akt; and 2) 28d CTB-SAP rats following intrathecal delivery of siRNA against the new synthesis of BDNF and inhibitors of MEK/ERK.

AIM 3:

Determine if COX1/2-induced inflammation differentially impacts the magnitude of pLTF observed in 7d and 28d CTB-SAP rats following moderate AIH.

Rationale: Patients with neuromuscular diseases/injuries experience systemic inflammation that hinders the function of the neural networks responsible for breathing (Perry, 2010; Teeling and Perry, 2009). As discussed above, we observe enhanced pLTF in 7d CTB-SAP rats, and speculate this enhancement is elicited through activation of Gs-A_{2A}-dependent mechanisms that utilize the new synthesis of TrkB and subsequent PI3K/Akt signaling. In contrast, we have observed that the amount of pLTF exhibited by 28d CTB-SAP treated rats is similar to that of 28d control and naïve rats, suggesting that pLTF is elicited through Gq-5-HT_2 receptor-dependent mechanisms that utilize the new synthesis of BDNF and downstream signaling through MEK/ERK (Nichols et al., 2018). When inflammation is evoked with the delivery of lipopolysaccharide (LPS; a toll-like receptor 4 agonist (Lu et al., 2008; Triantafilou and Triantafilou, 2002), Gq pathway-induced pMF and moderate AIH-induced pLTF are nearly abolished. pLTF is restored with the administration of the non-steroidal anti-inflammatory drug, ketoprofen (Agosto-Marlin et al., 2018; Hocker et al., 2017; Huxtable et al., 2011; Huxtable et al., 2015; Huxtable et al., 2013; Vinit et al., 2011). In contrast, Gs pathway-induced pMF and severe AIH-induced pLTF are unaffected by LPS-induced inflammation, indicating that the Gs pathway is inflammation-resistant (Agosto-Marlin et al., 2017). Therefore, we speculate that because pLTF is elicited through inflammation-resistant Gs-dependent mechanisms in 7d CTB-SAP rats, and will be unaffected by ketoprofen treatment. In contrast, we postulate that

pLTF in 28d CTB-SAP rats is elicited through inflammation-sensitive Gq-dependent mechanisms, and will be enhanced following the administration of ketoprofen.

Hypotheses: pLTF following CTB-SAP is inflammation-resistant at 7d, while pLTF is inflammation-sensitive at 28d. As assessed by in vivo neurophysiology, following COX1/2 inhibition with ketoprofen (IP): 1) pLTF will be unaffected in 7d CTB-SAP rats; and 2) pLTF will be enhanced in 28d CTB-SAP.

AIM 4:

Determine if the pectoralis minor muscles are recruited to assist in maintaining eupneic ventilation.

Rationale: Despite significant respiratory motor neuron loss following CTB-SAP treatment, rats are able to maintain eupneic ventilation (Nichols et al., 2015b) (Fig. 1.2). Consistent to what has been observed in other spinal/neuromuscular diseases, our preliminary data shows that diaphragmatic output is decreased in CTB-SAP rats (data not shown). Respiratory compensation by extradiaphragmatic muscle groups has been documented (particularly the intercostals, abdominals, sternocleidomastoid, scalene, seratii, trapezii, and latissimus dorsi muscles) following diaphragmatic bilateral paralysis, spinal cord injury, ALS, and other diseases in which there is loss of motor neurons and/or skeletal muscle (Bennett et al., 2004; Bye et al., 1990; Harrison et al., 1971; Kreitzer et al., 1978b; Stone and Keltz, 1963). Furthermore, human and animal studies have shown that the compensation of extradiaphragmatic accessory inspiratory muscles varies highly upon

the severity of the disease, the presence/amount of muscular atrophy, the state of wakefulness, and the posture of the individual. The pectoralis minor muscle attaches to the medial border and superior surface of the coracoid process of the scapula. When the pectoralis minor muscles contract, they pull the upper rib cage upward and outward. Following diaphragmatic loss, it has been suggested that breathing switches from 'thoracic breathing' to 'chest breathing' (Schleifer et al., 2002), requiring accessory inspiratory muscles of chest, such as the pectoralis minor, to be engaged.

Hypotheses: Pectoralis minor amplitude will be increased in CTB-SAP rats, and these muscles contribute to the maintenance of eupneic ventilation.

CHAPTER 2: Divergent receptor utilization is necessary for phrenic long-term facilitation over the course of motor neuron loss following CTB-SAP intrapleural injections

Lauren F. Borkowski, Catherine L. Smith, Amy N. Keilholz, and Nicole L. Nichols

Department of Biomedical Sciences, Dalton Cardiovascular Research Center, University of Missouri, Columbia, MO 65211

Abbreviated Title: pLTF requires distinct receptors after intrapleural CTB-SAP

2.1- ABSTRACT

Intrapleural injection of cholera toxin B conjugated to saporin (CTB-SAP) mimics respiratory motor neuron death and respiratory deficits observed in rat models of neuromuscular diseases. 7d CTB-SAP rats elicit enhanced phrenic long-term facilitation (pLTF) primarily through TrkB and PI3K/Akt-dependent mechanisms (*i.e*., Gs-pathway, which can be initiated by adenosine 2A (A_{2A}) receptors in naïve rats), while 28d CTB-SAP rats elicit moderate pLTF though BDNF and MEK/ERK-dependent mechanisms (*i.e*., Gq-pathway, which is typically initiated by serotonin (5-HT) receptors in naïve rats). Here, we tested the hypothesis that pLTF following CTB-SAP is: 1) A_{2A} receptor-dependent at 7d; and 2) 5-HT receptor-dependent at 28d. Adult Sprague Dawley male rats were anesthetized, paralyzed, ventilated, and were exposed to acute intermittent hypoxia (AIH; 3, 5 min bouts of 10.5% O_2) following bilateral, intrapleural injections at 7d and 28d of: 1) CTB-SAP (25 mg), or 2) un-conjugated CTB and SAP (control). Intrathecal C_4 delivery included either the: 1) A_{2A} receptor antagonist (MSX-3; 10 mM; 12 ml); or 2) 5-HT receptor antagonist (methysergide; 20 mM; 15 ml). pLTF was abolished with A_{2A} receptor inhibition in 7d, not 28d, CTB-SAP rats *vs*. controls ($p<0.05$), while pLTF was abolished following 5-HT receptor inhibition in 28d, not 7d, CTB-SAP rats *vs*. controls ($p<0.05$). Additionally, 5-HT_{2A} receptor expression was unchanged in CTB-SAP rats *vs*. controls, while 5-HT_{2B} receptor expression was decreased in CTB-SAP rats *vs*. controls ($p<0.05$). This study furthers our understanding of the contribution of differential receptor activation to pLTF and its implications for breathing following respiratory motor neuron death.

2.2- INTRODUCTION

Understanding and harnessing mechanisms of phrenic motor facilitation (pMF) are currently being investigated as a means by which ventilation can be rescued or maintained in patients with neuromuscular diseases and/or injuries that result in respiratory motor neuron loss. pMF is a persistent increase in phrenic nerve activity that can be elicited by a pharmacological stimulus, and phrenic long-term facilitation (pLTF) is a form of pMF that is elicited by exposure to bouts of acute intermittent hypoxia (AIH-induced pLTF) (Baker-Herman and Mitchell, 2008; Baker and Mitchell, 2000; Dale-Nagle et al., 2010; Mitchell et al., 2001). The amount of phrenic output elicited depends on the severity of AIH and occurs through two distinct pathways (Nichols et al., 2012). Naïve adult rats exposed to moderate AIH (35-55 mmHg PaO_2) induces pLTF through a Gq-serotonin (5-HT)-receptor-dependent pathway, where serotonin is released in the phrenic motor nucleus and binds to $5-HT_2$ receptors on or near phrenic motor neurons (Bach and Mitchell, 1996). Subsequent activation of protein kinase C theta (PKCθ) (Devinney et al., 2015; Devinney et al., 2013) leads to the new synthesis of brain-derived neurotrophic factor (BDNF) (Baker-Herman et al., 2004; McGuire and Ling, 2004) which binds to the mature TrkB receptor (Baker-Herman et al., 2004) and causes MEK/ERK activation/phosphorylation (Hoffman et al., 2012) to ultimately result in moderate pLTF. pLTF occurs at a greater magnitude when naïve adult rats are exposed to severe bouts of AIH (25–35 mmHg PaO_2) and requires a Gs-adenosine (A_{2A}) receptor-dependent pathway. This severe AIH exposure causes adenosine to be released into the extracellular space and activates A_{2A} receptors, which leads to the activation of protein kinase B (pAkt) *via* phosphatidylinositol 3-kinases (PI3K), and ultimately results in enhanced pLTF (Agosto-Marlin et al., 2017; Devinney et

al., 2013; Golder et al., 2008; Hoffman and Mitchell, 2011; Nichols et al., 2012). Our goal is to understand which underlying mechanisms are required to evoke pLTF following respiratory motor neuron loss so that we can harness these mechanisms to preserve and/or maintain breathing in the future.

Intrapleural injection of cholera toxin B conjugated to saporin (CTB-SAP) induces targeted respiratory motor neuron death (Nichols et al., 2018; Nichols et al., 2015b). Briefly, when CTB-SAP is injected intrapleurally, the CTB component binds to and enters the axolemma of neurons inhabiting the intrapleural space, allowing for the entire CTB-SAP construct to enter the axons. Once inside, the construct is then retrogradely transported to the neuron cell bodies of phrenic and intercostal motor neurons in the cervical (C3-5) and thoracic (T2-7) spinal cord, respectively (Lencer and Tsai, 2003; Mantilla et al., 2009; Nichols et al., 2015b). CTB and SAP will then dissociate once inside the motor neuron cell bodies (Llewellyn-Smith et al., 2000). SAP then binds to ribosomes and disables protein synthesis, which results in motor neuron cell death *via* mechanisms of apoptosis (Llewellyn-Smith et al., 1999; Lujan et al., 2010). We have previously reported significant respiratory motor neuron death in rats at 7 day (d; ~60% loss) and 28d (~75% loss) post-CTB-SAP treatment compared to controls (rats intrapleurally injected with unconjugated CTB+SAP) (Nichols et al., 2018; Nichols et al., 2015b). However, eupneic breathing is maintained in 7d and 28d CTB-SAP rats despite significant respiratory motor neuron loss and a decrease in phrenic output (Nichols et al., 2015b). In addition, we have previously reported that AIH-induced pLTF following CTB-SAP-induced respiratory motor neuron loss is enhanced at 7d, but is more moderate and is similar to that of naïve controls at 28d (Borkowski and Nichols, 2020; Nichols et al., 2018).

Although the underlying mechanisms required for producing varying magnitudes of AIH-induced pLTF following CTB-SAP-induced phrenic motor neuron death at 7d and 28d are yet to be fully discerned, pLTF is elicited predominately through TrkB and PI3K/Akt-dependent mechanisms in 7d CTB-SAP treated rats, and through BDNF and MEK/ERK-dependent mechanisms in 28d CTB-SAP treated rats (Borkowski and Nichols, 2020). The goal of the current study was to continue to understand and further delineate the mechanisms that underlie the differences in AIH-induced pLTF at 7d and 28d post-CTB-SAP induced phrenic motor neuron loss by determining the receptors required to evoke pLTF in these rats. Therefore, we hypothesized that A_{2A} receptors are required to elicit enhanced AIH-induced pLTF in 7d CTB-SAP, while 5-HT receptors are required to elicit moderate pLTF in 28d CTB-SAP rats. To study this, 7d and 28d CTB-SAP rats were given inhibitors to target A_{2A} (MSX-3) and 5-HT (methysergide) receptors through intrathecal delivery. In doing so, we found that pLTF is elicited through Gs-A_{2A} receptor mechanisms in 7d CTB-SAP treated rats, whereas Gq-5-HT receptor mechanisms induce pLTF in 28d CTB-SAP treated rats.

2.3 METHODS

Animals

Experiments were conducted on adult (3–4 months old) male Sprague Dawley rats (Envigo Colony 208; Indianapolis, IN). Rats were housed in pairs and maintained under a 12:12 light:dark cycle. Animals had access to a standard commercial pelleted diet and water *ad libitum*. All procedures in this manuscript were approved by the Institutional Animal Care and Use Committee at the University of Missouri in accordance with National Institutes of

Health Guide for the Care and Use of Laboratory Animals. The University of Missouri is an AAALAC-accredited institution that operates under Animal Welfare Assurance ID A3394-01.

Intrapleural Injections

Rats received bilateral intrapleural injections (6mm deep, fifth intercostal space) using a 50 µl Hamilton syringe and a custom needle (6 mm, 23 gauge, semi-blunt to prevent lung puncture) while under isoflurane anesthesia (1.5% in 100% oxygen as previously described by Mantilla et al. (2009). Control rats were intrapleurally injected with cholera toxin B subunit (CTB; 20 µg dissolved in double distilled H_2O; Calbiochem; Billerica, MA) unconjugated to saporin (SAP; 25 µg dissolved in phosphate buffered saline (PBS); Advanced Targeting Systems; San Diego, CA) to enable comparisons for respiratory plasticity. CTB conjugated to saporin (CTB-SAP; 25 µg dissolved in PBS; Advanced Targeting Systems; San Diego, CA) was intrapleurally injected to target respiratory motor neurons as described previously (Nichols et al., 2015; 2018; Borkowski and Nichols, 2020). CTB-SAP treated rats also received an additional 20 µg of CTB dissolved in double distilled H_2O (Calbiochem; Billerica, MA) in their administered intrapleural injections for retrograde tracing and immunohistochemical purposes. Rats were then monitored for 24 hours following the intrapleural injections to ensure respiration was not compromised following intrapleural injections, and were housed for 7 or 28 days before the below surgical preparation and neurophysiological experiments were performed.

Surgical Preparation for In Vivo Neurophysiological Experiments

Experimental procedures were performed as described previously (*e.g.,* Hoffman et al., 2012, Nichols et al., 2018). Briefly, rats were isoflurane anesthetized, tracheotomized, and pump ventilated (Small Animal SAR-1000 Ventilator; CWE, Ardmore, PA, USA; tidal volume ~ 2.5 mL, frequency $\sim 70\text{--}80$ breaths per minute). Rats remained under isoflurane anesthesia (3.5% in 50% O_2, balance N_2) throughout surgical procedures before being converted to urethane anesthesia over 15–20 min (1.85 g kg^{-1}, *i.v.*) while isoflurane was slowly withdrawn. Once completely converted to urethane anesthesia, rats were then paralyzed for neuromuscular blockade using pancuronium bromide (2.5 mg kg^{-1}, i.v.). Rats were given a 1:2:0.13 mixture of 6% Hetastarch (in 0.9% sodium chloride), lactated Ringer's solution, and 8.4% sodium bicarbonate *via* continuous intravenous infusion (1.5–6 mL kg^{-1} h^{-1}) to maintain body fluid and acid-base. Lack of the pressor responses or obvious respiratory neural responses to a toe pinch with a hemostat was used to confirm the adequacy of anesthesia before and immediately after surgical and neurophysiological protocols were complete. Body temperature was maintained (37 ± 1 °C) with a custom-made heated surgical table, and was assessed with a rectal thermometer (Physitemp, Clifton, NJ, USA). Throughout the surgical preparation, end-tidal PCO_2 (P_{ETCO2}) was maintained at ~45 mmHg and monitored with a flow-through carbon dioxide analyzer designed to sufficiently measure response time for P_{ETCO2} measurements in rats (CapStar-100, CWE, Ardmore, PA).

Rats were bilaterally vagotomized and blood pressure was monitored in the right femoral artery by the insertion of a polyethylene catheter (PE50 ID: 0.58 mm, OD: 0.965 mm; Intramedic, MD, USA) connected to a pressure transducer (APT300 Pressure

Transducer, Harvard Apparatus, Holliston, MA, USA). Arterial blood samples were taken during baseline, the first hypoxic episode, and at 15, 30 and at 60 min post-AIH and analyzed for partial pressures of O_2 (PO_2) and CO_2 (PCO_2) using a blood gas analyzer (ABL80 Flex, Radiometer, Brea, CA).

Through a dorsal approach, the left phrenic nerve was isolated, distally cut, desheathed, and covered with a saline soaked cotton ball until it was placed on a bipolar silver electrode (described in the following section). For delivery of drugs *via* an intrathecal approach (see below), a medial incision was first made along the spinal column and the muscle was removed over the C2-3 vertebrate. A laminectomy was performed at C2, and a small incision was made in the dura where a soft silicone catheter (2 Fr; Access Technologies, Skokie, IL) was then inserted subdurally 3– 4 mm caudal from the incision until the tip rested over the C4 segment to deliver drugs or vehicle from a 50µl Hamilton syringe as described below. Because isoflurane dampens phrenic nerve output, a minimum of 1 hour was allowed following the conversion to urethane anesthesia before neurophysiological recordings began to eliminate this effect.

In Vivo Neurophysiological Recordings

The left phrenic nerve was submerged in mineral oil and placed on bipolar silver electrodes to record nerve activity. Neural signals were amplified (10,000 ×), band-pass filtered (300– 10,000 Hz, Model 1800, A-M Systems, Carlsborg, WA, USA), full-wave rectified, and integrated (50 ms time constant, MA-821, CWE Inc., Ardmore, PA, USA). Integrated nerve bursts were digitized (8 kHz) and analyzed using a WINDAQ data acquisition system (DATAQ Instruments, Akron, OH, USA). Apneic and recruitment thresholds were

determined at least 1-hour post urethane anesthesia conversion. First, ventilation was increased and P_{ETCO2} was reduced until rhythmic nerve bursts had ceased (*i.e.*, apneic threshold). After 1 minute of nerve cessation, the ventilator rate was decreased and P_{ETCO2} was slowly increased until the resumption of rhythmic nerve bursts occurred (*i.e.*, recruitment threshold). To establish baseline conditions, P_{ETCO2} was held approximately 2 mmHg above the recruitment threshold until stabilization of neural activity had occurred (≥ 15 min). A baseline arterial blood sample was taken to document baseline blood gas levels. Following baseline measurements, rats were exposed to three 5-min episodes of isocapnic (± 1.5 mmHg) acute intermittent hypoxia [10% inspired O_2, arterial PO_2 (PaO_2): 35–45 mmHg] separated by 5-min intervals of baseline O_2 conditions (50% inspired O_2, PaO_2: ≥ 150 mmHg). Rats were returned to baseline inspired O_2 levels after the third bout of hypoxia, and inspired O_2 levels were maintained for the duration of the experiments. Manipulation of inspired CO_2 and/or the ventilation rate was done to maintain isocapnic arterial PCO_2 ($PaCO_2$) within ± 1.5 mmHg of the respective baseline value.

To test the hypothesis that differential G-coupled protein receptors are utilized to elicit the differential pLTF observed in 7d and 28d CTB-SAP treated rats, rats were intrathecally injected at spinal cord segment C4 with either an A_{2A} receptor antagonist (MSX-3; 10μM; Millipore-Sigma), a 5-HT receptor antagonist (methysergide; methy; 20mM; Millipore-Sigma), or the vehicle (artificial cerebral spinal fluid; aCSF; veh) prior to acute intermittent hypoxia exposure; drugs and aCSF were prepared and delivered as previously described (Nichols et al., 2012). Approximately 5 min after veh, 5 min after MSX-3, or 10-15 min after methy delivery, animals were exposed to either AIH or no AIH (time control; TC), and phrenic nerve activity was recorded for 60 min after AIH or TC.

7d control treated groups included three groups that received AIH treatment: 1) MSX-3 (n=6), 2) methy (n=6), and 3) veh (n=6); and three TC groups: 1) MSX-3 TC (n=3), 2) methy TC (n=3), and 3) veh TC (n=4). 28d control treated groups included three groups that received AIH treatment: 1) MSX-3 (n=6), 2) methy (n=6), and 3) veh (n=5); and three TC groups: 1) MSX-3 TC (n=4), 2) methy TC (n=3), and 3) veh TC (n=3). 7d CTB-SAP treated groups included three groups that received AIH treatment: 1) MSX-3 (n=6), 2) methy (n=6), and 3) veh (n=5); and three TC groups: 1) MSX-3 TC (n=3), 2) methy TC (n=3), and 3) veh TC (n=4). 28d CTB-SAP treated groups included three groups that received AIH treatment: 1) MSX-3 (n=5), 2) methy (n=5), and 3) veh (n=5); and three TC groups: 1) MSX-3 TC (n=3), 2) methy TC (n=3), and 3) veh TC (n=3). There were no statistical differences between 7d and 28d control rats treated with the vehicle, so these were grouped together (con veh; n=11). Additionally, multiple previous studies have demonstrated minimal experimental drift in TC experiments, and because we observed no apparent differences in TC groups (no AIH), all TC treated rats were grouped together per treatment (*i.e.,* MSX-3, methysergide, or veh) within control and CTB-SAP rats for statistical analyses. Not only did this grouping minimize the number of animals used to achieve the national standards for animal research, but it also assured that drugs or vehicle did not elicit unexpected pMF (*i.e.*, a time-dependent drift in time control experiments).

Immunohistochemistry

Tissue used for staining was obtained from a separate set of rats that did not receive any drug treatment during neurophysiological experiments than those used for the current neurophysiological studies. Rats were transcardially perfused with cold

4% paraformaldehyde in phosphate buffered saline (0.1 M PBS, pH 7.4). Immediately following perfusion, spinal cords were removed, post-fixed (4% paraformaldehyde in 0.1 M PBS) at 4°C overnight, and then cryoprotected in graded sucrose (20% sucrose for 3 days and 30% sucrose for an additional 3 days) at 4°C until sinking. Transverse sections (40 μm thick) of the spinal cord were then made using a freezing-sliding microtome (Leica SM 2000R, Germany), and stored at -20°C in an antifreeze solution (30% glycerol, 30% ethylene glycol, 40% PBS). To evaluate 5-HT$_{2A}$ and 5-HT$_{2B}$ receptor expression in the phrenic motor nucleus of 7d and 28d control and CTB-SAP rats, six sections from spinal cord segment C4 were selected for each animal (5-HT$_{2A}$: control, n =16; 7d CTB-SAP, n= 8; 28d CTB-SAP, n=8; 5-HT$_{2B}$: control, n=15; 7d CTB-SAP, n=7; 28d CTB-SAP, n=7).

Tissue was washed with 1X PBS three times for five minutes on a shaker at room temperature. Sections were then incubated at room temperature in a blocker solution (1X PBS + 0.2% Triton + 5% normal donkey serum) on a shaker for one hour. Then sections were incubated in primary antibody solution (1X PBS + 0.1% Triton + 5% normal donkey serum + antibody against CTB (goat, 1:2000, Calbiochem) and either 5-HT$_{2A}$ (rabbit polyclonal, 1:200; Neuromics, Edina, MN) or 5-HT$_{2B}$ (rabbit polyclonal, 1:300; Neuromics, Edina, MN)) overnight at 4°C on a shaker as conducted previously (Borkowski et al., 2020; Nichols et al., 2018; Nichols et al., 2015b). The following day, tissue was washed three times for five minutes at room temperature on a shaker in 1X PBS and incubated for two hours at room temperature on a shaker in the dark in secondary antibody solution (1X PBS + 0.1% Triton + 5% normal donkey serum + donkey anti-goat Alexa-Fluor 555 (1:1000; Molecular Probes, Eugene, OR) and donkey anti-mouse Alexa-Fluor

488 (1:1000; Molecular Probes, Eugene, OR). Tissue was then washed again while covered in 1X PBS three times for five minutes on a shaker at room temperature. The tissue was then mounted on positively charged glass slides (Thermo Fisher Scientific, Waltham, MA) dried, preserved with ProLong™ Gold anti-fade reagent (Thermo Fisher Scientific, Waltham, MA), and covered with a coverslip. Covered slides were stored at 4°C until imaging was performed.

Imaging and ImageJ Analysis

Photomicrographs were taken on an Olympus BX51 microscope containing a three-axis motorized stage (Ludl Electronic Products, Hawthorne, NY) with a monochrome digital camera (ORCA, Hamamatsu, Bridgewater, NJ) along with Neurolucida software (version 10, MicroBrightField, Willston, VT) at the same settings for all images per antibody per group (*i.e.*, gains for images: 555 (CTB) = 18, 488 (5-HT$_{2A}$) = 42, 488 (5-HT$_{2B}$) = 66). The photomicrographs were taken at 20x magnification to encompass the CTB-labelled phrenic motor neurons in the C$_4$ cervical spinal cord (Boulenguez et al., 2007; Mantilla et al., 2009; Nichols et al., 2015b; Watson et al., 2009). The following camera settings and filter cubes for CTB positive cells and 5-HT$_{2A/B}$ receptor expression were used to ensure appropriate fluorescence: Bright-field, Alexa Fluor 488 [excitation (ex.): λ480 nm; emission (em.): λ510 nm] and Alexa Fluor 555 [ex. λ555 nm; em. λ588]. Densitometry of the 5-HT$_{2A}$ and 5-HT$_{2B}$ receptors were performed on Z-stacked (5µm in z-plane per image) images by creating a region of interest that encompassed the CTB labeled phrenic motor neurons of the phrenic motor nucleus (same region of interest used for all images) and the surrounding non-phrenic ventral horn. Images were taken and analyzed as 8-bit

stacks at a resolution of 1024 x 1024 (366.67μm x 366.67μm). Thresholds in ImageJ for analysis of immunopositivity were: 5-HT2A: 130-170 and 5-HT2B: 95-135. Using ImageJ, immunopositive pixels for 5-HT2A and 5-HT2B receptor expression were evaluated within the phrenic motor nucleus and in the non-phrenic ventral horn in which optical density of 5-HT2A and 5-HT2B receptors was expressed as an average density per section/animal. The fractional area occupied by 5-HT2A and 5-HT2B receptors in raw image files was also computed by ImageJ (Nichols et al., 2015), and was interpreted as the percentage of the total field within the phrenic motor nucleus occupied by label positive pixels for 5-HT2A and 5-HT2B receptors. The fractional area occupied by 5-HT2A or 5-HT2B receptors in raw image files was calculated manually for the non-phrenic ventral horn by subtracting the region of interest encompassing the phrenic motor nucleus from the remaining field of the image. Total labeled positive pixels were determined for the phrenic motor nucleus (fractional area multiplied by total pixels in the phrenic motor nucleus) and for the entire ventral horn (fractional area multiplied by total pixels in the ventral horn).

Statistical Analysis

Integrated phrenic nerve burst amplitudes were averaged over 1 min during baseline and 15, 30, and 60 min after AIH. Because peak integrated inspiratory phrenic nerve bursts at baseline were not different within treatment groups, nerve bursts were normalized to baseline measurements to quantify the magnitude of pLTF (expressed as a percent change in baseline). Statistical comparisons between treatment groups for integrated phrenic nerve burst amplitude were done using a Friedman repeated measures ANOVA on ranks design due to the failure of normality. Statistical comparisons between treatment groups for blood

gases and mean arterial pressure were done using a two-way ANOVA with repeated-measures. Since there were no differences between successive hypoxic exposure within groups (p>0.05, data not shown), comparisons of the short-term hypoxic phrenic response were made using a one-way ANOVA, in which phrenic burst amplitude during the fifth minute of hypoxic episodes was averaged from all three episodes. For TC rats receiving no AIH exposure, a two-way ANOVA with repeated-measures design was performed; since there were no differences among them, they were grouped into single TC groups per treatment *(i.e.,* MSX-3, methy, veh) within control and CTB-SAP rats (MSX-3 TC control, n=7; MSX-3 TC CTB-SAP, n=6; methy TC control, n=6; methy TC CTB-SAP, n=6; veh TC control, n=7; veh TC CTB-SAP, n=7). A Kruskal-Wallis one-way ANOVA on ranks was used when comparing integrated phrenic nerve burst amplitude across groups at 60 min post-hypoxia. Since there were no statistical differences in neither fractional area, nor optical density between 7d and 28d control animals for 5-HT$_{2A}$ or 5-HT$_{2B}$ receptor expression, control animals were grouped together. A two-way ANOVA was used to compare 5-HT$_{2A}$ or 5-HT$_{2B}$ receptor optical density and fractional area in the phrenic motor nucleus and the non-phrenic ventral horn within and across groups. When significant ANOVA differences were detected, individual comparisons were made with either a Fisher's least significant difference *post hoc* test (blood gases, mean arterial pressure, short term hypoxia response, and receptor expression), Student-Newman-Keuls or Dunn's *post hoc* tests (amplitude) (Sigma Plot version 13.0; Systat Software Inc., San Jose, CA, USA), and were considered significant if $p < 0.05$; all values are expressed as means ± S.E.M.

2.4- RESULTS

Blood Gases and Mean Arterial Pressures

$PaCO_2$ was successfully maintained within 1.5 mmHg from its baseline value in all groups (Table 2.1), despite minor significant differences within and across groups. Because changes in $PaCO_2 > 1.5$ mmHg from baseline can influence pLTF, any observed changes in integrated phrenic nerve burst amplitude following AIH in the current study are not attributed to differences in chemoreceptor feedback (Bach and Mitchell, 1996). Drugs were not given prior to baseline, so any significant differences in $PaCO_2$ cannot be attributed to the drug delivery. Additionally, we speculate that significant differences in PaO_2 across groups for baseline and 60 mins post-hypoxia were not biologically relevant due to the successful regulation of PaO_2 above 150 mmHg at baseline, within the target range for AIH (35-45mmHg), then again above 150 mmHg post-hypoxia for the remainder of the study (Table 2.1). For mean arterial pressure, changes in mean arterial pressure of <20 mmHg from baseline values have minimal effect on respiratory activity in rats (Bach and Mitchell, 1996; Walker and Jennings, 1996), for which no groups had a significant difference in mean arterial pressure from baseline (<20 mmHg) at 60 mins post-hypoxia (Table 2.1) in the current study. As expected, all groups exposed to AIH had a significant decrease in blood pressure during hypoxia exposure from baseline MAP, and PaO_2 and mean arterial pressure differed among groups when AIH *vs*. TCs were compared during hypoxic episodes (Table 2.1). Thus, the differential pLTF expression observed in this study was not affected by differences in blood gases or blood pressure regulation.

Short-Term Hypoxic Phrenic Responses

All AIH-treated groups had hypoxic responses that were significantly increased *vs.* corresponding time control (TC) groups since TC groups were not exposed to AIH and therefore did not have a hypoxic response (Fig. 2.1; $p<0.05$). 7d CTB-SAP rats treated with the vehicle had a hypoxic response that was greater than all groups except for 7d CTB-SAP rats treated with methy (Fig.2.1; $p<0.05$). This observed enhancement in the hypoxic phrenic response in 7d CTB-SAP rats has been previously reported (Nichols et al., 2018). The hypoxic response for 7d CTB-SAP rats treated with methy was significantly greater than all control groups, regardless of treatment, and from 28d CTB-SAP rats treated with the vehicle and MSX-3 (Fig. 2.1; $p<0.05$). 28d CTB-SAP rats treated with methy had a significantly greater response to hypoxia than 7d controls treated with MSX-3 or methy (Fig. 2.1; $p<0.05$). Finally, the response to hypoxia was significantly greater in 7d CTB-SAP rats treated with MSX-3 compared to the respective control group of the same treatment (Fig. 2.1; $p<0.05$).

AIH-Induced pLTF in 7d, not 28d, CTB-SAP Treated Rats Requires A_{2A} Receptor Activation

The purpose of the current study is to understand the underlying receptor-dependent mechanisms that contribute to the different amounts of pLTF observed in CTB-SAP rats. As mentioned, previous studies have shown that AIH-induced pLTF is enhanced in 7d CTB-SAP treated rats compared to control rats and 28d CTB-SAP treated rats (Nichols et al., 2018). Additionally, we have reported that the enhanced pLTF observed in 7d CTB-SAP treated rats requires the new synthesis of TrkB and predominately PI3K/Akt signaling

(Borkowski and Nichols, 2020). Therefore, we hypothesized that because A_{2A} receptor activation induces enhanced pLTF and this receptor is upstream of PI3K/Akt signaling (Agosto-Marlin et al., 2017; Devinney et al., 2013; Golder et al., 2008; Hoffman and Mitchell, 2011; Nichols et al., 2012), A_{2A} receptors would be necessary for the enhanced pLTF observed in 7d CTB-SAP rats. Representative neurograms following veh, MSX-3 (A_{2A} receptor antagonist), or methy (5-HT receptor antagonist) pre-treatment are shown for 7d CTB-SAP rats in Fig. 2.2A-C and for 28d CTB-SAP rats in Fig. 2.3A-C. As expected, 7d CTB-SAP rats treated with the vehicle elicited the previously observed enhanced pLTF compared to the moderate amount of pLTF elicited by controls and respective time control treated animals at all time points ($p<0.05$; Figs. 2.2 & 2.4). 7d control rats treated with the vehicle also had a significant increase in pLTF from baseline at 30 and 60 min post-AIH ($p<0.05$; Fig. 2.2D & 2.4), and was significantly different from its respective TC at 60 min ($p<0.05$; Fig. 2.2D & 2.4). In congruence with our hypothesis, when 7d CTB-SAP rats were given the A_{2A} receptor inhibitor (MSX-3), pLTF was essentially abolished at all time points in the study and was not different from baseline or TC values ($p>0.05$), and was significantly decreased at 60 mins from 7d CTB-SAP rats pre-treated with the vehicle or methysergide ($p<0.05$; Fig. 2.2E & 2.4). There was no effect on pLTF in 7d control rats following A_{2A} receptor inhibition as shown by the significant increase from baseline at 30 and 60 min post-AIH ($p<0.05$; Fig. 2.2D & Fig. 2.4), and the lack of significant difference in pLTF magnitude between 7d control rats treated with MSX-3 and 7d controls treated with the vehicle 30 and 60 min post-AIH exposure ($p>0.05$; Fig. 2.2D & Fig. 2.4).

Similar to what was observed in 7d control rats pre-treated with MSX-3 resulting in A2A receptor inhibition, pLTF was unaffected by A2A receptor inhibition in 28d control rats ($p > 0.05$; Fig. 2.3D). In 28d control rats pre-treated with MSX-3, pLTF increased from baseline at 30 and 60 min post-hypoxia ($p < 0.05$), and elicited the same moderate magnitude of pLTF observed in 28d control rats pre-treated with the vehicle ($p > 0.05$; Fig. 2.3D & 2.4). 28d CTB-SAP rats pre-treated with the vehicle also elicit a moderate amount of pLTF, which has been previously reported (Nichols et al., 2018), that is similar to that of controls pre-treated with the vehicle ($p > 0.05$; Figs. 2.3 & 2.4). pLTF was not affected by A2A receptor inhibition in 28d CTB-SAP rats as shown by the increase from baseline at all time points post-AIH ($p < 0.05$; Fig. 2.3), and the lack of difference from vehicle treated control and 28d CTB-SAP rats 60 min post-hypoxia ($p > 0.05$; Fig. 2.4).

AIH-Induced pLTF in 28d, not 7d, CTB-SAP Treated Rats Requires 5-HT Receptor Activation

As stated above, we have observed that the amount of pLTF exhibited by 28d CTB-SAP treated rats is similar to that of control rats, suggesting the underlying pathways used to elicit pLTF may be similar (Nichols et al., 2018), and we recently reported that 28d CTB-SAP rats elicit pLTF through BDNF and subsequent MEK/ERK signaling (see Chapter 3) (Borkowski and Nichols, 2020). Therefore, we hypothesized that 28d CTB-SAP rats elicit moderate pLTF through Gq-5-HT receptor-dependent mechanisms. As expected, when control 7d or 28d rats were administered methy to inhibit 5-HT receptor signaling, pLTF was abolished from vehicle treated controls and was not different from respective TC groups ($p > 0.05$), despite the initial significant increase observed in 28d control rats from

baseline at 15 min post-hypoxia (Figs. 2.2D, 2.3D, & Fig. 2.4). 7d control rats pre-treated with methy exhibited significantly less pLTF from 7d controls pre-treated with the veh at 30 and 60 min, and from those pretreated with MSX-3 at 60 min ($p<0.05$; Fig. 2.2D & Fig. 2.4). However, 7d CTB-SAP rats treated with methy had phrenic nerve output that was increased from baseline at all time points ($p<0.05$) but was not different from 7d CTB-SAP rats treated with the vehicle at all time points ($p>0.05$), and also was increased from its respective TC group at 30 and 60 min as well as from 7d CTB-SAP rats pre-treated with MSX-3 at 60 min ($p<0.05$; Fig. 2.2 E & Fig. 2.4). 28d CTB-SAP rats also had an abolishment of pLTF following methy treatment as shown by the significant decrease in pLTF from respective vehicle treated rats, the lack of increase in pLTF from baseline, and the lack of difference in pLTF from its respective TC group ($p>0.05$; Fig. 2.3E & Fig. 2.4). Taken together, these data indicate that 5-HT receptor activation is required for pLTF in 28d CTB-SAP rats, while pLTF in 7d CTB-SAP rats is unaffected by 5-HT receptor antagonist delivery.

5-HT$_{2A}$ Receptor Expression is Unchanged, while 5-HT$_{2B}$ Receptors are Decreased in CTB-SAP Rats vs. controls

Representative photomicrographs for 5-HT$_{2A}$ and 5-HT$_{2B}$ receptors from transverse sections of spinal cord segment C$_4$ from control, 7d CTB-SAP and 28d CTB-SAP rats are shown in Figs. 2.5 & 2.6 A-F, respectively. 5-HT$_{2A}$ and 5-HT$_{2B}$ receptor positive staining was evaluated at 20x magnification in both the CTB-labelled (red) phrenic motor nucleus (PMN; indicated by the dashed white circle) and the non-PMN (area outside of the region of interest). When evaluating 5-HT$_{2A}$ receptor expression in terms of optical density and

fractional area, 5-HT2A receptor expression in CTB-SAP rats was unchanged from controls within the PMN and non-PMN (Fig. 2.5 G & H). 5-HT2A receptors appear to exist not only on the membranes of phrenic motor neurons and neurons in the non-PMN, but on membranes of other cell types as well (Fig. 2.5 A-F). 5-HT2B receptor expression expressed as optical density and fractional area is decreased from controls in 7d and 28d CTB-SAP rats in the PMN but is unchanged in the non-PMN (Fig. 2.6 G & H). Again, 5-HT2B receptors appear to be located on the cell membrane of phrenic motor neurons and neurons in the non-PMN as well as on other non-neuron cell types (Fig. 2.6 A-F). These data suggests that 5-HT2A receptor expression is unchanged in CTB-SAP rats from controls, while 5-HT2B receptor expression is decreased in CTB-SAP rats from controls, regardless of time point.

2.5- DISCUSSION

When bilateral intrapleural injections of CTB-SAP (25 µg) are given, respiratory motor neurons die, but breathing under normoxic conditions is maintained in unanesthetized rats (Nichols et al., 2015b). However, breathing during maximal chemosensory stimulation is compromised following CTB-SAP treatment (Nichols et al., 2015b), indicating that the loss of respiratory motor neurons induced by 25 µg of CTB-SAP leads to an inability to maintain breathing in response to challenge. Previous studies in vagotomized, pump-ventilated, anesthetized, and paralyzed rats following moderate AIH exposure have shown that not only do 7d CTB-SAP rats elicit respiratory plasticity *(i.e.*, pLTF), but it is enhanced from that of control and 28d CTB-SAP rats, through a predominantly Gs-dependent TrkB and PI3K/Akt signaling pathway (Borkowski and Nichols, 2020; Nichols et al., 2018). In

contrast, control and 28d CTB-SAP rats elicit moderate pLTF through Gq-dependent BDNF and MEK/ERK signaling (Borkowski and Nichols, 2020). The purpose of the current study was to investigate whether A_{2A} and 5-HT receptors involved in Gs and Gq-dependent signaling, respectively, that are upstream of the previously investigated intracellular targets (TrkB and PI3K/Akt *vs*. BDNF and MEK/ERK) are required for AIH-induced pLTF in CTB-SAP rats. Here, we demonstrate that distinct receptor activation is responsible for the differential AIH-induced pLTF exhibited at 7d and 28d following CTB-SAP-induced respiratory motor neuron loss. The major findings of this study include: 1) A_{2A} receptor activation is required for pLTF in 7d CTB-SAP treated rats; 2) pLTF is elicited *via* 5-HT receptor activation in 28d CTB-SAP rats; and 3) 5-HT_{2A} receptor expression was unchanged while 5-HT_{2B} receptor expression was decreased in the phrenic motor nucleus of CTB-SAP rats *vs*. controls. These findings are consistent with our previously published work that following AIH exposure: 1) 7d CTB-SAP rats elicit enhanced pLTF through Gs-dependent signaling that requires downstream TrkB and PI3K/Akt activation with upstream A_{2A} receptor activation; and 2) 28d CTB-SAP rats elicit moderate pLTF through Gq-dependent signaling that requires downstream BDNF synthesis and MEK/ERK activation with upstream 5-HT receptor activation.

Requirement of Distinct Receptors for pLTF following CTB-SAP-Induced Respiratory Motor Neuron Loss

Enhanced pLTF in 7d CTB-SAP rats is elicited predominately through TrkB and PI3K/Akt-dependent mechanisms (Borkowski and Nichols, 2020), which are downstream of A_{2A} receptor activation. In the current study, our data demonstrate the necessity for A_{2A}

receptor activation since pLTF was nearly abolished with A2A receptor antagonism in 7d CTB-SAP rats (Figs. 2.2 & 2.4). We did not observe this same abolishment, nor an enhancement of pLTF, when MSX-3 (A2A receptor antagonist) was intrathecally delivered to 28d CTB-SAP rats. This indicates that A2A receptors are not required for pLTF and that they are not constraining Gq mechanisms of pLTF in 28d CTB-SAP rats (Figs. 2.3 & 2.4). Therefore, it can be concluded from this data that Gs-A2A receptor-dependent signaling is required for enhanced pLTF in 7d CTB-SAP rats but does not contribute to moderate pLTF observed in 7d control, 28d control, or 28d CTB-SAP rats.

Moderate pLTF in 28d CTB-SAP treated rats requires BDNF and MEK/ERK-dependent mechanisms (Borkowski and Nichols, 2020), which are downstream of 5-HT2 receptor activation (Bach and Mitchell, 1996; Baker-Herman et al., 2004; Hoffman et al., 2012). To investigate the requirement of 5-HT receptors in CTB-SAP rats, methysergide (broad-spectrum 5-HT receptor antagonist) was intrathecally delivered to block 5-HT receptor activation. Although a broad-spectrum 5-HT receptor antagonist was used in the current study, we speculate that pLTF in 28d CTB-SAP rats is elicited through 5-HT2 receptors since pLTF was nearly abolished by methysergide (Figs. 2.3 & 2.4), which is similar to what is observed in control and naïve rats (Bach and Mitchell, 1996; Tadjalli and Mitchell, 2019), while methysergide had essentially no effect on pLTF in 7d CTB-SAP rats (Figs. 2.2 & 2.4). Taken together with our previous studies that evaluated downstream mechanisms of pLTF in CTB-SAP rats, it can be concluded that like control rats, 28d CTB-SAP rats elicit pLTF through Gq-5-HT receptor-dependent signaling pathways. Furthermore, we believe that these same mechanisms are utilized in CTB-SAP rats to elicit ventilatory long-term facilitation in unanesthetized (vagally intact) rats following moderate

AIH exposure because it has been previously published that moderate AIH induces ventilatory (Nakamura et al., 2010; Olson Jr et al., 2001) and diaphragmic (Navarrete-Opazo and Mitchell, 2014; Terada and Mitchell, 2011) LTF in naïve rats. This indicates that mechanisms of pLTF are not dictated by anesthesia nor vagotomy.

5-HT2 receptor isoform expression and potential utilization in pLTF

In order to design future studies to potentially harness 5-HT2 receptors in 28d CTB-SAP rats, it was necessary to first determine if 5-HT2 receptor isoform (2A *vs*. 2B) expression was affected in CTB-SAP rats. Thus, we evaluated C4 5-HT2A/B receptor expression in the phrenic motor nucleus (PMN) and non-PMN, and observed no difference in 5-HT2A receptor expression in 7d and 28d CTB-SAP rats from controls (Fig. 2.5), while 5-HT2B receptor expression was decreased in 7d and 28d CTB-SAP rats from controls (Fig. 2.6). The requirement for these specific isoforms for pLTF at each time point has yet to be investigated in CTB-SAP treated rats.

It is known that pMF *via* 5-HT2A activation is NADPH oxidase-independent, while 5-HT2B-induced pMF is NADPH oxidase-dependent (MacFarlane et al., 2011). Gq-5-HT-receptor-dependent pLTF in naïve rats also requires ROS formation *via* NADPH oxidase activity since ROS disinhibits phosphatase action on PKC (*i.e.,* ROS formation allows pLTF to be evoked) (MacFarlane and Mitchell, 2007; MacFarlane and Mitchell, 2008; Wilkerson et al., 2008). At this time, it is unknown whether NADPH oxidase and ROS formation are necessary for pLTF in CTB-SAP treated rats. Since pLTF elicited by moderate AIH in naïve rats requires NADPH oxidase and ROS formation (MacFarlane and Mitchell, 2007; MacFarlane and Mitchell, 2008), we speculate that 5-HT2B receptor

activation is required for moderate pLTF observed in the 28d CTB-SAP rats even though 5-HT2B receptor activation is decreased. We speculate that 7d CTB-SAP rats do not require NADPH oxidase activity because pLTF is being elicited predominately through Gs-dependent signaling that does not require the formation of ROS.

On the other hand, 5-HT2A receptor expression was not different from controls with CTB-SAP treatment at 7d and 28d within the phrenic motor nucleus, nor the greater ventral horn (Fig. 2.5). It has been shown that activation of both 5-HT2A and 5-HT2B receptors are required for moderate AIH-induced pLTF in naïve rats (Tadjalli and Mitchell, 2019). Furthermore, Tadjalli and Mitchell found that blocking downstream MEK/ERK inhibition blocked 5-HT2A, but not 5-HT2B, receptor activated pMF, indicating differential downstream activation of these receptor isoforms (Tadjalli and Mitchell, 2019). We have previously reported the requirement for MEK/ERK signaling in 28d CTB-SAP rats, and that 7d CTB-SAP rats also utilize MEK/ERK signaling but to a lesser degree compared to 28d CTB-SAP rats (Borkowski and Nichols, 2020). Thus, it is possible that CTB-SAP rats are utilizing the upstream 5-HT2A receptor to elicit NADPH oxidase-independent pLTF. However, we currently show that delivery of the 5-HT receptor antagonist does not have an effect on pLTF in 7d CTB-SAP rats, but we have not ruled out if there is a convergence of Gs and Gq downstream pathways and suggest that this should be further investigated. Furthermore, we posit that 5-HT2A receptor expression is unchanged in control, 7d CTB-SAP, and 28d CTB-SAP rats because 5-HT2A receptors are utilized synergistically with A2A or 5-HT2B receptor activation simultaneously to contribute to pLTF. Since receptor expression does not determine receptor functionality, future studies will need to evaluate the contribution of each 5-HT2 receptor isoform and the necessity of NADPH oxidase/ROS

formation for pLTF in 7d and 28d CTB-SAP rats to determine if pLTF is being constrained or if pLTF could be enhanced by 5-HT2 receptor isoform activation or inhibition.

As shown in the photomicrographs, 5-HT2A/B receptors exist on other neural cells (*e.g.*, microglia and astrocytes) that are not CTB(+) phrenic motor neurons (Figs. 2.5 & 2.6; red). Krabbe et al. found that *in vitro* microglial migration is facilitated by serotonin and ATP (Krabbe et al., 2012). Thus, it is possible that CTB-SAP-induced respiratory motor neuron death itself could lead to the release of ATP and signal microglial migration to respiratory motor nuclei. Although we have not examined 5-HT2A/B receptor expression on microglia, it may be that the lack of difference between groups when evaluating 5-HT2A receptors is due to expression on resident microglia, which have been shown to be upregulated in CTB-SAP rats (Nichols et al., 2015b). It is also possible that 5-HT2A receptor utilization is not the primary receptor pathway for pLTF in all groups, and therefore, there is no difference in receptor expression. In other words, 5-HT2A receptor expression may be unchanged because 5-HT2A receptor activation for pLTF is used as a fail-safe mechanism when all other methods of pLTF fail. Lastly, serotonin release has been shown to activate 5-HT2A/B receptors and contribute to cytokine exosome release (Glebov et al., 2015). The activation of 5-HT2A receptors on microglia has been shown to suppress TNF-α and IL-6 production (Nau Jr et al., 2013), while 5-HT2B receptor activation on microglia attenuates phagocytic activity (Krabbe et al., 2012), indicating differential utilization of each isoform in response to injury. Thus, the interaction between mechanisms of pLTF and other cell types (*e.g.,* microglia) following CTB-SAP-induced respiratory motor neuron loss should be further investigated.

Cross-talk inhibition between the Gs and Gq pathways

It is well documented that the Gs pathway constrains moderate AIH-induced pLTF through the A2A receptor (Hoffman et al., 2010). However, because we did not see an enhancement in pLTF in 28d CTB-SAP rats with A2A receptor inhibition, we conclude that these receptors are not constraining pLTF, and that pLTF is occurring directly through the activation of the Gq-5-HT2 receptor pathway (Figs. 2.3 & 2.4). Therefore, it may not be beneficial to enhance pLTF with A2A receptor agonism at this time point. Conversely, when naïve rats are exposed to severe AIH, A2A receptors become activated leading to an enhanced pLTF, which can be abolished by 5-HT2A/B receptor agonism (Perim et al., 2018; Perim et al., 2019). Again, we did not see an enhancement in pLTF in the 7d CTB-SAP rats with 5-HT receptor antagonism, indicating that these receptors are not constraining pLTF (Figs. 2.2 & 2.4). This study utilized a broad spectrum 5-HT receptor antagonist, which can act on 5-HT7 receptors and influence Gs-dependent signaling mechanisms. However, we know that 5-HT7 receptor activation constrains pLTF (Hoffman and Mitchell, 2013), and that Gs-dependent signaling can still occur through the A2A receptors – this would lead to enhanced pLTF in 28d CTB-SAP rats if cross-talk inhibition on Gs-dependent signaling was alleviated by the blockade of Gq-dependent signaling through inhibition of 5-HT2 receptors with methysergide, which we did not observe (Figs. 2.3 & 2.4). Future studies should focus on delivering A2A and 5-HT2A/B receptor agonists to determine if pMF can be elicited in CTB-SAP rats, and if AIH-induced pLTF can be further enhanced in CTB-SAP rats.

Mechanisms of pLTF in CTB-SAP rats vs. other models of neurodegeneration

Our findings for pLTF following CTB-SAP-induced respiratory motor neuron loss are somewhat in contrast to what has been reported in other rodent models of degeneration or injury. Previous studies in a rat model of amyotrophic lateral sclerosis (SOD1[G93A]) showed that despite progressive motor neuron loss, end-stage SOD1[G93A] rats elicit pLTF when exposed to moderate AIH. End-stage SOD1[G93A] rats actually have an enhanced pLTF (Nichols et al., 2015a) that is elicited *via* Gq-pathway dependent mechanisms that require the new synthesis of BDNF and subsequent MEK/ERK signaling without any evidence of Gs-dependent pathway contribution to this enhancement (Nichols et al., 2017). pLTF has also been investigated in rats following bilateral cervical dorsal rhizotomy (C3-C5), and it was found that enhanced pLTF observed 28d post-injury was 5-HT2 receptor-dependent (Kinkead et al., 1998). Thus, these studies are in contrast to some extent with our current and previous findings in CTB-SAP rats where 7d rats elicit an enhancement in pLTF that requires Gs-pathway dependent mechanisms, but 28d rats elicit a moderate amount of pLTF that requires Gq-pathway dependent mechanisms (Borkowski and Nichols, 2020; Nichols et al., 2018). In contrast, our findings in CTB-SAP rats are quite similar to what has been found in rats with C2 hemisection as a model of cervical spinal cord injury in which these rats elicit pLTF through A2A receptor activation during early injury (1-2 weeks post-injury) when serotonergic innervation is compromised (Dale-Nagle et al., 2010; Golder and Mitchell, 2005). Serotonergic neurons begin to recover 8 weeks post-injury and pLTF is then elicited through Gq-5-HT2-dependent signaling (Golder and Mitchell, 2005), which is similar to what we observe in our 28d CTB-SAP rats. Furthermore, in rats with a mid-cervical contusion (C3/C4), tidal volume and AIH-induced LTF were not impacted by

the systemic administration of either 5-HT or A2A receptor antagonism (Wen et al., 2019). However, 5-HT2A receptor inhibition attenuated frequency while A2A receptor inhibition enhanced frequency following AIH exposure in rats given a mid-cervical contusion, and the necessity of 5-HT2A receptor activation for frequency LTF increased over time in this mid-cervical contusion injury rat model (Wen et al., 2019). Together with our findings, these studies show that enhancement of phrenic output can be elicited through both Gq and Gs pathways in a time-dependent manner throughout the progression of disease or injury, and that both pathways should be taken into consideration when exploring therapeutic options.

Significance and Conclusions

Here, we utilized the intrapleural CTB-SAP model to further delineate mechanisms of AIH-induced pLTF over the course of respiratory motor neuron death. In studying these underlying mechanisms, we hope to aid in the development of pharmacological interventions to prolong respiratory deficits from occurring in patients with neuromuscular diseases. Furthermore, previous and current studies show that pLTF is elicited by different mechanisms throughout the course of disease. Specifically, pLTF is A2A receptor-dependent following 7d (early) of CTB-SAP-induced respiratory motor neuron loss, and is 5-HT receptor-dependent following 28d (late) of CTB-SAP-induced respiratory motor neuron loss. By recognizing that mechanisms of pLTF differ temporally, we can more appropriately approach treating respiratory deficits in patients with neuromuscular diseases based on the stage (early *vs*. late) of motor neuron disease, and provide multiple avenues

for interventions (*e.g.,* A2A or 5-HT receptor activation could be harnessed) when one therapy/treatment does not work.

2.6- NEW & NOTEWORTHY

The current study investigates underlying receptor-dependent mechanisms contributing to phrenic long-term facilitation (pLTF) following CTB-SAP-induced respiratory motor neuron death at 7d and 28 d. We found that A2A receptors are required for enhanced pLTF in 7d CTB-SAP rats, while 5-HT receptors are required for moderate pLTF in 28d CTB-SAP rats. Targeting these time-dependent mechanisms have implications for breathing maintenance over the course of many neuromuscular diseases.

2.7- ACKNOWLEDGEMENTS

2.8- GRANTS

2.9- AUTHOR CONTRIBUTIONS

Author contributions: L.F.B. and N.L.N. in conception and design of research; L.F.B., C.L.S., A.N,K., and N.L.N. performed experiments; L.F.B., C.L.S., and N.L.N. analyzed data; L.F.B., C.L.S., and N.L.N. interpreted results; L.F.B. prepared figures; L.F.B. drafted manuscript; L.F.B., C.L.S., A.N.K., and N.L.N. edited and revised manuscript; and L.F.B., C.L.S., A.N.K, and N.L.N. approved final version of manuscript.

Experimental Groups	P_{aCO_2} (mmHg) baseline	HX	60 min	P_{aO_2} (mmHg) baseline	HX	60 min	MAP (mmHg) baseline	HX	60 min
With AIH									
Veh									
CON	49.6±0.8	49.9±0.8[f]	49.3±0.9[f]	285±9[afgh]	35.8±1.4[b]	275±7[ag]	115±4[a]	69±4[b]	108±4[a]
7d CS	52.2±1.3	52.3±1.2	52.2±1.5	253±21[a]	35.0±1.9[b]	242±14[a]	125±4[a]	76±7[b]	116±4[a]
28d CS	51.7±1.4	52.3±1.4	51.5±1.2	296±8[acfgh]	37.8±1.2[b]	290±14[acg]	123±6[a]	76±10[b]	107±6[a]
MSX-3									
7d CON	46.9±2.7[c]	46.6±2.8[bcd]	47.0±2.5[c]	245±29[ab]	35.0±2.4[b]	261±14[abg]	112±6[a]	72±5[b]	110±10[a]
7d CS	45.5±1.9[cde]	45.8±1.9[cde]	46.1±2.0[cd]	235±36[ab]	37.8±3.3[b]	223±23[ab]	114±7[a]	65±5[b]	113±4[a]
28d CON	47.9±1.9	48.4±1.9	47.7±2.0	308±10[acfgh]	37.3±2.0[b]	289±15[acg]	121±11[a]	95±17[efgh]	110±9
28d CS	49.8±2.8	50.1±2.4[f]	50.7±2.8[f]	303±10[acfgh]	39.8±1.5[b]	295±17[acfg]	112±7[a]	68±9[bi]	96±7[a]
Methy									
7d CON	45.8±1.4[cd]	44.9±1.3[cd]	45.3±1.7[cd]	232±32[ab]	35.0±2.5[b]	255±19[ab]	109±8[a]	67±11[b]	118±7[a]
7d CS	46.5±0.8[cd]	46.8±0.7[cd]	46.9±1.0[c]	313±10[acfgh]	36.2±0.9[b]	293±9[acg]	99±11[acd]	69±10[bi]	96±8[af]
28d CON	46.4±1.5[cd]	46.2±1.3[cd]	46.6±1.3[cd]	290±16[afgh]	37.3±3.0[b]	276±13[ag]	118±4[a]	74±6[b]	110±7[a]
28d CS	50.1±1.3	50.4±1.2[f]	49.7±1.5	304±13[acfgh]	35.4±1.6[b]	273±5[ag]	117±4[a]	70±7[bi]	100±7[a]
Without AIH (TCs)									
CON Veh	46.3±1.5	46.9±1.3	46.1±1.5	262±11	285±10	256±11	116±6	113±6	120±8
CS Veh	48.1±1.3	48.4±1.7	48.1±1.4	274±24	286±25	282±12	103±6[a]	119±19	109±10
CON MSX-3	51.1±2.1	51.4±1.9	51.1±2.1	312±3	317±1	306±6	116±3	112±5	105±7
CS MSX-3	49.0±1.5	49.0±1.2	50.3±2.4	294±11	294±9	248±7	107±7	118±6	108±2
CON Methy	48.3±1.0	49.2±1.2	47.8±0.8[a]	305±11	310±12	303±13	112±9	104±10	109±10
CS Methy	49.5±1.9	49.9±1.7	49.1±1.9	317±9	314±10	294±12	111±8	113±6	103±6

Table 2.1: Arterial PCO_2, PO_2 and mean arterial pressure (MAP) during baseline, hypoxia (HX) and 60 minutes post-hypoxia for control (CON) and CTB-SAP (CS) treated rats with acute intermittent hypoxia (AIH) or without AIH (time-control or TC). Rats received intrathecal delivery of either: 1) vehicle (aCSF; veh); 2) A2A receptor antagonist (MSX-3); or 3) broad spectrum 5-HT receptor antagonist (methysergide; methy). Significant differences within groups included *versus* hypoxia ([a]), and across groups included *versus*: respective TC ([b]), 7d CTB-SAP veh ([c]), 28d CTB-SAP veh ([d]), CON veh ([e]), 7d CON methy ([f]), 7d CTB-SAP MSX-3 ([g]), 7d CON MSX-3 ([h]), and 28d CON MSX-3 ([i]). Values are expressed as means ± S.E.M. Differences were considered significant if p<0.05.
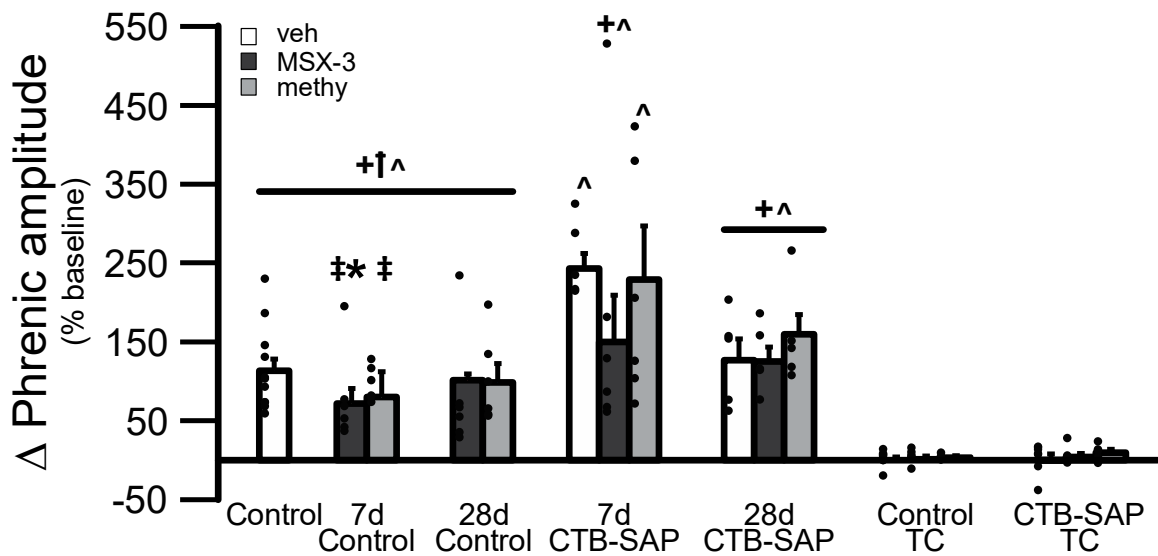
Figure 2.1: Short-term phrenic nerve hypoxic response in 7d & 28d control and CTB SAP treated rats. Short-term phrenic nerve hypoxic responses were compared in 7d and 28d control and CTB-SAP treated rats pre-treated with vehicle (aCSF; veh), MSX-3, or methysergide (methy). As expected, all treatment groups exposed to AIH had a significantly greater hypoxic response *vs.* the respective TC group (^). 7d CTB-SAP rats pre-treated with vehicle had a short-term hypoxic response that was greater than all groups, with the exception of 7d CTB-SAP rats pre-treated with methy (+). 7d CTB-SAP rats pre-treated with methy had a short-term hypoxic response that was greater than all control groups and 28d CTB-SAP rats pre-treated with vehicle or MSX-3 (†). 7d CTB-SAP rats pre-treated with MSX-3 had a greater short-term hypoxic response *vs.* the respective control (*). 7d control rats pre-treated with MSX-3 and methy had a short-term hypoxic response that was decreased from 28d CTB-SAP rats pre-treated with methy (‡). Values are means ± SEM, and all significant differences are *p*<0.05.
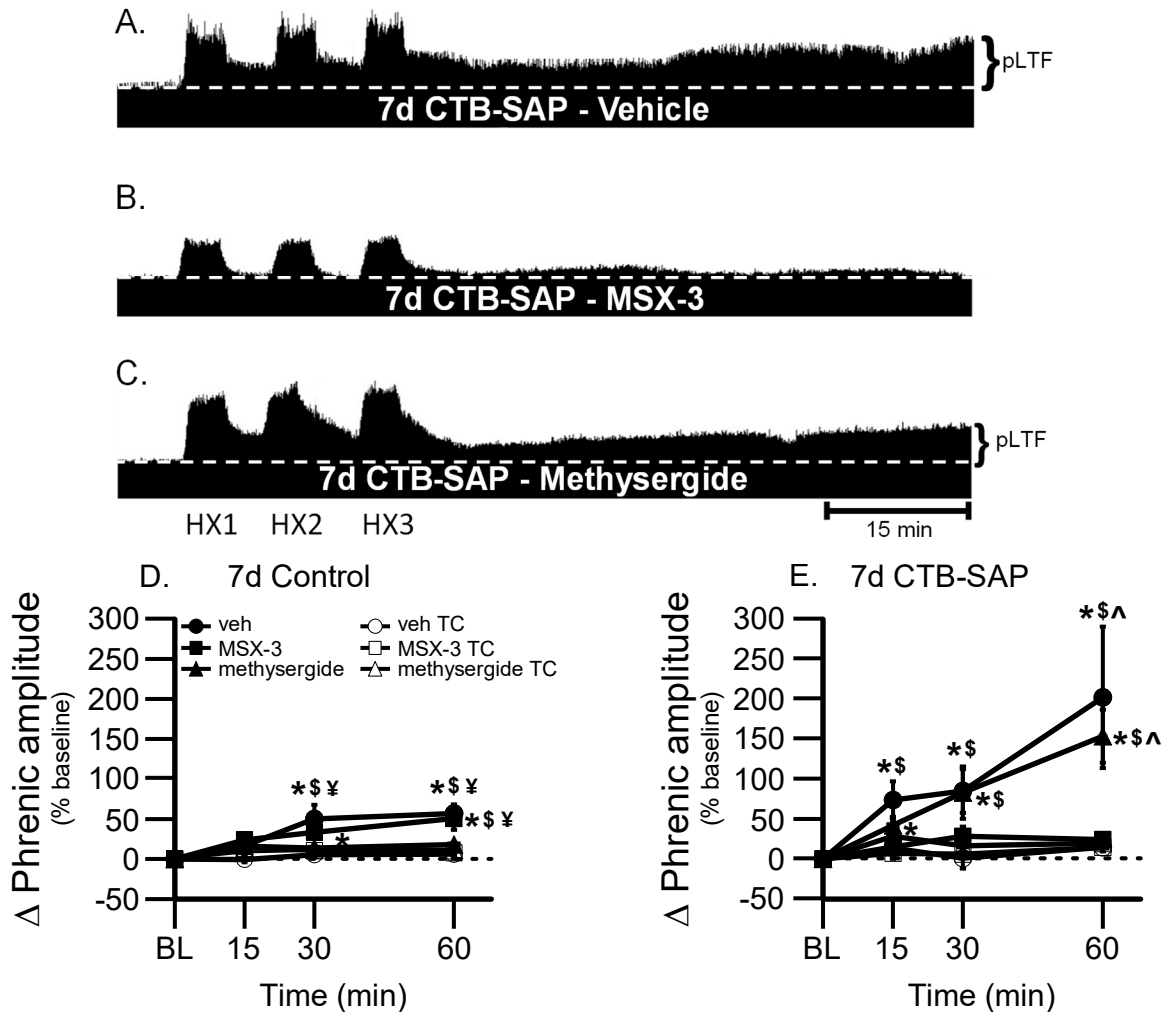
Figure 2.2: pLTF in 7d treated rats. A-C. Representative traces of compressed, integrated phrenic nerve activity before and after AIH in 7d CTB-SAP rats pre-treated with vehicle (veh; **A.**), MSX-3 (**B.**), or methysergide (**C.**). Baseline is indicated in each trace by a white, dashed line. AIH elicits an enhanced pLTF in 7d CTB-SAP rats pre-treated with veh and methysergide, while pLTF appears nearly abolished with MSX-3 pre-treatment. **D.** and **E.** Phrenic burst amplitude (expressed as a percent change from baseline) in 7d control (**D.**) and 7d CTB-SAP (**E.**) rats pre-treated with veh, veh TC, MSX-3, MSX-3 TC, methysergide, or methysergide TC. pLTF was significantly increased from baseline (*) at 30 and 60 min post-hypoxia in 7d control rats pre-treated veh or MSX-3 (**D.**), and at all time points in 7d CTB-SAP rats pre-treated with veh or methysergide (**E.**). pLTF was significantly increased from respective TCs ($) at 30 and 60 min in 7d control rats (**D.**), at all time points for 7d CTB-SAP rats (**E.**) pre-treated with veh, at 60 min for 7d control rats pre-treated with MSX-3 (**D**), and at 30 and 60min in 7d CTB-SAP rats pre-treated with methysergide (**E.**). pLTF was significantly increased at 30 and 60 min and at 60 min in 7d control rats pre-treated with veh or MSX-3, respectively, from 7d control rats pre-treated with methysergide (¥) (**D**). Lastly, pLTF was significantly increased in 7d CTB-SAP rats pre-treated with veh or methysergide from 7d CTB-SAP rats pre-treated with MSX-3 (^) at 60 min post-hypoxia (**E.**). Values are means ± SEM, and all significant differences are $p < 0.05$.
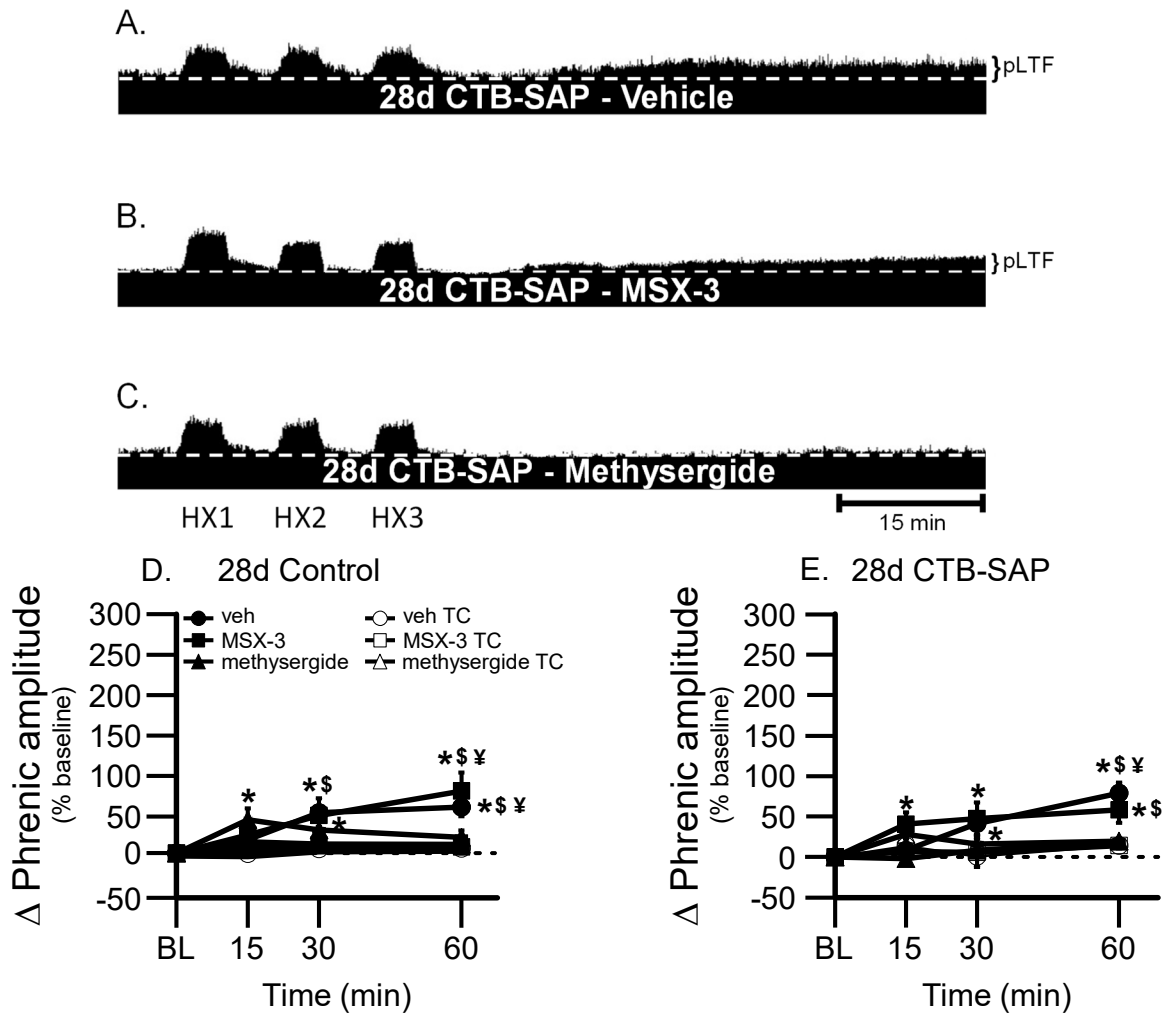
Figure 2.3: pLTF in 28d treated rats. A-C. Representative traces of compressed, integrated phrenic nerve activity before and after AIH in 28d CTB-SAP rats pre-treated with vehicle (veh; **A.**), MSX-3 (**B.**), or methysergide (**C.**). Baseline is indicated in each trace by a white, dashed line. AIH elicits moderate pLTF in 28d CTB-SAP rats pre-treated with veh and MSX-3, while pLTF appears nearly abolished with methysergide pre-treatment. **D.** and **E.** Phrenic burst amplitude (expressed as a percent change from baseline) in 28d control (**D.**) and 28d CTB-SAP (**E.**) rats pre-treated with veh, veh TC, MSX-3, MSX-3 TC, methysergide, or methysergide TC. pLTF was significantly increased from baseline (*) at 30 and 60 min post-hypoxia in 28d control rats pre-treated veh or MSX-3, and 15 min post-hypoxia following methysergide pre-treatment (**D.**). pLTF was significantly increased from baseline (*) at 30 and 60 min post-hypoxia in 28d CTB-SAP rats pre-treated with MSX-3, and at all time points following veh pre-treatment (**E.**). pLTF was significantly increased from respective TCs ($) at 30 and 60 min in 28d control rats (**D.**), and 60 min post-hypoxia in 28d CTB-SAP rats (**E.**) pre-treated with veh, and in 28d control and CTB-SAP rats pre-treated with MSX-3 at 60 min post-hypoxia. pLTF was significantly increased in 28d control rats pre-treated with veh or MSX-3 from 28d control rats pre-treated with methysergide (¥) at 60 min post-hypoxia (**D.**). pLTF was significantly increased in 28d CTB-SAP rats pre-treated with veh from 28d CTB-SAP rats pre-treated

with methysergide (¥) at 60 min post-hypoxia (**E.**). Values are means ± SEM, and all significant differences are $p<0.05$.
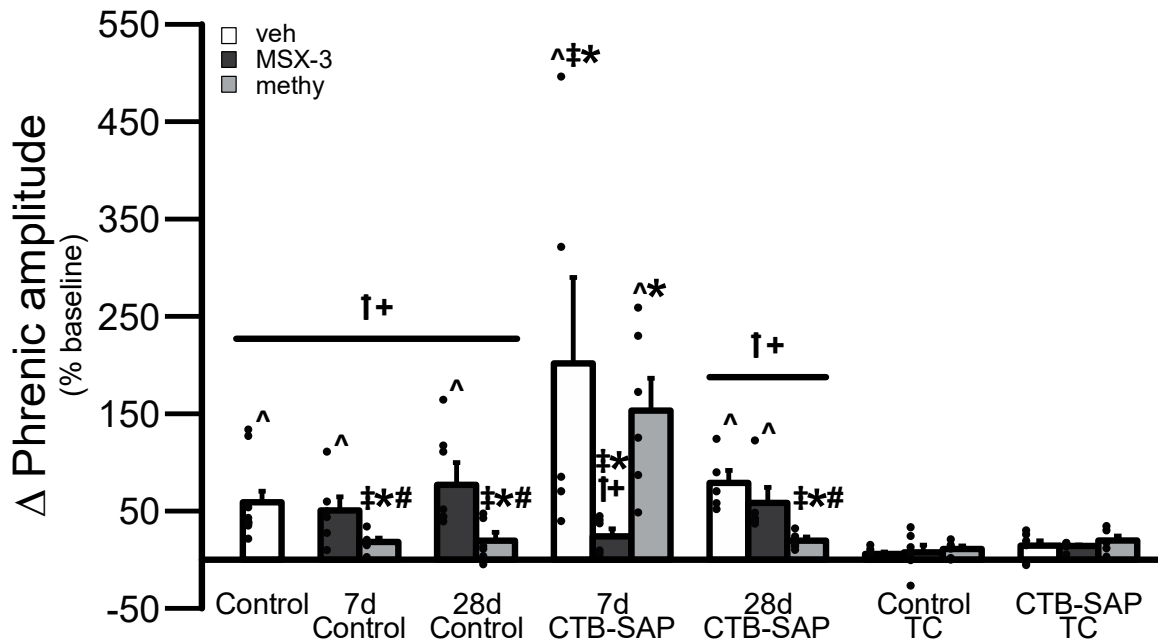
Figure 2.4: Direct comparisons of the change in phrenic amplitude (percent baseline) following AIH at 60 min post-hypoxia in 7d & 28d control and CTB-SAP treated rats. pLTF was compared in 7d and 28d control and CTB-SAP treated rats pre-treated with vehicle (veh), veh TC, MSX-3, MSX-3 TC, methysergide (methy), or methy TC. 7d and 28d control and CTB-SAP rats exhibited greater pLTF *vs.* the corresponding TC groups (^). pLTF was greater in control rats pre-treated with the veh (#) from control 7d and 28d rats and 28d CTB-SAP rats pre-treated with methy. 7d CTB-SAP rats pre-treated with veh exhibited pLTF that was significantly greater than all groups (+), with the exception of 7d CTB-SAP rats pre-treated with methy. 28d control rats pre-treated with MSX-3 (*) exhibited pLTF that was significantly less than that of 7d CTB-SAP rats pre-treated with veh or methy, and greater than 7d control, 28d control, and 28d CTB-SAP rats pre-treated with methy as well as 7d CTB-SAP rats pre-treated with MSX-3. 7d and 28d control and CTB-SAP rats exhibited pLTF that was significantly decreased from 7d CTB-SAP pre-treated with methy (Ɨ) regardless of pre-treatment, with the exception of 7d CTB-SAP veh treated rats. Lastly, 7d control, 28d control, and 28d CTB-SAP rats pre-treated with methy as well as 7d CTB-SAP rats pre-treated with MSX-3 elicited pLTF that was significantly decreased from 28d CTB-SAP rats pre-treated with veh (‡). Values are means ± SEM, and all significant differences are $p < 0.05$.
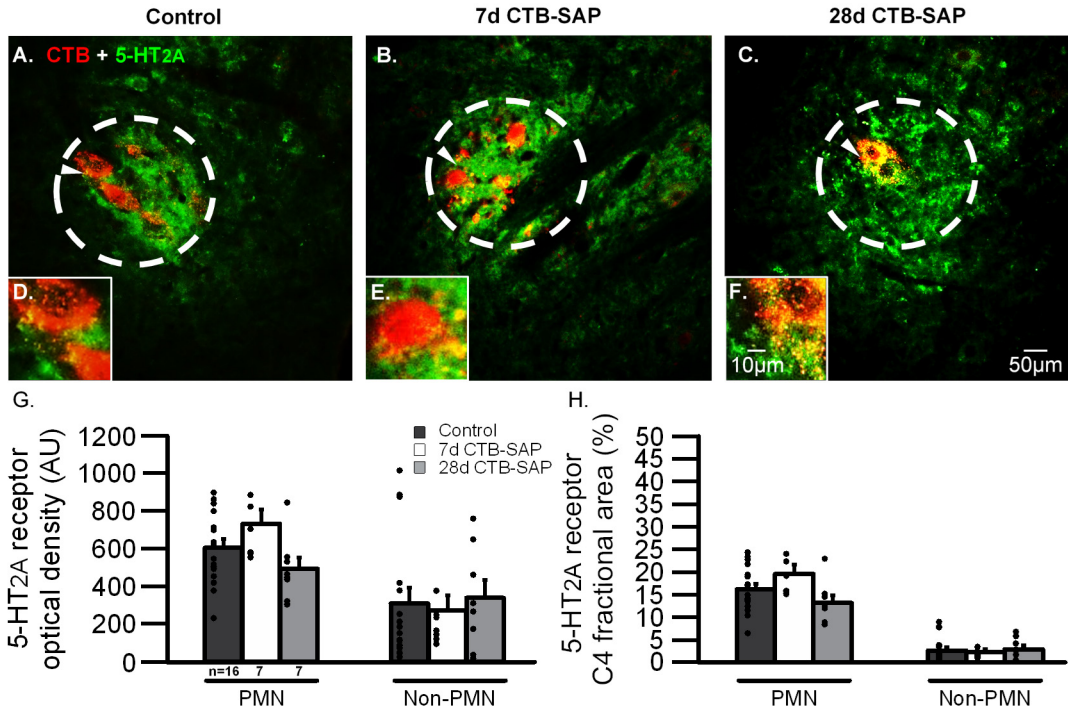
**Figure 2.5: 5-HT2A receptor expression in controls and CTB-SAP treated rats.** The representative photomicrographs display phrenic motor neurons (CTB; red) and 5-HT2A (green) receptor expression within the phrenic motor nucleus (PMN; white dashed circle) and the non-phrenic ventral horn (Non-PMN; area outside of the white dashed circle) from C4 spinal cord sections at 20x (**A-C.**) and 40x (**D-F.**) magnification in control (**A.** and **D.**), 7d CTB-SAP (**B.** and **E.**), and 28d CTB-SAP (**C.** and **F.**) treated rats. The white arrows in the 20x magnification images indicate which neurons are displayed in the 40x insets. 5-HT2A receptor expression is represented as optical density (AU; **G.**) and fractional area (**H.**) in the PMN and Non-PMN. 5-HT2A optical density and fractional area were not significantly different between groups within the PMN or within the Non-PMN (p>0.05).
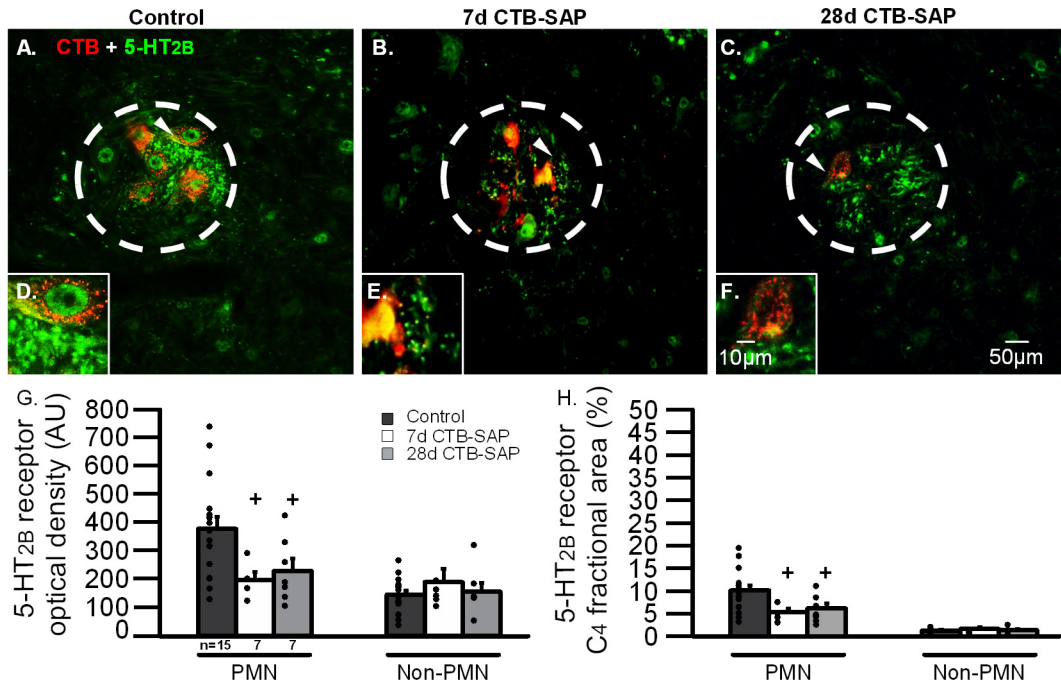
Figure 2.6: 5-HT2B receptor expression in controls and CTB-SAP treated rats. The representative photomicrographs display phrenic motor neurons (CTB; red) and 5-HT2B (green) receptor expression within the phrenic motor nucleus (PMN; white dashed circle) and the non-phrenic ventral horn (Non-PMN; area outside of the white dashed circle) from C4 spinal cord sections at 20x (**A-C.**) and 40x (**D-F.**) magnification in control (**A. and D.**), 7d CTB-SAP (**B. and E.**), and 28d CTB-SAP (**C. and F.**) treated rats. The white arrows in the 20x magnification images indicate which neurons are displayed in the 40x insets. 5-HT2B receptor expression is represented as optical density (AU; **G.**) and fractional area (**H.**) in the PMN and Non-PMN. 5-HT2B optical density and fractional area were decreased in the PMN in 7d and 28d CTB-SAP treated rats compared to control rats (+; $p<0.05$), but no significant differences were detected between groups within the Non-PMN ($p>0.05$).

CHAPTER 3: Differential mechanisms are required for phrenic long-term facilitation over the course of motor neuron loss following CTB-SAP intrapleural injections

Lauren F. Borkowski and Nicole L. Nichols

Department of Biomedical Sciences, Dalton Cardiovascular Research Center, University of Missouri, Columbia, MO 65211

Abbreviated Title: Mechanisms of pLTF following intrapleural CTB-SAP

3.1- ABSTRACT

Selective elimination of respiratory motor neurons using intrapleural injections of cholera toxin B fragment conjugated to saporin (CTB-SAP) mimics motor neuron death and respiratory deficits observed in rat models of neuromuscular diseases. This CTB-SAP model allows us to study the impact of motor neuron death on the output of surviving phrenic motor neurons. After 7(d) days of CTB-SAP, phrenic long-term facilitation (pLTF, a form of respiratory plasticity) is enhanced, but returns towards control levels at 28d. However, the mechanism responsible for this difference in magnitude of pLTF is unknown. In naïve rats, pLTF predominately requires 5-HT2 receptors, the new synthesis of BDNF, and MEK/ERK signaling; however, pLTF can alternatively be induced *via* A_{2A} receptors, the new synthesis of TrkB, and PI3K/Akt signaling. Since A_{2A} receptor-dependent pLTF is enhanced in naïve rats, we suggest that 7d CTB-SAP treated rats utilize the alternative mechanism for pLTF. Here, we tested the hypothesis that pLTF following CTB-SAP is: 1) TrkB and PI3K/Akt, not BDNF and MEK/ERK, dependent at 7d; and 2) BDNF and MEK/ERK, not TrkB and PI3K/Akt, dependent at 28d. Adult Sprague Dawley male rats were anesthetized, paralyzed, ventilated, and were exposed to acute intermittent hypoxia (AIH; 3, 5 min bouts of 10.5% O_2) following bilateral, intrapleural injections at 7d and 28d of: 1) CTB-SAP (25 µg), or 2) un-conjugated CTB and SAP (control). Intrathecal C_4 delivery included either: 1) small interfering RNA that targeted BDNF or TrkB mRNA; 2) UO126 (MEK/ERK inhibitor); or 3) PI828 (PI3K/Akt inhibitor). Our data suggest that pLTF in 7d CTB-SAP treated rats is elicited primarily through TrkB and PI3K/Akt-dependent mechanisms, whereas BDNF and MEK/ERK-dependent mechanisms induce

pLTF in 28d CTB-SAP treated rats. This project increases our understanding of respiratory plasticity and its implications for breathing following motor neuron death.

3.2- INTRODUCTION

Neuromuscular/neurodegenerative diseases (*e.g.*, Pompe disease, spinal muscular atrophy (SMA), progressive muscular atrophy, and amyotrophic lateral sclerosis (ALS)) and injuries (*e.g.*, spinal cord injury) result in loss of respiratory motor neurons, which subsequently leads to respiratory muscle weakness and/or paralysis, ventilator dependence, and ultimately death (Boentert et al., 2017; Bourke et al., 2001; Lechtzin et al., 2002; Lyall et al., 2001; Nichols et al., 2013b; Nogués et al., 2002; Wong et al., 2002). However, breathing is somehow maintained before ventilatory failure occurs. For example, patients with ALS and a genetic rat model of ALS (SOD1^{G93A}) maintain breathing until disease end-stage (Lyall et al., 2001; Nichols et al., 2013a). Although genetic models have been used to study the effects of motor neuron loss in the aforementioned diseases, these models also develop global symptoms that make it difficult to understand solely the effects of respiratory motor neuron loss. To specifically study the effects caused by respiratory motor neuron loss, we utilize intrapleural injections of cholera toxin B conjugated to saporin (CTB-SAP) to induce targeted respiratory motor neuron death (Nichols et al., 2018).

When CTB-SAP is injected intrapleurally, the CTB component binds to and enters the axolemma of neurons inhabiting the intrapleural space, allowing for the entire CTB-SAP construct to enter the axons. The construct is then retrogradely transported to the neuron cell bodies of phrenic and intercostal motor neurons in the cervical (C3-5) and thoracic (T2-7) spinal cord, respectively (Lencer and Tsai, 2003; Mantilla et al., 2009;

Nichols et al., 2015b). Once inside the cell bodies, CTB and SAP will then dissociate (Llewellyn-Smith et al., 2000) allowing SAP to bind to ribosomes. This binding disables protein synthesis resulting in motor neuron cell death over a matter of hours to days *via* mechanisms of apoptosis (Llewellyn-Smith et al., 1999; Lujan et al., 2010). Significant respiratory motor neuron death is observed in 7 day (d) and 28d CTB-SAP treated rats compared to control rats (unconjugated CTB+SAP injection) (Nichols et al., 2015b). Despite respiratory motor neuron loss and a decrease in phrenic output, eupneic breathing is maintained while breathing in response to maximum chemoreceptor activation is decreased in CTB-SAP treated rats (Nichols et al., 2015b).

One way that eupneic breathing is potentially maintained over the course of motor neuron loss is *via* compensatory mechanisms such as respiratory plasticity. We speculate these are mechanisms that enable surviving motor neurons to increase their output in order to compensate for the loss of neighboring motor neurons. This long-lasting increase in phrenic motor output is a form of phrenic plasticity known as phrenic motor facilitation (pMF) (Mitchell et al., 2001). pMF can be elicited pharmacologically (*e.g.*, *via* activation of Gq- or Gs-coupled receptors) or physiologically (*e.g.*, *via* acute intermittent hypoxia (AIH)). AIH-induced phrenic plasticity is specifically termed phrenic long-term facilitation (pLTF). pLTF occurs through the activation of Gq ($5-HT_{2A/B}$) (Bach and Mitchell, 1996; Fuller et al., 2001; MacFarlane and Mitchell, 2007; MacFarlane et al., 2011) or Gs-coupled receptor-dependent pathways (A_{2A} or $5-HT_7$) (Hoffman et al., 2010; Hoffman and Mitchell, 2013). Moderate exposure to AIH (35-55 mmHg PaO_2) in naïve adult rats leads to the induction of pLTF through serotonin (5-HT) release in the phrenic motor nucleus. 5-HT_2 receptors on or near phrenic motor neurons in the phrenic motor nucleus of the C3-6

spinal cord then become activated (Bach and Mitchell, 1996). Protein kinase C theta (PKCθ) is subsequently activated,(Devinney et al., 2015; Devinney et al., 2013) and leads to the new synthesis of brain-derived neurotrophic factor (BDNF) (Baker-Herman et al., 2004; McGuire and Ling, 2004). BDNF then binds to the mature TrkB receptor (Baker-Herman et al., 2004), which then activates MEK and the phosphorylation of ERK (Hoffman et al., 2012), ultimately resulting in pLTF. pLTF also requires reactive oxygen species (ROS) formation *via* NADPH oxidase activity since ROS disinhibits phosphatase action on PKC (*i.e.,* ROS formation allows pLTF to be evoked) (MacFarlane and Mitchell, 2008; MacFarlane et al., 2011).

As mentioned above, activation of spinal metabotropic receptors coupled to Gs proteins, such as adenosine 2A (A2A) (Golder et al., 2008) or 5-HT7 receptors (Hoffman and Mitchell, 2011), can also result in pMF. Pharmacological A2A receptor agonism-induced pMF requires the new synthesis of an immature TrkB isoform that is thought to signal from within phrenic motor neurons through auto-activation (Golder et al., 2008). pMF induced *via* the activation of A2A receptor agonism occurs independently from 5-HT receptor activation (Golder et al., 2008). Physiological A2A receptor activation occurs when naïve rats are exposed to more severe AIH (*i.e.*, 25–35 mmHg PaO_2). This leads to the release of adenosine into the extracellular space and activates adenosinergic mechanisms of pLTF, which includes the activation of protein kinase B (pAkt) *via* phosphatidylinositol 3-kinases (PI3K) (Agosto-Marlin et al., 2017; Devinney et al., 2013; Golder et al., 2008; Hoffman and Mitchell, 2011; Nichols et al., 2012). This severe protocol of AIH elicits pLTF that is enhanced from those rats exposed to the moderate AIH protocol (Nichols et al., 2012). Interestingly, when exposed to moderate AIH (35-55 mmHg PaO_2),

7d CTB-SAP rats exhibit enhanced pLTF that is similar to the amount of A2A receptor-induced pLTF, while 28d CTB-SAP rats exhibit a more moderate amount of pLTF that is similar to that of 5-HT2 receptor-induced pLTF in naïve rats (Baker-Herman et al., 2004; Fuller et al., 2000). However, the underlying mechanisms required for producing varying amounts of AIH-induced pLTF following CTB-SAP-induced phrenic motor neuron death have yet to be understood.

Using the CTB-SAP model, we aim to understand and delineate the underlying mechanisms of AIH-induced pLTF that are activated following phrenic motor neuron loss at 7d and 28d. Therefore, we hypothesized that 7d CTB-SAP rats elicit enhanced AIH-induced pLTF through TrkB and PI3K/Akt mechanisms, while 28d CTB-SAP rats elicit moderate pLTF through BDNF and MEK/ERK signaling mechanisms. Using intrathecal delivery of siRNAs to target BDNF and TrkB mRNA or inhibitors to target MEK/ERK or PI3K/Akt activity, we found that pLTF is elicited predominately through TrkB and PI3K/Akt-dependent mechanisms in 7d CTB-SAP treated rats, whereas BDNF and MEK/ERK-dependent mechanisms induce pLTF in 28d CTB-SAP treated rats.

3.3- METHODS

Animals

Experiments were conducted on adult (3–4 months old) male Sprague Dawley rats (Envigo Colony 208; Indianapolis, IN). Rats were housed in pairs and maintained under a 12:12 light:dark cycle. Animals had access to a standard commercial pelleted diet and water *ad libitum*. All procedures in this manuscript were approved by the Institutional Animal Care and Use Committee at the University of Missouri in accordance with National Institutes of

Health Guide for the Care and Use of Laboratory Animals. The University of Missouri is an AAALAC-accredited institution that operates under Animal Welfare Assurance ID A3394-01.

Intrapleural injections

Rats received bilateral intrapleural injections (6mm deep, fifth intercostal space) using a 50 µl Hamilton syringe and a custom needle (6 mm, 23 gauge, semi-blunt to prevent lung puncture) while under isoflurane anesthesia (1.5% in 100% oxygen as previously described by Mantilla et al. (2009). Control rats were intrapleurally injected with cholera toxin B subunit (CTB; 25 µg dissolved in doubly distilled H_2O; Calbiochem; Billerica, MA) unconjugated to saporin (SAP; 25 µg dissolved in phosphate buffered saline (PBS); Advanced Targeting Systems; San Diego, CA) to enable comparisons for respiratory plasticity. CTB conjugated to saporin (CTB-SAP; 25 µg dissolved in PBS; Advanced Targeting Systems; San Diego, CA) was intrapleurally injected to target respiratory motor neurons as described previously (Nichols et al., 2015; 2017). CTB-SAP treated rats also received an additional 20 µg of CTB dissolved in double distilled H_2O (Calbiochem; Billerica, MA) in their administered intrapleural injections. Rats were then monitored to ensure respiration was not compromised following intrapleural injections and were housed for 7 or 28 days before the below surgical preparation and neurophysiological experiments were performed.

Surgical Preparation

Experimental procedures were performed as described previously (*e.g.,* Hoffman et al., 2012, Nichols et al., 2018). Briefly, rats were isoflurane anesthetized, tracheotomized, and ventilated (Small Animal SAR-1000 Ventilator; CWE, Ardmore, PA, USA; tidal volume ~ 2.5 mL, frequency ~ 70–80 breaths per minute). Rats remained under isoflurane anesthesia (3.5% in 50% O_2, balance N_2) throughout surgical procedures before being converted to urethane anesthesia over 15–20 min (1.85 g kg^{-1}, *i.v.*) while isoflurane was slowly withdrawn. Once converted to urethane anesthesia, rats were then paralyzed using pancuronium bromide for neuromuscular blockade (2.5 mg kg^{-1}, i.v.). To maintain body fluid and acid-base balance, rats were given a 1:2:0.13 mixture of 6% Hetastarch (in 0.9% sodium chloride), lactated Ringer's solution, and 8.4% sodium bicarbonate *via* continuous intravenous infusion (1.5–6 mL kg^{-1} h^{-1}). Lack of the pressor responses or obvious respiratory neural responses to a toe pinch with a hemostat was used to confirm the adequacy of anesthesia before and immediately after surgical and neurophysiological protocols were complete. Body temperature was maintained (37 ± 1 °C) with a custom-made heated surgical table, and was accessed with a rectal thermometer (Physitemp, Clifton, NJ, USA). Throughout the surgical preparation, end-tidal PCO_2 (P_{ETCO2}) was maintained at ~45 mmHg and monitored with a flow-through carbon dioxide analyzer designed to sufficiently measure response time for P_{ETCO2} measurements in rats (CapStar-100, CWE, Ardmore, PA).

Rats were bilaterally vagotomized and blood pressure was monitored in the right femoral artery by the insertion of a polyethylene catheter (PE50 ID: 0.58 mm, OD: 0.965 mm; Intramedic, MD, USA) connected to a pressure transducer (APT300 Pressure

Transducer, Harvard Apparatus, Holliston, MA, USA). Arterial blood samples were taken during baseline, the first hypoxic episode, and at 15, 30 and at 60 min post-AIH and analyzed for partial pressures of O_2 (PO_2) and CO_2 (PCO_2), pH, and base excess (BE) using a blood gas analyzer (ABL80 Flex, Radiometer, Brea, CA).

Through a dorsal approach, the left phrenic nerve was isolated, distally cut, desheathed, and covered with a saline soaked cotton ball until it was placed on a bipolar silver electrode (described in the following section). For intrathecal delivery of drugs (see below), a laminectomy was performed at cervical level 2 (C_2), and a small incision was made in the dura. A soft silicone intrathecal catheter (2 Fr; Access Technologies, Skokie, IL) was caudally inserted subdurally (3-4 mm) until the tip of the catheter rested over the phrenic motor nucleus in the C_4 section of the spinal cord. The catheter was attached to a 50 µl Hamilton syringe filled with drug or vehicle solutions as described below. A minimum of 1 hour was allowed following the conversion to urethane anesthesia before neurophysiological recordings began to eliminate the dampening effect of isoflurane on phrenic nerve output.

Neurophysiological Recordings

The left phrenic nerve was submerged in mineral oil and placed on bipolar silver electrodes to record nerve activity. Neural signals were amplified (10,000 ×), band-pass filtered (300–10,000 Hz, Model 1800, A-M Systems, Carlsborg, WA, USA), full-wave rectified, and integrated (50 ms time constant, MA-821, CWE Inc., Ardmore, PA, USA). Integrated nerve bursts were digitized (8 kHz) and analyzed using a WINDAQ data acquisition system (DATAQ Instruments, Akron, OH, USA).

Experimental Protocol

Apneic and recruitment thresholds were determined at least 1-hour post urethane anesthesia conversion. First, ventilation was increased and P_{ETCO2} was reduced until rhythmic nerve bursts had ceased (*i.e.*, apneic threshold). After 1 minute of nerve cessation, the ventilator rate was decreased and P_{ETCO2} was slowly increased until the resumption of rhythmic nerve bursts occurred (*i.e.*, recruitment threshold). To establish baseline conditions, P_{ETCO2} was held approximately 2 mmHg above the recruitment threshold until stabilization of neural activity had occurred ($\geq$15 min). A baseline arterial blood sample was taken to document baseline blood gas levels. Following baseline measurements, rats were exposed to three 5-min episodes of isocapnic ($\pm$1.5 mmHg) acute intermittent hypoxia [10% inspired O_2, arterial PO_2 (PaO_2): 35–45 mmHg] separated by 5-min intervals of baseline O_2 conditions (50% inspired O_2, PaO_2: $\geq$150 mmHg). Rats were returned to baseline inspired O_2 levels after the third bout of hypoxia, and inspired O_2 levels were maintained for the duration of the experiments. Manipulation of inspired CO_2 and/or the ventilation rate was done to maintain isocapnic arterial PCO_2 ($PaCO_2$) within $\pm$1.5 mmHg of the respective baseline value.

Intrathecal Drug Delivery Protocol

To test the hypothesis that new spinal TrkB and/or BDNF protein synthesis are required for AIH-induced pLTF, small interfering RNAs (siRNAs) targeting BDNF and TrkB mRNA were injected *via* an intrathecal catheter over the cervical spinal cord ($\sim$C4) before AIH to prevent the translation and new BDNF or TrkB protein synthesis. TrkB siRNAs were obtained as a pool of four 21-nucleotide duplexes (siTrkB; ON-TARGET plus,

Dharmacon; gene, *Rat NTRK2*; GenBank Accession No. NM 012731, Lafayette, CO); this same pool has been shown previously to effectively block new TrkB synthesis using the same experimental preparation.(Golder et al., 2008) BDNF siRNAs were also obtained as a pool of four 21-nucleotide duplexes (siBDNF; ON-TARGET plus, Dharmacon; gene, *Rat BDNF*; GenBank accession number, NM012513); these same pool has also previously been shown to prevent new synthesis of spinal BDNF in the same experimental preparation.(Baker-Herman et al., 2004) We used a nontargeting siRNA sequence (siNT; ON-TARGETplus Nontargeting siRNA #1; Dharmacon) as a negative control for potential non-specific effects of siRNAs. siRNAs were reconstituted with siRNA universal buffer (Dharmacon), and stored at $-20°C$. Stock siTrkB or siBDNF (4 µl of 5 µM solution) was combined with: siNT (4 µl of 5 µM solution) so that the same amount of total siRNA was used for all groups; the transfection reagent, oligofectamine (32 µl, Invitrogen, Carlsbad, CA); and RNase-free water (160 µl, final concentration: 100 nM), and incubated at room temperature for 20 min. siNT experiments were performed by taking the stock siNT solution (8 µl of 5 µM solution), oligofectamine (32 µl), and RNase-free water (160 µl; final concentration, 100 nM), and then incubated as described above. siRNAs were slowly injected 2h before baseline measurements and AIH exposures and were performed over the C4 spinal segment *via* an intrathecal catheter (two, 10 µl injections separated by 10 min). 7d control treated control groups included three groups that received AIH treatment: 1) siBDNF (n=6), 2) siTrkB (n=6), and 3) siNT (n=8); and one group that received no AIH treatment: time controls (TCs; 32 µl oligofectamine, 168 µl of RNase-free water; n=4). 28d control treated control groups included three groups that received AIH treatment: 1) siBDNF (n=7), 2) siTrkB (n=6), and 3) siNT (n=8); and one group that received no AIH

treatment: TCs (n=4). 7d CTB-SAP treated groups included three groups that received AIH treatment: 1) siBDNF (n=6), 2) siTrkB (n=6), and 3) siNT (n=6), and one group that received no AIH treatment: TCs (n=3). 28d CTB-SAP treated groups included three groups that received AIH treatment: 1) siBDNF (n=6), 2) siTrkB (n=8), and 3) siNT (n=8); and one group that received no AIH treatment: TCs (n=4). All TC treated rats were grouped together within control and CTB-SAP rats. Approximately 2h after siRNA delivery, animals were exposed to either AIH or no AIH (TC), and phrenic nerve activity was recorded for 60 min after AIH or sham AIH.

Additionally, selective inhibitors were intrathecally injected for MEK/ERK (UO126, [1,4-diamino-2,3-dicyano-1,4-bis(o-aminophenylmercapto)butadiene; 12 µl, 100 µM; MEK/ERK inhibitor; Promega]), and PI3K/Akt (PI828 [2-(4-Morpholinyl)-8-(4-aminopheny)l–4H-1-benzopyran-4-one; 12 µl, 100 µM; PI3K/Akt inhibitor; Tocris Bioscience]) to evaluate their involvement in AIH-induced pLTF. 7d control treated groups included the following: 1) UO126 + AIH (n=7), 2) UO126 TC (n=4), 3) PI828 + AIH (n=7), 4) PI828 TC (n=3), and 5) vehicle + AIH (12 µl, 20% DMSO; n=6). 28d control treated groups included the following: 1) UO126 + AIH (n=6), 2) UO126 TC (n=4), 3) PI828 + AIH (n=7), 4) PI828 TC (n=4), and 5) vehicle + AIH (n=8). 7d CTB-SAP treated groups included the following: 1) UO126 + AIH (n=6), 2) UO126 TC (n=4), 3) PI828 + AIH (n=7), 4) PI828 TC (n=3), and 5) vehicle + AIH (n=6). 28d CTB-SAP treated groups included the following: 1) UO126 + AIH (n=7), 2) UO126 TC (n=5), 3) PI828 + AIH (n=7), 4) PI828 TC (n=3), and 5) vehicle + AIH (n=8). All TC treated rats were grouped together within control and CTB-SAP rats. Approximately 20 min after drug or vehicle

delivery, animals were exposed to either AIH or no AIH (TC), and phrenic nerve activity was recorded for 60 min after AIH or sham AIH.

Data and Statistical Analysis

Integrated phrenic nerve burst amplitudes were averaged over 1 min during baseline and 15, 30, and 60 min after AIH. Peak integrated inspiratory phrenic nerve bursts at baseline were similar within treatment groups; thus nerve bursts were normalized to baseline measurements to appropriately quantify the magnitude of pLTF (expressed as a percentage change from baseline). Statistical comparisons between treatment groups for AIH studies (amplitude, $PaCO_2$, PaO_2, pH, BE, and mean arterial pressure) were done using a two-way ANOVA with a repeated-measures design. Comparisons of the short-term hypoxic phrenic response were made using a one-way ANOVA, in which phrenic burst amplitude during the fifth minute of the first hypoxic episode was compared. For TC rats receiving no AIH exposure, a two-way ANOVA with repeated-measures design was performed; since there were no differences among them, they were grouped into a single TC group within control and CTB-SAP rats (siTC control, n=8; siTC CTB-SAP, n=7; UO126 TC control, n=8; UO126 TC CTB-SAP, n=9; PI828 TC control, n=7; and PI828 TC CTB-SAP, n=6). A one-way ANOVA was used when comparing phrenic nerve burst amplitudes across groups at 60 min post-hypoxia. A one-way ANOVA with ranks was used when comparing phrenic nerve burst frequency (expressed as an absolute change from baseline (bursts/min)) across groups at 60 min post-hypoxia. When significant ANOVA differences were detected, individual comparisons were made with Fisher's least significant difference post hoc test (Sigma Plot version 13.0; Systat Software Inc., San Jose, CA, USA). Differences between

the groups were considered significant if $p < 0.05$; all values are expressed as means ± S.E.M.

3.4- RESULTS

Blood gases and mean arterial pressures

Despite small but significant differences within and across groups for $PaCO_2$, it was successfully maintained within 1.5 mmHg from its baseline value in all groups (Tables 3.1 & 3.2). Therefore, changes in integrated phrenic nerve burst amplitude following AIH are not attributed to differences in chemoreceptor feedback (changes >1.5 mmHg of baseline in $PaCO_2$ can influence pLTF; Bach and Mitchell, 1996). While apneic and recruitment thresholds were significantly different in some instances (AT: control siTC *vs*. 7d control siBDNF (p=0.036), control siTC *vs*. 28d control siBDNF (p=0.017), 7d CTB-SAP siNT *vs*. 7d CTB-SAP siTrkB (p=0.026), 28d CTB-SAP siNT *vs*. 7d CTB-SAP siTrkB (p=0.037), control UO126 TC *vs*. 28d control vehicle (p=0.022), 7d control vehicle *vs*. 28d control vehicle (p=0.040), 28d control vehicle *vs*. 28d control UO126 (p=0.049); RT: control siTC *vs*. 7d control siBDNF (p=0.037), CTB-SAP PI828 TC *vs*. 7d CTB-SAP PI828 (p=0.024), 7d control vehicle *vs*. 7d CTB-SAP PI828 (p=0.037), 7d CTB-SAP PI828 *vs*. 28d control UO126 (p=0.045), 7d CTB-SAP PI828 *vs*. 28d control PI828 (p=0.045), and 7d control vehicle *vs*. 28d control vehicle (p=0.042); data not shown), drugs were not given prior to apneic and recruitment threshold acquisition and cannot contribute to differences in $PaCO_2$. Since PaO_2 was successfully regulated above 150 mmHg at baseline and remained above 150 mmHg post-hypoxia, and was held within the target range for AIH (35-45mmHg) (Tables 3.1 & 3.2), we speculate that significant differences for PaO_2

across groups for baseline and 60 mins post-hypoxia were likely not biologically relevant. For mean arterial blood pressure, slight but significant differences within groups were <20 mmHg at 60 mins post-hypoxia, and this was consistent among groups (Tables 3.1 & 3.2; changes in mean arterial pressure of <20 mmHg from baseline values have minimal effect on respiratory activity in rats (Walker and Jennings, 1995; Bach and Mitchell, 1996)). As expected, PaO_2 and mean arterial pressure differed among groups when AIH *vs*. TCs were compared during hypoxic episodes. There were no differences detected for pH in rats that received intrathecal siRNA pre-treatment, whereas there were small but significant differences for pH in rats that received pre-treatment of intrathecal vehicle or inhibitors for MEK/ERK (UO126) or PI3K/Akt (PI828) (Supplementary Tables 3.1 & 3.2). When comparing BE values, we did detect small but significant differences for rats pre-treated with intrathecal siRNA or vehicle or drug inhibitors, but BE was successfully maintained within 2.5 mEq*L^{-1} from its baseline value in all groups (Supplementary Tables 3.1 & 3.2). Thus, the differential pLTF expression observed in this study was not affected by differences in blood gases or blood pressure regulation.

Short-term hypoxic phrenic responses

Since time control (TC) groups were not exposed to AIH, these groups should not have a hypoxic response. Thus, all AIH-treated groups had hypoxic responses that were significantly increased *vs*. corresponding TC groups (Figs. 3.1A & 3.1B; respective TC *vs*. 7d control siNT (p<0.001), 7d control siBDNF (p<0.001), 7d control siTrkB (p<0.001), 28d control siNT (p<0.001), 28d control siBDNF (p=.030), 28 control siTrkB (p<0.001), 7d CTB-SAP siNT (p=0.002), 7d CTB-SAP siBDNF (p=0.004), 7d CTB-SAP siTrkB (p=0.004), 28d CTB-SAP siNT (p<0.001), 28d CTB-SAP siBDNF (p=0.049), 28 CTB-

SAP siTrkB (p=0.010), 7d control vehicle (p<0.001), 7d control UO126 (p=0.001), 7d control PI828 (p<0.001), 28d control vehicle (p<0.001), 28d control UO126 (p=0.005), 28d control PI828 (p=0.006), 7d CTB-SAP vehicle (p<0.001), 7d CTB-SAP UO126 (p=0.001), 7d CTB-SAP PI828 (p<0.001), 28d CTB-SAP vehicle (p<0.001), 28d CTB-SAP UO126 (p=0.005), and 28d CTB-SAP PI828 (p=0.009)). 7d CTB-SAP treated rats had an increased hypoxic response compared to 7d control rats pre-treated with the same siRNA (Fig. 3.1A; siNT (p<0.001), siBDNF (p=0.004), and siTrkB (p=0.004)). However, the short-term hypoxic phrenic response was decreased in 28d CTB-SAP rats pre-treated with siBDNF or siTrkB *vs.* all 7d CTB-SAP groups regardless of siRNA pre-treatment (Fig. 1A; 28d CTB-SAP siBDNF *vs.* 7d CTB-SAP siNT (p=0.002), 7d CTB-SAP siBDNF (p=0.010), and 7d CTB-SAP siTrkB (p=0.012); 28d CTB-SAP siTrkB *vs.* 7d CTB-SAP siNT (p=0.007), 7d CTB-SAP siBDNF (p=0.028), and 7d CTB-SAP siTrkB (p=0.032)), and it was decreased in 28d CTB-SAP rats pre-treated with siBDNF *vs.* 28d CTB-SAP rats pre-treated with siNT (Fig. 3.1A; p=0.048). The short-term hypoxic phrenic response was enhanced in vehicle treated 7d CTB-SAP rats *vs.* vehicle treated 7d control rats and 28d CTB-SAP rats pre-treated with vehicle (Fig. 3.1B; 7d CTB-SAP vehicle *vs.* 7d control vehicle (p=0.008), and 28d CTB-SAP vehicle (p=0.003)). 7d CTB-SAP rats pre-treated with PI828 had a hypoxic response that was significantly greater than 7d control rats pre-treated with PI828 and 28d CTB-SAP vehicle pre-treated rats (Fig. 3.1B; 7d CTB-SAP PI828 *vs.* 7d control PI828 (p=0.001) and 28d CTB-SAP vehicle (p=0.004)), whereas 7d controls pre-treated with PI828 had a hypoxic response that was significantly decreased *vs.* 28d controls pre-treated with vehicle (Fig. 1B; p=0.042). Lastly, vehicle treated 28d control rats and 7d CTB-SAP rats pre-treated with UO126 had hypoxic responses that were

significantly greater than 7d control rats pre-treated with UO126 (Fig. 3.1B; 7d control UO126 *vs*. 28d control vehicle (p=0.025), and 7d CTB-SAP UO126 (p=0.013)).

AIH-induced pLTF in 7d, not 28d, CTB-SAP treated rats is dependent on new TrkB synthesis

Previous studies have shown that AIH-induced pLTF is enhanced in 7d CTB-SAP treated rats compared to control rats and 28d CTB-SAP treated rats (Nichols et al., 2018). Thus, the purpose of the current study is to understand if underlying mechanisms contribute to the differential pLTF observed in CTB-SAP treated rats. One way we targeted the underlying mechanisms was to deliver intrathecal siBDNF or siTrkB. Representative phrenic neurograms are shown for AIH-exposed 7d CTB-SAP rats approximately 2h following siNT, siBDNF or siTrkB pre-treatment (Figs. 3.2A-C). As expected, pLTF in 7d control treated rats was abolished by siBDNF pre-treatment (significantly less than controls pre-treated with siNT (p<0.001) and siTrkB (p=0.001) at 60 min post-hypoxia; not different from controls pre-treated with siTC, p>0.05; Fig. 3.2D), which is consistent with new BDNF synthesis being required for pLTF in control treated rats. siTrkB and siNT pre-treatment in 7d controls had no effect on pLTF (p>0.05 for siTrkB *vs*. siNT; both significantly greater than rats pre-treated with siTC, both p<0.001; Fig. 3.2D). In contrast, siBDNF and siNT pre-treatment had no effect on pLTF in 7d CTB-SAP treated rats (p>0.05 for siBDNF *vs*. siNT; both significantly greater than rats pre-treated with siTC (30 min post-hypoxia: siNT, p<0.001; 60 min post-hypoxia: both p<0.001); Fig. 3.2E). Pre-treatment with siTrkB nearly abolished AIH-induced pLTF in 7d CTB-SAP rats (significantly less than pLTF exhibited by 7d CTB-SAP treated rats pre-treated with siNT

(15, 30, and 60 min post-hypoxia, all p<0.001) and siBDNF (15 min post-hypoxia, p=0.038; 60 min post-hypoxia, p=0.001); not different from CTB-SAP rats pre-treated with siTC, p>0.05, Fig. 3.2E). These data indicate that new TrkB synthesis contributes to AIH-induced pLTF in 7d CTB-SAP rats.

In contrast, we have observed that the amount of pLTF exhibited by 28d CTB-SAP treated rats is similar to that of 28d control treated rats, suggesting the underlying pathways used to elicit pLTF may be similar (Nichols et al., 2018). Representative phrenic neurograms are shown for AIH-exposed 28d CTB-SAP rats approximately 2h following siNT, siBDNF or siTrkB pre-treatment (Figs. 3.3A-C). As expected, siBDNF pre-treatment nearly abolished pLTF in 28d control and CTB-SAP treated rats (significantly less than 28d control and CTB-SAP treated rats pre-treated with siNT (control: 30 min post-hypoxia, p=0.016; 60 min post-hypoxia, p=0.003; CTB-SAP: 15 min post-hypoxia, p=0.038; 30 min post-hypoxia, p<0.001; 60 min post-hypoxia, p=0.002) and siTrkB (control: 30 min post-hypoxia, p=0.041; 60 min post-hypoxia, p=0.034; CTB-SAP: 30 min post-hypoxia, p=0.003; 60 min post-hypoxia, p=0.026); not different from rats pre-treated with siTC, p>0.05; Figs. 3.3D & 3.3E). However, siTrkB and siNT pre-treatment had no effect on pLTF in both groups (p>0.05 for siTrkB *vs*. siNT; both significantly greater than rats pre-treated with siTC (control siTrkB: 60 min post-hypoxia, p=0.012; control siNT: 60 min post-hypoxia, p<0.001; CTB-SAP siTrkB: 60 min post-hypoxia, p=0.031; CTB-SAP siNT: 60 min post-hypoxia, p=0.003; Figs. 3.3D & 3.3E). These data indicate that new BDNF synthesis is required for AIH-induced pLTF in 28d control and CTB-SAP treated rats.

Role of MEK/ERK and PI3K/Akt activity for pLTF in CTB-SAP treated rats

To further determine if underlying mechanisms contribute to the differential pLTF observed in CTB-SAP treated rats, we targeted the downstream signaling targets of BDNF and TrkB which include MEK/ERK and PI3K/Akt. Specifically, we intrathecally delivered UO126 or PI828 to inhibit MEK/ERK and PI3K/Akt signaling, respectively. Representative phrenic neurograms are shown for AIH-exposed 7d CTB-SAP rats approximately 20 mins following vehicle, UO126, or PI828 pre-treatment (Figs. 3.4A-C). UO126 pre-treatment abolished pLTF in 7d control rats (significantly less than controls pre-treated with vehicle (60 min post-hypoxia, $p<0.001$) and PI828 (60 min post-hypoxia, $p=0.017$); not different from controls pre-treated with UO126 TC, $p>0.05$; Fig. 3.4D), which is consistent with the requirement of MEK/ERK for pLTF in control rats. Pre-treatment with PI828 significantly attenuated AIH-induced pLTF in 7d CTB-SAP rats (significantly less than pLTF exhibited by 7d CTB-SAP treated rats pre-treated with vehicle (15 min post-hypoxia, $p=0.011$; 30 min post-hypoxia, $p=0.001$; 60 min post-hypoxia, $p<0.001$) and UO126 (15 min post-hypoxia, $p=0.049$; 30 min post-hypoxia, $p=0.027$; 60 min post-hypoxia, $p=0.022$); significantly greater than CTB-SAP rats pre-treated with PI828 TC (60 min post-hypoxia, $p=0.009$); Fig. 3.4E). Surprisingly, MEK/ERK inhibition also significantly attenuated pLTF in 7d CTB-SAP rats (significantly less than pLTF exhibited by 7d CTB-SAP treated rats pre-treated with vehicle (60 min post-hypoxia, $p<0.001$); significantly greater than CTB-SAP rats pre-treated with UO126 TC (15 min post-hypoxia, $p=0.030$; 30 min post-hypoxia, $p=0.001$; 60 min post-hypoxia, $p<0.001$); Fig. 3.4E). These data indicate that both MEK/ERK and PI3K/Akt activity are required for pLTF in 7d CTB-SAP rats, where PI3K/Akt has a greater contribution than

MEK/ERK activity (Fig. 3.4E). Overall, these data suggest that pLTF observed in 7d CTB-SAP treated rats is elicited through an alternative mechanism that utilizes new TrkB synthesis, and downstream signaling *via* PI3K/Akt and MEK/ERK.

As mentioned above, we hypothesized that 28d control treated rats and 28d CTB-SAP treated rats utilize the same underlying pathways to elicit pLTF since they exhibit a similar magnitude of pLTF (Nichols et al., 2018). Representative phrenic neurograms are shown for AIH-exposed 28d CTB-SAP rats approximately 20 mins following vehicle, UO126, or PI828 pre-treatment (Figs. 3.5A-C). As expected, UO126 pre-treatment abolished pLTF in 28d control and CTB-SAP treated rats (significantly less than 28d control and CTB-SAP treated rats pre-treated with vehicle (control: 60 min post-hypoxia, p=0.008; CTB-SAP: 60 min post-hypoxia, p=0.004) or PI828 (CTB-SAP: 60 min post-hypoxia, p=0.021); not different from rats pre-treated with UO126 TC, p>0.05; Fig. 3.5D & E). PI828 pre-treatment exhibited pLTF that was not different from vehicle pre-treatment for both 28d control and CTB-SAP groups (p>0.05; Figs. 3.5D & 3.5E). Thus, these data indicate that MEK/ERK activity is required for AIH-induced pLTF in 28d control and CTB-SAP treated rats.

An overall comparison of all groups is depicted in Fig. 3.6 for pLTF at 60 mins post-hypoxia. When comparing the two time points (7d *vs*. 28d) following siRNA pre-treatment, 7d CTB-SAP treated rats pre-treated with siNT exhibited significantly greater pLTF compared to 28d CTB-SAP treated rats with the same pre-treatment (p=0.019; Fig. 3.6A). 7d and 28d control rats pre-treated with siBDNF had pLTF that mirrored that of siTC pre-treatment, while pre-treatment with siTrkB had no effect on pLTF when compared to siNT pre-treated groups, regardless of time-point (p>0.05; Fig. 3.6A).

Similarly, pLTF in 28d CTB-SAP treated rats pre-treated with siBDNF mirrored that of siTC pre-treatment, and was reduced compared to 7d CTB-SAP treated rats pre-treated with siBDNF (p=0.001; Fig. 3.6A), while pLTF in 7d CTB-SAP rats pre-treated with siTrkB was not different *vs*. 28d CTB-SAP rats following the same pre-treatment (p>0.05; Fig. 3.6A). This confirms that new synthesis of BDNF is required for pLTF in controls and 28d CTB-SAP treated rats, but not 7d CTB-SAP treated rats. When comparing the two time points (7d *vs*. 28d) following pre-treatment with UO126 (MEK/ERK inhibitor) or PI828 (PI3K/Akt inhibitor), all drug treatments within the CTB-SAP group attenuated pLTF from 7d CTB-SAP rats pre-treated with the vehicle (all p<0.001; Fig. 3.6B). Concurrent with previous findings, 7d CTB-SAP rats pre-treated with the vehicle had an enhanced pLTF from 28d CTB-SAP rats of the same treatment (p<0.001; Fig. 3.6B) (Nichols et al., 2018). In control rats, MEK/ERK inhibition attenuated pLTF to that of TCs regardless of time point, suggesting MEK/ERK signaling is required for AIH-induced pLTF in control rats (7d control: p=0.006 *vs*. vehicle pre-treated rats; 28d control: p=0.030 *vs*. vehicle pre-treated rats; Fig. 3.6B). MEK/ERK inhibition also attenuated pLTF in 28d CTB-SAP rats when compared to 7d CTB-SAP rats of the same treatment (p=0.001; Fig. 3.6B). pLTF following PI3K/Akt pre-treatment was not different when comparing 7d to 28d controls or 7d to 28d CTB-SAP treated rats (p>0.05; Fig. 3.6B). These data confirm that pLTF in 7d CTB-SAP rats requires both MEK/ERK and PI3K/Akt activity, whereas 28d CTB-SAP rats require only MEK/ERK activity for pLTF. Lastly, we also compared phrenic nerve burst frequency at 60 min post-hypoxia (expressed as a percent change from baseline) for all groups (data not shown), in which we detected one significant difference: 28d CTB-SAP treated rats with vehicle pre-treatment exhibited significantly decreased

phrenic nerve burst frequency when compared to 7d control rats pre-treated with vehicle (p=0.020).

3.5- DISCUSSION

Here, we demonstrate that diverse underlying mechanisms may be responsible for the difference in pLTF seen at 7d and 28d following CTB-SAP-induced respiratory motor neuron loss. When bilateral intrapleural injections of CTB-SAP (25 μg) are given, respiratory motor neurons die, but breathing is maintained (Nichols et al., 2015b). Previous studies have shown that not only do 7d CTB-SAP rats elicit respiratory plasticity, but it is enhanced from that of control, and 28d CTB-SAP rats (Nichols et al., 2018). The major findings of this study include: 1) new TrkB synthesis and both MEK/ERK and PI3K/Akt activity are required for pLTF observed in 7d CTB-SAP treated rats; and 2) pLTF is elicited through BDNF and MEK/ERK signaling in 28d CTB-SAP rats.

Requirement for TrkB, and both PI3K/Akt and MEK/ERK signaling for pLTF in 7d CTB-SAP rats

Our findings in the current study suggest that initiation of the enhanced pLTF observed in 7d CTB-SAP rats is mediated predominately through new synthesis of TrkB (Figs. 3.2 & 3.6). As shown in previous studies, activation of the adenosine 2A (A_{2A}) receptor *via* pharmacological activation (Golder et al., 2008) or severe AIH (Nichols et al., 2012) requires the new synthesis of an immature TrkB isoform, activation of PI3K and Akt, and leads to enhanced pLTF. This A_{2A} induced phrenic plasticity occurs independently from the predominant mechanism which requires 5-HT_2 activation (Hoffman et al., 2012;

Nichols et al., 2012). Therefore, we hypothesized that the enhancement observed in 7d CTB-SAP rats was occurring through the same signaling pathway. Because siTrkB pre-treatment attenuated but did not completely abolish pLTF in 7d CTB-SAP rats ($p<0.05$; Figs. 3.2 & 3.6), we cannot eliminate the potential contributions of other pLTF signaling mechanisms, such as through BDNF and MEK/ERK signaling (Baker-Herman et al., 2004; Hoffman et al., 2012). Other signaling pathways that may contribute to the enhanced pLTF observed in 7d CTB-rats, but were not investigated in the current study, include signaling through α1-adrenoreceptors (Huxtable et al., 2014; Neverova et al., 2007), 5-HT7 receptors (Hoffman and Mitchell, 2013) which may require mammalian target of rapamycin (mTOR) (Fields et al., 2015), vascular endothelial growth factor (VEGF) (Dale-Nagle et al., 2011), or erythropoietin (EPO) (Dale and Mitchell, 2013). In addition, pre-treatment with inhibitors of either MEK/ERK or PI3K/Akt did not result in complete abolishment of pLTF in 7d CTB-SAP treated rats (Figs. 3.4 & 3.6); however, we suggest that PI3K/Akt has a greater contribution *vs*. MEK/ERK to pLTF observed in 7d CTB-SAP rats (pLTF following PI3K/Akt pre-treatment was attenuated when compared to pLTF following MEK/ERK pre-treatment; $p<0.05$; Figs. 3.4 & 3.6). Interestingly, blocking new synthesis of TrkB did not affect the phrenic response to hypoxia, as amplitude was not different from 7d CTB-SAP rats pre-treated with siNT ($p>0.05$; Fig. 3.1). Conversely, both MEK/ERK and PI3K/Akt inhibition attenuated the phrenic hypoxic response in 7d CTB-SAP rats *vs*. vehicle pre-treated 7d CTB-SAP rats ($p<0.05$; Fig. 3.1). We speculate that activation of both MEK/ERK and PI3K/Akt signaling contribute to pLTF in 7d CTB-SAP treated rats similar to what has been observed for VEGF-induced pMF (Dale-Nagle et al. 2011) either through:

1) separate mechanisms elicited by AIH exposure; or 2) that these signaling pathways converge on each other in a synergistic fashion to elicit pLTF.

Since we observe that TrkB synthesis and primarily PI3K/Akt signaling are required for pLTF in 7d CTB-SAP treated rats, we suggest that pLTF is dependent on A2A receptor activation in these rats. Following respiratory motor neuron loss induced by bilateral, intrapleural CTB-SAP (25 µg), we speculate phrenic plasticity elicited by activation of the A2A receptor and its downstream TrkB and PI3K/Akt pathway is an effective way to increase phrenic output, and maintain eupneic breathing. However, recent studies using a higher concentration of bilateral, intrapleural CTB-SAP (50 µg) that induced more severe respiratory motor neuron loss suggest otherwise (Seven et al., 2020). In studies further investigating the role of A2A receptor in neuroprotection using intrapleurally injected CTB-SAP (50 µg per bilateral injection), it was found that A2A receptors are significantly upregulated before peak phrenic motor neuron death occurs (Seven et al., 2020). This upregulation and activation directly contribute to the acceleration of phrenic motor neuron death. Blockade of the A2A receptor not only significantly increased phrenic motor neuron survival, but also improved diaphragmatic function (Seven et al., 2020). Therefore, the plasticity that we observe in 7d CTB-SAP rats (25 µg) may be in response to the activation of the A2A receptor through the accumulation of adenosine released from neighboring phrenic motor neuron cells experiencing neurotoxic apoptosis. Future studies will need to investigate the role of the A2A receptor in pLTF and neuroprotection following less severe respiratory motor neuron death induced by CTB-SAP (25 µg per bilateral injection) by: 1) determining if A2A receptor antagonism elicits an additive neuroprotective response to further enhance pLTF; and 2) determining if A2A

receptor agonism itself results in further enhanced pLTF, and if its activation is beneficial long-term to overcome respiratory deficits observed with maximal chemoreceptor activation. Furthermore, we suggest that different treatment options are required over the course of respiratory motor neuron loss, and that A_{2A} receptor activation is potentially beneficial when respiratory motor neuron loss is less severe.

BDNF and MEK/ERK signaling are utilized for pLTF in 28d CTB-SAP treated rats

Conversely, the current study has shown that pLTF in 28d CTB-SAP rats is similar in magnitude to control rats and naïve rats exposed to moderate AIH, as reported previously (Baker-Herman et al., 2004; Fuller et al., 2000; Hoffman et al., 2012; Nichols et al., 2018). This suggests that 28d CTB-SAP rats may also be eliciting plasticity through the same mechanisms as those documented in naïve rats (Baker-Herman et al., 2004; Hoffman et al., 2012). In short, AIH-induced pLTF requires the new synthesis of BDNF in 28d CTB-SAP treated rats (Figs. 3.3 & 3.6), similar to previous reports in naïve rats (Agosto-Marlin and Mitchell, 2017; Baker-Herman et al., 2004). Additionally, pre-treatment with the MEK/ERK inhibitor (UO126) abolished pLTF in 28d CTB-SAP rats (Figs. 3.5 & 3.6), consistent with previous studies in naïve and SOD1^{G93A} rats (Hoffman et al., 2012; Nichols et al., 2017). However, siTrkB and inhibition of PI3K/Akt had no effect on pLTF in 28d CTB-SAP rats (Figs. 3.3, 3.5, & 3.6). Additionally, it should be noted that no pre-treatment in 28d CTB-SAP treated rats resulted in a restored or greater magnitude of pLTF like what we observe in 7d CTB-SAP treated rats. Thus, the constraint on pLTF in 28d CTB-SAP treated rats remains unknown.

Since pLTF in 28d CTB-SAP treated rats was not enhanced following any pre-treatment in our study, we suggest that neither the G_q pathway (*i.e.*, BDNF and MEK/ERK) nor the G_s pathway (*i.e.*, TrkB and PI3K/Akt) are responsible for constraining pLTF. We speculate that this lack of enhancement may be due to the A_{2A} receptors no longer being activated to contribute to the pLTF exhibited in 28d treated rats. Additionally, phrenic plasticity has previously been shown to be constrained by peripheral and/or local influences such as inflammation. Specifically, inflammation abolishes phrenic plasticity induced by moderate AIH (*i.e.*, 5-HT$_2$ induced pLTF) or *via* 5-HT$_{2A/B}$ receptor pharmacological activation in naïve rats (Agosto-Marlin et al., 2018; Huxtable et al., 2011; Huxtable et al., 2015; Huxtable et al., 2013; Vinit et al., 2011). We have previously shown that microglial number is increased in the phrenic motor nucleus of CTB-SAP rats (Nichols et al., 2015b), and we have preliminary data that suggest systemically inhibiting inflammation (presumably caused by motor neuron death) using a nonsteroidal anti-inflammatory drug (ketoprofen) reveals enhanced pLTF in 28d CTB-SAP rats (Nichols and Tanner, 2018). Together, this suggests that inflammation may hinder pLTF in 28d CTB-SAP rats, and future studies will be focused on understanding what is responsible for this constraint (*e.g.*, cytokines such as TNF-a).

Lastly, the requirement for 5-HT$_{2A/B}$ receptor activation as well as their downstream signaling mechanisms in the initiation and maintenance of pMF and pLTF have been previously studied, and may be required in 28d CTB-SAP treated rats. For example, 5-HT$_2$ receptor activation and MEK/ERK signaling is required for the induction, but not the maintenance, of AIH-induced pLTF in naïve rats (Fuller et al., 2001; Hoffman et al., 2012). Furthermore, inhibition of MEK/ERK blocks 5-HT$_{2A}$, but not 5-HT$_{2B}$ pMF

(Fuller et al., 2001; Hoffman et al., 2012; Tadjalli and Mitchell, 2019). It is also known that pMF *via* 5-HT2A activation is NADPH oxidase-independent, while 5-HT2B-induced pMF is NADPH oxidase-dependent (MacFarlane et al., 2011). Following respiratory motor neuron loss in an ALS rodent model, it has been shown that inhibition of 5-HT receptors or downstream signaling modulators results in compromised breathing or pLTF, respectively (Nichols et al., 2014; Nichols et al., 2011; Nichols et al., 2017). In this same model, pre-symptomatic $SOD1^{G93A}$ rats exhibit NADPH oxidase-dependent AIH-induced pLTF, but pLTF becomes NADPH oxidase-independent at end-stage (Nichols et al., 2015a). Together, this suggests a differential requirement for 5-HT2A/B receptor activation over the course of disease. Here, we show that 28d CTB-SAP rats require new BDNF synthesis and MEK/ERK activity for pLTF (Figs. 3.3, 3.5 & 3.6). However, it remains unknown if 5-HT2A/B receptors are also required for pLTF, and if further activating these receptors would increase breathing in 28d CTB-SAP treated rats. Once the complete underlying mechanism for pLTF is elucidated in 28d CTB-SAP rats, pharmacological interventions at this time point can be tested to either maintain or elicit enhanced pLTF. Since the pathways evaluated in the current study are intracellular, future studies will be focused on the requirement of 5-HT2A/B and A2A receptors for pLTF in 7d and 28d CTB-SAP treated rats.

Significance

The CTB-SAP model effectively mimics the respiratory motor neuron loss and deficits observed in a variety of neuromuscular diseases. Studying AIH-induced pLTF in this model not only assists us in teasing out the underlying mechanisms of pLTF over the course

of motor neuron death, but also provides insight for potential targets for pharmacological or gene-therapy treatments to prevent respiratory deficits, ventilator dependence, and mortality. Additionally, because our data show that the mechanisms by which pLTF is elicited differs by time point, we must understand these mechanisms in order to pharmacologically target them in patients at varying stages of disease. This may provide insight as to why patients do not respond to therapy and pharmacological intervention in the same way. Finally, because symptoms vary vastly in motor neuron and neuromuscular diseases, it is important to investigate the multiple signaling pathways to provide more treatment options when one therapy does not work.

3.6- ACKNOWLEDGEMENTS

3.7- AUTHOR CONTRIBUTIONS

Experimental Groups	P_{aCO_2} (mmHg)			P_{aO_2} (mmHg)			MAP (mmHg)		
	baseline	HX	60 min	baseline	HX	60 min	baseline	HX	60 min
With AIH									
siNT									
7d CON	45.1±1.5[d]	44.1±1.8[d]	46.5±1.3[ad]	310±4[ab]	38.0±1[c]	269±7[a]	121±4[a]	84±7[c]	110±5[a]
7d CTB-SAP	49.5±1.5	49.6±1.6	51.0±2.1	296±8[ab]	39.1±1[c]	267±4[a]	114±4[ab]	72±6[c]	98±7[a]
28d CON	48.2±1.0[a]	46.7±1.1[d]	48.1±1.2[d]	303±19[ab]	40±3[c]	267±19[a]	115±7[ab]	87±7[c]	98±7
28d CTB-SAP	46.3±2.2[bd]	45.4±2.2[d]	47.8±1.9[ad]	305±11[ab]	41.3±1.3[c]	276±20[a]	110±6[a]	73±4[c]	103±5[a]
siBDNF									
7d CON	45.3±1.0[d]	45.1±1.2[d]	46.0±0.9[d]	301±7[ab]	38.5±1.4[c]	246±22[acde]	114±5[ab]	74±6[c]	95±5[a]
7d CTB-SAP	44.9±2.3[d]	45.2±3.1[d]	46.4±2.5[d]	290±11[a]	40.4±1.8[c]	276±7[a]	116±5[ab]	70±8[c]	102±7[a]
28d CON	48.5±3.1	47.8±3.2	47.9±3.3[d]	299±10[a]	40.0±1.5[c]	285±5[a]	127±6[a]	85±11[c]	101±9[a]
28d CTB-SAP	46.1±1.3[d]	45.3±1.4[d]	46.1±1.5[d]	307±6[ab]	41.7±1.0[c]	273±11[a]	107±7[a]	69±12[c]	103±7[a]
siTrkB									
7d CON	44.3±1.2[d]	43.5±1.4[d]	45.8±0.8[ad]	299±10[ab]	39.0±1.3[c]	271±12[a]	118±9[a]	72±5[c]	109±9[a]
7d CTB-SAP	47.9±1.3	48.8±1.4	47.8±1.2[d]	281±32[ad]	37.3±1.1[c]	257±26[ad]	118±6[a]	71±11[c]	111±6[a]
28d CON	53.2±1.4	52.8±1.3	54.6±1.5[a]	316±10[a]	38.6±0.9[c]	293±6[a]	119±14[ab]	92±13[c]	99±15
28d CTB-SAP	49.1±0.7	48.6±1.0	49.6±1.0	308±17[ab]	42.3±0.7[c]	265±19[a]	118±6[ab]	75±10[c]	93±7[a]
Without AIH (TCs)									
CON siTC	47.3±1.4[d]	47.8±1.5	47.7±1.3[d]	306±7	307±6	285±9	115±5	114±5	105±5
CTB-SAP siTC	50.1±2.4	49.8±2.2	50.5±3.4	302±10	303±8	283±12	112±6	122±12	104±11[a]

Table 3.1: Arterial PCO2, PO2 and mean arterial pressure (MAP) during baseline, hypoxia (HX) and 60 minutes post-hypoxia for control (CON) and CTB-SAP treated rats with acute intermittent hypoxia (AIH) or without AIH (time-control or TC). Rats received intrathecal delivery of siRNAs targeting BDNF (siBDNF), TrkB (siTrkB) or non-target (siNT) mRNA. Significant differences within groups included *versus* hypoxia ([a]), and 60 min ([b]), and across groups included *versus*: respective TC ([c]), 28d CON siTrkB ([d]), and 28d CON siBDNF ([e]). Values are expressed as means ± S.E.M. Differences were considered significant if $p<0.05$.

Experimental Groups	P_{aCO_2} (mmHg)			P_{aO_2} (mmHg)			MAP (mmHg)		
	baseline	HX	60 min	baseline	HX	60 min	baseline	HX	60 min
With AIH									
Vehicle									
7d CON	49.0±1.3	49.3±1.2	49.4±1.3	294±15[a]	39.7±2.3[c]	264±9[a]	108±9[a]	77±12[c]	106±4[a]
7d CTB-SAP	50.3±1.2	49.8±1.0	49.6±1.5	317±12[ab]	45.0±1.2[c]	273±9[ac]	108±8[a]	79±8[c]	110±9[a]
28d CON	51.2±1.0	50.9±0.9	51.1±1.2	263±21[ae]	42.1±2.5[c]	252±12[a]	107±4[a]	70±6[ce]	109±7[a]
28d CTB-SAP	51.1±0.6	50.8±0.7	51.5±0.7	249±17[a]	40.1±1.7[c]	246±20[a]	117±4[a]	80±12[c]	107±6[a]
UO126									
7d CON	48.0±1.1	48.1±1.2	47.9±1.3	285±10[a]	37.4±0.8[c]	271±7[a]	123±8[ac]	91±11	110±7[a]
7d CTB-SAP	45.5±1.9[bcdef]	46.4±1.9[cd]	47.0±1.6[c]	275±18[a]	38.0±1.7[c]	270±10[ac]	101±5[ai]	71±7[c]	97±8[a]
28d CON	45.8±2.0[def]	46.1±2.2[d]	46.6±1.1[g]	294±9[a]	37.5±1.7[c]	267±14[a]	127±9[acg]	91±9	107±10[a]
28d CTB-SAP	48.0±1.3	48.3±1.5[c]	47.4±1.5[c]	307±4[af]	39.3±1.5[c]	283±6[ac]	120±6[abg]	81±5	101±9[a]
PI828									
7d CON	45.6±1.5[def]	46.4±1.8[d]	46.1±1.5[defg]	302±10[af]	37.6±0.9[c]	278±12[a]	107±5[a]	80±7	100±6[a]
7d CTB-SAP	51.4±1.5	52.1±1.9	51.2±1.7	288±16[ab]	38.2±0.8[c]	260±15[a]	118±6[a]	87±10	106±9[a]
28d CON	45.0±1.9[defgh]	45.4±1.8[def]	45.5±1.4[defg]	303±8[af]	39.9±1.4[c]	282±5[a]	94±6[dfijk]	78±9	85±9[efhij]
28d CTB-SAP	50.5±1.0[b]	49.8±1.0	52.0±1.1[a]	300±9[af]	41.8±1.1[c]	275±9[a]	98±6[a]	79±13[c]	84±6[efhij]
Without AIH (TCs)									
CON UO126	48.2±2.0	48.5±1.8	47.8±1.5	284±27	287±26	289±10	100±6	110±11	91±7[a]
CTB-SAP UO126	52.6±3.0[a]	53.8±3.3	53.0±3.0	278±28[b]	280±27	222±35[a]	95±8[df]	93±11	96±5
CON PI828	46.0±2.4[def]	45.2±2.7[def]	45.9±2.1[defg]	298±8[f]	295±9	277±12	103±4	91±6	93±6
CTB-SAP PI828	52.7±1.5	52.9±1.8	52.8±1.6	280±30[b]	279±31	243±24[a]	102±7	106±7	85±9[aefhj]

Table 3.2: Arterial PCO$_2$, PO$_2$ and mean arterial pressure (MAP) during baseline, hypoxia (HX) and 60 minutes post-hypoxia for control (CON) and CTB-SAP treated rats with acute intermittent hypoxia (AIH) or without AIH (time-control or TC). Rats received intrathecal delivery of either: 1) vehicle (20% DMSO); or 2) MEK/ERK inhibitor (UO126); or 3) PI3K/Akt inhibitor (PI828). Significant differences within groups included *versus* hypoxia ([a]), and 60 min ([b]), and across groups included *versus*: respective TC ([c]), 7d CTB-SAP PI828 ([d]), 28d CON vehicle ([e]), 28d CTB-SAP vehicle ([f]), 28d CTB-SAP PI828 ([g]), 7d CTB-SAP vehicle ([h]), 28d CON UO126 ([i]), 7d CON UO126 ([j]), and 28d CTB-SAP UO126 ([k]). Values are expressed as means ± S.E.M. Differences were considered significant if p<0.05.

Experimental Groups	pH			BE $(mEq \cdot L^{-1})$		
	baseline	hypoxia	60 min	baseline	hypoxia	60 min
With AIH						
siNT						
7d CON	7.353±0.009	7.334±0.011	7.335±0.011	-1.1±0.6[a]	-2.7±0.9	-1.1±0.7[a]
7d CTB-SAP	7.329±0.010	7.324±0.010	7.314±0.015	-0.7±0.5	-1.2±0.4[c]	-1.0±0.5
28d CON	7.335±0.012	7.336±0.019	7.291±0.053	-0.7±0.9	-1.7±1.4	-1.5±1.2
28d CTB-SAP	7.328±0.012	7.321±0.014	7.348±0.018	-2.3±0.9[b]	-3.1±1.4	0.3±1.1[a]
siBDNF						
7d CON	7.348±0.010	7.345±0.007	7.368±0.013	-1.0±0.5	-1.5±0.9	0.6±1.2[ac]
7d CTB-SAP	7.345±0.011	7.347±0.011	7.350±0.011	-1.4±0.3	-2.8±0.9	-0.5±0.5[a]
28d CON	7.314±0.020	7.300±0.016	7.323±0.022	-2.4±0.5	-3.3±0.8	-1.6±0.9
28d CTB-SAP	7.335±0.011	7.310±0.011	7.333±0.020	-1.7±0.7[a]	-3.7±0.8	-2.1±1.1
siTrkB						
7d CON	7.357±0.015	7.357±0.008	7.368±0.013	-1.0±0.6	-1.4±0.8	0.6±0.7[ac]
7d CTB-SAP	7.345±0.014	7.330±0.019	7.347±0.018	-0.4±0.5	-1.0±0.8[c]	-0.2±0.9
28d CON	7.300±0.024	7.305±0.023	7.307±0.016	-1.5±1.2	-1.3±1.2	-0.2±0.8
28d CTB-SAP	7.313±0.007	7.310±0.012	7.318±0.014	-2.2±0.5	-3.0±1.0	-1.6±0.9
Without AIH (TCs)						
CON siTC	7.335±0.010	7.328±0.009	7.351±0.012	-1.1±0.9	-1.5±0.8	0.2±0.5[a]
CTB-SAP siTC	7.313±0.021	7.317±0.023	7.347±0.020	-1.7±0.7[b]	-1.6±1.0	0.6±0.2[ac]

Supplementary Table 3.1: pH and base excess (BE) during baseline, hypoxia (HX) and 60 minutes post-hypoxia for control (CON) and CTB-SAP treated rats with acute intermittent hypoxia (AIH) or without AIH (time-control or TC). Rats received intrathecal delivery of siRNAs targeting BDNF (siBDNF), TrkB (siTrkB) or non-target (siNT) mRNA. Significant differences within groups included *versus* hypoxia ([a]), and 60 min ([b]), and across groups included *versus*: 28d CTB-SAP siBDNF ([c]). Values are expressed as means ± S.E.M. Differences were considered significant if $p < 0.05$.

Experimental Groups	pH			BE (mEq*L^{-1})		
	baseline	hypoxia	60 min	baseline	hypoxia	60 min
With AIH						
Vehicle						
7d CON	7.340±0.016	7.333±0.016	7.333±0.022	-0.3±0.8[c]	-0.6±0.9[c]	-0.5±1.1
7d CTB-SAP	7.345±0.006[c]	7.337±0.013[c]	7.358±0.012[c]	0.8±0.4[cd]	-0.2±0.9	1.4±0.7[ac]
28d CON	7.330±0.011	7.325±0.011	7.345±0.009	-0.2±.4[c]	-0.7±0.7[c]	0.8±0.4[a]
28d CTB-SAP	7.325±0.006	7.330±0.007	7.340±0.009[c]	-0.6±0.5[b]	-0.2±0.6	0.8±0.6[c]
UO126						
7d CON	7.329±0.005[b]	7.316±0.007	7.351±0.004[a]	-1.4±0.4[b]	-2.4±0.5[f]	0.1±0.5[a]
7d CTB-SAP	7.328±0.014[b]	7.330±0.010	7.357±0.015[ac]	-2.2±1.1[bh]	-2.2±0.7	0.3±0.6[ac]
28d CON	7.352±0.014[ad]	7.328±0.016	7.368±0.016[ag]	-0.8±1.1[ab]	-2.3±1.4	0.9±1.0[a]
28d CTB-SAP	7.311±0.009	7.317±0.008	7.327±0.011[c]	-2.7±0.3[befhi]	-2.4±0.4[f]	-0.9±0.5[ah]
PI828						
7d CON	7.331±0.012	7.311±0.015	7.341±0.017[a]	-2.3±0.6[h]	-3.1±0.9[efhi]	-0.9±0.9[ah]
7d CTB-SAP	7.309±0.016	7.300±0.016	7.327±0.016[a]	-1.5±1.1	-2.0±1.2	-0.3±0.7[a]
28d CON	7.341±0.010[a]	7.316±0.012	7.344±0.014[a]	-1.8±0.8[ah]	-3.6±1.0[efhi]	-1.3±1.0[ah]
28d CTB-SAP	7.317±0.008	7.319±0.013	7.324±0.015	-1.3±0.8	-1.5±1.1	-0.1±0.9[a]
Without AIH (TCs)						
CON UO126	7.331±0.011	7.329±0.011	7.349±0.014	-1.3±0.3	-1.3±0.5	-0.2±0.6
CTB-SAP UO126	7.303±0.019[b]	7.293±0.020	7.281±0.032	-1.8±0.5	-2.1±0.6	-2.1±1.2
CON PI828	7.327±0.015[b]	7.329±0.013	7.354±0.020[a]	-2.5±0.7[b]	-2.8±0.6	-0.6±.8[a]
CTB-SAP PI828	7.310±0.013	7.308±0.015	7.303±0.020	-1.1±0.7	-1.2±0.7	-1.2±1.0

Supplementary Table 3.2: pH and base excess (BE) during baseline, hypoxia (HX) and 60 minutes post-hypoxia for control (CON) and CTB-SAP treated rats with acute intermittent hypoxia (AIH) or without AIH (time-control or TC). Rats received intrathecal delivery of either: 1) vehicle (20% DMSO); or 2) MEK/ERK inhibitor (UO126); or 3) PI3K/Akt inhibitor (PI828). Significant differences within groups included *versus* hypoxia ([a]), and 60 min ([b]), and across groups included *versus*: respective TC ([c]), 7d CTB-SAP PI828 ([d]), 28d CON vehicle ([e]), 28d CTB-SAP vehicle ([f]), 28d CTB-SAP PI828 ([g]), 7d CTB-SAP vehicle ([h]), and 7d CON vehicle ([i]). Values are expressed as means ± S.E.M. Differences were considered significant if $p < 0.05$.
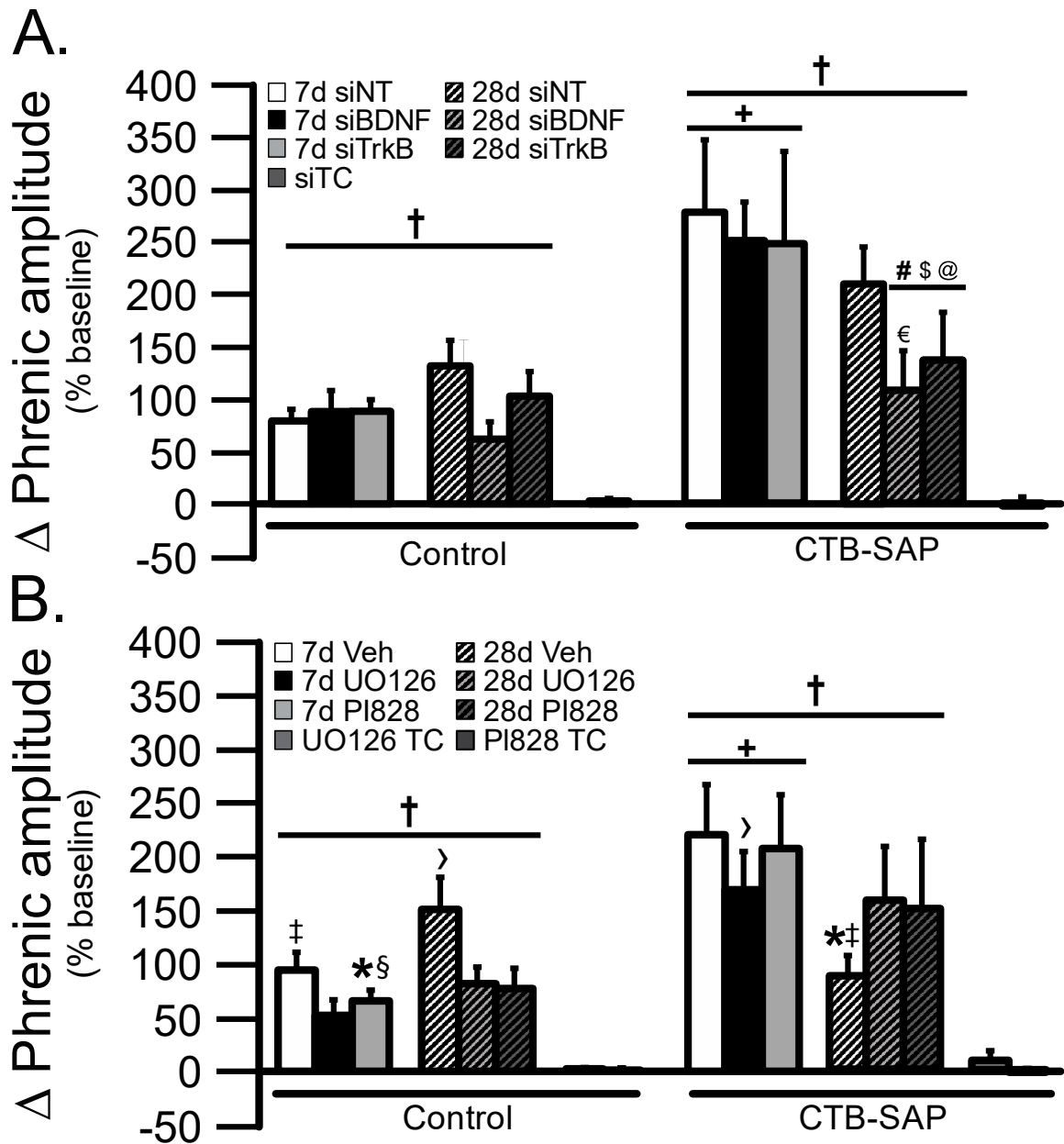
Figure 3.1: Short-term phrenic nerve hypoxic response in 7d & 28d control and CTB SAP treated rats. A. Short-term phrenic nerve hypoxic responses were compared in 7d and 28d control and CTB-SAP treated rats pre-treated with siNT, siBDNF, siTrkB, and siTC. As expected, all treatment groups exposed to AIH had a significantly greater hypoxic response *vs.* the corresponding siTC group (†). All 7d CTB-SAP rats pre-treated with siRNA had a significantly greater hypoxic response *vs.* respective pre-treated 7d control rats (+). 28d CTB-SAP rats pre-treated with siBDNF and siTrkB had hypoxic responses that were significantly less than 7d CTB-SAP rats pre-treated with siNT (#), 7d CTB-SAP rats pre-treated with siBDNF ($), and 7d CTB-SAP rats pre-treated with siTrkB (@). 28d CTB-SAP rats pre-treated with siNT had a significantly higher hypoxic response *vs.* 28d CTB-SAP rats pre-treated with siBDNF (€). **B.** Short-term phrenic nerve hypoxic responses were compared in 7 and 28d control and CTB-SAP treated rats pre-treated with

vehicle (DMSO), UO126, PI828, and TC for both inhibitors (UO126 TC and PI828 TC). As expected, all treatment groups exposed to AIH had a significantly greater hypoxic response *vs*. the corresponding TC group (†). All 7d CTB-SAP rats pre-treated with vehicle or inhibitors had a significantly greater hypoxic response *vs*. respective pre-treated 7d control rats (+). 7d CTB-SAP rats pre-treated with vehicle had a significantly greater hypoxic response compared to 7d controls pre-treated with vehicle, and 28d CTB-SAP rats with vehicle (‡). 7d CTB-SAP rats pre-treated with PI828 had a hypoxic response that was significantly greater than 7d control rats pre-treated with PI828, and 28d CTB-SAP rats pre-treated with vehicle (*). The hypoxic response in 7d control rats pre-treated with UO126 was significantly less than 7d CTB-SAP rats pre-treated with UO126, and 28d control rats pre-treated with vehicle (>). Lastly, 28d controls pre-treated with vehicle had a significantly greater hypoxic response compared to 7d controls pre-treated with PI828 (§). Values are means ± SEM, and all significant differences are $p < 0.05$.

Figure 3.2: pLTF in 7d siRNA treated rats. A–C, Representative traces of compressed, integrated phrenic nerve activity before and after AIH in 7d CTB-SAP rats pre-treated with siNT (**A**), siBDNF (**B**), or siTrkB (**C**). Baseline is indicated in each trace by a white, dashed line. AIH elicits pLTF in 7d CTB-SAP rats pre-treated with siNT and siBDNF, but appears to be reduced in rats pre-treated with siTrkB. **D, E.** Phrenic burst amplitude (expressed as a percent change from baseline) in 7d control (D) and 7d CTB-SAP (E) rats pre-treated with siNT, siBDNF, siTrkB, or siTC. pLTF was significantly increased from baseline (*) and siTC (†) at 60 min in 7d control rats pre-treated with siNT or siTrkB. In contrast, pLTF was significantly increased from baseline (*) at all time points in 7d CTB-SAP rats pre-treated with siNT or siBDNF, and from siTC at 30 (siBDNF) and 60 min post-hypoxia (both siBDNF and siNT (†)). pLTF in 7d CTB-SAP rats pre-treated with siTrkB was significantly reduced from 7d CTB-SAP rats pre-treated with siNT at all time points, and 7d CTB-SAP pre-treated with siBDNF at 15 min and 60 min post-hypoxia (#). Values are means ± SEM, and all significant differences are $p < 0.05$.
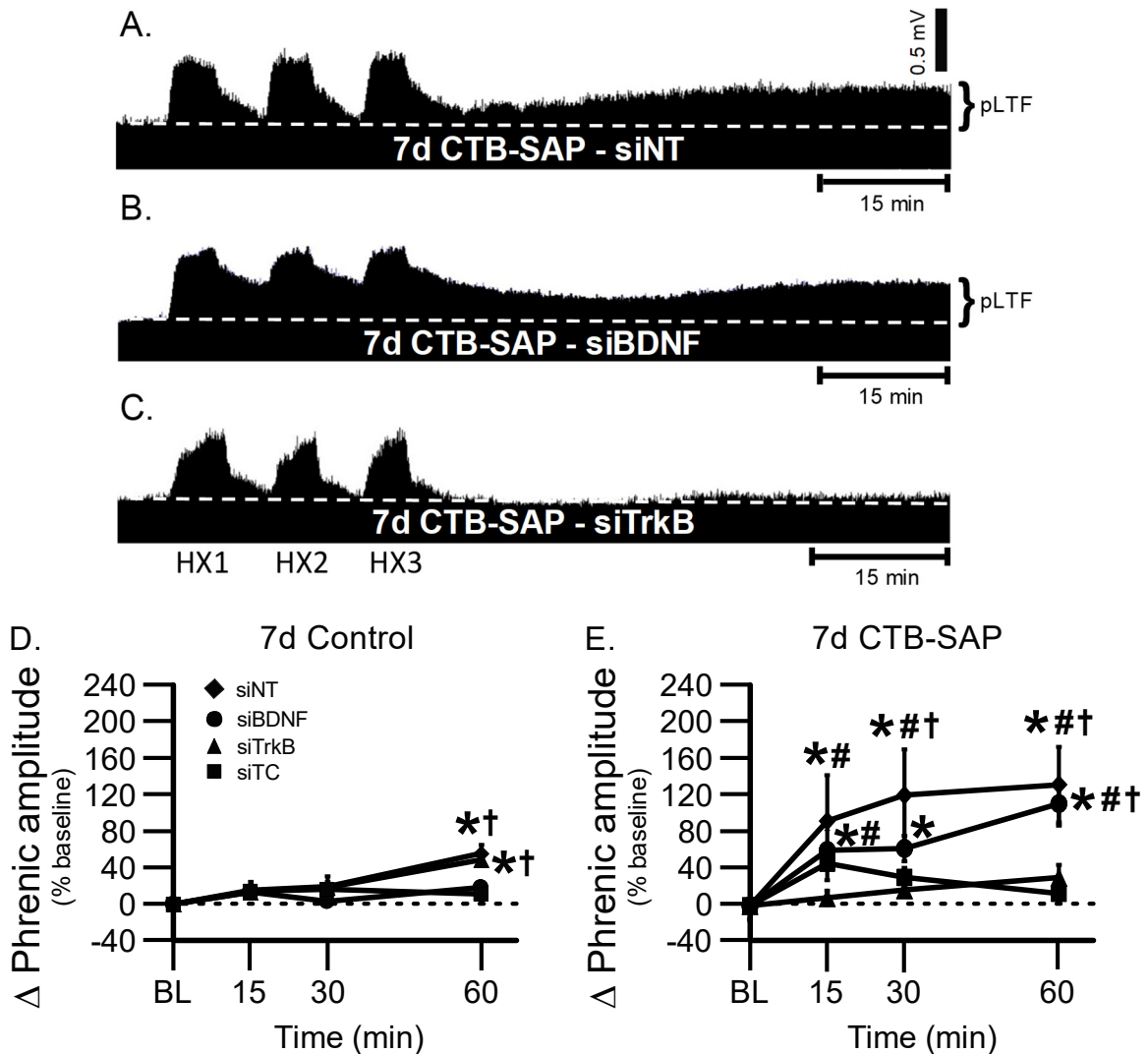
101

Figure 3.3: pLTF in 28d siRNA treated rats. A–C, Representative traces of compressed, integrated phrenic nerve activity before and after AIH in 28d CTB-SAP rats pre-treated with siNT **(A)**, siBDNF **(B)**, or siTrkB **(C)**. Baseline is indicated in each trace by a white, dashed line. AIH elicits pLTF in 28d CTB-SAP rats pre-treated with siNT and siTrkB, but appears to be reduced in rats pre-treated with siBDNF. **D, E.** Phrenic burst amplitude (expressed as a percent change from baseline) in 28d control (D) and 28d CTB-SAP (E) rats pre-treated with siNT, siBDNF, siTrkB, or siTC. pLTF was significantly increased from baseline (*) and siTC (†) in 28d control and CTB-SAP rats pre-treated with siNT at all time points post-hypoxia exposure *vs.* baseline and at 30 and 60 mins *vs.* siTC, and at 30 and 60 minutes in both groups pre-treated with siTrkB. In contrast, pLTF in 28d controls pre-treated with siBDNF was significantly reduced from 28d controls pre-treated with siNT and siTrkB at 30 and 60min post-hypoxia (+). Similarly, pLTF in 28d CTB-SAP treated rats pre-treated with siBDNF was significantly reduced from 28d CTB-SAP treated rats pre-treated with siTC at 15min post-hypoxia (†), siNT at all time points, and siTrkB at 30 and 60min post-hypoxia (+). Values are means ± SEM, and all significant differences are p<0.05.
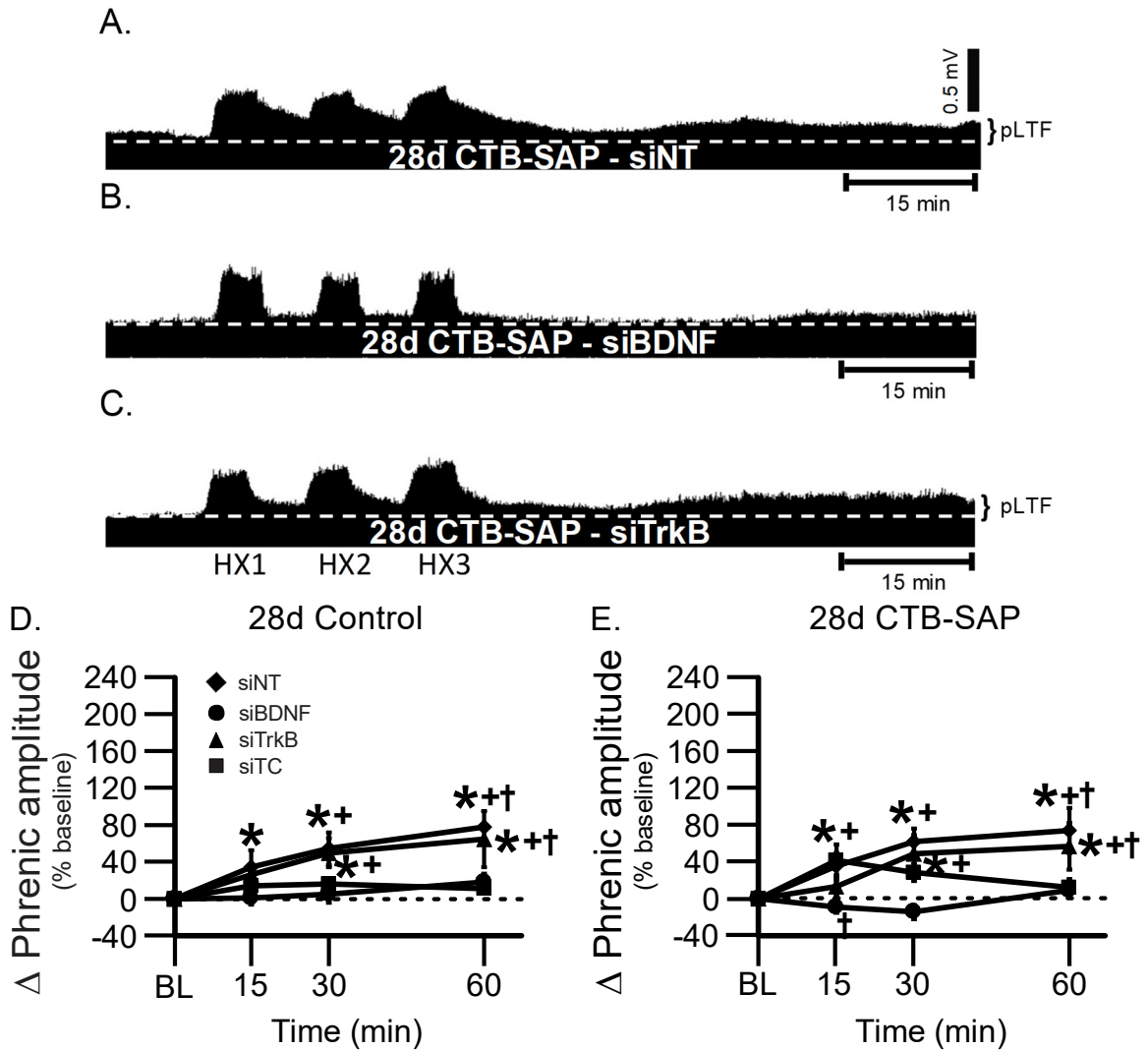
Figure 3.4: pLTF in 7d UO126 and PI828 treated rats. **A–C**, Representative traces of compressed, integrated phrenic nerve activity before and after AIH in 7d CTB-SAP rats pre-treated with vehicle (**A**; DMSO), a MEK/ERK inhibitor (**B**; UO126), or a PI3K/Akt inhibitor (**C**; PI828). Baseline is indicated in each trace by a white, dashed line. AIH elicits pLTF in 7d CTB-SAP rats pre-treated with the vehicle or UO126, but appears to be reduced in rats pre-treated with PI828. **D, E,** Phrenic burst amplitude (expressed as a percent change from baseline) in 7d control (D) and 7d CTB-SAP (E) rats pre-treated with vehicle, UO126, PI828, or drug inhibitor time controls (UO126 TC and PI828 TC). pLTF was significantly increased from baseline (*) in 7d control rats pre-treated with vehicle at 30 and 60 min, and at 60 min in rats pre-treated with PI828. Vehicle and PI828 pre-treated controls also exhibited pLTF that was significantly increased *vs*. TCs at 60 min post-hypoxia (vehicle *vs*. UO126 TC, +; vehicle and PI828 *vs*. PI828 TC, $). 7d CTB-SAP rats pre-treated with vehicle or UO126 exhibited significantly greater pLTF from baseline and TCs at all time points (vehicle *vs*. UO126 TC (+) and PI828 TC ($); UO126 *vs*. UO126 TC, +), and 60 min post-hypoxia in rats pre-treated with PI828 *vs*. baseline and PI828 TC ($). pLTF was

significantly reduced at 60 min post-hypoxia in 7d controls and 7d CTB-SAP treated rats pre-treated with UO126 *vs*. 7d controls and 7d CTB-SAP rats pre-treated with vehicle, as well as 7d controls pre-treated with PI828 (†). 7d CTB-SAP rats pre-treated with PI828 also exhibited significantly reduced pLTF at all time points *vs*. 7d CTB-SAP rats pre-treated with vehicle or UO126 (#). Values are means ± SEM, and all significant differences are $p<0.05$.
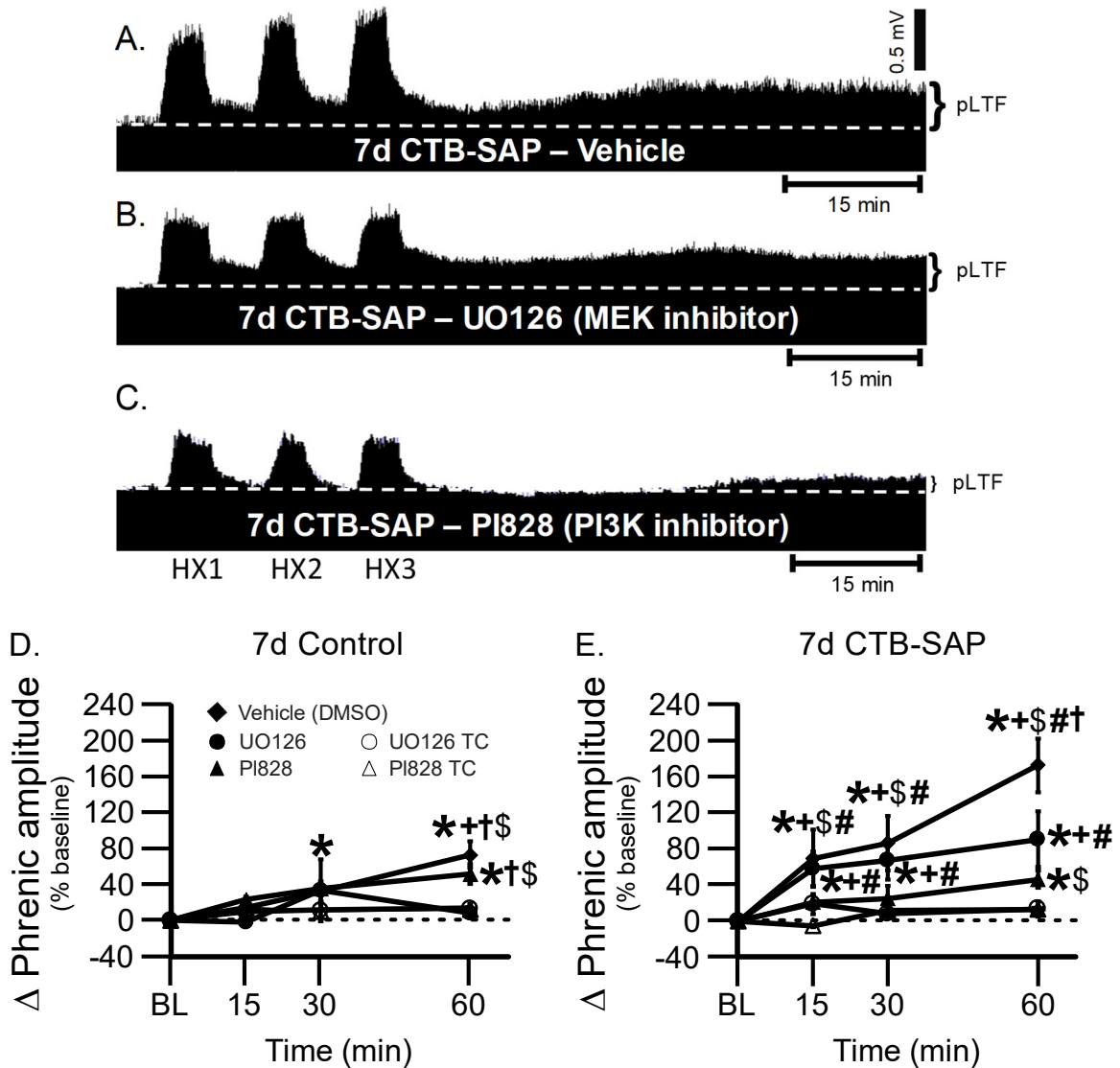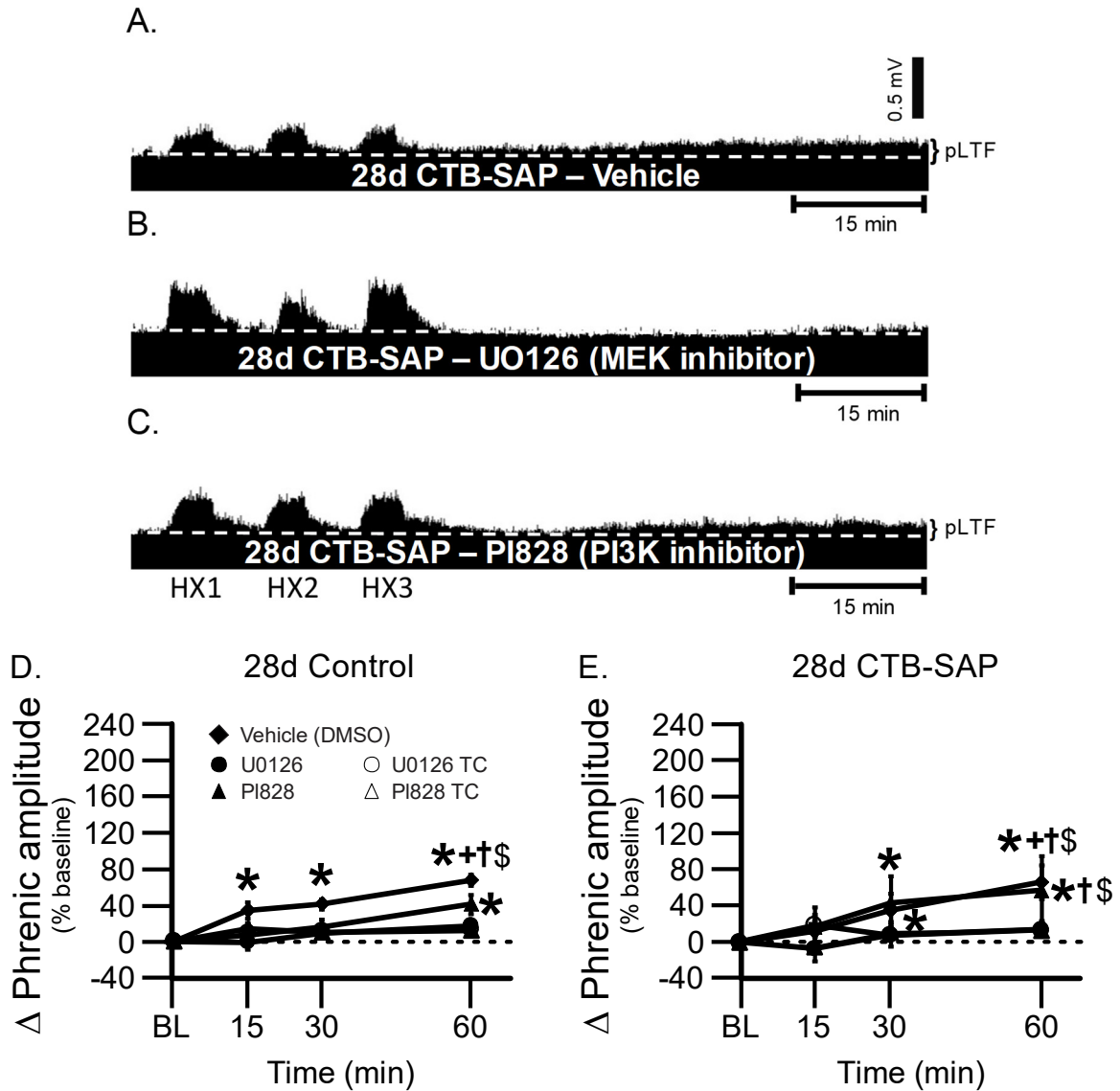
Figure 3.5: pLTF in 28d UO126 and PI828 treated rats. A–C, Representative traces of compressed, integrated phrenic nerve activity before and after AIH in 28d CTB-SAP rats pre-treated with vehicle (**A**; DMSO), a MEK/ERK inhibitor (**B**; UO126), or a PI3K/Akt inhibitor (**C**; PI828). Baseline is indicated in each trace by a white, dashed line. AIH elicits pLTF in 28d CTB-SAP rats pre-treated with the vehicle or PI828, but appears to be reduced in rats pre-treated with UO126. **D, E,** Phrenic burst amplitude (expressed as a percent change from baseline) in 28d control (D) and 28d CTB-SAP (E) rats pre-treated with vehicle, UO126, PI828 or drug inhibitor time controls (UO126 TC and PI828 TC). pLTF was significantly increased from baseline (*) in 28d control rats pre-treated with vehicle at all time points, and at 60 min post-hypoxia in rats pre-treated with PI828. Vehicle pre-treated 28d controls also exhibited pLTF that was significantly increased *vs.* TCs at 60 min post-hypoxia (vehicle *vs.* UO126 TC, +; vehicle *vs.* PI828 TC, $). Similarly, 28d CTB-SAP rats pre-treated with vehicle or PI828 exhibited significantly greater pLTF from baseline at 30 and 60min post-hypoxia, and from TCs at 60 min post-hypoxia (vehicle *vs.* UO126 TC (+) and PI828 TC ($); PI828 *vs.* PI828 TC, +). pLTF was significantly reduced

at 60 min post-hypoxia in 28d controls and 28d CTB-SAP treated rats pre-treated with UO126 *vs*. 28d controls and 28d CTB-SAP rats pre-treated with vehicle, and *vs*. 28d CTB-SAP treated rats pre-treated with PI828 (†). Values are means ± SEM, and all significant differences are p<0.05.
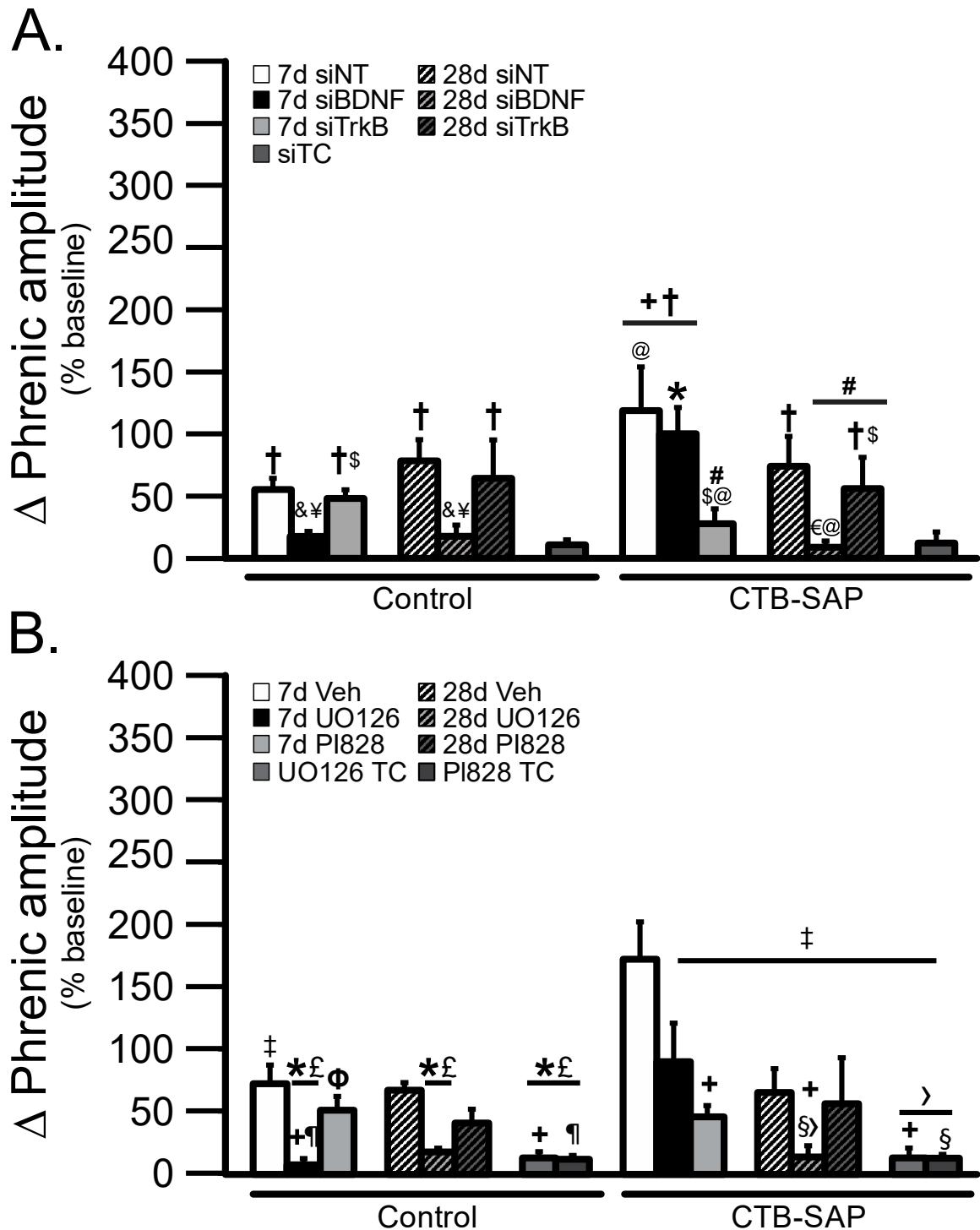
Figure 3.6: Direct comparisons of the change in phrenic amplitude (percent baseline) following AIH at 60 min post-hypoxia in 7d & 28d control and CTB-SAP treated rats.
A. pLTF was compared in 7d and 28d control and CTB-SAP treated rats pre-treated with siNT, siBDNF, siTrkB, and siTC. 7d and 28d control rats pre-treated with siNT and siTrkB had greater pLTF *vs.* the corresponding siTC group (†). 7d CTB-SAP rats pre-treated with siNT and siBDNF and 28d rats pre-treated with siNT and siTrkB had greater pLTF *vs.* the

corresponding siTC group (†). 7d CTB-SAP rats pre-treated with siNT and siBDNF elicited greater pLTF than that of respective 7d control rats (+). 7d and 28d control rats pre-treated with siBDNF had an attenuated pLTF from 28d control rats pre-treated with siNT (&) and siTrkB (¥). 28d CTB-SAP rats pre-treated with siBDNF had pLTF that was significantly attenuated from that of 7d CTB-SAP rats with the same pre-treatment (*), and from that of 28d CTB-SAP rats pre-treated with siTrkB (€). pLTF was reduced in 7d controls as well as 7d and 28d CTB-SAP treated rats pre-treated with siTrkB *vs*. 7d CTB-SAP rats pre-treated with siBDNF ($). 7d CTB-SAP rats pre-treated with siNT exhibited greater pLTF *vs*. 28d CTB-SAP rats pre-treated with siBDNF and 7d CTB-SAP rats as well as 28d CTB-SAP treated rats pre-treated with siTrkB (#). pLTF was significantly different when comparing 28d CTB-SAP treated rats pre-treated with siNT *vs*. 28d CTB-SAP rats pre-treated with siBDNF, and 7d CTB-SAP rats pre-treated with siNT or siTrkB (@). **B.** pLTF was compared in 7d and 28d control and CTB-SAP treated rats pre-treated with vehicle, UO126, PI828, and TC for both drug inhibitors (UO126 TC and PI828 TC). All CTB-SAP treatment groups and 7d control rats pre-treated with vehicle had significantly reduced pLTF *vs*. 7d CTB-SAP rats pre-treated with vehicle (‡). 7d and 28d control rats pre-treated with UO126 and control rats pre-treated with UO126 TC and PI828 TC had pLTF that was attenuated from 7d and 28d control rats pre-treated with vehicle (£ and *, respectively). 7d control rats and 28d CTB-SAP rats pre-treated with UO126, 7d CTB-SAP rats pre-treated with PI828, and control and CTB-SAP rats pre-treated with UO126 TC had pLTF that was significantly reduced from 7d CTB-SAP rats pre-treated with UO126 (+). 7d control rats pre-treated with UO126 and control rats pre-treated with PI828 TC had pLTF that was reduced from 7d control rats pre-treated with PI828 (¶). 7d CTB-SAP rats pre-treated with PI828 had pLTF that was greater than PI828 TC (Φ). 28d CTB-SAP rats pre-treated with UO126 and CTB-SAP rats pre-treated with PI828 TC had pLTF that was attenuated from 28d CTB-SAP rats pre-treated with PI828 (§). 28d CTB-SAP rats pre-treated with UO126 and CTB-SAP rats pre-treated with UO126 TC and PI828 TC had pLTF that was reduced from 28d CTB-SAP rats pre-treated with vehicle (>). Values are mean for each group ± SEM, and all significant differences are p<0.05.

CHAPTER 4: Nonsteroidal anti-inflammatory drug (ketoprofen) delivery differentially impacts phrenic long-term facilitation in rats with motor neuron death induced by intrapleural CTB-SAP injections

Lauren F. Borkowski, Amy N. Keilholz, Catherine L. Smith, Kaylie A. Canda, and Nicole L. Nichols*

Department of Biomedical Sciences, Dalton Cardiovascular Research Center, University of Missouri, Columbia, MO 65211

Abbreviated Title: Ketoprofen impacts pLTF following CTB-SAP

In revision at *Experimental Neurology*

4.1- ABSTRACT:

Intrapleural injections of cholera toxin B conjugated to saporin (CTB-SAP) selectively eliminates respiratory (*e.g.,* phrenic) motor neurons, and mimics motor neuron death and respiratory deficits observed in rat models of neuromuscular diseases. Additionally, microglial density increases in the phrenic motor nucleus following CTB-SAP. This CTB-SAP model allows us to study the impact of motor neuron death on the output of surviving phrenic motor neurons, and the underlying mechanisms that contribute to enhancing or constraining their output at 7 days (d) or 28d post-CTB-SAP injection. 7d CTB-SAP rats elicit enhanced phrenic long-term facilitation (pLTF) through the Gs-pathway (inflammation-resistant in naïve rats), while pLTF is elicited though the Gq-pathway (inflammation-sensitive in naïve rats) in control and 28d CTB-SAP rats. In 7d and 28d male CTB-SAP rats and controls, we evaluated the effect of cyclooxygenase-1/2 enzymes on pLTF by delivery of the nonsteroidal anti-inflammatory drug, ketoprofen (IP), and we hypothesized that pLTF would be unaffected by ketoprofen in 7d CTB-SAP rats, but pLTF would be enhanced in 28d CTB-SAP rats. In anesthetized, paralyzed and ventilated rats, pLTF was surprisingly attenuated in 7d CTB-SAP rats and enhanced in 28d CTB-SAP rats (both $p < 0.05$) following ketoprofen delivery. Additionally in CTB-SAP rats, microglia appeared to be more amoeboid in the phrenic motor nucleus, TNF-α expression appeared to be increased, and BDNF expression appeared to be increased but only at 28d. This study furthers our understanding of factors (*e.g.,* inflammation) that contribute to enhancing or constraining pLTF and its implications for breathing following respiratory motor neuron death.

Key words: respiratory plasticity; phrenic motor neuron death; inflammation; spinal cord; breathing; microglia

Highlights:

1) Ketoprofen constrains phrenic long-term facilitation in 7d CTB-SAP rats.

2) Ketoprofen enhances phrenic long-term facilitation in 28d CTB-SAP rats.

3) Inflammatory-associated marker expression is increased in CTB-SAP rats.

4) Microglia have amoeboid morphology in the phrenic motor nucleus in CTB-SAP rats.

Abbreviations: CTB (cholera toxin B), CTB-SAP (cholera toxin B conjugated to saporin), keto (ketoprofen), P_{ETCO_2} (partial pressure of end-tidal carbon dioxide), $PaCO_2$ (partial pressure of arterial carbon dioxide), PaO_2 (partial pressure of arterial oxygen), pLTF (phrenic long-term facilitation)

4.2- INTRODUCTION:

A variety of neuromuscular/neurodegenerative diseases (*e.g.*, spinal muscular atrophy (SMA), and amyotrophic lateral sclerosis (ALS)) and injuries (*e.g.*, spinal cord injury) result in respiratory motor neuron loss and diminished respiratory muscle output, and ultimately death by ventilatory failure (Boentert et al., 2017; Bourke et al., 2001; Lechtzin et al., 2002; Lyall et al., 2001; Nichols et al., 2013b; Nogués et al., 2002; Wong et al., 2002). Additionally, these patients experience systemic inflammation that hinders the function of the neural networks responsible for breathing (Perry, 2010; Teeling and Perry, 2009). However, breathing is maintained before mechanisms of compensation begin to fail, or respiratory motor neuron loss becomes too great. To specifically study the effects caused by respiratory motor neuron loss, we utilize intrapleural injections of cholera toxin B conjugated to saporin (CTB-SAP) to induce targeted respiratory motor neuron death (Borkowski and Nichols, 2020; Nichols et al., 2018; Nichols et al., 2015b).

Intrapleurally injected CTB-SAP results in phrenic [~40% survival in 7 day (d) CTB-SAP rats and ~25% survival in 28d CTB-SAP rats] and intercostal (~60% survival in 7d CTB-SAP rats and ~15% survival in 28d CTB-SAP rats) motor neuron loss and increased microglial density in the phrenic motor nucleus at 7d and 28d post-CTB-SAP treatment (Nichols et al., 2018; Nichols et al., 2015b). Interestingly, eupnea is maintained despite respiratory motor neuron loss (Nichols et al., 2015b). We speculate that the surviving respiratory neurons utilize mechanisms of plasticity, such as phrenic motor facilitation (pMF), to maintain eupnea. (Mitchell et al., 2001). Phrenic long-term facilitation (pLTF) is a form of pMF induced by acute intermittent hypoxia (AIH). In naïve rats, moderate AIH (35-55 mmHg PaO_2) elicits pLTF through Gq-dependent mechanisms

via serotonin 2 receptors (5-HT2) in the phrenic motor nucleus (Bach and Mitchell, 1996; Baker-Herman et al., 2004; Devinney et al., 2015; Devinney et al., 2013; Hoffman et al., 2012; McGuire and Ling, 2004). Conversely, severe AIH (*i.e.*, 25–35 mmHg PaO2) elicits enhanced pLTF through Gs-dependent mechanisms *via* A2A receptors (Agosto-Marlin and Mitchell, 2017; Devinney et al., 2013; Golder et al., 2008; Nichols et al., 2012). Interestingly, 7d CTB-SAP rats exhibit Gs-pathway dependent enhanced pLTF, while 28d CTB-SAP rats utilize the Gq-pathway for modest pLTF (Borkowski and Nichols, 2020; Nichols et al., 2018). However, it remains unknown if there are factors [*e.g.,* inflammation through cyclooxygenase 1 and 2 (COX-1 and 2)] contributing to the differential magnitude of pLTF exhibited in CTB-SAP rats.

Since microglial density is increased in the phrenic motor nucleus of CTB-SAP rats, we speculate that inflammation is one factor that contributes to differential pLTF. Gq pathway-induced pMF and moderate AIH-induced pLTF are nearly abolished by lipopolysaccharide (LPS; a toll-like receptor 4 agonist (Lu et al., 2008; Triantafilou and Triantafilou, 2002)) induced inflammation, but is restored with ketoprofen (non-steroidal anti-inflammatory drug) administration (Agosto-Marlin et al., 2018; Hocker et al., 2017; Huxtable et al., 2011; Huxtable et al., 2015; Huxtable et al., 2013; Vinit et al., 2011). In contrast, Gs pathway-induced pMF and severe AIH-induced pLTF are unaffected by LPS-induced inflammation, indicating that the Gs pathway is inflammation-resistant (Agosto-Marlin et al., 2017). However, the impact of inflammation (*e.g.*, COX-1 and 2 activation) on pLTF following CTB-SAP-induced respiratory motor neuron death has yet to be studied. Furthermore, it remains unknown if cells associated with inflammation such as microglia are activated in CTB-SAP rats, where activation is typically indicated by an

amoeboid morphological microglial phenotype (Graeber, 2010; Kettenmann et al., 2011; Kreutzberg, 1996; Sanagi et al., 2010). When there is an insult to the CNS, microglia will proliferate, rapidly migrate to the injury site, transition from ramified to amoeboid state (Graeber, 2010; Kreutzberg, 1996), and produce and release inflammatory-associated molecules (Huston and Tracey, 2011). Currently, changes in microglial morphology and inflammatory-associated markers following CTB-SAP-induced respiratory motor neuron death are unknown.

Here, we studied microglial morphology in the phrenic motor nucleus, cervical (C3-5) expression of inflammatory-associated markers, and how COX-1 and 2 mediated inflammation impacts pLTF in CTB-SAP treated rats. We hypothesized that microglia in the phrenic motor nucleus would have morphological characteristics that are consistent with activated microglia, and that cervical (C3-5) expression of inflammatory-associated markers would be increased in CTB-SAP rats. Furthermore, we hypothesized that pLTF would be unaffected by ketoprofen (nonsteroidal anti-inflammatory drug) in 7d CTB-SAP rats (Gs-pathway is inflammation resistant), but ketoprofen would enhance pLTF in 28d CTB-SAP rats (Gq-pathway is inflammation sensitive).

4.3- METHODS:

Animals

Experiments were conducted on adult (3–4 months old) male Sprague Dawley rats (Envigo Colony 208; Indianapolis, IN). Rats were housed in pairs and maintained under a 12:12 light:dark cycle. Animals had access to a standard commercial pelleted diet and water *ad libitum*. All procedures in this manuscript were approved by the Institutional Animal Care

and Use Committee at the University of Missouri in accordance with National Institutes of Health Guide for the Care and Use of Laboratory Animals. The University of Missouri is an AAALAC-accredited institution that operates under Animal Welfare Assurance ID A3394-01.

Intrapleural injections

Rats received bilateral intrapleural injections (6mm deep, fifth intercostal space) using a 50 µl Hamilton syringe and a custom needle (6 mm, 23 gauge, semi-blunt to prevent lung puncture) while under isoflurane anesthesia (1.5% in 100% oxygen as previously described by Mantilla et al. (2009). Control rats were intrapleurally injected with cholera toxin B subunit (CTB; 20 µg dissolved in doubly distilled H_2O; Calbiochem; Billerica, MA) unconjugated to saporin (SAP; 25 µg dissolved in phosphate buffered saline (PBS); Advanced Targeting Systems; San Diego, CA) to enable comparisons for respiratory plasticity. CTB conjugated to saporin (CTB-SAP; 25 µg dissolved in PBS; Advanced Targeting Systems; San Diego, CA) was intrapleurally injected to target respiratory motor neurons as described previously (Nichols et al., 2015; 2018; Borkowski and Nichols, 2020). CTB-SAP treated rats also received an additional 20 µg of CTB dissolved in double distilled H_2O (Calbiochem; Billerica, MA) in their administered intrapleural injections. Rats were then monitored to ensure respiration was not compromised following intrapleural injections, and were housed for 7 or 28 days before the below surgical preparation and neurophysiological experiments were performed.

Surgical Preparation for in vivo neurophysiological experiments

Experimental procedures were performed as described previously (*e.g.,* Hoffman et al., 2012, Nichols et al., 2018). Briefly, rats were isoflurane anesthetized, tracheotomized, and pump ventilated (Small Animal SAR-1000 Ventilator; CWE, Ardmore, PA, USA; tidal volume ~ 2.5 mL, frequency ~ 70–80 breaths per minute). Rats remained under isoflurane anesthesia (3.5% in 50% O_2, balance N_2) throughout surgical procedures before being converted to urethane anesthesia over 15–20 min (1.85 g kg^{-1}, *i.v.*) while isoflurane was slowly withdrawn. Once completely converted to urethane anesthesia, rats were then paralyzed for neuromuscular blockade using pancuronium bromide (2.5 mg kg^{-1}, i.v.). Rats were given a 1:2:0.13 mixture of 6% Hetastarch (in 0.9% sodium chloride), lactated Ringer's solution, and 8.4% sodium bicarbonate *via* continuous intravenous infusion (1.5–6 mL kg^{-1} h^{-1}) to maintain body fluid and acid-base balance. Lack of the pressor responses or obvious respiratory neural responses to a toe pinch with a hemostat was used to confirm the adequacy of anesthesia before and immediately after surgical and neurophysiological protocols were complete. Body temperature was maintained (37 ± 1 °C) with a custom-made heated surgical table, and was assessed with a rectal thermometer (Physitemp, Clifton, NJ, USA). Throughout the surgical preparation, end-tidal PCO_2 (P_{ETCO2}) was maintained at ~45 mmHg and monitored with a flow-through carbon dioxide analyzer designed to sufficiently measure response time for P_{ETCO2} measurements in rats (CapStar-100, CWE, Ardmore, PA).

Rats were bilaterally vagotomized and blood pressure was monitored in the right femoral artery by the insertion of a polyethylene catheter (PE50 ID: 0.58 mm, OD: 0.965 mm; Intramedic, MD, USA) connected to a pressure transducer (APT300 Pressure

Transducer, Harvard Apparatus, Holliston, MA, USA). Arterial blood samples were taken during baseline, the first hypoxic episode, and at 15, 30 and at 60 min post-AIH and analyzed for partial pressures of O_2 (PO_2) and CO_2 (PCO_2) using a blood gas analyzer (ABL80 Flex, Radiometer, Brea, CA).

Through a dorsal approach, the left phrenic nerve was isolated, distally cut, desheathed, and covered with a saline soaked cotton ball until it was placed on a bipolar silver electrode (described in the following section). Because isoflurane dampens phrenic nerve output, a minimum of 1 hour was allowed following the conversion to urethane anesthesia before neurophysiological recordings began to eliminate this effect.

In vivo Neurophysiological Recordings

The left phrenic nerve was submerged in mineral oil and placed on bipolar silver electrodes to record nerve activity. Neural signals were amplified (10,000 ×), band-pass filtered (300–10,000 Hz, Model 1800, A-M Systems, Carlsborg, WA, USA), full-wave rectified, and integrated (50 ms time constant, MA-821, CWE Inc., Ardmore, PA, USA). Integrated nerve bursts were digitized (8 kHz) and analyzed using a WINDAQ data acquisition system (DATAQ Instruments, Akron, OH, USA). Apneic and recruitment thresholds were determined at least 1-hour post urethane anesthesia conversion. First, ventilation was increased and P_{ETCO2} was reduced until rhythmic nerve bursts had ceased (*i.e.*, apneic threshold). After 1 minute of nerve cessation, the ventilator rate was decreased and P_{ETCO2} was slowly increased until the resumption of rhythmic nerve bursts occurred (*i.e.,* recruitment threshold). To establish baseline conditions, P_{ETCO2} was held approximately 2 mmHg above the recruitment threshold until stabilization of neural activity had occurred

(≥15 min). A baseline arterial blood sample was taken to document baseline blood gas levels. Following baseline measurements, rats were exposed to three 5-min episodes of isocapnic (±1.5 mmHg) acute intermittent hypoxia [10% inspired O_2, arterial PO_2 (PaO_2): 35–45 mmHg] separated by 5-min intervals of baseline O_2 conditions (50% inspired O_2, PaO_2: ≥150 mmHg). Rats were returned to baseline inspired O_2 levels after the third bout of hypoxia, and inspired O_2 levels were maintained for the duration of the experiments. Manipulation of inspired CO_2 and/or the ventilation rate was done to maintain isocapnic arterial PCO_2 ($PaCO_2$) within ±1.5 mmHg of the respective baseline value.

To test the hypothesis that inflammation plays a role in the differential pLTF observed in 7d and 28d CTB-SAP treated rats, rats were intraperitoneally (i.p.) injected with (S)-(+)-ketoprofen (keto; 12.5 mg/kg; Sigma-Aldrich, St. Louis, MO) or vehicle (veh; 50% ethanol and sterile saline; 100 µl/kg). 7d control treated groups included two groups that received AIH treatment: 1) keto (n=7), and 2) keto veh (n=6); and two groups that received no AIH treatment (time controls; TCs): 1) keto TC (n=3), and 2) keto veh TC (n=4). 28d control treated groups included two groups that received AIH treatment: 1) keto (n=7), and 2) keto veh (n=5); and two TC groups: 1) keto TC (n=4), and 2) keto veh TC (n=4). 7d CTB-SAP treated groups included two groups that received AIH treatment: 1) keto (n=6), and 2) keto veh (n=6); and two TC groups: 1) keto TC (n=3), and 2) keto veh TC (n=3). 28d CTB-SAP treated groups included two groups that received AIH treatment: 1) keto (n=8), and 2) keto veh (n=5); and two TC groups: 1) keto TC (n=4), and 2) keto veh TC (n=3). Since there were no apparent differences in TC groups (no AIH), and multiple previous studies demonstrating minimal experimental drift in time control experiments, all TC treated rats were grouped together per treatment (*i.e.,* keto and keto

veh) within control and CTB-SAP rats for statistical analyses. In this way, we were able to assure that drugs or vehicle did not elicit unexpected pMF (*i.e.*, a time-dependent drift in time control experiments), while minimizing animal use consistent with national standards for animal research. Approximately 3h after keto or keto veh delivery, animals were exposed to either AIH or no AIH (TC), and phrenic nerve activity was recorded for 60 min after AIH or sham AIH.

Immunohistochemistry

Tissue used for staining was obtained from a separate set of rats than those used for the current neurophysiological studies that did not receive any drug treatment during neurophysiological experiments. Immediately following neurophysiological protocols, rats were transcardially perfused with cold 4% paraformaldehyde in phosphate buffered saline (0.1 M PBS, pH 7.4). Spinal cords were immediately removed following perfusion, post-fixed (4% paraformaldehyde in 0.1 M PBS) at 4°C overnight, and then cryoprotected in graded sucrose (20% sucrose for 3 days and 30% sucrose for an additional 3 days) at 4°C until sinking. The spinal cords were transversely sectioned (40 μm thick) using a freezing-sliding microtome (Leica SM 2000R, Germany), and stored at -20°C in an antifreeze solution (30% glycerol, 30% ethylene glycol, 40% PBS). To evaluate microglial morphology in the phrenic motor nucleus of 7d and 28d control and CTB-SAP rats, six sections from C4 were selected for each animal (n=8 per group).

Tissue was washed with 1X PBS three times for five minutes on a shaker at room temperature. Sections were then incubated at room temperature in a blocker solution (1X PBS + 0.2% Triton + 5% normal donkey serum) on a shaker for one hour. Sections were

then incubated in primary antibody solution (1X PBS + 0.1% Triton + 5% normal donkey serum + antibody against CTB (goat, 1:2000, Calbiochem) and Cd11b (mouse 1:500, Bio-Rad)) overnight at 4°C on a shaker as conducted previously(Nichols et al., 2015b). The following day, tissue was washed three times for five minutes at room temperature on a shaker in 1X PBS. The tissue was then incubated for two hours at room temperature on a shaker in the dark in secondary antibody solution (1X PBS + 0.1% Triton + 5% normal donkey serum + donkey anti-goat Alexa-Fluor 555 (1:1000; Molecular Probes, Eugene, OR) and donkey anti-mouse Alexa-Fluor 488 (1:1000; Molecular Probes, Eugene, OR)). Tissue was then washed again while covered in 1X PBS three times for 5 minutes on a shaker at room temperature. The tissue was then mounted on positively charged glass slides (Thermo Fisher Scientific, Waltham, MA) and allowed to dry before ProLong™ Gold anti-fade reagent (Thermo Fisher Scientific, Waltham, MA) was applied, and a coverslip was put onto the slides. Covered slides were stored at 4°C until quantification of microglial morphology was performed.

Imaging

Photomicrographs were taken at the same settings for all images per antibody per group (*i.e.*, gains for images: 555 (CTB) = 744.95, 488 (Cd11b) = 799.11). The photomicrographs were taken using a Leica DM4000 confocal microscope at 20x magnification with Leica Application Suite X (LAS X) software to encompass the CTB-labelled phrenic motor neurons in the C4 cervical spinal cord (Boulenguez et al., 2007; Mantilla et al., 2009; Nichols et al., 2015b; Watson et al., 2009). Images were taken as 8-bit stacks at a resolution of 1024 x 1024 (366.67µm x 366.67µm).

Morphological Analysis of Microglia using IMARIS

Z stacks of all photomicrographs from all animals were opened in IMARIS software. The ROI set for the phrenic motor nucleus in the C4 sections was then used to create an ROI surface through the stack to incorporate 3D microglial projections. Once the high-resolution 3D surface was created, the CD11b+ cells were masked to eliminate background pixilation in order to more appropriately trace microglial processes. Starting points were then placed in the cell body of each microglia within the ROI. Seed points were then placed along the projections and the software automatically created a skeleton of the projections so 3D morphological attributes could be quantified. Filament length sum (primary projections from cell body), branch length (secondary projections), branch volume sum, filament volume sum, number of branches, number of end-points, filament distance from the origin sum, and the number of microglia within the ROI were quantified. Quantifications for each parameter were performed per microglia within the ROI. The microglial parameters were then averaged across microglia within the ROI and averaged per animal (n=8 animals per group). A decrease in filament length sum, branch length, number of branches, number of end-points, filament distance from the origin, in addition to an increase in filament and branch volume would be indicative of amoeboid morphology. A Sholl analysis was also performed to quantify the branching density for each microglia within the ROI based on the number of intersections the branches make with a series of concentric circles ($1\mu m$ apart). From the Sholl analysis, the process maximum (N_m, the maximum number of intersections for the cell), and the critical value (Cr, the distance from the cell body where N_m occurred) per microglia were evaluated. These parameters were then averaged across microglia in the ROI, and then averaged per

animal and subsequently per group. A decrease in the N_m and Cr would be indicative of amoeboid morphology.

qRT-PCR for inflammatory-associated marker expression

Cervical (C3-5, which encompasses the phrenic motor nucleus) expression of inflammatory-associated markers was evaluated in control and CTB-SAP rats that did not receive ketoprofen in order to characterize the inflammatory response following CTB-SAP-induced respiratory motor neuron loss. Rats were first perfused intracardially with 1X PBS, and the C3-5 spinal cord was isolated from each rat immediately after perfusion. Tissue homogenate samples were resuspended in TRI-reagent (Invitrogen, Waltham, MA), which was followed by total RNA isolation according to the manufacturer's instructions. qRT-PCR was then used to determine TNF-α, BDNF, iNOS, IL-10, IL-6, and Arg-1 gene expression. First, the RNA (1μg) prepared from tissue samples of individual rats was reverse-transcribed into first-strand cDNA using an oligo(dT)/random hexamer cocktail and M-MLV Reverse Transcriptase (Invitrogen, Waltham, MA). The cDNA was then used for qRT-PCR using iTaq^{tm} Universal SYBR® Green Supermix (BioRad Laboratories, Hercules, CA), forward and reverse primers (primer sequences that were utilized are listed in Table 1), and DEPC water. Primer specificity was assessed through NCBI BLAST analysis prior to use, and all dissociation curves had a single peak with an observed melting temperature consistent with the intended amplicon sequences. Relative gene expression normalized to 18S was determined by the ΔΔCt method, and data was expressed as the fold change relative to 18S expression.

Statistical Analysis

Integrated phrenic nerve burst amplitudes were averaged over 1 min during baseline and 15, 30, and 60 min after AIH. Peak integrated inspiratory phrenic nerve bursts at baseline were similar within treatment groups; thus nerve bursts were normalized to baseline measurements to appropriately quantify the magnitude of pLTF (expressed as a percentage change from baseline). Statistical comparisons between treatment groups for AIH studies (amplitude, $PaCO_2$, PaO_2, and mean arterial pressure) were done using a two-way ANOVA with a repeated-measures design. Since there were no differences between successive hypoxic exposure within groups ($p > 0.05$, data not shown), comparisons of the short-term hypoxic phrenic response were made using a one-way ANOVA, in which phrenic burst amplitude during the fifth minute of hypoxic episodes was averaged from all three episodes. For TC rats receiving no AIH exposure, a two-way ANOVA with repeated-measures design was performed; since there were no differences among them, they were grouped into single TC groups per treatment *(i.e.,* keto and keto veh) within control and CTB-SAP rats (keto veh TC control, n=8; keto veh TC CTB-SAP, n=6; keto TC control, n=7; keto TC CTB-SAP, n=7). A one-way ANOVA was used when comparing phrenic nerve burst amplitudes across groups at 60 min post-hypoxia. For parameters evaluated using IMARIS software in the phrenic motor nucleus, the 7d and 28d control and CTB-SAP rats were grouped together in their respective treatment groups because no differences were observed between time points within each treatment. A *t*-test was then performed to compare control to CTB-SAP rats. When significant ANOVA differences were detected, individual comparisons were made with Fisher's least significant difference post hoc test (Sigma Plot version 13.0; Systat Software Inc., San Jose, CA, USA). Differences between

the groups were considered significant if $p < 0.05$; all values are expressed as means ± S.E.M.

4.4- RESULTS:

Blood gases and mean arterial pressures

Despite small but significant differences within and across groups for $PaCO_2$, arterial PCO_2 ($PaCO_2$) was successfully maintained within 1.5 mm Hg from its baseline value in all groups (Table 4.2). Therefore, changes in integrated phrenic nerve burst amplitude following AIH is not attributed to differences in chemoreceptor feedback (changes >1.5 mmHg of baseline in $PaCO_2$ can influence pLTF; Bach and Mitchell, 1996). For AIH, PaO_2 was successfully regulated within the target range (35-45 mmHg), and remained above 150 mmHg at all time points post-hypoxia (Table 4.2). As expected, mean arterial pressure differed among groups when AIH *vs*. TCs were compared during hypoxic episodes, and slight but significant differences within groups were <20 mmHg at 60 mins post-hypoxia, and this was consistent among groups (Table 4.2; changes in mean arterial pressure of <20 mmHg from baseline values have minimal effect on respiratory activity in rats (Walker and Jennings, 1995; Bach and Mitchell, 1996)). Thus, the differential pLTF expression observed was not affected by differences in $PaCO_2$, PaO_2, or blood pressure regulation.

Short-term hypoxic phrenic responses

Since phrenic responses were not different across hypoxic episodes within AIH treated groups (p>0.05; data not shown), responses during the three episodes were combined in each rat and then compared across treatment groups (Fig. 4.1). Time control (TC) groups

were not exposed to AIH, and did not exhibit a significant change in amplitude during the sham AIH exposure as expected (Fig. 4.1). All AIH-treated groups had hypoxic responses that were significantly increased *vs*. corresponding TC groups (Fig. 4.1; $p<0.05$). Although all AIH groups elicited significant phrenic nerve hypoxic responses, 7d CTB-SAP rats pre-treated with keto veh had a greater phrenic nerve hypoxic response *vs.* all other treatment groups exposed to AIH, regardless of time point and pre-treatment (Fig. 4.1; $p<0.05$).

Ketoprofen delivery hinders pLTF at 7d, while it enhances pLTF in 28d CTB-SAP treated rats

The purpose of the current study is to understand if COX-1 and 2 mediated inflammation plays a role in the differential pLTF observed in CTB-SAP treated rats. Representative phrenic neurograms are shown for AIH-exposed 7d and 28d CTB-SAP rats approximately 3h following keto veh or keto (Figs. 4.2A, 4.2B, 3A, 4.3B). As expected, all groups exposed to AIH elicited pLTF that was significantly greater than baseline and corresponding TCs at 60 min (Figs. 4.2C, 2D, 4.3C, 4.3D, 4.4; $p<0.05$). However, when 7d CTB-SAP rats were pre-treated with keto, pLTF was attenuated from that of 7d CTB-SAP rats pre-treated with keto veh ($p<0.05$), and appeared similar to 7d control rats that received AIH regardless of pre-treatment (Figs. 4.2C, 4.2D, 4.4; $p>0.05$). In contrast, AIH-induced pLTF was enhanced when 28d CTB-SAP rats were pre-treated with keto compared to 28d CTB-SAP rats pre-treated with keto veh and 28d controls treated with keto or keto veh (Figs. 4.3C, 4.3D, 4.4; $p<0.05$). Interestingly, the enhanced pLTF observed in 28d CTB-SAP rats pre-treated with keto was similar to that of 7d CTB-SAP rats pre-treated with keto veh (Fig. 4.4; $p>0.05$). Together, these data indicate that inflammation

125

contributes to the enhanced pLTF observed in 7d CTB-SAP rats, and is constraining pLTF in 28d CTB-SAP rats.

Microglial morphological changes are exhibited in the phrenic motor nucleus of CTB-SAP rats

Neuroinflammation is mediated primarily through glial cells (*e.g.*, astrocytes, oligodendrocytes, and microglia). Microglia are the resident immune cells of the CNS that react to injury by undergoing phenotypic changes that are affiliated with pro- and anti-inflammatory states both molecularly and morphologically. Here, we evaluated morphological changes in microglia within the phrenic motor nucleus of CTB-SAP rats *vs*. controls using IMARIS software. Consistent with our previous findings (Nichols et al., 2015b), microglial number was increased in CTB-SAP rats compared to controls (Table 4.3 & Fig. 4.5). IMARIS software was also used to evaluate parameters that are indicative of ramified or amoeboid morphological states. The software was used to three-dimensionally mask immunopositive Cd11b pixels on the microglia within the phrenic motor nucleus (Fig. 4.5 A & B). Through an automated process performed by IMARIS software, starting points were then placed on the soma of the microglia and seed points were placed along the projections of the microglia (Fig. 4.5 C & D). The microglia were then cast into a 3D object in which filament and branching parameters were calculated from the starting point. Significant decreases in filament length (μm), filament distance from the origin (μm), and number of intersections were observed in CTB-SAP rats compared to controls (p<0.05; Table 4.3). This would suggest that the microglia in CTB-SAP rats are more amoeboid-like in morphological state. However, we did not observe significant

differences in other parameters that were studied including branch length, branch number, branch volume, filament volume, number of end points, and intersection distance (p>0.05; Table 4.3).

TNF-α expression appears increased in CTB-SAP rats, while BDNF expression only appears increased in 28d CTB-SAP rats

Cervical (C3-5, which encompasses the phrenic motor nucleus) inflammatory-associated marker expression was evaluated using qRT-PCR in control rats and in rats following CTB-SAP-induced respiratory motor neuron loss. qRT-PCR was performed on homogenate C3-5 samples to quantify fold changes for the following inflammatory-associated markers: TNF-α, iNOS, IL-6, BDNF, IL-10, and Arg-1). Preliminary data (Fig. 4.6) suggests that there is an increase in TNF-α expression in both 7d and 28d CTB-SAP rats *vs*. controls. Additionally, our preliminary data suggests that BDNF expression is increased in 28d CTB-SAP rats *vs*. 7d CTB-SAP and control rats (Fig. 4.6). No other inflammatory-associated markers (iNOS, IL-6, IL-10, or Arg-1) appear to be different between groups (Fig. 4.6). These data provide insight into time-dependent cytokine expression which may explain the differences in the response to ketoprofen at these time points.

4.5- DISCUSSION:

Here, we demonstrate that inflammatory-associated markers appear to be increased and pLTF following CTB-SAP induced respiratory motor neuron loss at 7d and 28d is differentially affected following ketoprofen delivery. When bilateral intrapleural injections of CTB-SAP (25 μg) are given, respiratory motor neurons die, but breathing is maintained

(Nichols et al., 2018; Nichols et al., 2015b). AIH-induced pLTF has been shown to be enhanced in 7d CTB-SAP treated rats compared to control rats and 28d CTB-SAP treated rats (Nichols et al., 2018), and it has been shown that 7d CTB-SAP rats predominately utilize the Gs pathway for pLTF whereas 28d CTB-SAP rats utilize the Gq pathway (Borkowski and Nichols, 2020). This enhancement is no longer observed at 7d in CTB-SAP rats pre-treated with ketoprofen (Figs. 4.2D & 4.4). Conversely, pre-treatment with ketoprofen enhanced pLTF in 28d CTB-SAP treated rats (Figs. 4.3D & 4.4). In addition, we see changes in microglial expression and morphology at these different time points, indicating they may play a role in the differences in the AIH-induced pLTF observed at 7d and 28d. The major findings of this study include: 1) COX-1 and 2 signaling contributes to the enhanced AIH-induced pLTF observed in 7d CTB-SAP rats; 2) COX-1 and 2 signaling constrains AIH-induced pLTF in 28d CTB-SAP rats; 3) microglia are morphologically amoeboid-like in the phrenic motor nucleus of CTB-SAP rats; and 4) TNF-α expression appears to be increased in 7d and 28d rats, and BDNF expression appears to be increased in only 28d CTB-SAP rats.

COX-1 and 2 signaling contributes to enhanced pLTF in 7d CTB-SAP rats, while it constrains pLTF in 28d CTB-SAP rats

Our findings in the current study suggest that initiation of the enhanced pLTF observed in 7d CTB-SAP rats is mediated in part by the activation of cyclooxygenase-1 and -2 (COX-1 and COX-2) enzymes and the downstream production of proinflammatory prostaglandins. When 7d CTB-SAP rats were pre-treated with the nonsteroidal COX-1 and COX-2 inhibitor ketoprofen, AIH-induced pLTF was no longer enhanced and appeared

similar to that of control rats pre-treated with keto veh (Figs. 4.2-4.4). Conversely, when 28d CTB-SAP rats were pre-treated with ketoprofen, AIH-induced pLTF was enhanced to that of 7d CTB-SAP rats pre-treated with keto veh (Figs. 4.3, 4.4). Consistent with prior studies, ketoprofen did not have an effect on pLTF in control rats (Huxtable et al., 2013). The results in the current study show that COX-1 and 2 signaling contributes to the enhanced pLTF in 7d CTB-SAP rats, but constrains pLTF exhibited by 28d CTB-SAP rats.

The mechanism(s) by which inflammation impacts pLTF following CTB-SAP-induced respiratory motor death at 7d and 28d remains unknown. However, since CTB-SAP intrapleural injections results in cell death through apoptotic mechanisms induced by saporin, we speculate that NF-kB and MAPK-mediated transcriptional signaling (Hanamsagar et al., 2012) is increased in dying respiratory motor neurons, which then stimulates the release of circulating pro-inflammatory cytokines such as tumor necrosis factor alpha (TNF- α; Fig. 6) andinterleukin-1 beta (IL-1β) (Kreutzberg, 1996). IL-1 and TNF-α receptors are located on neurons, microglia, and astrocytes (Lampron et al., 2013; Probert, 2015) indicating that inflammatory stimulation can be sensed and evoked between multiple cell types, as well as within cell types of the same phenotype. Our preliminary data suggest cervical TNF-α expression is increased in 7d CTB-SAP rats, which may contribute to inflammation resistant pLTF at this time point. As previously mentioned, inflammation can diminish pLTF in a variety of ways, one being through IL-1 receptor activation (Hocker and Huxtable, 2018). Although we did not measure IL-β expression in this study, we speculate that an initial increase in IL-1β in 7d CTB-SAP rats could be leading to increased p38 MAPK signaling. This signaling could increase glutamate release to the postsynaptic neuron (Kotlyarov et al., 1999) and contribute to the enhanced pLTF

observed in 7d CTB-SAP rats. This same signaling pathway has been shown to be vital in the abolishment of sustained intermittent hypoxia-induced and LPS-induced pLTF (Huxtable et al., 2015; Huxtable et al., 2013) that is Gq-dependent; therefore, this may be another way 7d CTB-SAP rats are resistant to inflammation-induced pLTF depression.

Furthermore, previous studies have shown that TNF-α signaling in the spinal cord interferes with spinal plasticity by increasing the trafficking of AMPA receptors to the post-synaptic membrane leading to an up-regulation of Ca^{2+} permeable Glutamate receptor 2 (GluR2)-lacking AMPA receptors that ultimately increase postsynaptic excitability (Beattie et al., 2002). TNF-α activity has also been shown to be sufficient for pMF and is required for a form of respiratory plasticity that results from reduction in central respiratory neural activity, known as inactivity-induced phrenic motor facilitation (iPMF) (Baertsch and Baker-Herman, 2013; Baker-Herman and Strey, 2011; Mahamed et al., 2011; Strey and Baker-Herman, 2012) (Broytman et al., 2013). Therefore, it is possible that TNF-α production alone can elicit pLTF in our model of CTB-SAP-induced respiratory motor neuron loss (which may explain why we no longer see pLTF enhancement in 7d CTB-SAP rats with COX-1 and COX-2 inhibition since we may be interfering with TNF-α signaling), and we speculate that CTB-SAP rats are exhibiting TNF-α dependent iPMF.

Additionally, we observe that TNF-α and BDNF appears to be increased in 28d CTB-SAP rats. When studied in the context of hypoxia, TLR4 expression was increased on microglia through HIF-1α (hypoxia-inducible factor 1α). This then leads to the release of pro-inflammatory mediators through the nuclear factor kappa-light-chain-enhancer of activated B cells (NF-κB) pathway (Hanamsagar et al., 2012; Yao et al., 2013). Although the mechanism is unknown, the expression of TNF-α has been shown to be dependent on

hypoxia-induced COX2 activation (Xing et al., 2015). Additionally, another study found that BDNF transcription is positively regulated by TNF-α in astroglia (Saha et al., 2006). Therefore, we speculate that the increase we observe in TNF-α is contributing to the simultaneous increase in BDNF in 28d CTB-SAP rats. When studied in spinal cord injury, suppression of BDNF was actually shown to be beneficial in the fact that it limits astrocyte proliferation and prevents astrogliosis (Tu et al., 2017). It may be possible that abnormal astrocyte proliferation and cytokine production is constraining pLTF in 28d CTB-SAP rats, and this is alleviated through the inhibition of COX2 and subsequent reduction in TNF-α dependent BDNF overproduction. Future studies will focus on microglial and astrocyte cytokine release and the interactions these cytokines have with the differential mechanisms of pLTF utilized by 7d and 28d CTB-SAP rats.

Microglial morphology is impacted in CTB-SAP treated rats

Under normal conditions, microglia are considered to be in a resting state, but are continually surveying the environment with ramified branching (Parkhurst and Gan, 2010; Raivich, 2005). Upon injury, microglia migrate to the site of injury and begin to undergo morphological changes that can be pro-inflammatory or anti-inflammatory. The number of microglia in the phrenic motor was significantly increased in CTB-SAP rats compared to controls when evaluated with IMARIS software (Table 4.3 & Fig. 4.5), which is consistent with our previous study (Nichols et al., 2015b). When we evaluated microglial morphological parameters using IMARIS software in the phrenic motor nucleus, we found that CTB-SAP rats had decreased primary branching and a smaller number of branch

intersections using the Sholl analysis, which is indicative of a more amoeboid-like morphological state compared to the microglia observed in controls.

Lastly, *in vitro* research has shown that serotonin and ATP facilitate microglial migration (Krabbe et al., 2012). Thus, it is possible that CTB-SAP-induced respiratory motor neuron death could lead to the release of ATP and signal microglial migration to respiratory motor nuclei. However, microglia are not the only cell types involved in neuroinflammation. Astrocytes should also be evaluated for their density, morphology, and molecular changes in CTB-SAP rats, since astrocytes are increased in neurogenerative disease models following respiratory motor neuron loss (Howland et al., 2002).

Significance

Since inflammation differentially affects AIH-induced pLTF at different time points following respiratory motor neuron death, future directions will be focused on understanding which underlying pro- and anti-inflammatory factors are produced by microglia in these motor nuclei in CTB-SAP treated rats. Additionally, we will focus on determining whether these factors impact pLTF and breathing (*e.g.,* contribute *vs*. constrain). Inflammatory responses (and associated cell types) following respiratory motor neuron death must be investigated further to better understand when and what type of intervention would be beneficial to improve breathing following respiratory motor neuron loss. Furthermore, by understanding differences in the mechanisms involved and the impact of inflammation on respiratory plasticity and breathing, we can more accurately treat patients with nonsteroidal drugs throughout varying stages of respiratory motor neuron loss.

4.6- ACKNOWLEDGEMENTS:

4.7- AUTHOR CONTRIBUTIONS:

Gene Name	Forward sequence (5')	Reverse sequence (5')
18s	CGGGTGCTCTTAGCTGAGTGTCCCG	CTCGGGCCTGCTTTGAACAC
TNF-α	TGCCACTTCATACCAGGAGA	CCGGAGTCCGTGATGTCTA
IL-6	GTGGCTAAGGACCAAGACCA	GGTTTGCCGAGTAGACCTCA
IL-10	AAGTGATGCCCCAGGCAGAGAA	AAATCGATGACAGCGTCGCAGC
Arginase-1	CCACGGTCTGTGGGAAAAGCCAAT	TTGCCATACTGT GGTCTCCACCCA
BDNF	CCCATCACAATCTCACGGTAATC	TGCGGAGGGTCTCCTATGAA
iNOS	AGGGAGTGTTGTTCCAGGTG	TCTGCAGGATGTCTTGAACG

Table 4.1: Primer sequences for qRT-PCR analyses.

Experimental Groups	P_{aCO_2} (mmHg)			P_{aO_2} (mmHg)			MAP (mmHg)		
	baseline	hypoxia	60 min	baseline	hypoxia	60 min	baseline	hypoxia	60 min
With AIH									
Keto veh									
7d CON	46.9±1.2	47.2±0.9	46.9±1.1	287±7[ab]	42.2±1.2[c]	258±16[a]	118±6	97±16	117±17
7d CTB-SAP	49.6±1.3	49.3±1.1	49.5±1.4	312±6[abcf]	39.8±1.3[c]	270±11[a]	108±5	85±8	101±8
28d CON	46.1±0.7[b]	45.9±0.6	47.4±0.4[a]	314±12[af]	42.8±1.2[c]	297±11[a]	106±7	87±11	98±6
28d CTB-SAP	46.7±1.7	46.4±1.7[e]	47.1±1.3	311±5[acf]	38.8±2.7[c]	288±13[a]	123±8[a]	80±16	108±6[a]
Keto									
7d CON	46.8±1.2	47.1±1.3	47.4±0.9	290±5[a]	40.9±2.0[c]	270±13[a]	104±6[a]	73±9[c]	124±21[a]
7d CTB-SAP	49.3±2.0[b]	48.3±1.3	50.7±1.4[a]	268±30[a]	36.0±1.9[c]	247±31[ad]	106±4[a]	80±5	92±17[g]
28d CON	47.9±1.0	48.5±1.2	48.3±1.5	306±10[a]	39.4±0.6[c]	295±13[af]	106±12	91±7[c]	86±12[gh]
28d CTB-SAP	50.1±1.1[d]	50.4±0.9[d]	50.7±1.0	316±4[abcf]	40.6±1.8[c]	280±11[a]	109±6[a]	75±6[c]	92±6[gh]
Without AIH (TCs)									
CON keto veh	49.4±1.6	49.3±1.8	49.7±1.7	290±13	293±11	279±7	108±3	108±5	105±4
CTB-SAP keto veh	49.2±0.8	49.8±1.0	49.3±1.1	254±18	271±11	279±11	108±6	109±6	110±6
CON keto	50.3±1.6[d]	50.2±1.7[d]	50.5±1.4	306±6	304±7	287±7	123±3	120±5	107±9
CTB-SAP keto	49.4±1.5	49.6±1.5	49.1±1.4	256±27	264±28	260±20	125±13	105±7	105±5

Table 4.2: Arterial PCO$_2$, PO$_2$ and mean arterial pressure (MAP) during baseline, hypoxia (HX) and 60 minutes post-hypoxia for control and CTB-SAP treated rats with acute intermittent hypoxia (AIH) or without AIH (time-control or TC). Rats received intrathecal delivery of ketoprofen (keto) or keto vehicle (veh). Significant differences within groups included *versus* hypoxia ([a]), and 60 min ([b]), and across groups included *versus*: respective TC ([c]), keto veh 28d CON ([d]), keto 28d CTB-SAP ([e]), keto 7d CTB-SAP ([f]), keto 7d CON ([g]), and keto veh 7d CON ([h]). Values are expressed as means ± 1 S.E.M. Differences were considered significant if p<0.05.

Phrenic Motor Nucleus	Control	CTB-SAP
Branch length (μm)	7.94 ± 0.11	7.90 ± 0.07
Branch number	5.44 ± 0.33	4.59 ± 0.32
Branch volume sum (μm^3)	50.2 ± 1.17	52.3 ± 1.03
Filament length sum (μm)	104 ± 4.50	89.1 ± 5.08[a]
Filament volume sum (μm^3)	656 ± 29.6	587 ± 35.8
Filament distance from the Origin sum (μm)	273 ± 3.15	264 ± 2.81[a]
Number of end-points	7.96 ± 0.38	6.88 ± 0.40
Number of microglia	7.33 ± 0.66	14.2 ± 1.29[a]
Number of intersections	5.83 ± 0.18	5.06 ± 0.18[a]
Intersection distance (μm)	7.91 ± 0.24	7.51 ± 0.26

Table 4.3. Morphology of microglia within the phrenic motor nucleus in control and CTB-SAP rats. Morphological parameters were averaged for each group, and compared between control and CTB-SAP treated rats. Significant decreases were observed for filament length sum (μm), filament distance from the origin sum (μm), and the max number of intersections in CTB-SAP rats *vs*. controls, while the number of microglia was significantly increased in CTB-SAP rats *vs*. controls ([a]).
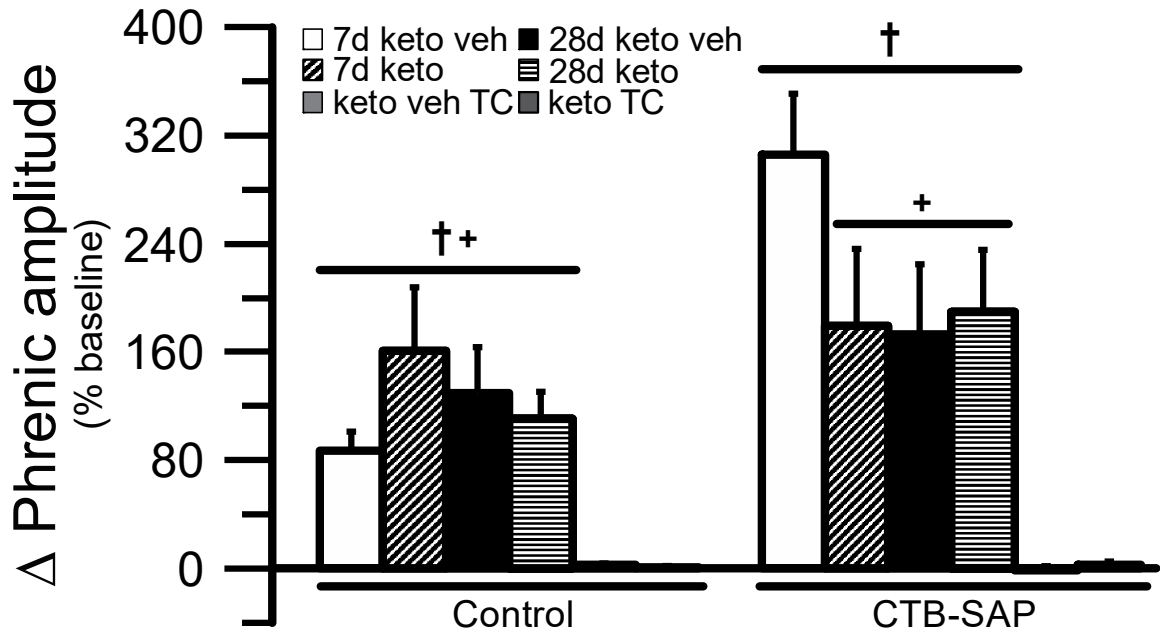
Figure 4.1: Short-term phrenic nerve hypoxic response in 7d & 28d control and CTB-SAP treated rats. Short-term phrenic nerve hypoxic responses were compared in 7d and 28d control and CTB-SAP treated rats pre-treated with ketoprofen (keto) or keto vehicle (keto veh). As expected, all treatment groups exposed to AIH had a significantly greater hypoxic response *vs.* the corresponding time control (TC) groups (†). 7d CTB-SAP rats pre-treated with keto veh had a greater phrenic nerve hypoxic response *vs.* all other treatment groups exposed to AIH (+).

Figure 4.2: pLTF in 7d treated rats. A & B, Representative traces of compressed, integrated phrenic nerve activity before and after AIH in 7d CTB-SAP rats pre-treated with keto veh (**A**) or keto (**B**). Baseline is indicated in each trace by a white, dashed line. AIH elicits an enhanced pLTF in 7d CTB-SAP rats pre-treated with keto veh, while pLTF appears to be more moderate with keto pre-treatment. **C, D**. Phrenic burst amplitude (expressed as a percent change from baseline) in 7d control (**C**) and 7d CTB-SAP (**D**) rats pre-treated with keto veh, keto veh TC, keto, or keto TC. pLTF was significantly increased from baseline (*) at all time points in 7d control rats pre-treated with keto and at 30 and 60 min post-hypoxia in those pre-treated with keto veh. pLTF was significantly increased from respective TCs at 60 min (†) in 7d control (**C**) and CTB-SAP (**D**) rats pre-treated with keto or keto veh. pLTF was significantly increased from baseline (*) at all time points in 7d CTB-SAP rats pre-treated with keto veh and at 60 min for those pre-treated with keto. 7d CTB-SAP rats pre-treated with keto had a pLTF that was significantly less than that of 7d CTB-SAP rats pre-treated with keto veh (#).
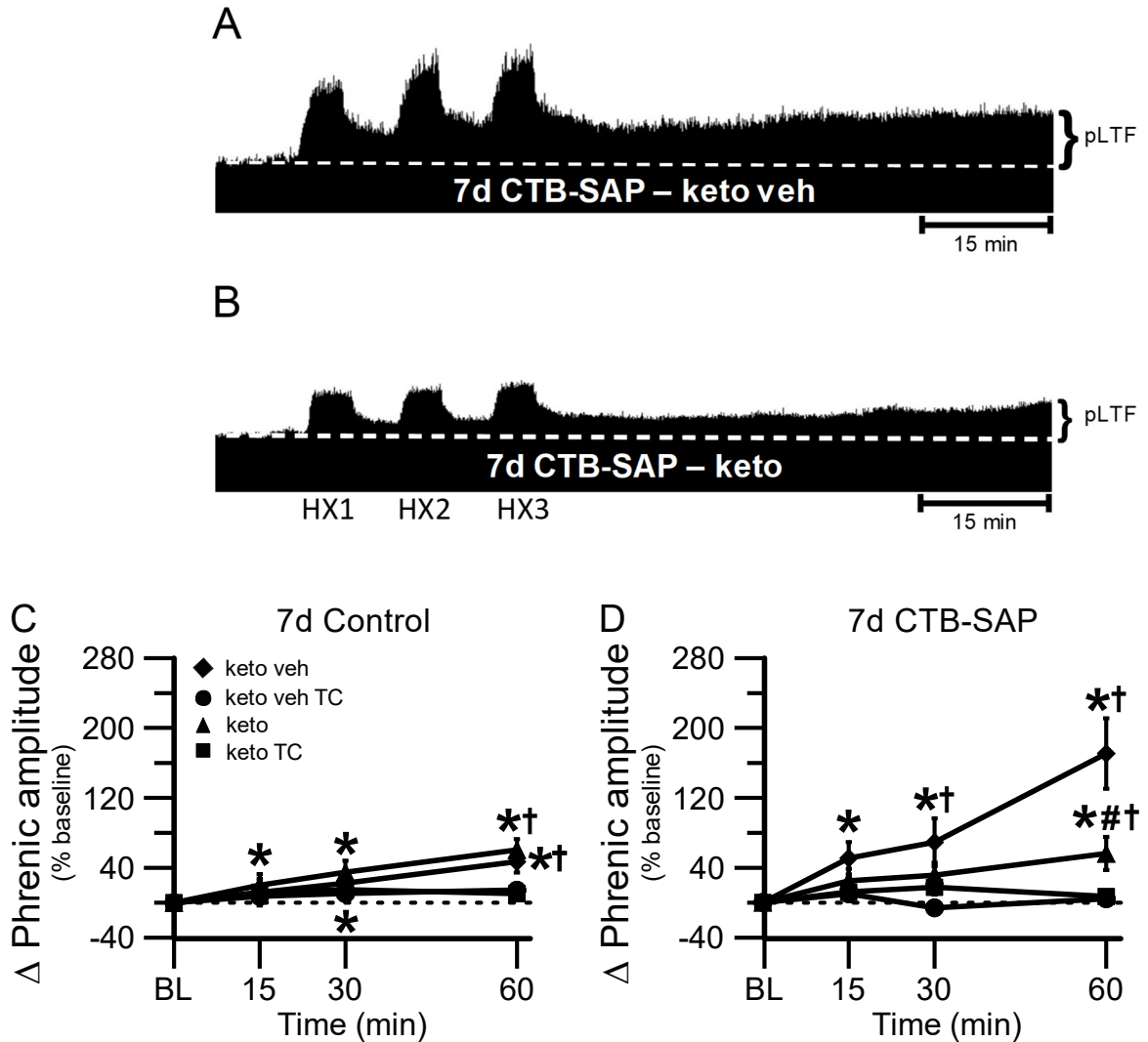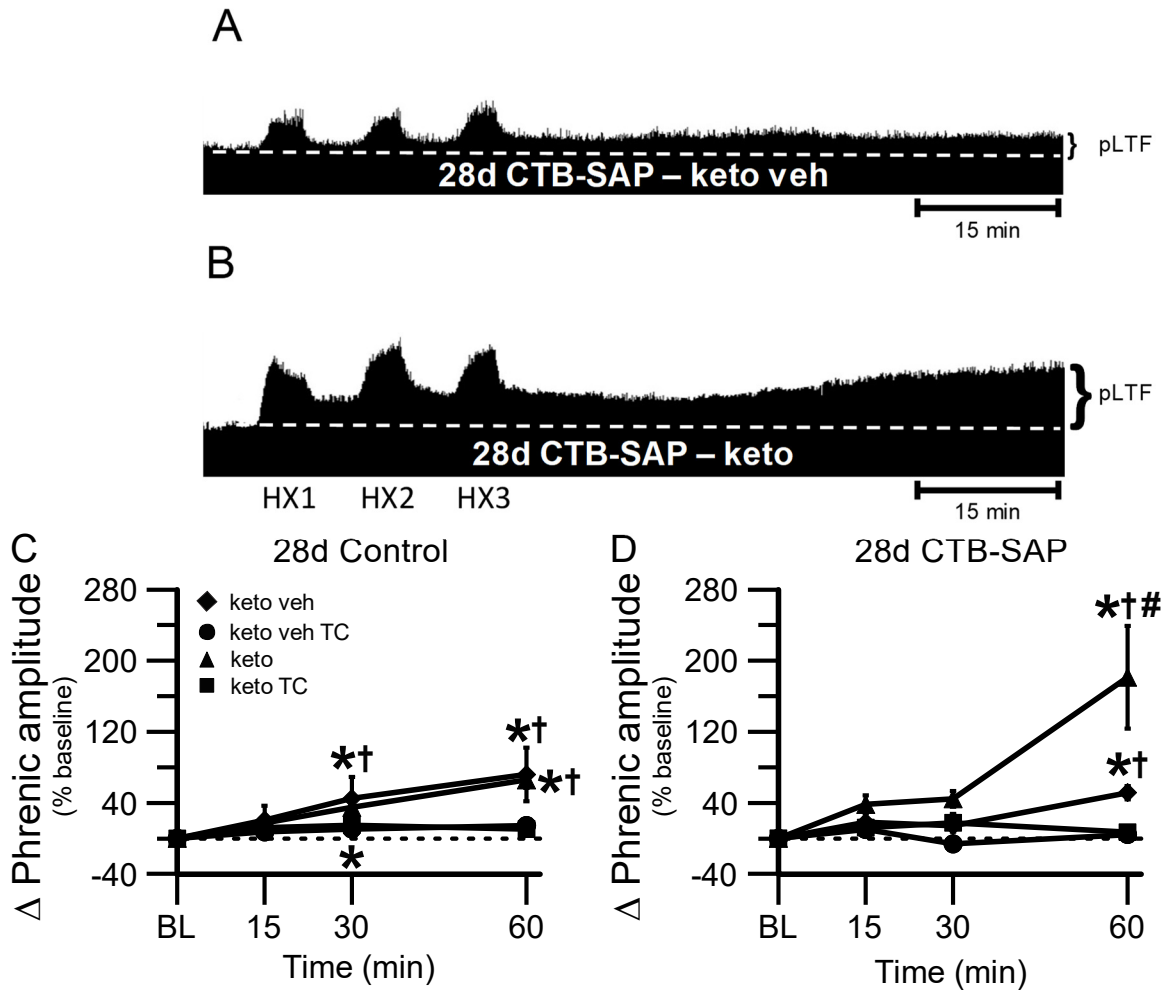
Figure 4.3: pLTF in 28d treated rats. A & B, Representative traces of compressed, integrated phrenic nerve activity before and after AIH in 28d CTB-SAP rats pre-treated with keto veh (**A**) or keto (**B**). Baseline is indicated in each trace by a white, dashed line. AIH elicits an enhanced pLTF in 28d CTB-SAP rats pre-treated with keto, while pLTF appears to be more moderate with keto veh pre-treatment. **C, D**. Phrenic burst amplitude (expressed as a percent change from baseline) in 28d control (**C**) and 28d CTB-SAP (**D**) rats pre-treated with keto veh, keto veh TC, keto, or keto TC. pLTF was significantly increased from baseline (*) at 30 and 60 min in 28d control rats pre-treated with keto veh and keto, and 60 min in 28d CTB-SAP rats with the same pre-treatments. pLTF was significantly greater than respective time controls at 30 and 60 min in 28d control rats pre-treated with keto veh, and at 60 min in 28d control and CTB-SAP rats pre-treated with keto and 28d CTB-SAP rats pre-treated with keto veh (†). 28d CTB-SAP rats pre-treated with keto had a significantly greater pLTF than that of 28d CTB-SAP rats pre-treated with keto veh (#).
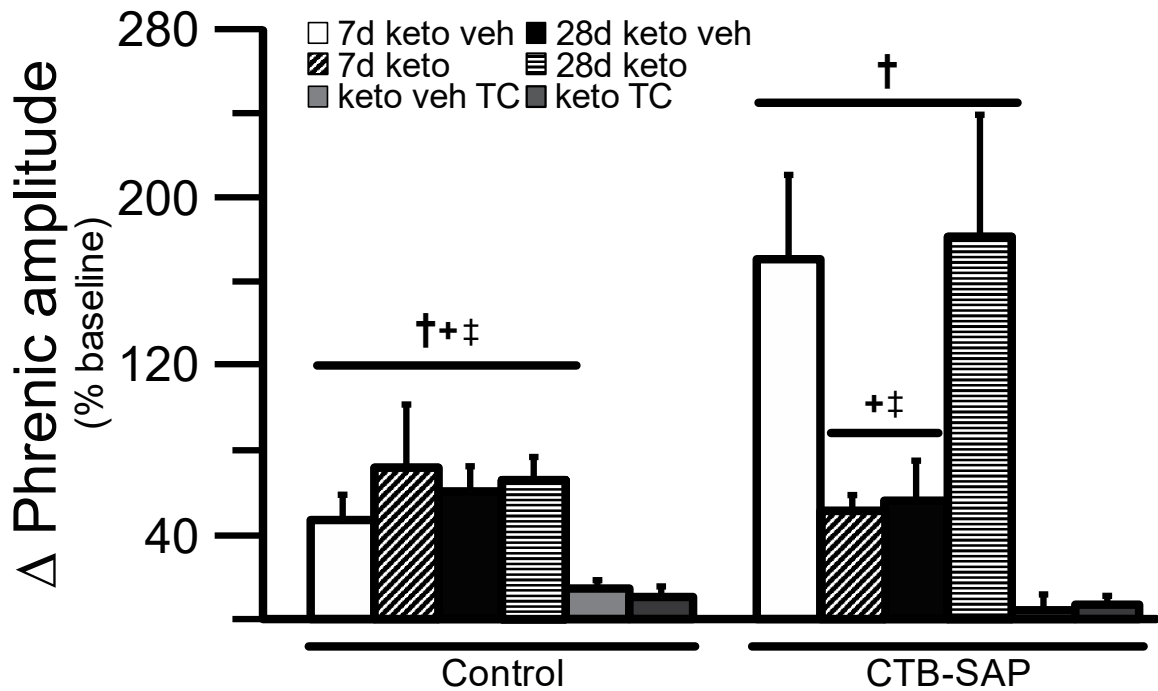
Figure 4.4: Direct comparisons of the change in phrenic amplitude (percent baseline) following AIH at 60 min post-hypoxia in 7d & 28d control and CTB-SAP treated rats. pLTF was compared in 7d and 28d control and CTB-SAP treated rats pre-treated with keto veh, keto, keto veh TC, or keto TC. 7d and 28d control and CTB-SAP rats exhibited greater pLTF *vs*. the corresponding TC groups (†). 7d CTB-SAP rats pre-treated with keto veh and 28d CTB-SAP rats pre-treated with keto had a pLTF that was significantly greater than all control groups, 28d CTB-SAP rats pre-treated with keto veh, and 7d CTB-SAP rats pre-treated with keto (+ and ‡, respectively).
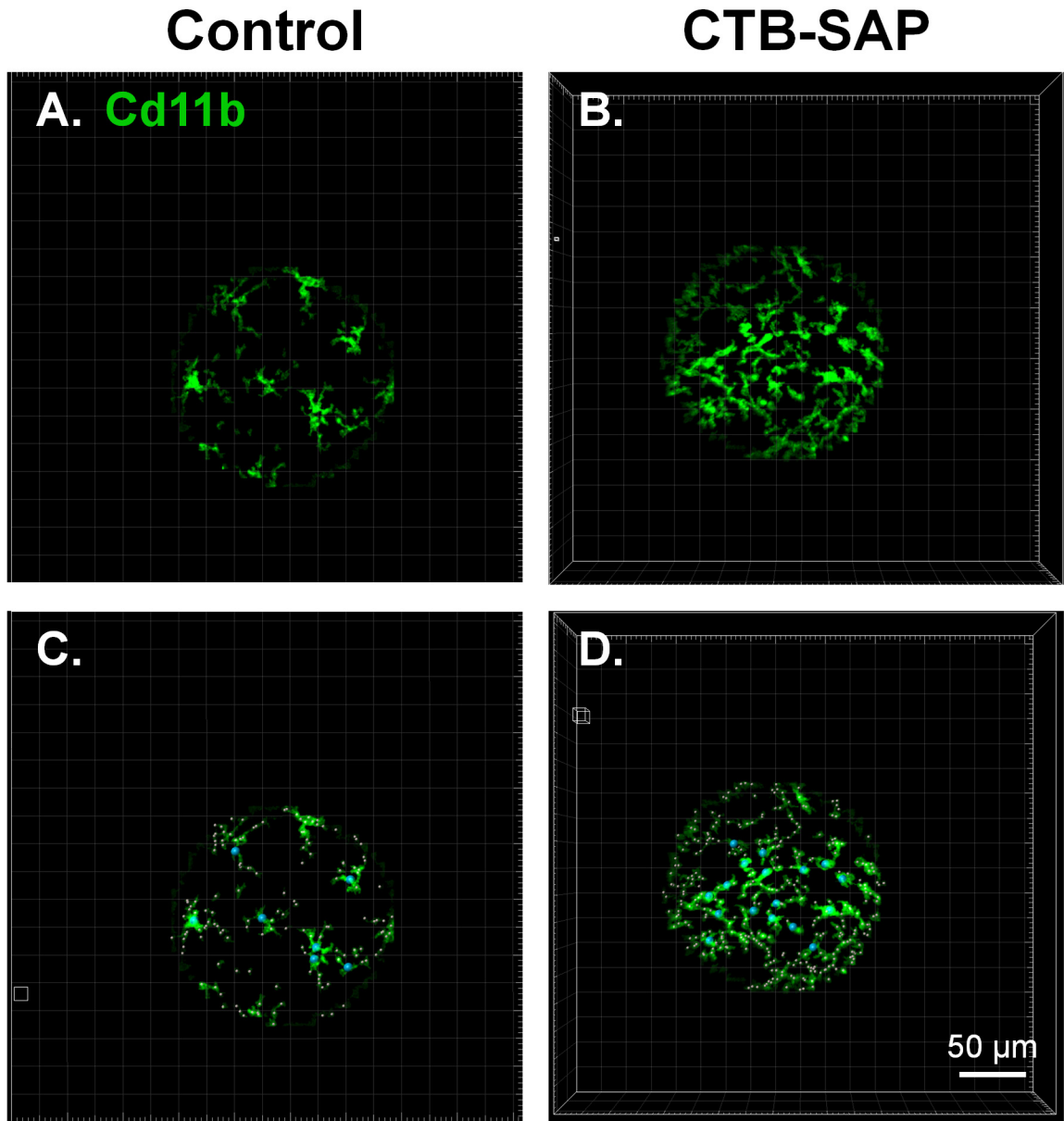
Figure 4.5. IMARIS analysis of microglial morphology in the phrenic motor nucleus in control and CTB-SAP rats. A-D. Representative images of Cd11b (green) labelled microglia within the phrenic motor nucleus from C4 cervical spinal cord segments from a control (**A & C**) and CTB-SAP (**B & D**) rat. Note, there is an increase in the number of microglia within the phrenic motor nucleus of the CTB-SAP rat as represented by the increase in green (**B**) *vs*. the control (**A**) rat. **C & D.** Images were masked to eliminate staining that was artifact, and starting points (blue circles) were inserted on the soma of the microglia. Seed points (pink small circles) were then inserted along the projections, and the IMARIS software then calculated various parameters related to filament and branch length and thickness. The closer the seed points are to the starting point, the shorter the projections are from the soma of the microglia, which is indicative of an amoeboid morphological state as depicted in CTB-SAP rats (**B & D**).
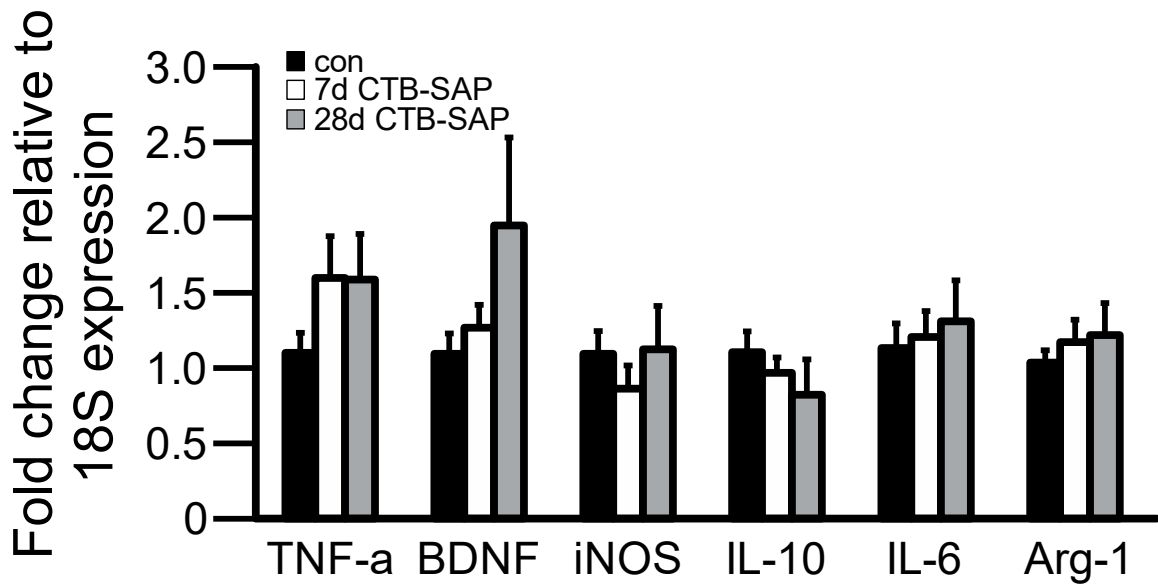
Figure 4.6. Cervical (C3-5) inflammatory-associated marker expression in control and CTB-SAP rats. Pro- and anti-inflammatory cytokine expression was evaluated in homogenate cervical spinal cord (C3-5) tissue encompassing the phrenic motor nucleus. Preliminary data thus far suggests that TNF-α expression is increased in 7d and 28d CTB-SAP rats *vs.* controls. In addition, BDNF expression also appears to be increased in 28d CTB-SAP rats *vs.* control and 7d CTB-SAP rats.

CHAPTER 5: Utilization of pectoralis minor accessory inspiratory muscles in a rodent model of respiratory motor neuron loss

Lauren F. Borkowski and Nicole L. Nichols

Department of Biomedical Sciences, Dalton Cardiovascular Research Center, University of Missouri, Columbia, MO 65211

Abbreviated Title: Pectoralis minor muscle utilization in CTB-SAP rats

5.1- ABSTRACT

In a novel model of respiratory motor neuron death [adult rats intrapleurally injected with cholera toxin B conjugated to saporin (CTB-SAP) which selectively eliminates phrenic and intercostal motor neurons], eupnea is maintained despite deficits in maximal ventilatory capacity. We hypothesized that the maintenance of eupnea following CTB-SAP-induced respiratory motor neuron loss may occur through the recruitment of accessory inspiratory muscles (*e.g.*, the pectoralis minor). Although not normally utilized during eupnea, these muscles become engaged during increased ventilatory demand, such as with exercise, injury, or disease (*e.g.*, ALS), to actively elevate the ribs upward and outward to move the chest wall. To test this hypothesis, we: 1) studied pectoralis minor output *via* electromyography (EMG) in anesthetized, spontaneously breathing control and CTB-SAP intrapleurally injected rats; and 2) studied breathing using whole-body plethysmography in awake, unanesthetized rats and pectoralis minor muscle output with EMG in anesthetized, spontaneously breathing control and CTB-SAP intrapleurally and intramuscularly injected rats. We found that pectoralis minor muscle activity is recruited but is not required for eupnea following CTB-SAP-induced respiratory motor neuron death. This indicates that the pectoralis minor muscles are not solely responsible for breathing maintenance, but may still be utilized in conjunction with other accessory muscles prior to ventilatory failure.

5.2- INTRODUCTION

Inspiration is primarily attributed to the diaphragm because it accounts for 70-80% of inspiratory tidal volume (Benditt, 2006; Hruska Jr, 1997). The diaphragm is a dome-shaped muscle at the base of the intrapleural cavity, separating the intrapleural space from the abdominal cavity. During inspiration, the diaphragm contracts, and the central tendon becomes more fixed as the dome flattens and moves downwards. This increases the pressure in the abdominal cavity while decreasing its volume and causes the vaulting outward of the abdominal wall (Kendall and Kendall, 1993). In addition, the scalene muscle groups are considered by some as primary inspiratory muscles because they are active during inspiration at all times to lift and expand the rib cage (De Troyer and Estenne, 1984), but are considered as secondary inspiratory muscles by others because they are not the main muscle used for tidal volume (Grassino et al., 1978; Saboisky et al., 2007). Although the diaphragm is the primary muscles of inspiration, secondary (accessory) inspiratory muscles can also be recruited to maintain tidal volume.

When there is an increase in respiratory demand (e.g. exercise, chronic obstructive pulmonary disease, etc.) or in cases of functional reduction of the primary inspiratory muscle (e.g. spinal cord injury (SCI), ALS, etc.), the accessory muscles (internal and external intercostals, parasternal intercostals, sternocleidomastoid, scalenes, pectoralis major and minor, serrati and trapezii) can become recruited to actively elevate the ribs upward and outward to move the chest wall and assist in tidal volume maintenance (Grassino et al., 1978; Hruska Jr, 1997; Loring and De Troyer, 1985). However, diseases and injuries resulting in the loss of respiratory motor neurons greatly impact phrenic nerve output to the diaphragm, and eventually ventilatory deficits and, ultimately, death ensue

(Bye et al., 1990)., However, breathing is maintained through mechanisms of compensation and the recruitment of the aforementioned accessory inspiratory muscles until disease or injury becomes too severe.

To study the impact of motor neuron loss on breathing, we use an inducible model of respiratory motor neuron loss in which cholera toxin B conjugated to saporin (CTB-SAP) is injected into the intrapleural space. CTB-SAP is taken into resident respiratory motor neurons and targeted death begins to occur within 3 days. Phrenic and intercostal motor neuron death is significantly greater in 7d and 28 CTB-SAP rats *vs*. controls (receiving unconjugated CTB + SAP) (Nichols et al., 2015b). Despite this significant loss in respiratory motor neurons and phrenic motor output, CTB-SAP rats are able to maintain eupnea and only experience breathing deficits during maximal chemosensory stimulation (Nichols et al., 2015b). Because this model recapitulates breathing maintenance despite respiratory motor neuron loss, we can investigate the recruitment of other accessory inspiratory muscles, specifically the pectoralis minor muscle. Therefore, we speculate that accessory inspiratory muscles (*e.g.*, the pectoralis minor) are recruited to maintain breathing to compensate for the loss of phrenic and intercostal motor neurons.

The pectoralis minor muscle is of particular interest in our model because the medial and lateral pectoral nerves originate from motor neurons located primarily in the ventral horn of the C5/C6 region of the cervical spinal cord (Aszmann et al., 2000; Moosman, 1980). In our model, we induce selective phrenic motor neuron death in the C3-6 cervical spinal cord with an intrapleural CTB-SAP injection. Therefore, we hypothesized that: 1) pectoralis minor muscle motor neurons are in close proximity to the phrenic motor nucleus in adult rats; 2) pectoralis minor muscle output is increased following intrapleural

CTB-SAP-induced respiratory motor neuron loss; and 3) pectoralis minor muscle motor neuron survival, pectoralis minor muscle activity, and breathing are all decreased following intramuscular (pectoralis minor) CTB-SAP injection.

5.3- METHODS

Animals

Experiments were conducted on adult (3–4 months old) male Sprague Dawley rats (Envigo Colony 208; Indianapolis, IN). Rats were housed in pairs and maintained under a 12:12 light:dark cycle. Animals had access to a standard commercial pelleted diet and water *ad libitum*. All procedures in this manuscript were approved by the Institutional Animal Care and Use Committee at the University of Missouri in accordance with National Institutes of Health Guide for the Care and Use of Laboratory Animals. The University of Missouri is an AAALAC-accredited institution that operates under Animal Welfare Assurance ID A3394-01.

Intrapleural and Pectoralis Minor Muscle Injections

Rats received bilateral intrapleural injections (6mm deep, fifth intercostal space) using a 50 µl Hamilton syringe and a custom needle (6 mm, 23 gauge, semi-blunt to prevent lung puncture) while under isoflurane anesthesia (1.5% in 100% oxygen as previously described by Mantilla et al. (2009). Control rats were intrapleurally injected with cholera toxin B subunit (CTB; 20 µg dissolved in doubly distilled H_2O; Calbiochem; Billerica, MA) unconjugated to saporin (SAP; 25 µg dissolved in phosphate buffered saline (PBS Advanced Targeting Systems; San Diego, CA) to enable comparisons for pectoralis minor

muscle recruitment. CTB conjugated to saporin (CTB-SAP; 25 µg dissolved in PBS; Advanced Targeting Systems; San Diego, CA) was intrapleurally injected to target respiratory motor neurons as described previously (Nichols et al., 2015; 2018; Borkowski and Nichols, 2020). To determine the requirement of the pectoralis minor muscle for the maintenance of eupnea, rats were bilaterally intrapleurally and intramuscularly (in the pectoralis minor muscle) injected with either control (CTB + SAP) or CTB-SAP under the conditions described above. Rats also received an additional bilateral injection of CTB conjugated to AlexaFluor 647 (CTB-AF647; intrapleural; 5 µg per side) and CTB conjugated to AlexaFluor 488 (CTB-AF488; intramuscularly, pectoralis minor muscle; 5 µg per side) for retrograde tracing. Rats were then monitored for 24 hours following the injections to ensure respiration was not compromised following intrapleural injections, and were housed for 7 or 28 days before electromyography was performed in only intrapleurally injected 7d and 28d control and CTB-SAP rats (n= 15 per group); or before bilaterally intrapleurally and intramuscularly injected (pectoralis minor muscle) control (n=7), 7d CTB-SAP (n=5) or 28d CTB-SAP (n=7) rats underwent whole-body plethysmography and electromyographical experiments as described below.

Whole-Body Plethysmography

Whole-body plethysmography was performed in awake, freely-moving rats to evaluate quantitative breathing measurements with altered inspired gas concentrations (gas concentrations controlled by Flow Commander, Therapeutiq Research, De Soto, KS). Rats were placed in a whole-body flow-through plethysmograph (Data Sciences International, St. Paul, MN) 7d or 28d post- intrapleural and intramuscular (pectoralis minor muscle)

injection of control or CTB-SAP. The rats acclimated to the chamber while breathing room air (21% O_2, balance N_2; flushed at ~ 3 L/min) for 15 minutes before ventilatory measurements were recorded for baseline conditions for an additional 15 minutes. Rats were then exposed a hypoxic + hypercapnic gas mixture (10.5% O_2/7% CO_2; 15 min). A pressure calibration signal, ambient and chamber pressures, and rat body mass were used to calculate breath-by-breath tidal volume (VT) (Drorbaugh and Fenn, 1955; Jacky, 1978), respiratory frequency, mean inspiratory flow (VT/Ti), minute ventilation ($\dot{V}E$), inspiratory time (Ti), expiratory time (Te), peak inspiratory flow (PIF), and peak expiratory flow (PEF). VT, $\dot{V}E$, and VT/Ti are reported normalized to body mass (per 100 g). Data were rejected if there was evidence of pressure fluctuations caused by gross body movements or sniffing behavior. At the conclusion of the study, rats were removed from the chambers and they were prepared for surgery for electromyographical experiments.

Surgical Preparation and in vivo Electromyographical Experiments

Rats were initially anesthetized using 4% isoflurane and the isoflurane was adjusted to maintain a spontaneous respiration rate of 60 breaths per minute ($\sim$ 2.5% isoflurane in 100% oxygen) throughout the brief surgical preparation. Rats were tracheotomized and cannulated in the femoral artery and vein for taking arterial blood gas samples and for urethane conversion, respectively. Urethane conversion (1.85 g kg^{-1}, *i.v.* infused at 6 ml/hr) then began in the supine position, and isoflurane was withdrawn to maintain a minimum respiratory rate of 60 breaths per minute. Once converted, a midline cut was made from the bottom to the top of the sternum and the skin was retracted to expose the entire left pectoralis minor muscle. The rat was then placed in the prone position in a mouth

clamp with the head of the rat turned 45° with an alligator clip slightly lifting the left front arm to stabilize the chest and arm of the animal, and an alligator clip attached to an arm of an immobile stand was used to secure a bipolar electrode during recording.

Once a consistent amplitude for the pectoralis minor muscle was established and the rat had been off isoflurane for at least 45 minutes (length of time the animal was under isoflurane for the surgical procedure and conversion to urethane), baseline recordings began. Pectoralis minor muscle recordings were collected in rats that were exposed to 30% FiO_2 for 20 minutes (PaO_2 ~150 mmHg; baseline) before being exposed to maximum chemosensory stimulation (hypoxia + hypercapnia; FiO_2 10.5% + $FiCO_2$ 10.5%; max) for five minutes.

Immunohistochemistry

A subset of naïve rats (n=3) were bilaterally injected into the pectoralis minor muscle with 5 µl per side of cholera toxin B subunit (CTB; 20 µg dissolved in doubly distilled H_2O; Calbiochem; Billerica, MA) to determine the location of the pectoralis minor muscle motor neurons within the ventral horn of the cervical spinal cord and their proximity to the phrenic motor nucleus. After 7d, rats were transcardially perfused with cold 4% paraformaldehyde in phosphate buffered saline (0.1 M PBS, pH 7.4). Spinal cords were immediately removed following perfusion, post-fixed (4% paraformaldehyde in 0.1 M PBS) at 4°C overnight, and then cryoprotected in graded sucrose (20% sucrose for 3 days and 30% sucrose for an additional 3 days) at 4°C until sinking. Transverse sections (40 µm thick) of the spinal cord were then collected using a freezing-sliding microtome (Leica SM 2000R, Germany), and stored at -20°C in an

antifreeze solution (30% glycerol, 30% ethylene glycol, 40% PBS) until immunohistochemistry was performed.

Six sections of tissue from C4-C7 were placed into wells and washed with 1X PBS three times for five minutes on a shaker at room temperature. Sections were then incubated at room temperature in a blocker solution (1X PBS + 0.2% Triton + 5% normal donkey serum) on a shaker for one hour. Sections were then incubated in primary antibody solution (1X PBS + 0.1% Triton + 5% normal donkey serum + antibody against CTB (goat, 1:2000, Calbiochem) and NeuN (mouse polyclonal, 1:500, Millipore) overnight at 4°C on a shaker as conducted previously (Nichols et al., 2015b). On the following day, tissue was washed three times for five minutes at room temperature on a shaker in 1X PBS. The tissue was then incubated for two hours at room temperature on a shaker in the dark in secondary antibody solution (1X PBS + 0.1% Triton + 5% normal donkey serum + donkey anti-goat Alexa-Fluor 555 (1:1000; Molecular Probes, Eugene, OR) and donkey anti-mouse Alexa-Fluor 488 (1:1000; Molecular Probes, Eugene, OR)). Subsequently, the tissue was then washed again while covered in 1X PBS three times for 5 minutes on a shaker at room temperature. The tissue was then mounted on positively charged glass slides (Thermo Fisher Scientific, Waltham, MA) and allowed to dry before ProLong™ Gold anti-fade reagent (Thermo Fisher Scientific, Waltham, MA) was applied, and a coverslip was put onto the slides. Covered slides were stored at 4°C until imaging of staining was performed.

Rats that received the intrapleural (+ CTB-AF647) and intramuscular pectoralis minor muscle (+ CTB-AF488) injections of the control (n=7) or CTB-SAP (7d and 28d; n=7 per group) were used to confirm phrenic motor neuron death and to quantify pectoralis motor neuron survival. Under sufficient urethane anesthetization, rats were immediately

perfused following electromyographical experiments as described above. Transcardial perfusion was performed with cold 4% paraformaldehyde in phosphate buffered saline (0.1 M PBS, pH 7.4). Spinal cords were immediately removed following perfusion, post-fixed (4% paraformaldehyde in 0.1 M PBS) at 4°C overnight, and then cryoprotected in graded sucrose (20% sucrose for 3 days and 30% sucrose for an additional 3 days) at 4°C until sinking. Transverse sections (40 µm thick) of the spinal cord were then collected using a freezing-sliding microtome (Leica SM 2000R, Germany), and stored at -20°C in an antifreeze solution (30% glycerol, 30% ethylene glycol, 40% PBS) until immunohistochemistry was performed. Because the CTB-AlexaFluor conjugates were already fluorescently tagged, all slicing, washing, mounting, and drying was done in the dark as to not to quench the fluorescence. Six sections were selected from C4-C7 and washed in 1X PBS three times for five minutes in the dark. Tissue was then mounted on positively charged glass slides (Thermo Fisher Scientific, Waltham, MA) and allowed to dry in the dark before ProLong™ Gold anti-fade reagent (Thermo Fisher Scientific, Waltham, MA) was applied, and a coverslip was put onto the slides. Covered slides were stored in the dark at 4°C until phrenic and pectoralis minor muscle motor neuron survival was quantified.

Imaging and Motor Neuron Counts

Photomicrographs were taken to determine the location of pectoralis minor motor neurons using a Leica DM4000 confocal microscope at 20x magnification with Leica Application Suite X (LAS X) software to encompass the putative phrenic motor nucleus in C4-C6 and CTB-labelled pectoralis motor neurons in the C4-C7 cervical spinal cord. Z-stacked (5µm

in z-plane per image) images were collected by creating a region of interest that encompassed the putative phrenic motor nucleus and pectoralis minor muscle motor neurons, and images were taken and analyzed as 8-bit stacks at a resolution of 1024 x 1024 (366.67μm x 366.67μm). CTB positive labeled cells were evaluated using ImageJ.

Similarly, for rats that received the double retrograde labeling of intrapleural CTB-AF647 and pectoralis minor muscle intramuscular CTB-488, live microscopy and photomicrographs were taken to determine the impact of CTB-SAP on pectoralis minor motor neuron survival. Z-stacked (5μm in z-plane per image) images were taken that encompassed CTB-AF647 positive phrenic motor neurons in the C4 section of the spinal cord and CTB-AF488 positive pectoralis minor muscle motor neurons in cervical sections C5-C7. Images were taken and analyzed as 8-bit stacks at a resolution of 1024 x 1024 (366.67μm x 366.67μm). CTB-647 positive phrenic motor neurons and CTB-AF488 pectoralis minor muscle motor neurons that were identified by positive staining of the cell body and a visible nucleus were manually quantified using ImageJ within the ventral horn by scrolling through the stack. The number of CTB-AF647 and CTB-AF488 motor neurons were counted from all rats in each group and compared between CTB–SAP and control rats using Microsoft Excel to allow for graphical and statistical comparisons. The number of phrenic motor neurons in the C4 segment was extrapolated from the 6 sections (length of the entire phrenic motor nucleus is ~ 2000 μm; 40 μm sections) and the number of surviving pectoralis minor motor neurons in the C5-C7 segments were extrapolated from the 6 sections (~ 6000 μm; 40 μm sections).

Statistical Analysis

Statistical comparisons between treatment groups to determine the recruitment of the pectoralis minor muscle in control and CTB-SAP rats only receiving the intrapleural injection were done using a Friedman repeated measures ANOVA on ranks design to the failure of normality. The data failed normality due to high variability in pectoralis minor muscle amplitude from animal to animal within groups and some did not pass the Grubb's outlier test, but we decided to include all data points since this is the first time the recruitment of the pectoralis minor muscle has been evaluated in a model of respiratory motor neuron death. Pectoralis minor muscle amplitude was not significantly different between control groups at baseline or max following only intrapleural injections, so only one control group (7d control) was used to evaluate pectoralis minor muscle amplitude following intrapleural and intramuscular injection. Following intrapleural and intramuscular control or CTB-SAP injection, pectoralis minor muscle amplitude was analyzed using a two-way RM ANOVA. Pectoralis minor muscle motor neuron survival in C$_5$-C$_7$ was evaluated using a One-Way ANOVA. All respiratory parameters in rats intrapleurally and intramuscularly injected with control or CTB-SAP were analyzed using a two-way RM ANOVA. Multiple linear regression analyses were performed between baseline or maximal pectoralis minor muscle amplitude with pectoralis minor muscle motor neuron survival, and baseline or maximal V_T/100g with pectoralis minor muscle motor neuron survival. When significant ANOVA differences were detected, individual comparisons were made with either a Fisher's least significant difference *post hoc* test (motor neuron survival, respiratory variables, and amplitude following intrapleural and intramuscular injections) or a Student-Newman-Keuls *post hoc* test (amplitude following

only intrapleural injections) (Sigma Plot version 13.0; Systat Software Inc., San Jose, CA, USA), and were considered significant if $p < 0.05$; all values are expressed as means ± S.E.M.

5.4-RESULTS

Pectoralis minor muscle motor neurons are in close proximity to the phrenic motor nucleus

To determine the location of the pectoralis minor muscle motor pool within the ventral horn of the cervical spinal cord, rats were intramuscularly injected with the cholera toxin B subunit for retrograde tracing. Spinal cord sections from cervical segments C4-C7 are shown in Fig. 5.1 (A-D, respectively). Pectoralis minor muscle motor neurons are labelled red (CTB) and motor neurons are labelled in green (NeuN), therefore pectoralis minor muscle motor neurons appear yellow because they are colocalized with both CTB and NeuN. The phrenic motor nucleus is present in sections C3-C6 of the adult rat spinal cord, but for the purpose of showing the location of the pectoralis minor muscle motor neurons, only C4-C7 of sections containing the putative phrenic motor nucleus (Boulenguez et al., 2007; Mantilla et al., 2009; Watson et al., 2009) and pectoralis minor motor neurons are shown. Our representative photomicrographs demonstrate that the pectoralis minor motor neurons are in close proximity to the phrenic motor nucleus, these motor neuron pools are exclusive from one another, and that the majority of pectoralis minor motor neurons exist in C5 and C6 (Fig. 5.1 B, C). Taken together, we speculate that the pectoralis minor motor neurons may respond to nearby dying phrenic motor neurons in our CTB-SAP model.

Pectoralis minor muscle output is increased following intrapleural CTB-SAP-induced respiratory motor neuron death

Compressed representative neurograms show raw pectoralis minor muscle amplitude in urethane anesthetized, spontaneously breathing control, 7d CTB-SAP, and 28d CTB-SAP rats (Fig 5.2 A-C). Pectoralis minor muscle amplitude was evaluated during baseline (normoxia; 30% FiO2) and during maximal chemosensory stimulation (max) (Fig 5.2 A-D). There were no differences in pectoralis minor muscle amplitude between 7d and 28d control rats); however these groups were separated for analysis to show time-point differences between controls and CTB-SAP rats at 7d and 28d (Fig 4.2 D). Even though 7d and 28d control rats were challenged with hypoxia + hypercapnia, pectoralis minor muscle amplitude did not increase from baseline with this challenge. During baseline, pectoralis minor muscle amplitude was increased in CTB-SAP rats compared to their respective controls ($p<0.05$). Additionally, 28d CTB-SAP rats had a significantly greater pectoralis minor muscle amplitude from 7d CTB-SAP rats at baseline ($p<0.05$). When pectoralis minor muscle amplitude was evaluated at max, we found that 7d CTB-SAP rats had a significant increase ($p<0.05$) in pectoralis minor muscle activity from its respective baseline amplitude, but that amplitude at max was not different from the respective 7d control group. During max, 28d CTB-SAP rats increased pectoralis minor muscle amplitude when challenged that was greater than any group within max and baseline conditions. These data suggest that the pectoralis minor muscle activity is recruited 7d post-CTB-SAP-induced respiratory motor neuron death, and to even a greater extent in 28d CTB-SAP rats, during baseline and max challenge.

Bilateral pectoralis minor intramuscular injections of CTB-SAP reduces motor neuron survival

We next wanted to determine if the pectoralis minor muscles were specifically recruited to maintain breathing. Therefore, we sought to eliminate pectoralis minor motor neurons in our model of CTB-SAP-induced respiratory motor neuron death following intrapleural injections. Control, 7d CTB-SAP, and 28d CTB-SAP rats were bilaterally injected with either the control or CTB-SAP (25 µg) intramuscularly into the pectoralis minor muscle in addition to their respective intrapleural injection. These injections also contained conjugated fluorescent retrograde tracers to evaluate phrenic (CTB-AF647) and pectoralis minor (CTB-AF488) motor neuron survival. We found that intrapleural injections of CTB-SAP does not impact pectoralis minor muscle motor neuron survival (data not shown). Following intrapleural and intramuscular injections of either the control (CTB + SAP) or CTB-SAP, pectoralis minor motor neuron survival in the C5-C7 cervical spinal cord was evaluated in control (Fig 5.3 A, D, G), 7d CTB-SAP (Fig 5.3 B, E, H), and 28d CTB-SAP (Fig 5.3 C, F, I) rats. Surviving and retrogradely-labeled pectoralis minor motor neurons are shown in green, and are primarily found in segments C5 and C6. As expected, bilateral intramuscular injections of CTB-SAP significantly reduced pectoralis minor motor survival in 7d (29% survival) and 28d (34% survival) CTB-SAP rats from controls ($p<0.05$).

CTB-SAP-induced pectoralis minor motor neuron death abolishes pectoralis minor muscle recruitment

Once pectoralis minor muscle motor neurons were significantly reduced following bilateral intramuscular CTB-SAP injections in the CTB-SAP intrapleural model, we wanted to assess if the pectoralis minor muscles were still recruited. Pectoralis minor muscle output using electromyography was performed in anesthetized, spontaneously breathing rats receiving both intrapleural and intramuscular injections of either the control or CTB-SAP (7d and 28d). Representative compressed neurograms of pectoralis minor muscle output are shown during baseline and max (Fig 5.4 A-C) in control, 7d CTB-SAP, and 28d CTB-SAP rats. Because we found that pectoralis minor muscle output was not different between control groups following only intrapleural injections (Fig. 5.1), we only performed EMG recordings in 7d control rats following intrapleural and intramuscular injections (Fig 5.4 A). We found that pectoralis minor muscles were no longer recruited during baseline, normoxia, exposure in CTB-SAP rats at 7d and 28d, and are not different from controls following pectoralis minor muscle motor neuron death (Fig 5.4). During max, control rats were once again not significantly recruited, and 7d CTB-SAP rats also did not recruit the pectoralis minor muscle following CTB-SAP induced pectoralis minor motor neuron death (Fig 5.3). Interestingly, 28d CTB-SAP rats receiving both the intrapleural and intramuscular injections of CTB-SAP were still able to recruit the pectoralis minor muscle at max ($p<0.05$), and this was greater than all groups during max and from its own baseline ($p<0.05$). Together, CTB-SAP-induced pectoralis minor motor neuron death eliminates pectoralis minor muscle recruitment in our model of intrapleural CTB-SAP-induced respiratory motor neuron death.

158

Pectoralis minor muscles are not required for eupnea

To determine if the recruitment of the pectoralis minor muscles were required for breathing maintenance, pectoralis minor muscle motor neurons were significantly reduced using intramuscular CTB-SAP injections in the CTB-SAP intrapleural model and breathing was evaluated using whole-body plethysmography. Briefly, awake, free-moving rats were placed in plethysmograph chamber and exposed to Baseline (normoxia) and combined hypoxia + hypercapnia (Max) following intramuscular and intrapleural injections of either the control or CTB-SAP (Fig. 5.5). Respiratory variables including tidal volume (VT; A), breathing frequency (B), minute ventilation ($\dot{V}E$; C), and mean inspiratory flow (VT/TI D) were assessed. Baseline breathing frequency was increased in 7d CTB-SAP rats from control rats ($p < 0.05$), and no deficits were observed at baseline for any of the variables in CTB-SAP rats compared to controls. All respiratory variables at max were increased from respective baseline values for all groups ($p < 0.05$). Additionally, all variables at max, except for breathing frequency, were decreased in both CTB-SAP treated groups *vs*. controls ($p < 0.05$). These deficits in breathing at max are consistent with our previous reports in rats that have intrapleural CTB-SAP-induced respiratory motor neuron loss (Nichols et al., 2015b). We also evaluated PIF, PEF, Ti, and Te (data not shown). There were no deficits observed at baseline following CTB-SAP treatment in PIF nor PEF *vs*. controls. During max, PIF was decreased in 7d CTB-SAP rats *vs*. controls and 28d CTB-SAP rats, while there was no significant difference in 28d CTB-SAP rats *vs*. controls. PEF was also decreased at max in 7d and 28d CTB-SAP rats *vs*. controls. Baseline inspiratory and expiratory time (Ti and Te, respectively) were decreased from controls in 7d CTB-SAP rats, but these deficits were no longer observed during max. Meanwhile, there was no

significant effect on inspiratory nor expiratory time at baseline nor max in 28d CTB-SAP rats *vs*. control rats. These data suggest that the pectoralis minor is not responsible for the maintenance of eupnea following intrapleural CTB-SAP-induced respiratory motor neuron loss.

Pectoralis minor motor neuron survival impacts tidal volume during maximal chemosensory stimulation

To further elucidate any impacts of pectoralis minor motor neuron death on pectoralis minor muscle amplitude or tidal volume, multiple linear regression analyses were performed. Multiple linear regression analyses were also performed to evaluate any relationship between pectoralis minor muscle amplitude and tidal volume following pectoralis minor motor neuron death. There was no significant relationship between pectoralis minor motor neuron survival and pectoralis minor muscle amplitude at baseline, nor at max ($p > 0.05$; data not shown). There was a slight trend for a relationship between pectoralis minor motor neuron survival and tidal volume at baseline (Fig 5.6 A; $p = 0.069$), there was a significant trend in the relationship between pectoralis minor motor neuron survival and tidal volume at max (Fig 5.6 B; $p = 0.049$). Pectoralis minor muscle amplitude also did not predict tidal volume following CTB-SAP-induced pectoralis minor motor neuron death at baseline, nor at max ($p > 0.05$; data not shown). Together, these data suggest that pectoralis minor motor neuron survival predicts maximal tidal volume.

5.5- DISCUSSION

To our knowledge, this is the first time the number of pectoralis minor motor neurons have been quantified in the C5-C7 spinal cord of the adult rat. Additionally, this is the first time the pectoralis minor muscle has been evaluated following CTB-SAP- induced respiratory motor neuron loss. The overall findings of this study include: 1) the pectoralis minor muscle motor neurons are found in the ventral horn of the C5-C7 spinal cord of the rat, and are exclusive from, but are in close proximity to the phrenic motor neurons; 2) pectoralis minor motor neuron survival is unaffected by intrapleural CTB-SAP-induced respiratory motor neuron loss; 3) pectoralis minor muscles are recruited during baseline and max in rats following CTB-SAP-induced respiratory motor neuron loss; 4) pectoralis minor muscle motor neurons can be selectively eliminated through intramuscular injections of CTB-SAP, and this abolishes pectoralis minor muscle recruitment; and 5) pectoralis minor muscles are not required for the maintenance of eupnea following CTB-SAP-induced respiratory motor neuron death. These overall results indicate that the pectoralis minor muscle is not a primary muscle of inspiration utilized for eupneic maintenance following CTB-SAP-induced respiratory motor neuron loss.

Pectoralis minor muscle and its implications in breathing maintenance

Here, we demonstrate that while pectoralis minor muscle activity is recruited in a rat model of CTB-SAP-induced respiratory motor neuron loss, this particular muscle group is not required for the maintenance of eupnea observed in this model. This does not eliminate a role for this muscle group in the instance of neuromuscular disease in the maintenance of eupnea. We know that with respiratory distress and loss of diaphragmatic output that

breathing switches 'thoracic breathing' to 'chest breathing' (Schleifer et al., 2002), indicating that the muscles of the shoulder girdle and neck become much more involved in the assistance of tidal volume maintenance. More specifically, sleep disordered breathing due to lack of diaphragmatic output in neuromuscular diseases leads to a poor prognosis. Better sleep and increased survival is correlated with accessory respiratory muscle recruitment during eupnea in patients with ALS compared to those patients whose accessory respiratory muscles are not recruited during eupnea (Arnulf et al., 2000). Additionally, we know that the pectoralis minor, specifically, has implications for breathing because individuals with Poland Syndrome have unilateral pectoral (major and minor) muscle hypoplasia and experience restrictive pulmonary dysfunction. This results in hypoventilation during wakefulness and sleep-disordered breathing (Cortés-Julián et al., 2017) due to the inability for the pectoralis minor muscle to sufficiently move the chest wall. Therefore, the pectoralis minor muscle does play a role in the maintenance of eupnea following neuromuscular disease, injury, and dysfunction due to its participation in chest wall movement, which is required for breathing during both physiological and pathological states.

How, when, and for how long these accessory inspiratory muscles become recruited following neuromuscular degeneration, and the neural circuits responsible for this recruitment are of high interest for exploration. Using the mouse model of ALS (SOD1^{G93A}), Romer et al. attempted to answer these questions by implanting telemetry devices with leads to the trapezii and scalene muscles. This group found that both muscles groups had high activity at rest that was correlated with breathing during early disease, but that this activity as it relates to breathing declines in late disease and the output of these

muscles are still functional but are not related to breathing. Additionally, it has been shown that glutamatergic neurons (e.g., V2a neurons) that synapse on phrenic motor neurons (Zholudeva et al., 2017) are sufficient for respiratory drive, but V2a neurons degenerate in ALS mice over the course of the disease (Romer et al., 2017). From this, it has been speculated that the loss of V2a neurons leads to a decline in excitatory drive to phrenic motor neurons throughout the disease (Romer et al., 2017). Following SCI, V2a neurons have been shown to increase their connections with phrenic motor neurons, indicating they may contribute to breathing preservation (Romer et al., 2017). During breathing at rest, the scalene and trapezius respiratory muscles are not normally active in naïve adult mice (Romer et al., 2017). When the excitability of V2a neurons was increased using designer receptors exclusively activated by designer drugs (DREADD), the scalene and trapezius respiratory muscles had increased output during normal breathing at rest (Romer et al., 2017). On the contrary, CNO injection in V2a-(G_i)DREADD mice exhibited increased bouts of trapezius and scalene activity after V2a neurons were inhibited (Jensen et al., 2019). This indicates that V2a neuron inhibition increases accessory inspiratory muscle recruitment. Further studies need to be conducted to directly link V2a neurons to the recruitment of the pectoralis minor muscle and whether increasing or decreasing their excitability contributes to recruitment of accessory inspiratory muscle recruitment and breathing maintenance in CTB-SAP rats.

Accessory muscle recruitment in other instances of labored breathing

The recruitment of pectoralis muscles and other accessory inspiratory muscles have been studied in other conditions that impact breathing such as heart failure and chronic

obstructive pulmonary disease. Patients with these diseases experience the feeling of breathlessness or shortness of breath, known as dyspnea, and can be used as a measure of prognosis and evaluation of treatment for each disease (Anzueto and Miravitlles, 2017; Sassi-Dambron et al., 1995; Zannad et al., 2013). Inspiratory dysfunction is a hallmark of heart failure, and diaphragmatic activity in patients with this disease has been of interest in recent years (Hughes et al., 1999; Kelley and Ferreira, 2017; Mancini et al., 1992; Meyer et al., 2001). In a recent study, diaphragm, scalene, and pectoralis minor muscle activity was evaluated using electromyography with surface electrodes in heart failure patients whom had entered the emergency room for dyspnea (Luiso et al., 2020). This study found that scalene and diaphragm had a significant direct relationship with the clinical dyspnea index, while pectoralis minor muscle activity did not (Luiso et al., 2020). These results are not surprising, however, because the diaphragm muscle itself is spared and was able to produce a robust signal despite the sensation of breathlessness. Therefore, once this muscle begins to become exhausted with long-term heart failure, the pectoralis minor muscle may be recruited to assist in the maintenance of eupnea. In the current study, we found that pectoralis minor muscle activity increases with CTB-SAP-induced respiratory motor neuron loss, but that these muscles are not required for eupneic ventilation. Following CTB-SAP-induced loss of pectoralis minor muscle motor neurons, breathing frequency is increased while inspiratory and expiratory time are decreased in 7d CTB-SAP *vs*. controls (Fig. 5.5). We speculate that either brainstem mechanisms are compensating for the loss of recruitment of the pectoralis minor muscles and/or that another accessory inspiratory muscle is recruited to compensate for the loss of diaphragmatic and pectoralis minor muscle output, thus resulting in no significant impact on overall eupnea in CTB-SAP rats.

Additionally, significant impact of the pectoralis minor muscles on the maintenance of eupneic breathing may not be observed because lack of diaphragmatic output has not yet become severe enough to rely on this particular accessory muscle group. Therefore, it will be important to determine if the pectoralis minor muscles become recruited when diaphragmatic output significantly decreases following CTB-SAP-induced respiratory motor neuron death in future studies.

In patients with chronic obstructive pulmonary disease, there is a progressive reduction in parenchymal elasticity and increased airflow limitations. This leads to prolonged contraction of respiratory muscles and an increased load on the respiratory muscles in an attempt to meet increased demand for ventilatory flow (Caruana-Montaldo et al., 2000; Paulin et al., 2003). A vicious cycle of increased neural and mechanical increases in ventilatory demand ensues leading to progressive severity in dyspnea. Prolonged contraction reduces contractile range of the respiratory muscles and causes mechanoreceptors in ventilatory neural networks to continue to fire to increase ventilation, which creates an even greater increase in ventilatory demand. When the pectoralis muscles were studied in COPD patients, pectoralis major and minor muscle area was less in patients with reduced lung function (severe airflow limitations), assessed by spirometry, and low resting oxygen saturations. These findings indicate a relationship between the pectoralis muscle group and respiratory mechanics. Therefore, it has been speculated that improving chest wall mobility through stretching and exercise could delay the progression of COPD in the early stages of the condition (Engel and Vemulpad, 2009). One study used surface electromyography to assess how stretching of accessory respiratory muscles (sternocleidomastoid, upper intercostals, diaphragm, and rectus abdominis) contributes to

breathing in COPD patients. This group found that with stretching, there was a decrease in respiratory effort and improved efficiency of inspiratory muscle activity. They concluded that aerobic training program, which was also used in this study, combined with respiratory muscle stretching reduces dyspnea and increases functional and ventilatory capacities in patients with COPD. Because we observe breathing deficits during maximal chemosensory stimulation following CTB-SAP-induced respiratory motor neuron loss, it may be beneficial to determine whether aerobic exercise and strengthening of the pectoralis minor muscles could correct or diminish these deficits. Additionally, it would be beneficial to study if there are any abnormalities and/or asynchrony in respiratory muscle recruitment in our model. For example, under physiological conditions, there is a slight lag between rib cage expansion and abdominal engagement to expand the chest (Heldt and McIlroy, 1987). This lag in engagement becomes greater in disease and can ultimately result in uncoordinated paradoxical breathing where the abdomen moves outward as the chest moves inward, leading to breathing deficits (Gaultier et al., 1987). This paradoxical breathing may be occurring following CTB-SAP-induced respiratory motor neuron loss during maximal chemosensory stimulation leading to breathing deficits, that may be corrected with pectoralis minor muscle strengthening.

#

Significance

The current study investigated the role of the pectoralis minor muscle following CTB-SAP-induced respiratory motor neuron loss. Even though we saw an increase in baseline pectoralis minor muscle output activity, we found that these muscles are not necessary for eupneic maintenance. However, pectoralis minor muscle activity may be indicative of

166

neuromuscular disease prognosis, and its potential synergistic contributions with other accessory inspiratory muscles in the maintenance of breathing should not be ignored. The pectoralis minor muscles, and other muscles of the shoulder girdle, could be targeted through stimulation or exercise/stretching to maintain ventilation late in neuromuscular disease and should be investigated.

5.6- NEW & NOTEWORTHY

To the best of our knowledge, this is the first time accessory inspiratory muscle (*e.g.,* pectoralis minor) output has been studied specifically in the context of respiratory motor neurons loss following intrapleural CTB-SAP injection. Although pectoralis minor activity is recruited, it is not required for breathing maintenance following CTB-SAP-induced respiratory motor neuron loss. This study furthers our understanding of the contribution of the pectoralis minor muscles following motor neuron loss.

5.7- ACKNOWLEDGEMENTS

5.8- GRANTS

5.9- AUTHOR CONTRIBUTIONS

Author contributions: L.F.B. and N.L.N. in conception and design of research; L.F.B. performed experiments; L.F.B. and N.L.N. analyzed data; L.F.B. and N.L.N. interpreted results; L.F.B. prepared figures; L.F.B. drafted manuscript; and L.F.B. and N.L.N. edited, revised, and approved final version of manuscript.
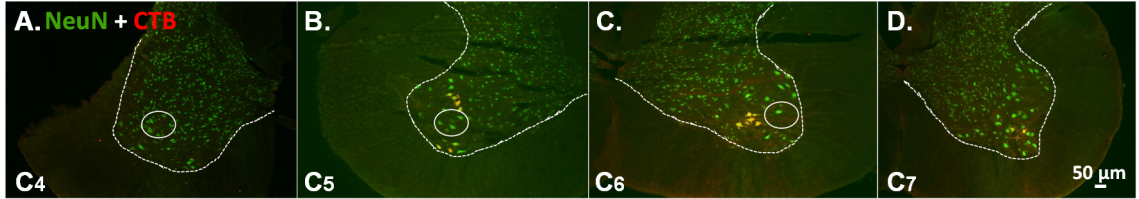
Figure 5.1: Location of the pectoralis minor muscle motor neurons in adult rats. A-D. The representative photomicrographs at 10x magnification depict spinal cord segments C4-C7 from a naïve rat, where the gray matter is outlined by a white dashed line and the putative phrenic motor nucleus is outlined by a white circle. CTB (red) was injected bilaterally into the pectoralis minor muscle group, neurons were labelled with NeuN (green), and double-labelled (CTB+NeuN) pectoralis minor muscle motor neurons appear yellow. Note, the representative photomicrographs depict that the putative phrenic motor nucleus is located in segments C4-C6 (**A-C**), and the pectoralis minor muscle motor neurons are located in segments C5-C7 and are in close proximity to the putative phrenic motor neurons (**B-D**).
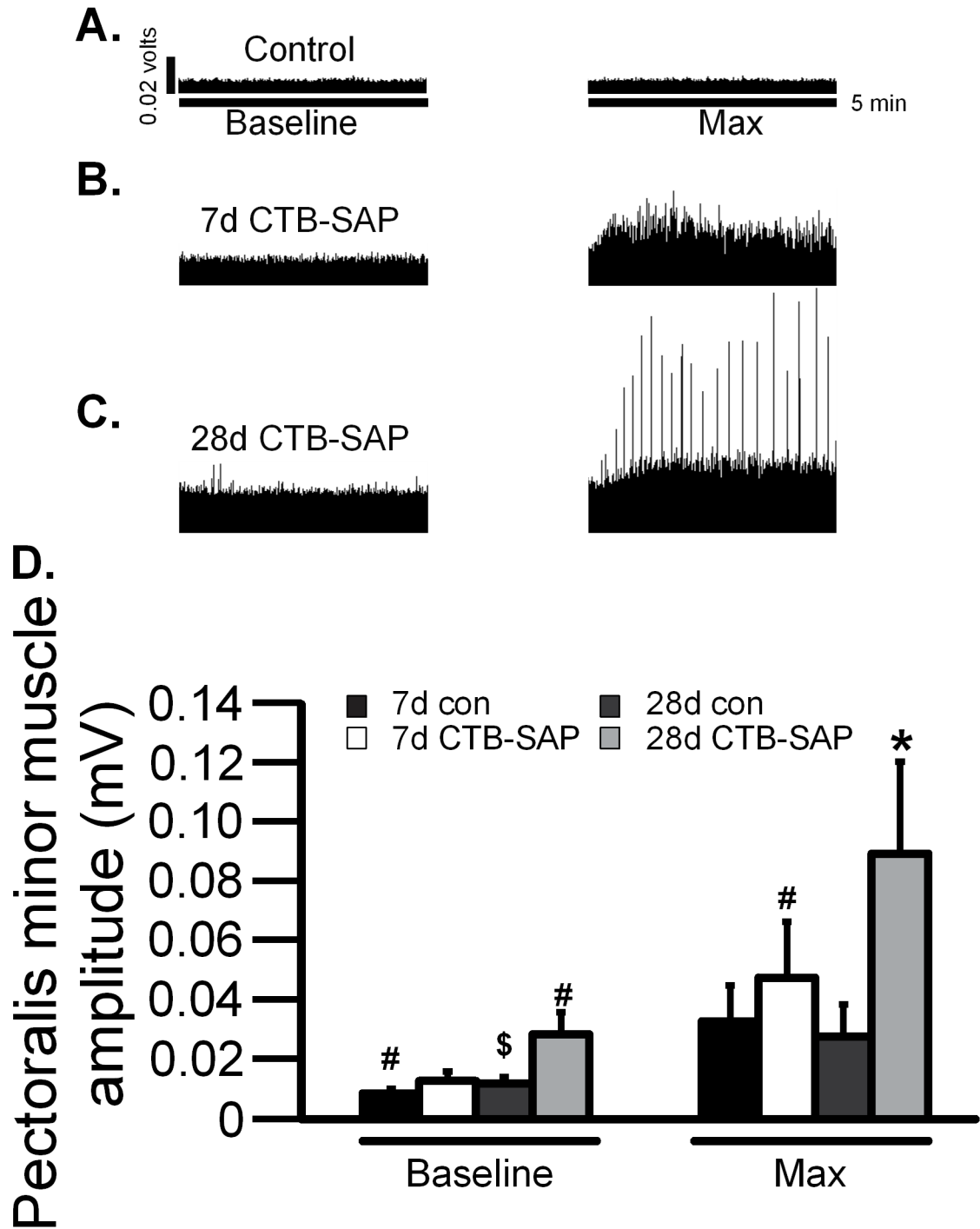
Figure 5.2: Pectoralis minor muscle output following intrapleural control or CTB-SAP injections in adult rats. A-C. Representative traces of integrated pectoralis minor muscle amplitude in control (**A.**), 7d CTB-SAP (**B.**), and 28d CTB-SAP (**C.**) rats. Spontaneous pectoralis minor muscle activity was recorded in all rats during normoxia (baseline) and in response to maximum chemosensory stimulation (max; hypercapnia + hypoxia). Large spikes indicate augmented breaths in the representative trace from the 28d

CTB-SAP rat. **D.** Pectoralis minor muscle output was measured and compared in 7d and 28d intrapleurally injected control (con; black and dark gray bars, respectively) and CTB-SAP (white and light gray bars, respectively) rats during baseline and max. Baseline pectoralis minor muscle amplitude in 7d and 28d CTB-SAP rats was greater than their respective controls, and baseline amplitude in 28d CTB-SAP rats was greater than that of 7d CTB-SAP rats (# *vs*. 7d CTB-SAP at baseline; $ *vs*. 28d CTB-SAP rats at baseline). Pectoralis minor muscle amplitude was significantly increased at max in 7d CTB-SAP rats *vs*. its respective baseline (#), and 28d CTB-SAP rats elicited a greater pectoralis minor muscle amplitude at max *vs*. all other groups during baseline and max (*). Values are expressed as means ± SEM, and all significant differences are p<0.05.

Control **7d CTB-SAP** **28d CTB-SAP**

A. CTB-AF488   B.   C.

C5

D.   E.   F.

C6

G.   H.   I.

C7

50 µm

J.

Figure 5.3: Pectoralis minor motor neuron survival following intrapleural and intramuscular control or CTB-SAP injections in adult rats. A-J. Representative photomicrographs at 20x magnification depict surviving pectoralis minor motor neurons (green; CTB-AlexaFluor488; CTB-AF488) from C5 (**A-C),** C6 (**D-F**), and C7 (**G-I**) spinal cord segments from intrapleurally and intramuscularly (pectoralis minor muscle) injected control (**A,D,G**), 7d CTB-SAP (**B,E,H**), and 28d CTB-SAP (**C,F,I**) rats. Note, the paucity of surviving pectoralis minor motor neurons in the CTB-SAP rats (**B,C,E,F,H,I**) *vs.* the control rat (**A,D,G**). **J.** Quantification of the number of surviving pectoralis minor motor neurons in cervical spinal cord segments C5-C7 (the length of the pectoralis motor nucleus) in control (white bar), 7d CTB-SAP (dark grey bar), and 28d CTB-SAP (black bar) treated rats. 7d and 28d CTB-SAP treated rats had significantly less surviving motor neurons compared to controls (* *vs.* control; $p<0.05$). All values are expressed as the mean $\pm$ SEM.

A.

0.02 volts

Control

Baseline

Max

5 min

B.

7d CTB-SAP

C.

28d CTB-SAP

D.

Pectoralis minor muscle amplitude (mV)

con
7d CTB-SAP
28d CTB-SAP

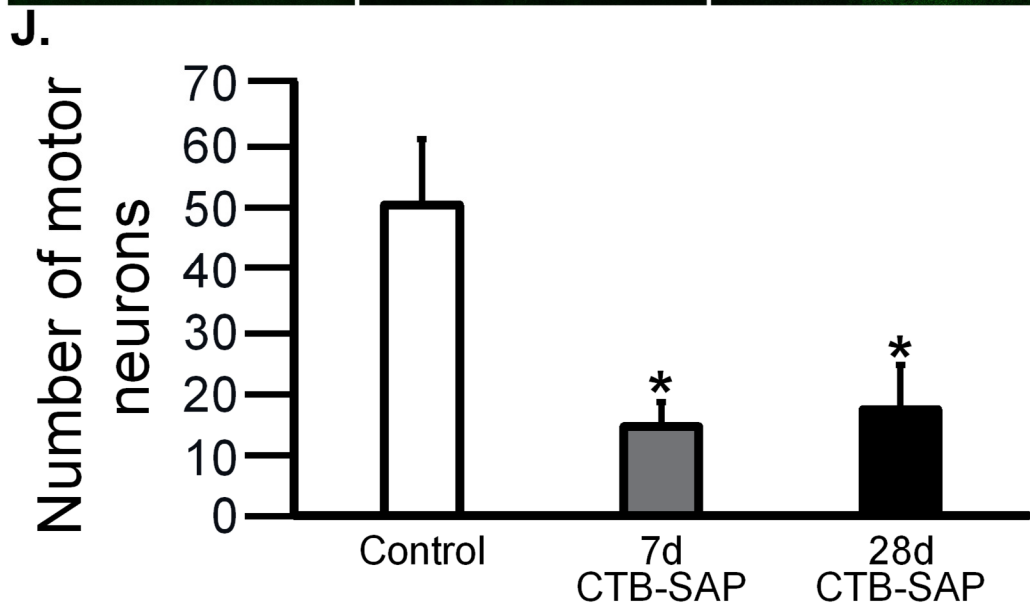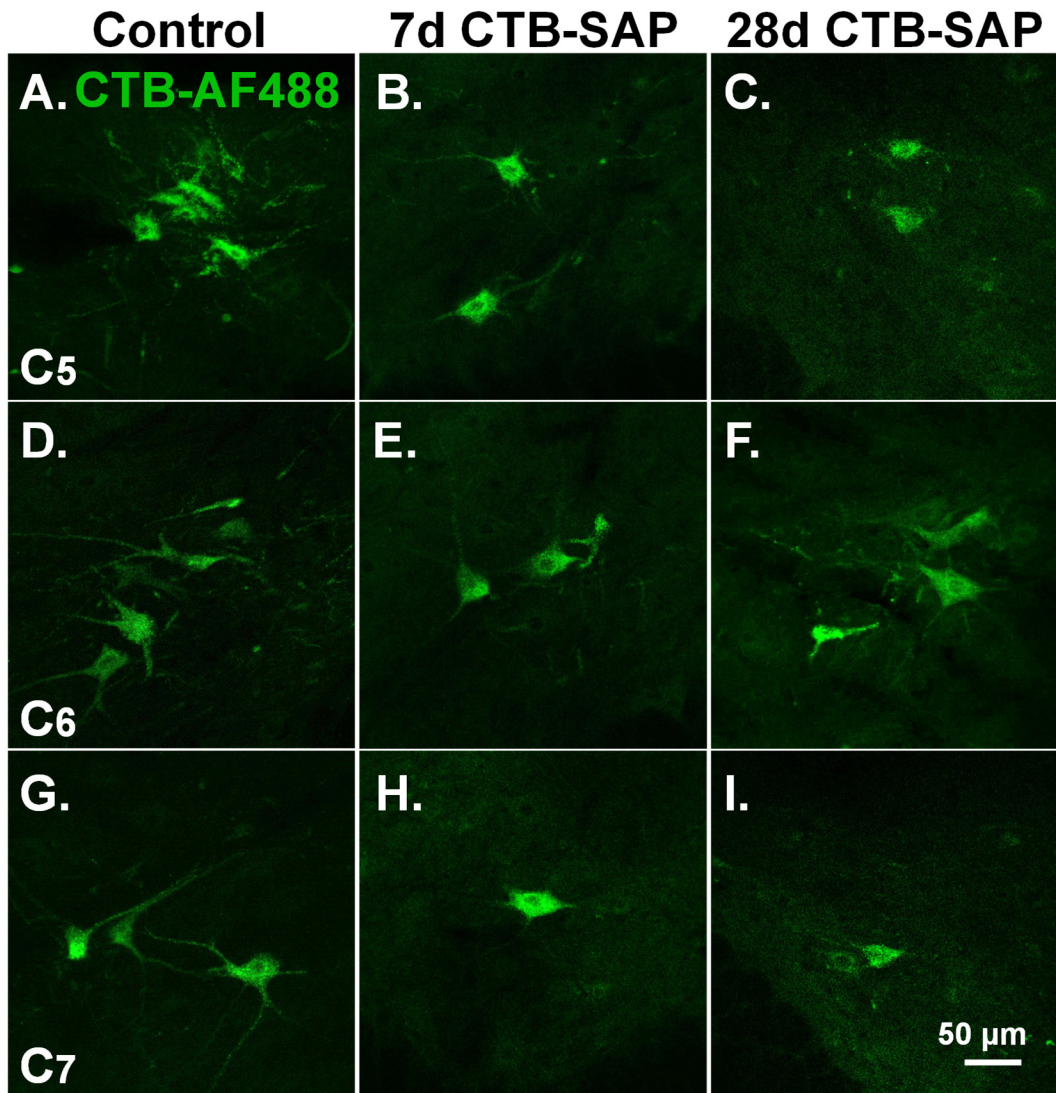Baseline

Max

*

+ +
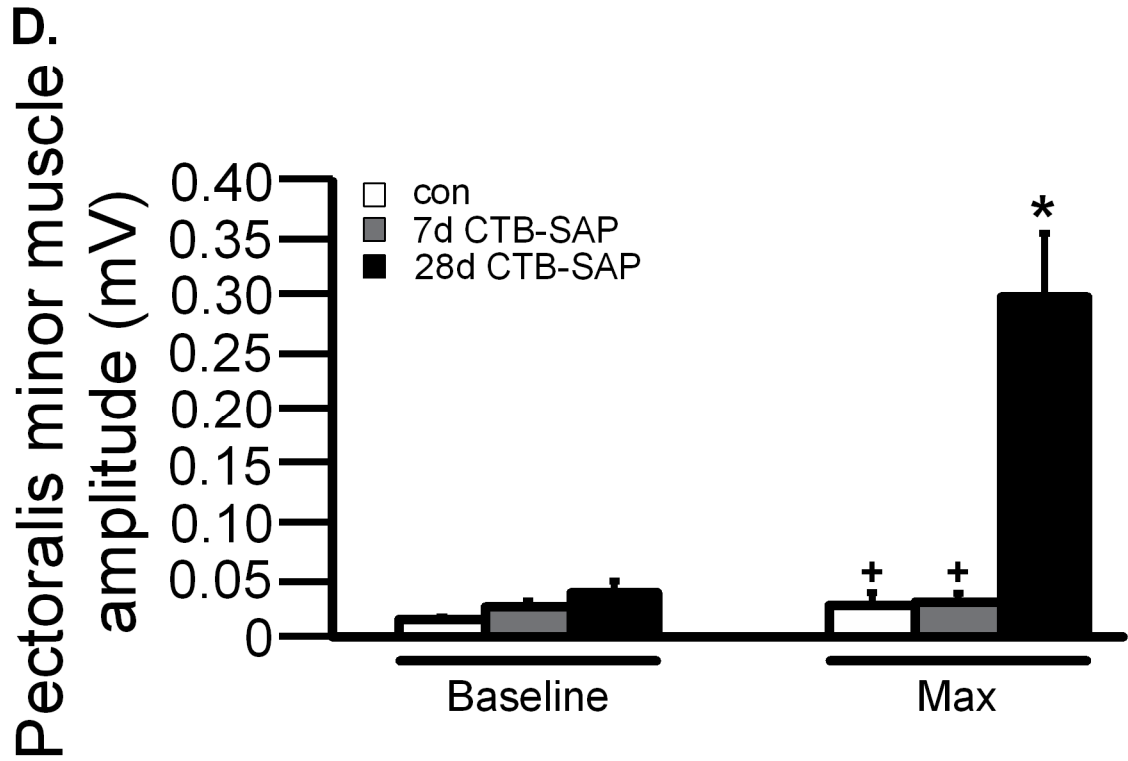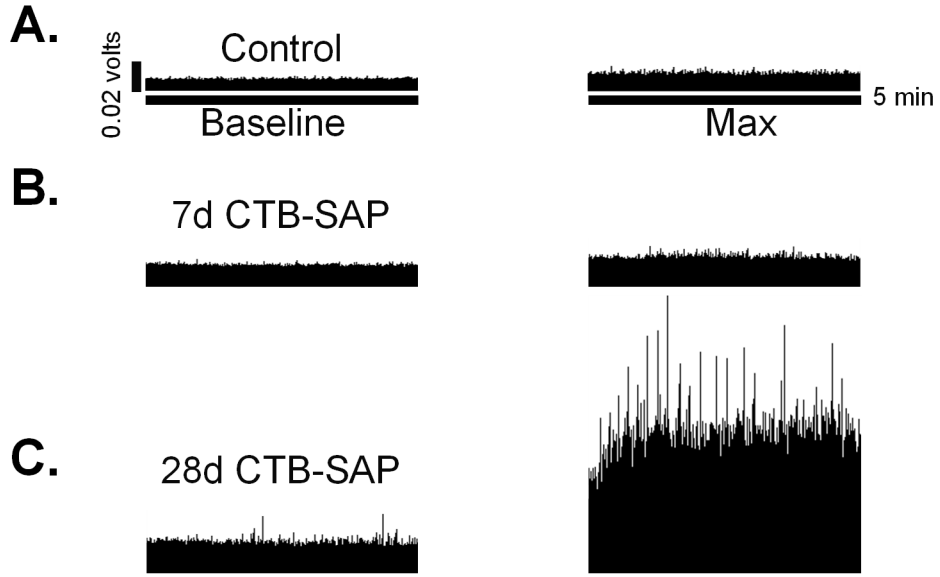
Figure 5.4: Pectoralis minor motor output following intrapleural and intramuscular control or CTB-SAP injections in adult rats. A-C. Representative traces of integrated pectoralis minor muscle amplitude following bilateral intrapleural and intramuscular CTB-SAP-induced phrenic and pectoralis minor motor neuron death in control (**A.**), 7d CTB-SAP (**B.**), and 28d CTB-SAP (**C.**) rats. Spontaneous pectoralis minor muscle activity was recorded in all rats during normoxia (baseline) and in response to maximum chemosensory stimulation (max; hypercapnia + hypoxia). Large spikes indicate augmented breaths in the representative trace from the 28d CTB-SAP rat. **D.** Pectoralis minor muscle output was measured in 7d and 28d intrapleurally and intramuscularly (pectoralis minor muscle) injected control (con; white bars) or CTB-SAP (gray and black bars, respectively) rats during normoxia (baseline) and maximal chemosensory stimulation (max; hypoxia + hypercapnia). Baseline pectoralis minor muscle amplitude in both CTB-SAP treated groups was unchanged from controls. Only 28d CTB-SAP rats had a significant increase in pectoralis minor muscle amplitude at max from its respective baseline (*), and this amplitude was significantly greater than controls and 7d CTB-SAP rats during max (+). Values are expressed as means ± SEM, and all significant differences are p<0.05.
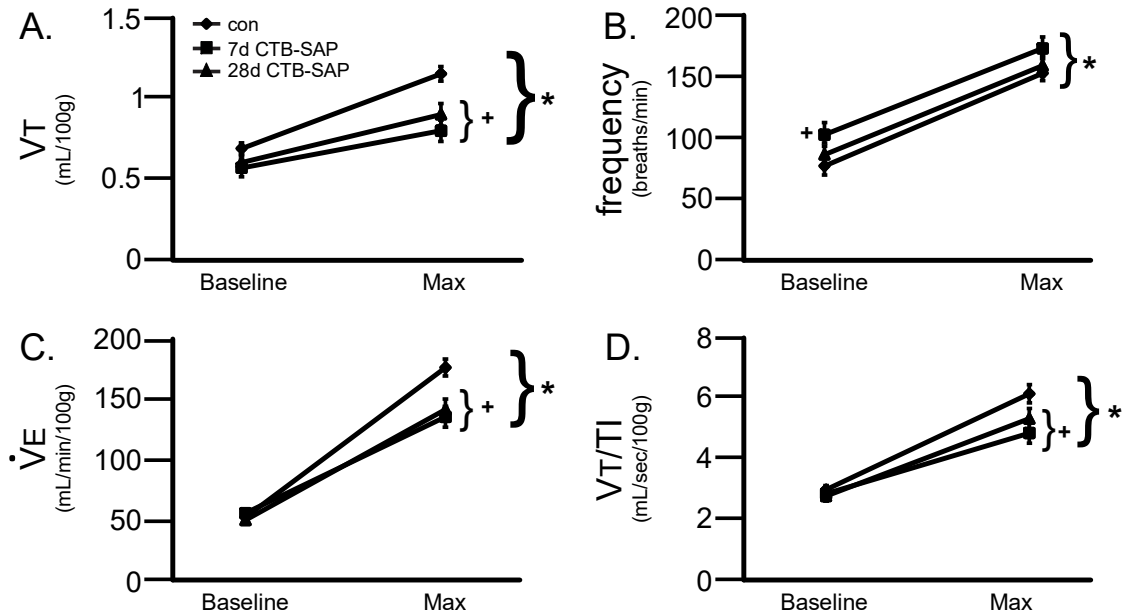
Figure 5.5: Respiratory variables following intrapleural and intramuscular control or CTB-SAP injections in adult rats. A-D. Respiratory variables including tidal volume (V_T; A), breathing frequency (B), minute ventilation ($\dot{V}_E$; C), and mean inspiratory flow (V_T/T_I D) were assessed in intrapleurally and intramuscularly (pectoralis minor muscle) injected control (con; diamond) or CTB-SAP treated rats (7d, square; 28d, triangle) during normoxia (baseline) and maximum chemosensory stimulation (max; hypoxia + hypercapnia). Baseline breathing frequency was increased in 7d CTB-SAP rats from control rats (+), and no deficits were observed at baseline for any of the variables in CTB-SAP rats compared to controls. All respiratory variables at max were increased from respective baseline values for all groups (*), but all variables at max, except for breathing frequency, were decreased in both CTB-SAP treated groups *vs*. controls (+). All values are expressed as means ± SEM, and all significant differences are p<0.05.

A. Baseline

$y = 0.0012x + 0.5306$
$R^2 = 0.1916$

B. Max

$y = 0.0023x + 0.7977$
$R^2 = 0.2202$
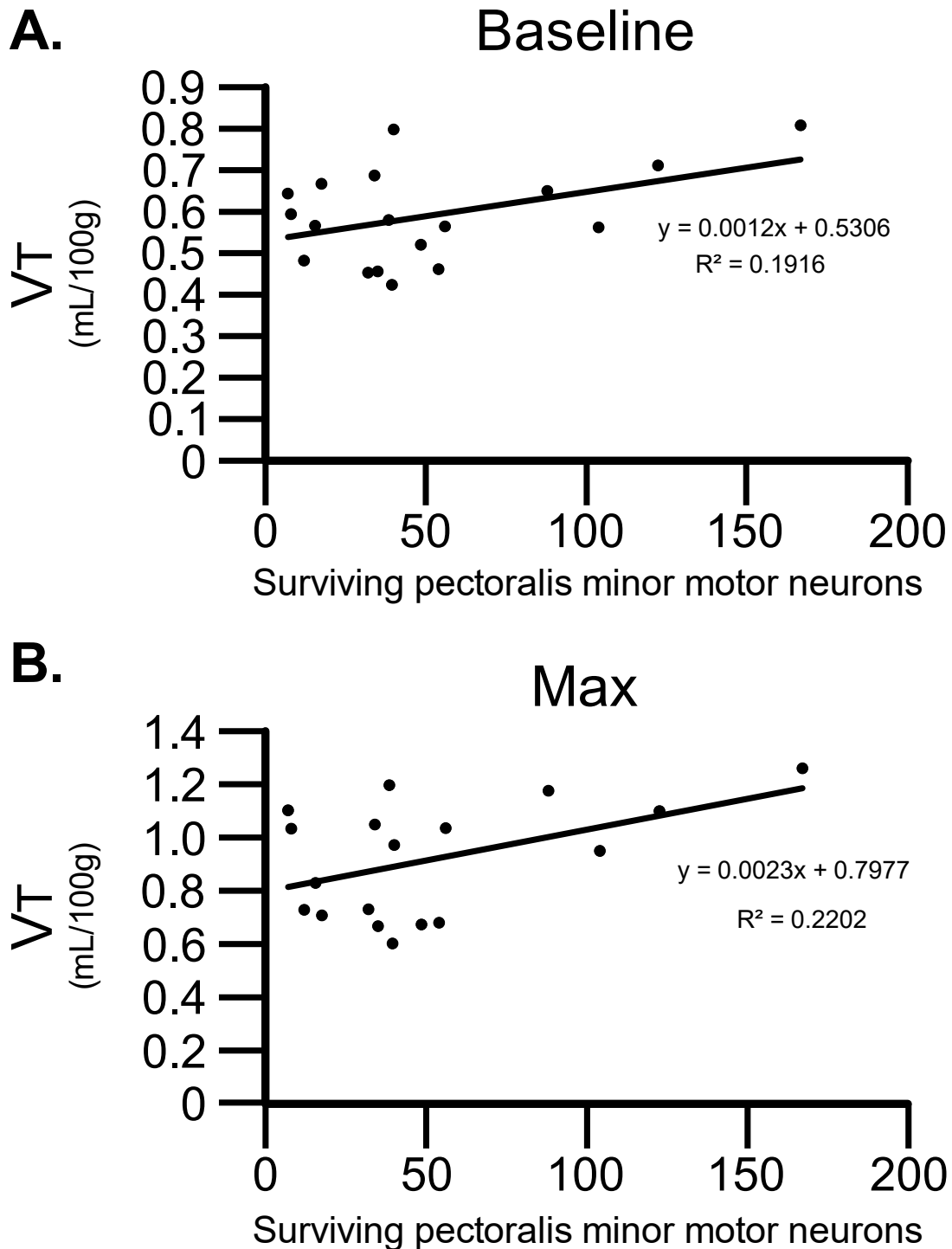
Figure 5.6: Regression analyses reveal significant correlations following intrapleural and intramuscular control or CTB-SAP injections in adult rats. Multiple regression analyses between baseline (**A**) or maximal (**B**) VT/100g with pectoralis minor motor neuron survival. Although not quite significant, there is a trend for a correlation between the number of surviving pectoralis minor motor neurons and baseline VT/100g (**A**; p=0.069). However, there is a significant correlation between the number of surviving

177

pectoralis minor motor neurons and maximum VT/100g (**B**; p =0.049); thus, pectoralis minor motor neuron survival predicts maximum VT/100g.

CHAPTER 6: DISCUSSION

The purpose of this dissertation is to explore potential targets for preserving respiratory function and increasing maximal ventilatory capacity following respiratory motor neuron death (Fig. 6.1). By using an inducible model of respiratory motor neuron death, we furthered our knowledge of the underlying G-coupled protein receptor-dependent mechanisms required for pLTF (Chapters 2 & 3), how COX1/2-induced inflammation differentially impacts pLTF (Chapter 4), and the recruitment of an accessory inspiratory muscle group (*e.g.,* pectoralis minor) (Chapter 5; Fig. 6.1). This dissertation also utilizes the CTB-SAP model to further examine the specific impact of respiratory motor neuron death on eupneic maintenance and maximal ventilatory capacity, which could provide insight for treatments in neuromuscular diseases or injuries. The following sections will discuss how the CTB-SAP model can be used to explore currently available treatment options for respiratory preservation used in human patients to better pinpoint timeframes in which these interventions should be used, the overall implications this research has in breathing preservation, other factors of consideration that impact the findings of the current research, pitfalls of the current research, and the overall conclusions of the current research.

6.1- Current Treatment Options for Respiratory Preservation Following Motor Neuron Death

Pharmaceutical treatment

Currently, there are pharmacological interventions for ALS and SCI, but their efficacy varies depending on the type and stage of the motor neuron disease/injury. This section will discuss pharmaceutical interventions that target G-coupled protein-dependent
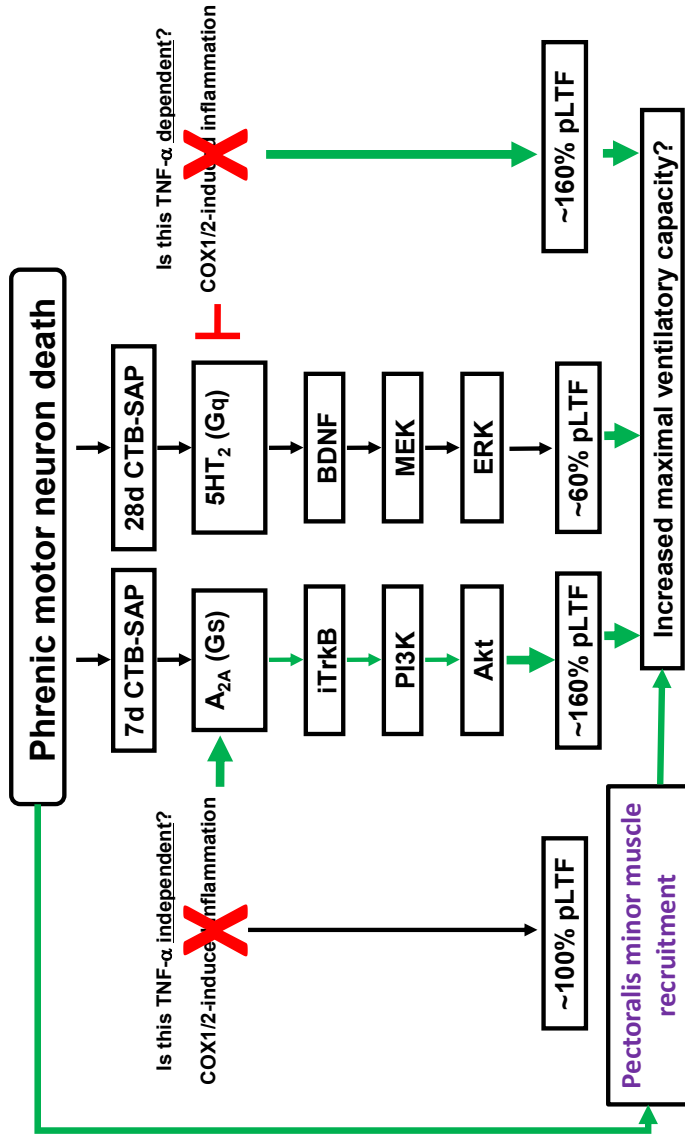
Figure 6.1. Schematic demonstrating the overall conclusions of the current dissertation. The schematic displays how mechanisms of pLTF and pectoralis minor muscle recruitment potentially contribute to increasing maximal ventilatory capacity in CTB-SAP rats. We have shown that enhanced pLTF in 7d CTB-SAP rats is elicited through A2A receptor activation (Chapter 2), requires the new synthesis of iTrkB, and occurs predominantly through downstream PI3K/Akt activation (Chapter 3). Meanwhile, pLTF in 28d CTB-SAP rats is elicited through 5-HT receptor activation (Chapter 2) and requires the new synthesis of BDNF followed by the subsequent activation of MEK/ERK (Chapter 3). We have also shown that COX1/2-induced inflammation contributes to the enhanced pLTF observed in 7d CTB-SAP rats since ketoprofen delivery attenuated pLTF (Chapter 4). COX1/2-induced inflammation constrains pLTF in 28d CTB-SAP rats because ketoprofen pre-treatment led to enhanced pLTF (Chapter 4). Additionally, we have preliminary data (data not shown) that pLTF is TNF-α independent at 7d and TNF-α dependent at 28d. Therefore, other inflammatory factors should be investigated to determine their necessity for enhanced pLTF in 7d CTB-SAP rats. The mechanisms of pLTF (Chapter 2-4) and the recruitment of the pectoralis minor muscle (Chapter 5) investigated in the current dissertation are strategies that can be harnessed to increase maximal ventilatory capacity following CTB-SAP-induced respiratory motor neuron loss.

180

mechanisms and the accumulation of reactive oxygen species, both of which are mechanisms relevant to the differential mechanisms of pLTF observed in our CTB-SAP model. Following CTB-SAP-induced respiratory motor neuron death, we have determined the amount of phrenic and intercostal motor neuron death that has occurred at 7d and 28d (Nichols et al., 2015b) and the differential G-coupled protein-dependent signaling mechanisms responsible for the difference in magnitude of pLTF in 7d and 28d rats. Therefore, we can use these different time points to investigate when the current treatments available to human patients that interfere with these known pathways of pLTF should be used for the most beneficial effects on breathing preservation/maintenance. We know that respiratory drive and pLTF are elicited through glutamatergic signaling, and pLTF is eliminated with NMDA receptor antagonism in anesthetized naïve rats (Chitravanshi and Sapru, 1996; McCrimmon et al., 1989; McGuire et al., 2005; Steenland et al., 2006). Although we have not directly tested the necessity of the NMDA receptor in the CTB-SAP model, we speculate that the excitatory events elicited by NMDA receptor activation are necessary for G-coupled receptor dependent mechanisms of pLTF observed in the CTB-SAP model. However, glutamatergic excitotoxity must be considered following CTB-SAP-induced respiratory motor neuron loss because we are trying to enhance pLTF in 28d CTB-SAP rats to that of 7d CTB-SAP (from ~ 60% pLTF to ~ 160% pLTF; Fig. 6.1) rats by targeting components of Gq and Gs-signaling, respectively, to ultimately increase maximal ventilatory capacity. Therefore, if harnessing one of these G-coupled protein-dependent mechanisms leads to a prolonged increase in glutamatergic signaling through NMDA receptor activation, we may initially enhance pLTF but contribute to glutamatergic excitotoxicity and motor neuron death.

Riluzole, a benzothiazole, is approved for the treatment of ALS due to its demonstration of neuroprotective potential *in vitro* and *in vivo* (Bryson et al., 1996) where patients experienced prolonged survival and/or time to tracheotomy following Riluzole treatment (Bryson et al., 1996). Riluzole affects neurons by inhibiting excitatory amino acid release, inhibiting events following stimulation of excitatory amino acid (*N*-methyl-D-aspartate (NMDA)) receptors by interfering with G protein-dependent mechanisms, and stabilizing the inactivated state of voltage-dependent sodium channels (Bryson et al., 1996). With ALS progression, it is thought that increased central drive followed by increased extracellular concentrations and respiratory nuclei release of glutamate is one way that motor neuron death occurs, therefore, Riluzole reduces excitotoxicity by modulating glutamatergic signaling. Similarly, when Gacyclidine (NMDA receptor antagonist) was delivered (1 mg/kg; i.v.) 10, 30, 60 and 120 min after spinal contusion injury (T7–T9) in rats, significant benefits were observed after 18 days following Gacyclidine treatment 10 min post-injury *vs*. untreated controls and rats treated at any other time point (Gaviria et al., 2000). These benefits included quicker walking recovery, a decrease in damaged spinal cord tissue that correlated with improved motor performance, and increased somatosensory evoked potential amplitudes (Gaviria et al., 2000). These studies indicate suppressing glutamatergic signaling is beneficial. Because we have shown that CTB-SAP rats elicit pLTF through G-coupled protein receptor-dependent signaling mechanisms, we speculate Riluzole treatment would abolish pLTF in our model. This does not mean Riluzole should not be investigated in the CTB-SAP model, because the mechanism by which this drug interferes with G-coupled protein receptor signaling has yet to be delineated and may have beneficial effects depending on which pathway it interacts

with at 7d and 28d (Gs *vs*. Gq, respectively). However, because Gacyclidine had beneficial effects following SCI early on when serotonergic innervation is significantly reduced, it is possible that Gacyclidine would contribute to improving maximal ventilatory capacity in 7d CTB-SAP rats since they have characteristics that are similar to that of SCI such as a reduction in serotonin terminals (data not shown), and an increase in A2A receptor expression (preliminary data not shown), and utilize Gs-A2A receptor-dependent signaling (Chapters 2 & 3).

Although we have not investigated glutamate receptor expression, nor the necessity for glutamatergic receptor activation for pLTF in the CTB-SAP model, we know that cervical contusion and SCI results in an increase in glutamatergic interneuron innervation to phrenic motor neurons with increased terminal sprouting and synaptic strength. Normally, VGLUT2(+) excitatory interneurons are not necessary for normal breathing, but their innervation of phrenic motor neurons is increased and they directly contribute to breathing following cervical contusion and SCI (Satkunendrarajah et al., 2018). On the other hand, excitotoxicity due to excessive glutamate signaling is very detrimental in SCI, and pharmacological intervention to prevent deterioration is difficult due to the acute time-course of glutamate release following trauma (Faden et al., 1989). In regard to SCI, there is an initial peak in glutamate release that decreases in a graded manner over the following hours in the rat model of spinal contusion (Farooque et al., 1996). Conveniently, CTB-SAP rats have a known time point for when significant phrenic and intercostal motor neuron death occurs (3d post-intrapleural injection). Therefore, using the known information above we can investigate changes in interneuron innervation to the affected nuclei, determine the contributions of VGLUT2(+) excitatory interneurons and their implications

for breathing, and determine a glutamate-signaling time-course to prevent further motor neuron deterioration through glutamatergic excitotoxicity in the CTB-SAP model. Glutamatergic signaling also has implications in accessory inspiratory muscle recruitment. In SOD1^{G93A} rats, trans-diaphragmatic pressure is impaired at the late stages of disease, and the recruitment of accessory inspiratory muscles has been thought to occur through glutamatergic V2a neurons (Romer et al., 2017). Blocking glutamate signaling may not be beneficial in SOD1^{G93A} rats and may exacerbate respiratory failure. We have shown that the accessory inspiratory muscle group, the pectoralis minor muscles, become recruited following CTB-SAP-induced respiratory motor neuron death. Although we do not know how these muscles are being recruited in response to CTB-SAP-induced respiratory motor neuron death, they may rely on VGLUT2(+) excitatory interneurons and/or glutamatergic V2a neurons. Thus, blocking glutamatergic signaling may block the recruitment of accessory inspiratory muscles and may result in breathing deficits at baseline and further exacerbate the deficits observed at max. As shown in Chapter 5, the pectoralis minor muscle motor neurons are in close proximity to the phrenic motor nucleus, so any intervention that targets glutamatergic modulation in the phrenic motor pool may have an effect on the pectoralis minor motor pool as well and result in further deficits in maximal ventilatory capacity.

As addressed above, ROS production has implications in pLTF and has been targeted for therapy in human patients with neuromuscular diseases/injuries. In naïve rats, pMF requires the production of reactive oxygen species through the activation of NADPH oxidase (NOX) (MacFarlane and Mitchell, 2007; MacFarlane and Mitchell, 2009). However, oxidative damage is upregulated in both familial and sporadic cases of ALS and

should be investigated as a target to treat a broader group of affected individuals (Beal et al., 1997). Similar to glutamatergic activation, ROS production is necessary for pMF but the overproduction of free radicals contributes to disease progression. Edaravone (3-methyl-1-phenyl-2-pyrazolin-5-one, MCI-186) is another pharmaceutical drug approved for and used to treat ALS that is thought to elicit its neuroprotective effects through scavenging free radicals (Shichinohe et al., 2004; Uno et al., 2005). Following motor symptom onset in SOD1^{G93A} mice, mice administered Edaravone had a delay in disease progression, a reduction in spinal SOD1 deposits, and a reduction in oxidative damage (Ito et al., 2008). Edaravone did not significantly extend survival of SOD1^{G93A} mice and is speculated to not be sufficient in slowing progression of bulbar or respiratory symptoms (Ito et al., 2008). In ALS patients, Edaravone significantly reduced lipid oxidation and prolonged the decline in functional parameters (*e.g.,* speech, handwriting, walking, breathing) (Yoshino and Kimura, 2006). Although we have not directly investigated the role of NOX and ROS production following CTB-SAP-induced respiratory motor neuron death, we have shown that pLTF in 28d CTB-SAP rats is elicited through Gq-5-HT receptor-dependent mechanisms. Additionally, we have speculated that because the magnitude of pLTF in 28d CTB-SAP rats is similar to that of naïve rats, that 5-HT2B receptors are the required isoform for pLTF at 28d. Therefore, NOX signaling and ROS production would be required for pLTF in 28d CTB-SAP rats and we speculate that treatment with Edaravone will eliminate the ~60% pLTF observed at this time point. Because 7d CTB-SAP rats elicit enhanced pLTF through Gs-A2A receptor-dependent signaling, we speculate that ROS scavenging would further contribute to enhance pLTF at

7d, because normally Gs signaling is inhibited by AIH-induced transient ROS production and PKC phosphorylation (Lai et al., 1997; Zimmermann and Taussig, 1996).

Edaravone has also been studied in models of SCI immediate after injury to the spinal cord (primary injury) and several weeks after the injury where functional and structural deficits in neural tissue persist (secondary injury) (Tator and Fehlings, 1991). Secondary injury is thought to be driven by radical-mediated lipid peroxidation which makes neural cell membranes particularly vulnerable (Hall et al., 1992; Taoka et al., 1995). This may have implications in the CTB-SAP model where intrapleural CTB-SAP injections induce a primary injury through the initial significant lesioning of phrenic and intercostal motor neurons at 3d and 7d, and induce a secondary injury through further motor neuron death (although not quite significant for phrenic) and potential lipid peroxidation at 28d. In rats with a spinal contusion injury (6 wks after injury), intravenous infusion of Edaravone 1 hour prior to sacrifice significantly attenuated lipid peroxide formation in spinal cord homogenate, significantly spared white matter in the spinal cord, and resulted in a significantly higher motor score than untreated rats (Ohta et al., 2005). Based on rodent models of SCI and contusion, Edaravone should be further investigated to determine whether it can prolong lesioning of respiratory motor neurons or prevent lipid peroxide formation from 7d to 28d following CTB-SAP treatment. Additionally, if Edaravone can preserve the lesioning, it may prevent or restore the deficits in maximal ventilatory capacity in 28d rats.

Finally, although we use the CTB-SAP model to better understand underlying mechanisms of pLTF to try to develop treatments to restore/preserve breathing, treatments in human patients have focused on cell-based therapies through the infusion of human

embryonic stem cells (hESCs). Following the hESC treatment, all five patients (who were either paraplegic or quadriplegic) showed significant improvement in their ability to balance while sitting, control and sensation of bowel and bladder, and significant increases in power and movement of both lower and upper limbs (Shroff and Gupta, 2015). It has been suggested that hESC treatment contributes to restoration following SCI through providing compensation for demyelination, promotion of axonal regeneration, and directing regenerated axons to appropriate targets (Cao and Feng, 2009). Furthermore, it has been found that Edaravone treatment can actually further improve hESC treatment by inducing these cells to differentiate into neuron-like cells that expressed the neuronal and synaptic makers in a dose-dependent fashion *in vitro* (Shi et al., 2018). This treatment combination as well as its effects on respiratory motor neurons following cervical SCI should be investigated and could even be investigated in ALS models for translational treatment options for patients with these ailments. Furthermore, this combined treatment should be performed in our CTB-SAP model to determine if these same benefits are observed and at what time point (3d, 7d, or 28d) these interventions should take place to provide the greatest benefit to ventilatory capacity while minimizing deleterious effects to the motor neurons themselves.

Intermittent Hypoxia Exposure: Good or Bad?

There is much debate as to whether intermittent hypoxia exposure is beneficial or detrimental following respiratory motor neuron loss. This variability in beneficial effects is due to the protocol of exposure (the severity of hypoxia, the duration, and the repetitiveness of the exposure), and the type of neuromuscular disease or injury. We have

187

shown that 3, 5-min bouts of AIH (35–45 mmHg PaO_2) elicits a significant difference in the magnitude of pLTF at different time points following CTB-SAP-induced respiratory motor neuron death (7d *vs*. 28d; Chapters 2-4) (Nichols et al., 2018). We have also shown that despite the same AIH protocol, 7d CTB-SAP rats elicit enhanced pLTF through A_{2A} receptor activation, while 28d CTB-SAP rats elicit pLTF through 5-HT receptor activation (likely $5-HT_2$ receptors) (Chapter 2). However, we have yet to determine if this same magnitudes of pLTF can be elicited following daily protocols of AIH pre-conditioning. In naïve rats, daily low-dose AIH pre-conditioning (<15 episodes/day for 7 days) (Wilkerson and Mitchell, 2009) or mild chronic intermittent hypoxia (CIH; ~6 episodes/hr, 12hr/day, 72 episodes/day) enhances pLTF (Fuller et al., 2003; Ling et al., 2001). On the other hand, pLTF is abolished following 1-7 days of moderate CIH (15 episodes/hr, 8 hr/day; 120 episodes/day)(Huxtable et al., 2015). Naïve rats elicited enhanced pLTF following CIH (10–12% O_2/air, 2–5 min intervals, 8–12 hrs/night) through serotonin-dependent mechanisms (Ling et al., 2001). To more closely recapitulate the episodic bouts of hypoxia experienced by patients with sleep disordered breathing, other groups used CIH exposure with shorter hypoxic episodes (5–12% O_2, 15s episodes with 5 min intervals, 8h/day) and found that serotonin signaling and ROS formation was required for pLTF (Peng and Prabhakar, 2003). Therefore, this protocol may be beneficial in our 28d CTB-SAP rats in eliciting either enhanced pLTF and/or ventilatory long-term facilitation since we demonstrate these rats utilize serotonin-dependent mechanisms to elicit pLTF in the studies discussed in the current dissertation (Chapter 2).

Acute intermittent hypoxia has been used to treat SCI and spinal contusion patients and rodent models. Following AIH, enhanced respiratory and non-respiratory (limb) motor

function was observed in patients and rodents with chronic incomplete spinal cord injury (SCI) (Trumbower et al., 2012; Vinit et al., 2009). In the first two weeks following a C2 spinal hemisection (C2HS), serotonergic innervation of the phrenic motor nucleus is significantly decreased and, therefore AIH does not elicit pLTF on the side of the injury (Golder and Mitchell, 2005). However, by 8 weeks, AIH-induced pLTF is restored as serotonergic innervation is simultaneously restored (Golder and Mitchell, 2005). One-week post-C2HS there is potential for restoring breathing capacity following daily AIH (dAIH). Following dAIH, there was an increase in tidal volume during hypercapnia, an increase in the response of phrenic motor output to graded levels of hypercapnia, an increase in evoked action potentials both ipsilateral and contralateral to the injury, and pLTF was observed (Barr et al., 2007). Because we know that serotonergic innervation is significantly decreased immediately following the injury and we know that in our model 7d CTB-SAP elicit plasticity through Gs-A$_{2A}$ receptor dependent pathways, dAIH may be beneficial for increasing ventilatory capacity in our model at this time point. Once pLTF is then Gq-5-HT$_2$ receptor dependent by 28d following CTB-SAP-induced respiratory motor neuron death, CIH exposure with shorter hypoxic episodes may enhance pLTF at this time point.

Muscle Pacing

As discussed in Chapter 5 and in the previous section, there have been studies that have evaluated the impact of acute or chronic hypoxia exposure on other muscles of respiration at different time points in a variety of neuromuscular diseases and injuries, as well as the mechanisms by which accessory respiratory muscle recruitment is occurring. In the CTB-

SAP model we found that diaphragmatic output decreases during baseline and max breathing over the course of respiratory motor neuron loss (Chapter 5, data not shown). At the same time, the pectoralis minor, an accessory inspiratory muscle, is recruited during baseline and max in CTB-SAP rats (Chapter 5). Interestingly, the recruitment of the pectoralis minor occurs in 7d CTB-SAP rats during baseline even though diaphragmatic output is not yet significantly decreased from controls at this time (Chapter 5, data not shown). Although we showed that the pectoralis minor becomes recruited, it is not necessary for eupnea. However, we do have data to suggest that pectoralis minor muscle motor neuron survival can predict tidal volume during max, indicating it may have a role in preserving maximal ventilatory capacity (Chapter 5). The purpose of this section is to discuss strategies by which primary muscles of respiration can be preserved and/or accessory muscles can be stimulated to prolong respiratory deficits.

Pacing the diaphragm is a non-invasive strategy that has been used in ALS patient to prolong ventilator dependence. The goal of diaphragmatic pacing (specifically, low-frequency pacing) is to preserve diaphragmatic function, prevent diaphragmatic atrophy, promote the development of oxidative fatigue-resistant type 1 muscle fibers (Acker et al., 1987; Marzocchi et al., 1990; Peterson et al., 1994), and delay the necessity of mechanical ventilation prior to respiratory failure (Gonzalez-Bermejo et al., 2016). We have found that there is a marginal reduction in diaphragmatic output in 7d CTB-SAP rats *vs*. controls at baseline, while there is a significant reduction in diaphragmatic output in 28d CTB-SAP rats *vs*. controls at baseline (Chapter 5, data not shown). During max, diaphragmatic output is significantly compromised in 7d and 28d CTB-SAP rats *vs*. controls (Chapter 5, data not shown). Additionally, we found that pectoralis minor muscles are recruited over the course

of CTB-SAP-induced respiratory motor neuron loss at baseline and max (Chapter 5), and although are not necessary for baseline breathing, they may be necessary for breathing at max. Together, these data indicate that diaphragmatic pacing and/or pectoralis minor muscle pacing should be investigated to compensate for loss of diaphragmatic output to restore maximal ventilatory capacity.

In ALS patients that had moderate respiratory involvement (forced vital capacity 60–80% predicted), diaphragmatic pacing resulted in serious adverse effects (capnothorax or pneumothorax, acute respiratory failure, venous thromboembolism) and significantly decreased survival (Gonzalez-Bermejo et al., 2012). The authors, therefore, do not promote diaphragmatic pacing as an early treatment for respiratory function in ALS patients. This must be taken into consideration when evaluating the outcomes of diaphragmatic pacing in CTB-SAP rats. Because diaphragmatic output is not yet significantly impacted and there are no deficits in baseline breathing compared to controls in 7d CTB-SAP rats, diaphragmatic pacing may actually induce respiratory deficits at baseline. In another study, ALS patients were implanted laparoscopically with diaphragm electrodes for diaphragmatic conditioning, which resulted in positive respiratory outcomes including greater movement of the diaphragm, increased thickness of the diaphragm muscle, prolonged the decrease in forced vital capacity, increased median survival, and attenuated the number of deaths due to ventilatory failure (Onders et al., 2014). The differences in outcomes in these studies evaluating diaphragmatic pacing may be a result of Onders et al. excluding patients with severe bulbar symptoms, the time of intervention, and/or the diaphragm pacing frequency/protocol. We suspect that these same respiratory and muscular benefits will be observed in our 28d CTB-SAP treated rats where diaphragmatic

output is most greatly affected at baseline and max. Regarding the pectoralis minor, we suspect that pacing this muscle will also be beneficial in terms of muscle movement and fiber type preservation, as well as eliminating the respiratory deficits observed at max in both 7d and 28d CTB-SAP rats. Discrepancies in patient outcomes in the aforementioned studies may be due to whether there was upper *vs.* lower or upper and lower motor neuron dysfunction, and which motor neurons were more greatly affected.

In SCI patients, the preservation of phrenic nerve and diaphragmatic activity is crucial in the outcome of the implantation of stimulation electrodes. Thus far in the CTB-SAP model of respiratory motor neuron death, we know the amount of motor neuron death that has occurred, when there is a significant reduction in diaphragmatic activity, and when the pectoralis minor muscles become recruited. For incomplete SCI, which is similar in motor neuron survival to the CTB-SAP model, the laparoscopic approach for electrode implantation allows for mapping of the motor end plate within the muscle that correspond to phrenic nerve insertion. In the thoracic cavity, the phrenic nerve divides into three or four branches that insert into the left and right diaphragm in a cranial orientation (Onders et al., 2004a). To appropriately place diaphragmatic electrodes for pacing, the injured and spared diaphragm is determined by stimulating these different branches and seeing if diaphragmatic contraction occurs (Onders et al., 2004b). Appropriate placement of stimulating electrodes and diaphragmatic pacing lead to three-fourths of patients with cervical SCI being successfully weaned off the ventilator in an average of ten days post-placement and pacing. Additionally, one-third of the study group reached a point of independent breathing, without a ventilator or the necessity of the electrodes, and the electrodes were eventually removed (Posluszny Jr et al., 2014). Mapping could be

beneficial in the CTB-SAP model to specifically determine how each branch of the phrenic and the sections of the diaphragm that each branch innervates is affected by motor neuron loss. Similarly, mapping of the pectoralis minor muscle can be done by stimulating the medial or lateral nerves that innervate the pectoralis minor muscle to determine which nerve more greatly contributes to pectoralis minor muscle contraction. Ultimately, knowing which branch(es) of the phrenic and sections of the diaphragm are most greatly affected by motor neuron loss would be beneficial for precisely placing electrodes for diaphragmatic pacing to effectively increase diaphragmatic output, delay ventilator dependence, and prolong respiratory deficits from occurring in individuals suffering from respiratory deficits due to motor neuron loss.

Finally, sleep disordered breathing is a hallmark characteristic of neurodegenerative disorders. During REM sleep, skeletal muscle activity (including the accessory muscles of respiration) and diaphragm strength is reduced, which can lead to significant hypoventilation (Bye et al., 1990). We have yet to investigate whether there are reductions in diaphragmatic or pectoralis minor muscle output during REM sleep in CTB-SAP rats, and if these reductions in primary and accessory muscle output result in respiratory deficits. If sleep leads to reductions in either diaphragmatic or pectoralis minor muscle output and results in respiratory deficits in CTB-SAP rats, then pacing of these muscles should be evaluated separately and together during hours of wakefulness or sleep, and across sleep-wake cycles to determine if respiratory deficits can be mitigated.

6.2- pLTF and Inflammation

Inflammation is another hallmark of neuromuscular diseases and/or injury and impacts respiratory function. Neurodegenerative diseases and injuries elicit inflammation and activate the immune cells, microglia, of the CNS (Beers et al., 2006; Beers et al., 2011; Fendrick et al., 2007; Philips and Robberecht, 2011; Sanagi et al., 2010). It is unclear if and when inflammation is beneficial to motor neuron preservation or detrimental to those surviving motor neurons (Beers et al., 2006); however, it is known that long-term systemic inflammation interferes with neural networks responsible for breathing and hinders their function (Perry, 2010; Teeling and Perry, 2009). Using the CTB-SAP model, we aimed to understand how early (7d) and late (28d) COX-1/2-induced inflammation impacted pLTF and how this knowledge could be used to improve maximal ventilatory capacity (Fig. 6.1).

As addressed in Chapter 4, we found that COX-1 and 2 mechanisms either contribute to or constrain pLTF over the course of motor neuron loss in CTB-SAP rats. We established in Chapters 2 and 3 that pLTF in 7d CTB-SAP rats is enhanced and occurs through Gs-dependent pathways (Borkowski and Nichols, 2020), and it is known that Gs-dependent mechanisms of pMF and pLTF are inflammation-resistant (Agosto-Marlin et al., 2017). Additionally, we established in Chapters 2 and 3 that pLTF in 28d CTB-SAP rats is elicited through Gq-dependent mechanisms, and it is known that inflammation through the administration of lipopolysaccharide (LPS) abolishes Gq-dependent pMF and pLTF (Lu et al., 2008; Triantafilou and Triantafilou, 2002). We found that inflammation contributed to the enhanced pLTF observed in 7d CTB-SAP rats, which was abolished with the administration of the non-steroidal anti-inflammatory drug ketoprofen (IP). Conversely, we found that COX-1 and 2 mechanisms constrain pLTF in 28d CTB-SAP

rats because pLTF was enhanced when ketoprofen was administered. We also evaluated microglial morphology in the phrenic motor nucleus and cervical (C3-5) inflammatory-associated marker gene expression in CTB-SAP rats. We found that microglia appear more ameboid in the phrenic motor nucleus, which is indicative of activation. Sadly, NSAID use for the treatment of ALS has not shown to have a significant effect prolonging the progression of disease. Additionally, long-term steroid treatment to alleviate inflammation has actually been affiliated with pectoral muscle atrophy due to the induction of muscle catabolism (Vivier et al., 2019), which would be detrimental to the recruitment of this muscle group for the preservation of breathing. Therefore, more specific targets of inflammation should be investigated so that an entire signaling pathway is not inhibited that may actually have some positive effects (*e.g.,* COX-1 and COX-2 overall signaling).

We conducted qRT-PCR on markers of inflammation and found that these could be targets that are either contributing to or constraining pLTF, and that blocking one of these targets could enhance pLTF and breathing following CTB-SAP-induced respiratory motor neuron death. Endotoxin or prolonged hypoxia exposure-induced (8hrs) inflammation reduces ventilation and inhibits serotonin (Gq)- dependent AIH-induced pLTF, which can be alleviated by the administration of ketoprofen or with p38 MAPK inhibition (Huxtable et al., 2011; Huxtable et al., 2015; Huxtable et al., 2013; Vinit et al., 2011). On the other hand, A2A-dependent mechanisms of pLTF are unaffected by endotoxin-induced inflammation (Agosto-Marlin et al., 2017), and TNF-α is actually sufficient and necessary for pMF (Baertsch and Baker-Herman, 2013; Baker-Herman and Strey, 2011; Mahamed et al., 2011; Strey and Baker-Herman, 2012) (Broytman et al., 2013). TNF-α itself can activate downstream signaling of PI3K and PKC (Strey and Baker-

Herman, 2012; Yin et al., 2012), while constraining Gq-dependent mechanisms of pLTF (Huxtable et al., 2011). Our preliminary data suggest that TNF-α is increased in CTB-SAP rats at both 7d and 28d, but we speculate that TNF-α is contributing to the observed enhanced pLTF in the 7d CTB-SAP rats. Additionally, we speculate that TNF-α is constraining pLTF in 28d CTB-SAP rats, since we see enhancement in 28d CTB-SAP rats with COX-1 and 2 inhibition. In addition to an increase in TNF-α in our 28d CTB-SAP rats, BDNF also appears to be increased. We have previously determined that BDNF is required for pLTF in 28d CTB-SAP rats (Borkowski and Nichols, 2020), so now we must determine if BDNF activity is being constrained by TNF-α, and if the enhanced pLTF we observe following ketoprofen treatment is due to the inhibition of TNF-α. As discussed in Appendix I, there is interplay between TNF-α and BDNF. It is possible that TNF-α is either constraining downstream Gq signaling or that it is contributing to the feed-forward production of BDNF. Thus, a TNF-α inhibitor should be given prior to AIH exposure to further delineate the effect TNF-α has on pLTF following CTB-SAP-induced respiratory motor neuron loss at 7d and 28d. Understanding what cytokines are being produced and how they interfere with mechanisms of pLTF elicited at 7d and 28d post-CTB-SAP-induced respiratory motor neuron death could provide insight into targeted treatment for respiratory maintenance in this model. More specifically, as shown by our results, it would not be beneficial to give an NSAID or COX1/2 inhibitor following acute respiratory motor neuron death, but it would be beneficial to give an NSAID or COX1/2 inhibitor following chronic respiratory motor neuron death (Chapter 4 & Fig. 6.1).

6.3- Considerations and Pitfalls

CTB-SAP Model vs. Other Models of Motor Neuron Death

A major point of discussion that should be addressed with the CTB-SAP model of induced respiratory motor neuron death is its recapitulation of neuromuscular diseases and/or injuries. First, the mechanism by which neuromuscular diseases result in motor neuron death is highly debated and is disease/injury specific. Conveniently, we know the exact mechanism by which saporin induces motor neuron death through apoptotic mechanisms. Other diseases can have both genetic and sporadic causes, and if the cause is unknown, the disease/injury may be harder to prolong because only symptoms are targeted for treatment. A genetic cause accounting for approximately 20% of familial ALS cases is through mutations in the copper/zinc superoxidedismutase-1 (SOD-1) gene. This mutation leads to a toxic gain of function of the SOD1 enzyme through the formation of free radicals (Vucic and Kiernan, 2009). Another issue with SOD1 mutations is that they can lead to misfolding of the SOD1 peptide, leading to disruption in proteosomic function and axonal transport systems through intracellular aggregate formation (Bruijn et al., 1998; Williamson and Cleveland, 1999; Zetterström et al., 2007). When mechanisms of cell death were investigated in motor neurons overexpressing SOD1, it was determined that SOD1 triggers endoplasmic reticulum stress through dysfunction of endoplasmic reticulum (ER)-associated degradation machinery. This then resulted in activation of the apoptosis signal-regulating kinase 1 (ASK1)-dependent cell death pathway (Nishitoh et al., 2008). Although this has not been determined as the sole mechanism of SOD1 mutation-induced cell death, it is not a shared mechanism of CTB-SAP-induced cell death. Spinal muscular atrophy (SMA) is also linked to genetic mutations, deletions, or rearrangements

in the survival motor neuron 1 and 2 (SMN1, SMN2) genes (Lefebvre et al., 1995). Why motor neurons are vulnerable to changes in SMN1 and SMN2 genes and exact mechanisms by which these changes induce pathogenesis have been speculated but remain unknown. What is known is that SMN protein is localized in ribonucleoprotein granules in the neurites and growth cones of primary motor neurons and is thought to interact with β-actin (Rossoll et al., 2003). When there are low concentrations of SMN protein, there is a reduction in β-actin protein in axons and growth cones, which results in in axonal outgrowth and pathfinding defects making primary motor neurons dysfunctional (McWhorter et al., 2003; Zhang et al., 2003). These are genetic contributions of neuromuscular disease, whereas the CTB-SAP model has a known mode of inducing motor neuron death. Therefore, it is important to determine the cause of motor neuron pathology in order to produce a therapy that prevents or prolongs the death of motor neurons through interference with the genetic mutation or interference with downstream apoptotic signaling mechanisms. The CTB-SAP model can provide insight as potential therapies to preserve breathing function, but our model only induces respiratory motor neuron death and does not address the effects of global motor neuron death and the prolonged CNS inflammatory response.

Secondly, the rate at which motor neurons are lost is not consistent across neuromuscular diseases or injuries and the motor pools most greatly affected differ amongst neuromuscular diseases or injuries and prognosis. For example, spinal cord injury results in the immediate loss of spinal motor neurons at the site of injury and leads to the impairment of neural pathways descending from the site of injury (Zimmer et al., 2007). Hemisection at the second cervical segment results in immediate disruptions in ipsilateral

descending respiratory projections to the phrenic nucleus, and leads to hemiparalysis of the diaphragm and allows for the study of respiratory deficits because the respiratory motor neurons affected and spared are known (Goshgarian, 2003; Zimmer et al., 2007). In the case of neurodegenerative diseases, however, motor neuron degeneration occurs incrementally and allows for mechanisms of compensation and deficits only appear when either motor neuron loss becomes too great and/or compensatory mechanisms fail, which is what is observed in SOD1^{G93A} rodent models of ALS. While our CTB-SAP-induced model of targeted respiratory motor neuron loss mimics the respiratory deficits observed at end-stage in the SOD1^{G93A} rat model (decreased phrenic nerve activity (Nichols et al., 2013b), increased microglial density (Alexianu et al., 2001), and preserved tidal volume during eupnea (Dale et al., 2006)) (Nichols et al., 2014; Nichols et al., 2013b), we observe significant motor neuron death occurring as early as 3d post-treatment (Nichols et al., 2015b). This significant loss of respiratory motor neurons occurs much more quickly in our model than in the SOD1^{G93A} model. Therefore, mechanisms of respiratory plasticity observed in the CTB-SAP model may be more consistent with those observed in the C2 hemisection model than the SOD1^{G93A} model. Because we know the amount of death occurring at 3d, 7d, and 28d post-CTB-SAP treatment, we can use this model to investigate other time points between 7d and 28d or after 28d to provide information as to when: 1) G-coupled protein receptor-dependent mechanisms of pLTF switch (Gs to Gq); 2) mechanisms of COX1/2-induced inflammation switch from contributing to constraining pLTF; 3) diaphragmatic output first becomes significantly decreased from controls and the amount of phrenic motor neuron loss that contributes to this reduction in output; and 4)

accessory muscles begin to be recruited and/or become required for eupnea and maximal ventilatory capacity (Fig. 6.1)

6.4- Future Directions

Determine the underlying mechanism(s) of pLTF in female CTB-SAP rats

Currently, we have only published data following CTB-SAP-induced respiratory motor neuron death in male Sprague-Dawley rats. We know that pLTF in female rats is dependent on the estrous cycle in naïve rats; pLTF is not present when circulating estradiol levels are low (estrus or diestrus) or following ovariectomy in young female rats, which is restored with estrogen supplementation (Barok et al.; Zabka et al., 2001b). Similarly, normally cycling female rats exposed to AIH (5 × 5 min episodes; 10% O_2) during proestrus elicited ventilatory plasticity 60 min following AIH exposure, which was shown by a progressive increase in minute ventilation (McIntosh and Dougherty, 2019; Zabka et al., 2001b). Female rats in estrus did not elicit any respiratory changes following AIH, which is concurrent with pLTF studies (McIntosh and Dougherty, 2019). Female rats do elicit pLTF when exposed to severe bouts of AIH, but the magnitude is estrous cycle-dependent and enhanced when estradiol levels are increased (Dougherty). This indicates that estradiol interferes with mechanisms of plasticity following severe AIH exposure. Severe AIH elicits Gs-A2A receptor dependent pLTF in male naïve rats(Nichols et al., 2012; Nichols and Mitchell, 2021), and we observe the utilization of this same signaling pathway in male CTB-SAP rats at 7d; therefore, estradiol may impact Gs signaling. Surprisingly, we have preliminary data that suggests that female Sprague-Dawley rats do elicit pLTF, but they do not elicit enhanced pLTF during any stage of the estrogen cycle following CTB-SAP-

induced respiratory motor neuron death at neither 7d nor 28d. Therefore, we speculate that ventilatory plasticity would also not occur in these female CTB-SAP rats.

What we do know is that testosterone is required for plasticity because pLTF is decreased in aged male rats with reduced circulating testosterone levels (Zabka et al., 2001a). Following the removal of the testes, severe and moderate AIH-induced pLTF is also eliminated in male rats (Dougherty; Dougherty et al., 2018; Grittner et al., 2021). When these males are given supplemental testosterone, pLTF is restored, but under the conditions that testosterone can effectively be converted to estradiol. These results indicate that estradiol and activation of estrogen (E2) receptors are the components that are necessary for pLTF in both males and females (Dougherty et al., 2018; Grittner et al., 2021; Zabka et al., 2006). Furthermore, as discussed in the previous section regarding inflammation, lipopolysaccharide-induced inflammation increases pro-inflammatory cytokines, with a greater increase in males. In LPS treated females, there was a significant reduction in pro-inflammatory genes expressed by microglia following E2 treatment. This reduction was not observed in male rats under the same treatments (Gardner et al., 2016). This suggests that microglia from males have a greater pro-inflammatory response to LPS, which we believe is contributing to the observed enhancement in pLTF in our 7d CTB-SAP treated male rats. Therefore, it is possible that estrogen signaling is constraining pLTF by interfering with mechanisms of inflammation. We have yet to evaluate markers of inflammation in CTB-SAP treated female rats.

Determine if receptors required to evoke pLTF are utilized for eupnea in CTB-SAP rats

Because we have determined that there is a difference in the requirement of Gq and Gs receptors and downstream signaling pathways in 7d *vs*. 28d CTB-SAP rats that contribute to the differential magnitude of pLTF elicited at these time points, the next step would be to determine if these same pathways are utilized to maintain eupnea. Previous studies have indicated that A2A receptor activation improves ventilation in rats that had a cervical spinal cord injury (Golder et al., 2008). In addition, studies in brainstem slices demonstrated that the endogenous activation of 5-HT2A is required for the generation of the respiratory rhythm *in vitro* (Peña and Ramirez, 2002), and thus, may contribute to maintaining eupnea. However, whether A2A and/or 5-HT2A/B receptors assist in the maintenance of eupneic ventilation following CTB-SAP treatment has yet to be determined. Therefore, we speculate that A2A receptors are required for eupneic ventilation in 7d (but not 28d) rats, and 5-HT2 receptors are required for eupneic ventilation in 28d (but not 7d) rats. I had conducted a pilot study to determine if 3 days of intraperitoneal injections of A2A (MSX-3) or 5-HT (methysergide) would impact breathing in 7d and 28d control and CTB-SAP treated rats, but I did not see any impact on breathing parameters. Therefore, I have proposed the following methods to ensure drug delivery directly to the cervical spinal cord to evaluate the impact of Gq and Gs mechanisms on breathing.

Male Sprague-Dawley rats would have an osmotic minipump implanted near the scapula with the silicone catheter inserted subdurally and secured over the phrenic motor nucleus in the C4 section of the spinal cord for the delivery of either the A2A (MSX-3), 5-HT (methysergide), or 5-HT2A/B (ketanserin) receptor antagonists to evaluate the role of Gq and Gs receptors, as studied in Chapter 2. The same experiment can be repeated using

siRNAs against BDNF and TrkB or protein inhibitors to target PI3K/Akt or MEK/ERK signaling, as studied in Chapter 3. Rats would be allowed 3d of recovery before receiving an intrapleural injection of either: 1) CTB–SAP (25 µg), or 2) unconjugated CTB and SAP (*i.e.,* control; (CTB + SAP). This recovery period is necessary because we know inflammation differentially impacts pLTF, as described in Appendix I, so we would want to eliminate this variable. Whole-body plethysmography would then be performed on rats either 7- or 28-days post-injection. Respiratory parameters including respiratory frequency, tidal volume and minute ventilation would be recorded in freely-moving rats while they are breathing room air (*i.e.*, baseline; 30 min of 21% O_2, balance nitrogen (N_2)), followed by hypercapnia (21% O_2, 7% carbon dioxide (CO_2), balance $N2$; 5 min), and hypoxia + hypercapnia conditions (10.5% O_2/7% CO_2; 5 min; *i.e.*, maximum ventilatory capacity or Max). In doing so, it can be determined exactly what factors impact breathing with delivery specifically to the cervical spinal cord which encompasses the phrenic motor nucleus.

Determine the recruitment of other accessory muscle groups and the neural networks involved

Extradiaphragmatic inspiratory muscle groups (such as the intercostal and sternocleidomastoid muscles) may be recruited first to compensate for breathing in 7d and 28d CTB-SAP rats, but it may not be necessary for the pectoralis minor muscles to be recruited to move the chest wall until the diaphragm can no longer contract enough to maintain adequate tidal volume (*i.e.*, greater than 28d). Other studies have shown that the external intercostal, sternocleidomastoid, abdominal, and scalene muscles are recruited following bilateral diaphragmatic hemiparalysis, ALS, and spinal cord injury (Bennett et

al., 2004; Bye et al., 1990; Harrison et al., 1971; Kreitzer et al., 1978a; Stone and Keltz, 1963). Thus, future studies could be focused on determining which accessory muscles get recruited following CTB-SAP treatment, how much their amplitude changes from 7d to 28d of treatment, and if the amplitude changes based on state of wakefulness and/or anesthesia. This can be achieved through the implantation of telemetry devices to evaluate which muscles are affected or recruited first, as well as to what extent each muscle group is affected or recruited following respiratory motor neuron death. After determining the contributions or deficits elicited by each muscle group, these muscles could then be evaluated again following AIH exposure to determine if these muscles elicit plasticity and could be further recruited. Additional studies could evaluate the amplitude of the nerve supply to these muscles (*e.g.*, the accessory nerve and the medial and lateral brachial nerves) to see if CTB-SAP treatment induces alternative nerve bed compensation for the maintenance of eupneic ventilation. In other words, is eupneic ventilation maintained due to increased nerve output to accessory inspiratory musculature in response to CTB-SAP-induced respiratory motor neuron death?

Some muscle fiber types are much more susceptible (type I muscle fibers are less susceptible that type II) to atrophy in neuromuscular disease states and these muscle fibers undergo denervation and reinnervation with progressive motor neuron loss. In the SOD1^{G93A} mouse model of ALS, axonal detachment of motor neuron terminals from muscle occurs at 47 days while symptom onset isn't observed until 90 days (Fischer et al., 2004) resulting in a significant drop in muscle fiber force (˜60%) in pre-symptomatic SOD1^{G93A} mice (Hegedus et al., 2008). Since type I fibers are utilized for eupneic breathing in humans and animals (Polla et al., 2004) and eupneic ventilation is maintained following

CTB-SAP treatment, we suggest type I fibers in the pectoralis minor muscles will be unaffected following CTB-SAP treatment while type II fibers, which are recruited when respiratory demand increases (Polla et al., 2004), will be decreased following CTB-SAP treatment contributing to the deficits observed during max. Future histological studies could be performed on the diaphragm and pectoralis minor muscles (and possibly other accessory inspiratory muscles) to determine: 1) fiber type characterization and distribution base on myosin heavy-chain isoforms; and 2) how fiber type is affected by CTB-SAP-induced respiratory motor neuron death in terms of atrophy, size/type characterization, and distribution.

6.5- Overall Conclusions

The current studies investigated underlying G-coupled protein receptor-dependent mechanisms of AIH-induced respiratory plasticity, the impact of COX1/2-induced inflammation on respiratory plasticity, and the recruitment of the pectoralis minor muscle in an effort to further our understanding of breathing function preservation following CTB-SAP-induced respiratory motor neuron death and to develop targets to increase maximal ventilatory capacity (Fig. 6.1). In terms of respiratory plasticity, we know that the magnitude of respiratory plasticity elicited in 7d CTB-SAP rats is enhanced compared to 28d CTB-SAP and control rats. The current studies found that the observed enhancement in pLTF at 7d occurs through the activation of (Gs)-A_{2A} receptors and primarily through downstream PI3K/Akt signaling (Chapters 2 & 3). Conversely, we found that similar to controls and naïve rats, 28d rats elicit pLTF that is more moderate through the activation of (Gq)-5-HT receptors, presumably 5-HT_2 receptors, and subsequent MEK/ERK

signaling (Chapters 2 & 3). Additionally, I found that COX1/2-induced inflammation contributes to enhanced pLTF in 7d CTB-SAP rats, while it constrains pLTF in 28d CTB-SAP rats. These findings suggest differences in pLTF pathways and inflammatory responses following early *vs*. late respiratory motor neuron loss, and that these pathways can be targeted to enhance pLTF in patients experiencing neurodegeneration from disease or injury in an effort to delay mechanical ventilatory dependence and improve quality of life. More specifically, it is important that there are multiple pathways of plasticity because determining the stage of disease can be clinically difficult. Therefore, if targeting one G-coupled protein receptor mechanism does not improve pLTF or ventilation, then another mechanism(s) could be targeted and result in a beneficial outcome. This dissertation also provides further insight as to when anti-inflammatory drugs should be given to patients with neuromuscular diseases/injuries. NSAID treatment does not seem to be beneficial early on in terms of breathing maintenance through mechanisms of pLTF. However, because patients usually do not seek medical attention until there is significant clinical presentation of a disease/injury, NSAIDs may be useful in contributing to pLTF and breathing maintenance at this time.

Additionally, I investigated the role of an accessory inspiratory muscle, the pectoralis minor muscle, and its recruitment and contribution to breathing maintenance following CTB-SAP-induced respiratory motor neuron death. I found that 7d CTB-SAP rats recruit pectoralis minor muscle activity, which is even more greatly recruited in 28d CTB-SAP rats. When the role of these muscles was evaluated for their contributions to breathing, it was found that these muscles are not necessary for eupnea, but may have implications for minimizing breathing deficits during maximal chemosensory stimulation.

This does not eliminate the role of these muscles in the overall maintenance of breathing following respiratory motor neuron death, as they may be stimulated (directly, or indirectly through AIH exposure) for breathing maintenance.

LIST OF REFERENCES

Acker, M.A., J.D. Mannion, W.E. Brown, S. Salmons, J. Henriksson, T. Bitto, D.R. Gale, R. Hammond, and L.W. Stephenson. 1987. Canine diaphragm muscle after 1 yr of continuous electrical stimulation: its potential as a myocardial substitute. *Journal of Applied Physiology* 62:1264-1270.

Agosto-Marlin, I.M., and G.S. Mitchell. 2017. Spinal BDNF-induced phrenic motor facilitation requires PKCθ activity. *Journal of neurophysiology* 118:2755-2762.

Agosto-Marlin, I.M., N.L. Nichols, and G.S. Mitchell. 2017. Adenosine-dependent phrenic motor facilitation is inflammation resistant. *Journal of neurophysiology* 117:836-845.

Agosto-Marlin, I.M., N.L. Nichols, and G.S. Mitchell. 2018. Systemic inflammation inhibits serotonin receptor 2-induced phrenic motor facilitation upstream from BDNF/TrkB signaling. *Journal of neurophysiology* 119:2176-2185.

Alexianu, M.E., M. Kozovska, and S.H. Appel. 2001. Immune reactivity in a mouse model of familial ALS correlates with disease progression. *Neurology* 57:1282-1289.

Anzueto, A., and M. Miravitlles. 2017. Pathophysiology of dyspnea in COPD. *Postgraduate medicine* 129:366-374.

Arnulf, I., T. Similowski, F. Salachas, L. Garma, S. Mehiri, V. Attali, V. Behin-Bellhesen, V. Meininger, and J.-P. Derenne. 2000. Sleep disorders and diaphragmatic function in patients with amyotrophic lateral sclerosis. *American journal of respiratory and critical care medicine* 161:849-856.

Aszmann, O.C., M. Rab, L. Kamolz, and M. Frey. 2000. The anatomy of the pectoral nerves and their significance in brachial plexus reconstruction. *The Journal of hand surgery* 25:942-947.

Aznar, J.P., J. Urbano, E.G. Laborda, P.Q. Moreno, and L.F. Vergara. 1996. Breast and pectoralis muscle hypoplasia: A mild degree of Poland's syndrome. *Acta Radiologica* 37:759-762.

Bach, K.B., and G.S. Mitchell. 1996. Hypoxia-induced long-term facilitation of respiratory activity is serotonin dependent. *Respiration physiology* 104:251-260.

Baertsch, N.A., and T.L. Baker-Herman. 2013. Inactivity-induced phrenic and hypoglossal motor facilitation are differentially expressed following intermittent vs. sustained neural apnea. *Journal of applied physiology* 114:1388-1395.

Baker-Herman, T.L., D.D. Fuller, R.W. Bavis, A.G. Zabka, F.J. Golder, N.J. Doperalski, R.A. Johnson, J.J. Watters, and G.S. Mitchell. 2004. BDNF is necessary and sufficient for spinal respiratory plasticity following intermittent hypoxia. *Nature neuroscience* 7:48.

Baker-Herman, T.L., and G.S. Mitchell. 2008. Determinants of frequency long-term facilitation following acute intermittent hypoxia in vagotomized rats. *Respiratory physiology & neurobiology* 162:8-17.

Baker-Herman, T.L., and K.A. Strey. 2011. Similarities and differences in mechanisms of phrenic and hypoglossal motor facilitation. *Respiratory physiology & neurobiology* 179:48-56.

Baker, T., and G. Mitchell. 2000. Episodic but not continuous hypoxia elicits long-term facilitation of phrenic motor output in rats. *The Journal of physiology* 529:215-219.

Barok, R., J. Grittner, and B. Dougherty. The Long-Term Impact of Ovariectomy on Ventilation and Expression of Phrenic Long-Term Facilitation in Female Rats. *The FASEB Journal* 35:

Barr, M.R.L., C.M. Sibigtroth, and G.S. Mitchell. 2007. Daily acute intermittent hypoxia improves respiratory function in rats with chronic cervical spinal hemisection. In Wiley Online Library.

Bartley, J. 2011. Breathing and temporomandibular joint disease. *Journal of Bodywork and movement therapies* 15:291-297.

Bascom, A.T., A. Sankari, H.G. Goshgarian, and M.S. Badr. 2015. Sleep onset hypoventilation in chronic spinal cord injury. *Physiological reports* 3:e12490.

Beal, M.F., R.J. Ferrante, S.E. Browne, R.T. Matthews, N.W. Kowall, and R.H. Brown Jr. 1997. Increased 3-nitrotyrosine in both sporadic and familial amyotrophic lateral sclerosis. *Annals of Neurology: Official Journal of the American Neurological Association and the Child Neurology Society* 42:644-654.

Beattie, E.C., D. Stellwagen, W. Morishita, J.C. Bresnahan, B.K. Ha, M. Von Zastrow, M.S. Beattie, and R.C. Malenka. 2002. Control of synaptic strength by glial TNFα. *Science* 295:2282-2285.

Beers, D.R., J.S. Henkel, Q. Xiao, W. Zhao, J. Wang, A.A. Yen, L. Siklos, S.R. McKercher, and S.H. Appel. 2006. Wild-type microglia extend survival in PU. 1 knockout mice with familial amyotrophic lateral sclerosis. *Proceedings of the National Academy of Sciences* 103:16021-16026.

Beers, D.R., W. Zhao, B. Liao, O. Kano, J. Wang, A. Huang, S.H. Appel, and J.S. Henkel. 2011. Neuroinflammation modulates distinct regional and temporal clinical responses in ALS mice. *Brain, behavior, and immunity* 25:1025-1035.

Benditt, J.O. 2006. The neuromuscular respiratory system: physiology, pathophysiology, and a respiratory care approach to patients. *Respiratory care* 51:829-839.

Bennett, J., H. Dunroy, D. Corfield, N. Hart, A. Simonds, M. Polkey, and M. Morrell. 2004. Respiratory muscle activity during REM sleep in patients with diaphragm paralysis. *Neurology* 62:134-137.

Benot, A., and J. Lopez-Barneo. 1990. Feedback inhibition of Ca2+ currents by dopamine in glomus cells of the carotid body. *European Journal of Neuroscience* 2:809-812.

Berlowitz, D.J., D.J. Brown, D.A. Campbell, and R.J. Pierce. 2005. A longitudinal evaluation of sleep and breathing in the first year after cervical spinal cord injury. *Archives of physical medicine and rehabilitation* 86:1193-1199.

Bianchi, A.L., M. Denavit-Saubie, and J. Champagnat. 1995. Central control of breathing in mammals: neuronal circuitry, membrane properties, and neurotransmitters. *Physiological reviews* 75:1-45.

Boentert, M., S. Wenninger, and V.A. Sansone. 2017. Respiratory involvement in neuromuscular disorders. *Current opinion in neurology* 30:529-537.

Borkowski, L.F., T.A. Craig, O.E. Stricklin, K.A. Johnson, and N.L. Nichols. 2020. 5-HT2A/B receptor expression in the phrenic motor nucleus in a rat model of ALS (SOD1G93A). *Respiratory Physiology & Neurobiology* 103471.

Borkowski, L.F., and N.L. Nichols. 2020. Differential mechanisms are required for phrenic long-term facilitation over the course of motor neuron loss following CTB-SAP intrapleural injections. *Experimental Neurology* 113460.

Boulenguez, P., C. Gestreau, S. Vinit, J.-C. Stamegna, A. Kastner, and P. Gauthier. 2007. Specific and artifactual labeling in the rat spinal cord and medulla after injection of monosynaptic retrograde tracers into the diaphragm. *Neuroscience letters* 417:206-211.

Bourke, S., P. Shaw, and G. Gibson. 2001. Respiratory function vs sleep-disordered breathing as predictors of QOL in ALS. *Neurology* 57:2040-2044.

Broytman, O., N.A. Baertsch, and T.L. Baker-Herman. 2013. Spinal TNFα is necessary for inactivity-induced phrenic motor facilitation. *The Journal of physiology* 591:5585-5598.

Bruijn, L.I., M.K. Houseweart, S. Kato, K.L. Anderson, S.D. Anderson, E. Ohama, A.G. Reaume, R.W. Scott, and D.W. Cleveland. 1998. Aggregation and motor neuron toxicity of an ALS-linked SOD1 mutant independent from wild-type SOD1. *Science* 281:1851-1854.

Bryson, H.M., B. Fulton, and P. Benfield. 1996. Riluzole. *Drugs* 52:549-563.

Bye, P., E.R. Ellis, F.G. Issa, P.M. Donnelly, and C.E. Sullivan. 1990. Respiratory failure and sleep in neuromuscular disease. *Thorax* 45:241-247.

Campbell, E. 1955. An electromyographic examination of the role of the intercostal muscles in breathing in man. *The Journal of physiology* 129:12-26.

Cao, F.-j., and S.-q. Feng. 2009. Human umbilical cord mesenchymal stem cells and the treatment of spinal cord injury. *Chinese medical journal* 122:225-231.

Caruana-Montaldo, B., K. Gleeson, and C.W. Zwillich. 2000. The control of breathing in clinical practice. *Chest* 117:205-225.

Chang, A.J. 2017. Acute oxygen sensing by the carotid body: from mitochondria to plasma membrane. *Journal of Applied Physiology* 123:1335-1343.

Chitravanshi, V., and H. Sapru. 1996. NMDA as well as non-NMDA receptors mediate the neurotransmission of inspiratory drive to phrenic motoneurons in the adult rat. *Brain research* 715:104-112.

Conforti, L., I. Bodi, J.W. Nisbet, and D.E. Millhorn. 2000. O2-sensitive K+ channels: role of the Kv1. 2 α-subunit in mediating the hypoxic response. *The Journal of physiology* 524:783-793.

Cortés-Julián, G., H.B. Bushra-Nuritu, R. Buenfil-Fuentes, and J.A.M. Rajme. 2017. Modified Ravitch procedure for left Poland syndrome combined with pectus excavatum. *The Annals of thoracic surgery* 104:e337-e339.

Dale-Nagle, E.A., M.S. Hoffman, P.M. MacFarlane, and G.S. Mitchell. 2010. Multiple pathways to long-lasting phrenic motor facilitation. In New frontiers in respiratory control. Springer, 225-230.

Dale-Nagle, E.A., I. Satriotomo, and G.S. Mitchell. 2011. Spinal vascular endothelial growth factor induces phrenic motor facilitation via extracellular signal-regulated kinase and Akt signaling. *Journal of Neuroscience* 31:7682-7690.

Dale, E., L. Nashold, S. Mahamed, C. Svendsen, and G. Mitchell. 2006. Sustained ventilatory capacity in a rat model of amyotrophic lateral sclerosis (ALS). In Wiley Online Library.

Dale, E.A., and G.S. Mitchell. 2013. Spinal vascular endothelial growth factor (VEGF) and erythropoietin (EPO) induced phrenic motor facilitation after repetitive acute intermittent hypoxia. *Respiratory physiology & neurobiology* 185:481-488.

De Troyer, A., and M. Estenne. 1984. Coordination between rib cage muscles and diaphragm during quiet breathing in humans. *Journal of Applied Physiology* 57:899-906.

Devinney, M.J., D.P. Fields, A.G. Huxtable, T.J. Peterson, E.A. Dale, and G.S. Mitchell. 2015. Phrenic long-term facilitation requires PKCθ activity within phrenic motor neurons. *Journal of Neuroscience* 35:8107-8117.

Devinney, M.J., A.G. Huxtable, N.L. Nichols, and G.S. Mitchell. 2013. Hypoxia-induced phrenic long-term facilitation: emergent properties. *Annals of the New York Academy of Sciences* 1279:143-153.

Devinney, M.J., N.L. Nichols, and G.S. Mitchell. 2012. Spinal A2A receptor inhibition reveals phrenic motor facilitation following moderate sustained hypoxia. In Federation of American Societies for Experimental Biology.

Dougherty, B. The Influence of Circulating Sex Hormones on Severe Intermittent Hypoxia-Induced Phrenic Long-Term Facilitation in Female and Male Rats. *The FASEB Journal* 35:

Dougherty, B.J., E. Tyurina, and D. McIntosh. 2018. Spinal Conversion of Testosterone to Estradiol for the Expression of Phrenic Long-term Facilitation in Adult Male Rats. *The FASEB Journal* 32:878.873-878.873.

Dröge, W. 2002. Free radicals in the physiological control of cell function. *Physiological reviews*

Drorbaugh, J.E., and W.O. Fenn. 1955. A barometric method for measuring ventilation in newborn infants. *Pediatrics* 16:81-87.

Engel, R.M., and S. Vemulpad. 2009. Progression to chronic obstructive pulmonary disease (COPD): Could it be prevented by manual therapy and exercise during the 'at risk'stage (stage 0)? *Medical hypotheses* 72:288-290.

Faden, A.I., P. Demediuk, S.S. Panter, and R. Vink. 1989. The role of excitatory amino acids and NMDA receptors in traumatic brain injury. *Science* 244:798-800.

Farooque, M., L. Hillered, A. Holtz, and Y. Olsson. 1996. Changes of extracellular levels of amino acids after graded compression trauma to the spinal cord: an experimental study in the rat using microdialysis. *Journal of neurotrauma* 13:537-548.

Feldman, J., G.S. Mitchell, and E. Nattie. 2003. Breathing: rhythmicity, plasticity, and chemosensitivity. *Annu Rev Neurosci* 26:239-266.

Fendrick, S.E., Q.-S. Xue, and W.J. Streit. 2007. Formation of multinucleated giant cells and microglial degeneration in rats expressing a mutant Cu/Zn superoxide dismutase gene. *Journal of neuroinflammation* 4:1-12.

Fields, D.P., S. Springborn, and G.S. Mitchell. 2015. Spinal 5-HT7 receptors induce phrenic motor facilitation via EPAC-mTORC1 signaling. *Journal of neurophysiology* 114:2015-2022.

Fischer, L.R., D.G. Culver, P. Tennant, A.A. Davis, M. Wang, A. Castellano-Sanchez, J. Khan, M.A. Polak, and J.D. Glass. 2004. Amyotrophic lateral sclerosis is a distal axonopathy: evidence in mice and man. *Experimental neurology* 185:232-240.

Frankel, H., J. Coll, S. Charlifue, G. Whiteneck, B. Gardner, M. Jamous, K. Krishnan, I. Nuseibeh, G. Savic, and P. Sett. 1998. Long-term survival in spinal cord injury: a fifty year investigation. *Spinal cord* 36:

Fuller, D., K. Bach, T. Baker, R. Kinkead, and G. Mitchell. 2000. Long term facilitation of phrenic motor output. *Respiration physiology* 121:135-146.

Fuller, D., A. Zabka, T. Baker, and G. Mitchell. 2001. Selected contribution: phrenic long-term facilitation requires 5-HT receptor activation during but not following episodic hypoxia. *Journal of applied physiology* 90:2001-2006.

Fuller, D.D., F.J. Golder, E. Olson Jr, and G.S. Mitchell. 2006. Recovery of phrenic activity and ventilation after cervical spinal hemisection in rats. *Journal of Applied Physiology* 100:800-806.

Fuller, D.D., S.M. Johnson, E.B. Olson, and G.S. Mitchell. 2003. Synaptic pathways to phrenic motoneurons are enhanced by chronic intermittent hypoxia after cervical spinal cord injury. *Journal of Neuroscience* 23:2993-3000.

Gardner, A.N., B.J. Dougherty, and J.J. Watters. 2016. Differential Responses of Male and Female Microglia to LPS and Estrogen May Contribute to Sexually Dimorphic Effects of Inflammation on Phrenic Long-term Facilitation. *The FASEB Journal* 30:992.991-992.991.

Gaultier, C., J. Praud, E. Canet, M. Delaperche, and A. d'Allest. 1987. Paradoxical inward rib cage motion during rapid eye movement sleep in infants and young children. *Journal of developmental physiology* 9:391-397.

Gaviria, M., A. Privat, P. d'Arbigny, J.-M. Kamenka, H. Haton, and F. Ohanna. 2000. Neuroprotective effects of a novel NMDA antagonist, Gacyclidine, after experimental contusive spinal cord injury in adult rats. *Brain research* 874:200-209.

Glebov, K., M. Löchner, R. Jabs, T. Lau, O. Merkel, P. Schloss, C. Steinhäuser, and J. Walter. 2015. Serotonin stimulates secretion of exosomes from microglia cells. *Glia* 63:626-634.

Golder, F., D. Fuller, M. Lovett-Barr, S. Vinit, D. Resnick, and G. Mitchell. 2011. Breathing patterns after mid-cervical spinal contusion in rats. *Experimental neurology* 231:97-103.

Golder, F.J., and G.S. Mitchell. 2005. Spinal synaptic enhancement with acute intermittent hypoxia improves respiratory function after chronic cervical spinal cord injury. *Journal of Neuroscience* 25:2925-2932.

Golder, F.J., L. Ranganathan, I. Satriotomo, M. Hoffman, M.R. Lovett-Barr, J.J. Watters, T.L. Baker-Herman, and G.S. Mitchell. 2008. Spinal adenosine A2a receptor activation elicits long-lasting phrenic motor facilitation. *Journal of Neuroscience* 28:2033-2042.

Golder, F.J., P.J. Reier, P.W. Davenport, and D.C. Bolser. 2001. Cervical spinal cord injury alters the pattern of breathing in anesthetized rats. *Journal of Applied Physiology* 91:2451-2458.

Gonzalez-Bermejo, J., C. Morélot-Panzini, F. Salachas, S. Redolfi, C. Straus, M.-H. Becquemin, I. Arnulf, P.-F. Pradat, G. Bruneteau, and A.R. Ignagni. 2012. Diaphragm pacing improves sleep in patients with amyotrophic lateral sclerosis. *Amyotrophic Lateral Sclerosis* 13:44-54.

Gonzalez-Bermejo, J., C. Morélot-Panzini, M.-L. Tanguy, V. Meininger, P.-F. Pradat, T. Lenglet, G. Bruneteau, N. Le Forestier, P. Couratier, and N. Guy. 2016. Early diaphragm pacing in patients with amyotrophic lateral sclerosis (RespiStimALS): a randomised controlled triple-blind trial. *The Lancet Neurology* 15:1217-1227.

Gonzalez, C., L. Almaraz, A. Obeso, and R. Rigual. 1994. Carotid body chemoreceptors: from natural stimuli to sensory discharges. *Physiological reviews* 74:829-898.

Goshgarian, H.G. 2003. Invited review: the crossed phrenic phenomenon: a model for plasticity in the respiratory pathways following spinal cord injury. *Journal of applied physiology* 94:795-810.

Goshgarian, H.G. 2009. The crossed phrenic phenomenon and recovery of function following spinal cord injury. *Respiratory physiology & neurobiology* 169:85-93.

Graeber, M.B. 2010. Changing face of microglia. *Science* 330:783-788.

Grassino, A., M. Goldman, J. Mead, and T. Sears. 1978. Mechanics of the human diaphragm during voluntary contraction: statics. *Journal of Applied Physiology* 44:829-839.

Grittner, J., S. Miller, and B. Dougherty. 2021. Conversion of Testosterone to Estradiol is Necessary for the Development of Long-term Facilitation in Adult Male Rats. *The FASEB Journal* 35:

Guyenet, P.G., and D.A. Bayliss. 2015. Neural control of breathing and CO2 homeostasis. *Neuron* 87:946-961.

Hall, E., P. Yonkers, P. Andrus, J. Cox, and D. Anderson. 1992. Biochemistry and pharmacology of lipid antioxidants in acute brain and spinal cord injury. *Journal of neurotrauma* 9:S425-442.

Hanamsagar, R., M.L. Hanke, and T. Kielian. 2012. Toll-like receptor (TLR) and inflammasome actions in the central nervous system. *Trends in immunology* 33:333-342.

Harrison, B., J. Collins, K. Brown, and T. Clark. 1971. Respiratory failure in neuromuscular diseases. *Thorax* 26:579-584.

Hayashi, F., C. Hinrichsen, and D.R. McCrimmon. 2003. Short-term plasticity of descending synaptic input to phrenic motoneurons in rats. *Journal of applied physiology* 94:1421-1430.

Hegedus, J., C. Putman, N. Tyreman, and T. Gordon. 2008. Preferential motor unit loss in the SOD1G93A transgenic mouse model of amyotrophic lateral sclerosis. *The Journal of physiology* 586:3337-3351.

Heldt, G.P., and M.B. McIlroy. 1987. Dynamics of chest wall in preterm infants. *Journal of applied physiology* 62:170-174.

Hocker, A.D., and A.G. Huxtable. 2018. IL-1 receptor activation undermines respiratory motor plasticity after systemic inflammation. *Journal of Applied Physiology* 125:504-512.

Hocker, A.D., J.A. Stokes, F.L. Powell, and A.G. Huxtable. 2017. The impact of inflammation on respiratory plasticity. *Experimental neurology* 287:243-253.

Hoffman, M., F. Golder, S. Mahamed, and G. Mitchell. 2010. Spinal adenosine A2A receptor inhibition enhances phrenic long term facilitation following acute intermittent hypoxia. *The Journal of physiology* 588:255-266.

Hoffman, M., and G. Mitchell. 2011. Spinal 5-HT7 receptor activation induces long-lasting phrenic motor facilitation. *The Journal of physiology* 589:1397-1407.

Hoffman, M., and G. Mitchell. 2013. Spinal 5-HT7 receptors and protein kinase A constrain intermittent hypoxia-induced phrenic long-term facilitation. *Neuroscience* 250:632-643.

Hoffman, M.S., N.L. Nichols, P.M. MacFarlane, and G.S. Mitchell. 2012. Phrenic long-term facilitation after acute intermittent hypoxia requires spinal ERK activation but not TrkB synthesis. *Journal of applied physiology* 113:1184-1193.

Howland, D.S., J. Liu, Y. She, B. Goad, N.J. Maragakis, B. Kim, J. Erickson, J. Kulik, L. DeVito, and G. Psaltis. 2002. Focal loss of the glutamate transporter EAAT2 in a transgenic rat model of SOD1 mutant-mediated amyotrophic lateral sclerosis (ALS). *Proceedings of the National Academy of Sciences* 99:1604-1609.

Hruska Jr, R.J. 1997. DYSFUNCTIONAL, RESPIRATORY MECHANICS ON OROFACIAL PAIN. *Dental Clinics of North America* 41:211.

Hughes, P.D., M.I. Polkey, M. Lou Harris, A.J. Coats, J. Moxham, and M. Green. 1999. Diaphragm strength in chronic heart failure. *American journal of respiratory and critical care medicine* 160:529-534.

Huston, J.M., and K.J. Tracey. 2011. The pulse of inflammation: heart rate variability, the cholinergic anti-inflammatory pathway and implications for therapy. *Journal of internal medicine* 269:45-53.

Huxtable, A., S. Vinit, J. Windelborn, S. Crader, C. Guenther, J. Watters, and G. Mitchell. 2011. Systemic inflammation impairs respiratory chemoreflexes and plasticity. *Respiratory physiology & neurobiology* 178:482-489.

Huxtable, A.G., P.M. MacFarlane, S. Vinit, N.L. Nichols, E.A. Dale, and G.S. Mitchell. 2014. Adrenergic α1 receptor activation is sufficient, but not necessary for phrenic long-term facilitation. *Journal of Applied Physiology* 116:1345-1352.

Huxtable, A.G., S.M. Smith, T.J. Peterson, J.J. Watters, and G.S. Mitchell. 2015. Intermittent hypoxia-induced spinal inflammation impairs respiratory motor plasticity by a spinal p38 MAP kinase-dependent mechanism. *Journal of Neuroscience* 35:6871-6880.

Huxtable, A.G., S.M. Smith, S. Vinit, J.J. Watters, and G.S. Mitchell. 2013. Systemic LPS induces spinal inflammatory gene expression and impairs phrenic long-term facilitation following acute intermittent hypoxia. *Journal of applied physiology* 114:879-887.

Ito, H., R. Wate, J. Zhang, S. Ohnishi, S. Kaneko, H. Ito, S. Nakano, and H. Kusaka. 2008. Treatment with edaravone, initiated at symptom onset, slows motor decline and decreases SOD1 deposition in ALS mice. *Experimental neurology* 213:448-455.

Jacky, J. 1978. A plethysmograph for long-term measurements of ventilation in unrestrained animals. *Journal of Applied Physiology* 45:644-647.

Jensen, V.N., K. Seedle, S.M. Turner, J.N. Lorenz, and S.A. Crone. 2019. V2a neurons constrain extradiaphragmatic respiratory muscle activity at rest. *Eneuro* 6:

Kelley, R.C., and L.F. Ferreira. 2017. Diaphragm abnormalities in heart failure and aging: mechanisms and integration of cardiovascular and respiratory pathophysiology. *Heart failure reviews* 22:191-207.

Kettenmann, H., U.-K. Hanisch, M. Noda, and A. Verkhratsky. 2011. Physiology of microglia. *Physiological reviews* 91:461-553.

Khurram, O.U., M.J. Fogarty, S. Rana, P. Vang, G.C. Sieck, and C.B. Mantilla. 2019. Diaphragm muscle function following midcervical contusion injury in rats. *Journal of Applied Physiology* 126:221-230.

Kinkead, R., W.-Z. Zhan, Y. Prakash, K.B. Bach, G.C. Sieck, and G.S. Mitchell. 1998. Cervical dorsal rhizotomy enhances serotonergic innervation of phrenic motoneurons and serotonin-dependent long-term facilitation of respiratory motor output in rats. *Journal of Neuroscience* 18:8436-8443.

Kotlyarov, A., A. Neininger, C. Schubert, R. Eckert, C. Birchmeier, H.-D. Volk, and M. Gaestel. 1999. MAPKAP kinase 2 is essential for LPS-induced TNF-α biosynthesis. *Nature cell biology* 1:94-97.

Krabbe, G., V. Matyash, U. Pannasch, L. Mamer, H.W. Boddeke, and H. Kettenmann. 2012. Activation of serotonin receptors promotes microglial injury-induced motility but attenuates phagocytic activity. *Brain, behavior, and immunity* 26:419-428.

Kreitzer, S.M., N.T. Feldman, N.A. Saunders, and R.H. Ingram Jr. 1978a. Bilateral diaphragmatic paralysis with hypercapnic respiratory failure: a physiologic assessment. *The American journal of medicine* 65:89-95.

Kreitzer, S.M., N.A. Saunders, H.R. Tyler, and R.H. Ingram Jr. 1978b. Respiratory muscle function in amyotrophic lateral sclerosis. *American Review of Respiratory Disease* 117:437-447.

Kreutzberg, G.W. 1996. Microglia: a sensor for pathological events in the CNS. *Trends in neurosciences* 19:312-318.

Kumar, P., and N.R. Prabhakar. 2011. Peripheral chemoreceptors: function and plasticity of the carotid body. *Comprehensive Physiology* 2:141-219.

Lai, H.-L., T.-H. Yang, R.O. Messing, Y.-H. Ching, S.-C. Lin, and Y. Chern. 1997. Protein kinase C inhibits adenylyl cyclase type VI activity during desensitization of the A2a-adenosine receptor-mediated cAMP response. *Journal of Biological Chemistry* 272:4970-4977.

Lampron, A., A. ElAli, and S. Rivest. 2013. Innate immunity in the CNS: redefining the relationship between the CNS and Its environment. *Neuron* 78:214-232.

Lane, M.A., K.-Z. Lee, D.D. Fuller, and P.J. Reier. 2009. Spinal circuitry and respiratory recovery following spinal cord injury. *Respiratory physiology & neurobiology* 169:123-132.

Lechtzin, N., C.M. Wiener, D.M. Shade, L. Clawson, and G.B. Diette. 2002. Spirometry in the supine position improves the detection of diaphragmatic weakness in patients with amyotrophic lateral sclerosis. *Chest* 121:436-442.

Lee, K.-Z. 2019. Impact of cervical spinal cord contusion on the breathing pattern across the sleep-wake cycle in the rat. *Journal of Applied Physiology* 126:111-123.

Lee, K.-Z., and S.-H. Hsu. 2017. Compensatory function of the diaphragm after high cervical hemisection in the rat. *Journal of neurotrauma* 34:2634-2644.

Lee, K.-Z., and H.-C. Kuo. 2017. Vagal control of breathing pattern after midcervical contusion in rats. *Journal of neurotrauma* 34:734-745.

Lefebvre, S., L. Bürglen, S. Reboullet, O. Clermont, P. Burlet, L. Viollet, B. Benichou, C. Cruaud, P. Millasseau, and M. Zeviani. 1995. Identification and characterization of a spinal muscular atrophy-determining gene. *Cell* 80:155-165.

Lencer, W.I., and B. Tsai. 2003. The intracellular voyage of cholera toxin: going retro. *Trends in biochemical sciences* 28:639-645.

Lian, T., and R.J. Ho. 1997. Cholera toxin B-mediated targeting of lipid vesicles containing ganglioside GM1 to mucosal epithelial cells. *Pharmaceutical research* 14:1309-1315.

Ling, L., D.D. Fuller, K.B. Bach, R. Kinkead, E.B. Olson, and G.S. Mitchell. 2001. Chronic intermittent hypoxia elicits serotonin-dependent plasticity in the central neural control of breathing. *Journal of Neuroscience* 21:5381-5388.

Liu, J., X. Wei, C. Zhao, S. Hu, J. Duan, G. Ju, M.T. Wong-Riley, and Y. Liu. 2011. 5-HT induces enhanced phrenic nerve activity via 5-HT2A receptor/PKC mechanism in anesthetized rats. *European journal of pharmacology* 657:67-75.

Lladó, J., C. Haenggeli, A. Pardo, V. Wong, L. Benson, C. Coccia, J.D. Rothstein, J.M. Shefner, and N.J. Maragakis. 2006. Degeneration of respiratory motor neurons in the SOD1 G93A transgenic rat model of ALS. *Neurobiology of disease* 21:110-118.

Llewellyn-Smith, I.J., C. Martin, L.F. Arnolda, and J.B. Minson. 2000. Tracer-toxins: cholera toxin B-saporin as a model. *Journal of neuroscience methods* 103:83-90.

Llewellyn-Smith, I.J., C.L. Martin, L.F. Arnolda, and J.B. Minson. 1999. Retrogradely transported CTB–saporin kills sympathetic preganglionic neurons. *Neuroreport* 10:307-312.

López-Barneo, J., P. González-Rodríguez, L. Gao, M.C. Fernández-Agüera, R. Pardal, and P. Ortega-Sáenz. 2016. Oxygen sensing by the carotid body: mechanisms and role in adaptation to hypoxia. *American Journal of Physiology-Cell Physiology* 310:C629-C642.

López-Barneo, J., P. Ortega-Sáenz, R. Pardal, A. Pascual, and J. Piruat. 2008. Carotid body oxygen sensing. *European Respiratory Journal* 32:1386-1398.

Lopez-Barneo, J., R. Pardal, R. Montoro, T. Smani, J. García-Hirschfeld, and J. Urena. 1999. K+ and Ca2+ channel activity and cytosolic [Ca2+] in oxygen-sensing tissues. *Respiration physiology* 115:215-227.

López-López, J., C. Gonzalez, and M. Perez-Garcia. 1997. Properties of ionic currents from isolated adult rat carotid body chemoreceptor cells: effect of hypoxia. *The Journal of Physiology* 499:429-441.

Loring, S., and A. De Troyer. 1985. Actions of the respiratory muscles. *" The Thorax"(Lung biology in health and disease; v. 29)* 327:

Lu, Y.-C., W.-C. Yeh, and P.S. Ohashi. 2008. LPS/TLR4 signal transduction pathway. *Cytokine* 42:145-151.

Luiso, D., J.A. Villanueva, L.C. Belarte-Tornero, A. Fort, Z. Blázquez-Bermejo, S. Ruiz, R. Farré, J. Rigau, J. Martí-Almor, and N. Farré. 2020. Surface respiratory electromyography and dyspnea in acute heart failure patients. *PloS one* 15:e0232225.

Lujan, H.L., G. Palani, J.D. Peduzzi, and S.E. DiCarlo. 2010. Targeted ablation of mesenteric projecting sympathetic neurons reduces the hemodynamic response to pain in conscious, spinal cord-transected rats. *American Journal of Physiology-Regulatory, Integrative and Comparative Physiology* 298:R1358-R1365.

Lyall, R., N. Donaldson, M. Polkey, P. Leigh, and J. Moxham. 2001. Respiratory muscle strength and ventilatory failure in amyotrophic lateral sclerosis. *Brain* 124:2000-2013.

MacFarlane, P., and G. Mitchell. 2007. Serotonin-induced phrenic long-term facilitation requires reactive oxygen species signaling via the NADPH oxidase complex. *Soc Neurosci Abst* 520:

MacFarlane, P., and G. Mitchell. 2008. Respiratory long-term facilitation following intermittent hypoxia requires reactive oxygen species formation. *Neuroscience* 152:189-197.

MacFarlane, P., and G. Mitchell. 2009. Episodic spinal serotonin receptor activation elicits long-lasting phrenic motor facilitation by an NADPH oxidase-dependent mechanism. *The Journal of physiology* 587:5469-5481.

MacFarlane, P., S. Vinit, and G. Mitchell. 2011. Serotonin 2A and 2B receptor-induced phrenic motor facilitation: differential requirement for spinal NADPH oxidase activity. *Neuroscience* 178:45-55.

Mahamed, S., K.A. Strey, G.S. Mitchell, and T.L. Baker-Herman. 2011. Reduced respiratory neural activity elicits phrenic motor facilitation. *Respiratory physiology & neurobiology* 175:303-309.

Mancini, D.M., D. Henson, J. LaManca, and S. Levine. 1992. Respiratory muscle function and dyspnea in patients with chronic congestive heart failure. *Circulation* 86:909-918.

Mansel, J.K., and J.R. Norman. 1990. Respiratory complications and management of spinal cord injuries. *Chest* 97:1446-1452.

Mantilla, C.B., S.M. Greising, W.-Z. Zhan, Y.B. Seven, and G.C. Sieck. 2013. Prolonged C2 spinal hemisection-induced inactivity reduces diaphragm muscle specific force with modest, selective atrophy of type IIx and/or IIb fibers. *Journal of applied physiology* 114:380-386.

Mantilla, C.B., W.-Z. Zhan, and G.C. Sieck. 2009. Retrograde labeling of phrenic motoneurons by intrapleural injection. *Journal of neuroscience methods* 182:244-249.

Marzocchi, M., R.T. Brouillette, L.M. Klemka-Walden, S.L. Heller, D.E. Weese-Mayer, B.S. Brozanski, J. Caliendo, M. Daood, M.N. Ilbawi, and C.E. Hunt. 1990. Effects of continuous low-frequency pacing on immature canine diaphragm. *Journal of Applied Physiology* 69:892-898.

McCrimmon, D., J. Smith, and J. Feldman. 1989. Involvement of excitatory amino acids in neurotransmission of inspiratory drive to spinal respiratory motoneurons. *Journal of Neuroscience* 9:1910-1921.

McGuire, M., and L. Ling. 2004. Activation of protein kinase C near/in phrenic motoneurons is required for phrenic long-term facilitation in rats. *Am J Respir Crit Care Med* 169:A433.

McGuire, M., Y. Zhang, D.P. White, and L. Ling. 2005. Phrenic long-term facilitation requires NMDA receptors in the phrenic motonucleus in rats. *The Journal of physiology* 567:599-611.

McIntosh, D., and B.J. Dougherty. 2019. Development of ventilatory long-term facilitation is dependent on estrous cycle stage in adult female rats. *Respiratory physiology & neurobiology* 264:1-7.

McWhorter, M.L., U.R. Monani, A.H. Burghes, and C.E. Beattie. 2003. Knockdown of the survival motor neuron (Smn) protein in zebrafish causes defects in motor axon outgrowth and pathfinding. *The Journal of cell biology* 162:919-932.

Meyer, F.J., M.M. Borst, C. Zugck, A. Kirschke, D. Schellberg, W. Kübler, and M. Haass. 2001. Respiratory muscle dysfunction in congestive heart failure: clinical correlation and prognostic significance. *Circulation* 103:2153-2158.

Mitchell, G.S., T.L. Baker, S.A. Nanda, D.D. Fuller, A.G. Zabka, B.A. Hodgeman, R.W. Bavis, K.J. Mack, and E. Olson Jr. 2001. Invited review: Intermittent hypoxia and respiratory plasticity. *Journal of Applied Physiology* 90:2466-2475.

Montoro, R., J. Urena, R. Fernandez-Chacon, G. Alvarez de Toledo, and J. Lopez-Barneo. 1996. Oxygen sensing by ion channels and chemotransduction in single glomus cells. *The Journal of General Physiology* 107:133-143.

Moosman, D.A. 1980. Anatomy of the pectoral nerves and their preservation in modified mastectomy. *The American Journal of Surgery* 139:883-886.

Nakamura, A., E.B. Olson Jr, J. Terada, J.M. Wenninger, G.E. Bisgard, and G.S. Mitchell. 2010. Sleep state dependence of ventilatory long-term facilitation following acute intermittent hypoxia in Lewis rats. *Journal of applied physiology* 109:323-331.

Nattie, E. 1999. CO2, brainstem chemoreceptors and breathing. *Progress in neurobiology* 59:299-331.

Nattie, E., and A. Li. 2012. Respiration and autonomic regulation and orexin. In Progress in brain research. Elsevier, 25-46.

Nau Jr, F., B. Yu, D. Martin, and C.D. Nichols. 2013. Serotonin 5-HT 2A receptor activation blocks TNF-α mediated inflammation in vivo. *PloS one* 8:e75426.

Navarrete-Opazo, A., and G.S. Mitchell. 2014. Recruitment and plasticity in diaphragm, intercostal, and abdominal muscles in unanesthetized rats. *Journal of applied physiology* 117:180-188.

Neverova, N.V., S.A. Saywell, L.J. Nashold, G.S. Mitchell, and J.L. Feldman. 2007. Episodic stimulation of α1-adrenoreceptors induces protein kinase C-dependent persistent changes in motoneuronal excitability. *Journal of Neuroscience* 27:4435-4442.

Nicaise, C., D.M. Frank, T.J. Hala, M. Authelet, R. Pochet, D. Adriaens, J.-P. Brion, M.C. Wright, and A.C. Lepore. 2013. Early phrenic motor neuron loss and transient respiratory abnormalities after unilateral cervical spinal cord contusion. *Journal of neurotrauma* 30:1092-1099.

Nicaise, C., T.J. Hala, D.M. Frank, J.L. Parker, M. Authelet, K. Leroy, J.-P. Brion, M.C. Wright, and A.C. Lepore. 2012a. Phrenic motor neuron degeneration compromises phrenic axonal circuitry and diaphragm activity in a unilateral cervical contusion model of spinal cord injury. *Experimental neurology* 235:539-552.

Nicaise, C., R. Putatunda, T.J. Hala, K.A. Regan, D.M. Frank, J.-P. Brion, K. Leroy, R. Pochet, M.C. Wright, and A.C. Lepore. 2012b. Degeneration of phrenic motor neurons induces long-term diaphragm deficits following mid-cervical spinal contusion in mice. *Journal of neurotrauma* 29:2748-2760.

Nichols, N., R. Johnson, I. Satriotomo, and G. Mitchell. 2014. Neither serotonin nor adenosine-dependent mechanisms preserve ventilatory capacity in ALS rats. *Respiratory physiology & neurobiology* 197:19-28.

Nichols, N.L., T.A. Craig, and M.A. Tanner. 2018. Phrenic long-term facilitation following intrapleural CTB-SAP-induced respiratory motor neuron death. *Respiratory physiology & neurobiology* 256:43-49.

Nichols, N.L., E.A. Dale, and G.S. Mitchell. 2012. Severe acute intermittent hypoxia elicits phrenic long-term facilitation by a novel adenosine-dependent mechanism. *Journal of applied physiology* 112:1678-1688.

Nichols, N.L., G. Gowing, I. Satriotomo, L.J. Nashold, E.A. Dale, M. Suzuki, P. Avalos, P.L. Mulcrone, J. McHugh, and C.N. Svendsen. 2013a. Intermittent hypoxia and stem cell implants preserve breathing capacity in a rodent model of amyotrophic

lateral sclerosis. *American journal of respiratory and critical care medicine* 187:535-542.

Nichols, N.L., and G.S. Mitchell. 2021. Mechanisms of severe acute intermittent hypoxia-induced phrenic long-term facilitation. *Journal of Neurophysiology* 125:1146-1156.

Nichols, N.L., P.L. Mulcrone, J.J. Watters, C.N. Svendsen, and G.S. Mitchell. 2011. Enhanced phrenic long-term facilitation (pLTF) following intermittent hypoxia in a rat ALS model (SOD1G93A) is attenuated by spinal siRNAs targeting BDNF and TrkB synthesis. In Federation of American Societies for Experimental Biology.

Nichols, N.L., I. Satriotomo, L.L. Allen, A.M. Grebe, and G.S. Mitchell. 2017. Mechanisms of enhanced phrenic long-term facilitation in SOD1G93A rats. *Journal of Neuroscience* 37:5834-5845.

Nichols, N.L., I. Satriotomo, D.J. Harrigan, and G.S. Mitchell. 2015a. Acute intermittent hypoxia induced phrenic long-term facilitation despite increased SOD1 expression in a rat model of ALS. *Experimental neurology* 273:138-150.

Nichols, N.L., and M.A. Tanner. 2018. Inflammation Differentially Impacts Phrenic Long-term Facilitation (pLTF) in Rats with Motor Neuron Death Induced by Intrapleural CTB-saporin Injections. *The FASEB Journal* 32:625.617-625.617.

Nichols, N.L., J. Van Dyke, L. Nashold, I. Satriotomo, M. Suzuki, and G. Mitchell. 2013b. Ventilatory control in ALS. *Respiratory physiology & neurobiology* 189:429-437.

Nichols, N.L., S. Vinit, L. Bauernschmidt, and G.S. Mitchell. 2015b. Respiratory function after selective respiratory motor neuron death from intrapleural CTB–saporin injections. *Experimental neurology* 267:18-29.

Nishitoh, H., H. Kadowaki, A. Nagai, T. Maruyama, T. Yokota, H. Fukutomi, T. Noguchi, A. Matsuzawa, K. Takeda, and H. Ichijo. 2008. ALS-linked mutant SOD1 induces ER stress-and ASK1-dependent motor neuron death by targeting Derlin-1. *Genes & development* 22:1451-1464.

Nogués, M.A., A.J. Roncoroni, and E. Benarroch. 2002. Breathing control in neurological diseases. *Clinical Autonomic Research* 12:440-449.

Nurse, C.A. 2010. Neurotransmitter and neuromodulatory mechanisms at peripheral arterial chemoreceptors. *Experimental physiology* 95:657-667.

Nurse, C.A., and N.A. Piskuric. 2013. Signal processing at mammalian carotid body chemoreceptors. In Seminars in cell & developmental biology. Elsevier, 22-30.

Ohta, S., Y. Iwashita, H. Takada, S. Kuno, and T. Nakamura. 2005. Neuroprotection and enhanced recovery with edaravone after acute spinal cord injury in rats. *Spine* 30:1154-1158.

Olson Jr, E., C. Bohne, M. Dwinell, A. Podolsky, E. Vidruk, D. Fuller, F. Powell, and G. Mitchel. 2001. Ventilatory long-term facilitation in unanesthetized rats. *Journal of Applied Physiology* 91:709-716.

Onders, R.P., H. Aiyar, and J.T. Mortimer. 2004a. Characterization of the Human Diaphragm Muscle with Respect to the Phrenic Nerve Motor Points for Diaphragmatic Pacing/DISCUSSION. *The American surgeon* 70:241.

Onders, R.P., A.F. DiMarco, A.R. Ignagni, H. Aiyar, and J.T. Mortimer. 2004b. Mapping the phrenic nerve motor point: the key to a successful laparoscopic diaphragm pacing system in the first human series. *Surgery* 136:819-826.

Onders, R.P., M. Elmo, C. Kaplan, B. Katirji, and R. Schilz. 2014. Final analysis of the pilot trial of diaphragm pacing in amyotrophic lateral sclerosis with long-term follow-up: diaphragm pacing positively affects diaphragm respiration. *The American Journal of Surgery* 207:393-397.

Parkhurst, C.N., and W.-B. Gan. 2010. Microglia dynamics and function in the CNS. *Current opinion in neurobiology* 20:595-600.

Paulin, E., A.F. Brunetto, and C.R.F. Carvalho. 2003. Effects of a physical exercises program designed to increase thoracic mobility in patients with chronic obstructive pulmonary disease. *J Pneumol* 29:287-294.

Peña, F., and J.-M. Ramirez. 2002. Endogenous activation of serotonin-2A receptors is required for respiratory rhythm generation in vitro. *Journal of Neuroscience* 22:11055-11064.

Peng, Y.-J., and N.R. Prabhakar. 2003. Reactive oxygen species in the plasticity of respiratory behavior elicited by chronic intermittent hypoxia. *Journal of applied physiology* 94:2342-2349.

Perim, R.R., D.P. Fields, and G.S. Mitchell. 2018. Cross-talk inhibition between 5-HT2B and 5-HT7 receptors in phrenic motor facilitation via NADPH oxidase and PKA. *American Journal of Physiology-Regulatory, Integrative and Comparative Physiology* 314:R709-R715.

Perim, R.R., D.P. Fields, and G.S. Mitchell. 2019. Protein kinase Cδ constrains the S-pathway to phrenic motor facilitation elicited by spinal 5-HT7 receptors or severe acute intermittent hypoxia. *The Journal of physiology* 597:481-498.

Perry, V.H. 2010. Contribution of systemic inflammation to chronic neurodegeneration. *Acta neuropathologica* 120:277-286.

Peterson, D.K., M. Nochomovitz, T. Stellato, and J. Mortimer. 1994. Long-term intramuscular electrical activation of the phrenic nerve: safety and reliability. *IEEE transactions on biomedical engineering* 41:1115-1126.

Philips, T., and W. Robberecht. 2011. Neuroinflammation in amyotrophic lateral sclerosis: role of glial activation in motor neuron disease. *The Lancet Neurology* 10:253-263.

Polla, B., G. D'antona, R. Bottinelli, and C. Reggiani. 2004. Respiratory muscle fibres: specialisation and plasticity. *Thorax* 59:808-817.

Posluszny Jr, J.A., R. Onders, A.J. Kerwin, M.S. Weinstein, D.M. Stein, J. Knight, L. Lottenberg, M.L. Cheatham, S. Khansarinia, and S. Dayal. 2014. Multicenter review of diaphragm pacing in spinal cord injury: successful not only in weaning from ventilators but also in bridging to independent respiration. *Journal of Trauma and Acute Care Surgery* 76:303-310.

Probert, L. 2015. TNF and its receptors in the CNS: The essential, the desirable and the deleterious effects. *Neuroscience* 302:2-22.

Raivich, G. 2005. Like cops on the beat: the active role of resting microglia. *Trends in neurosciences* 28:571-573.

Rana, S., G.C. Sieck, and C.B. Mantilla. 2017. Diaphragm electromyographic activity following unilateral midcervical contusion injury in rats. *Journal of neurophysiology* 117:545-555.

Romer, S.H., K. Seedle, S.M. Turner, J. Li, M.L. Baccei, and S.A. Crone. 2017. Accessory respiratory muscles enhance ventilation in ALS model mice and are activated by excitatory V2a neurons. *Experimental neurology* 287:192-204.

Rossoll, W., S. Jablonka, C. Andreassi, A.-K. Kröning, K. Karle, U.R. Monani, and M. Sendtner. 2003. Smn, the spinal muscular atrophy–determining gene product, modulates axon growth and localization of β-actin mRNA in growth cones of motoneurons. *The Journal of cell biology* 163:801-812.

Saboisky, J.P., R.B. Gorman, A. De Troyer, S.C. Gandevia, and J.E. Butler. 2007. Differential activation among five human inspiratory motoneuron pools during tidal breathing. *Journal of applied physiology* 102:772-780.

Saha, R.N., X. Liu, and K. Pahan. 2006. Up-regulation of BDNF in astrocytes by TNF-α: a case for the neuroprotective role of cytokine. *Journal of Neuroimmune Pharmacology* 1:212-222.

Sajkov, D., R. Marshall, P. Walker, I. Mykytyn, R.D. McEvoy, J. Wale, H. Flavell, A.T. Thornton, and R. Antic. 1998. Sleep apnoea related hypoxia is associated with cognitive disturbances in patients with tetraplegia. *Spinal cord* 36:231-239.

Sanagi, T., S. Yuasa, Y. Nakamura, E. Suzuki, M. Aoki, H. Warita, Y. Itoyama, S. Uchino, S. Kohsaka, and K. Ohsawa. 2010. Appearance of phagocytic microglia adjacent to motoneurons in spinal cord tissue from a presymptomatic transgenic rat model of amyotrophic lateral sclerosis. *Journal of neuroscience research* 88:2736-2746.

Sassi-Dambron, D.E., E.G. Eakin, A.L. Ries, and R.M. Kaplan. 1995. Treatment of dyspnea in COPD: a controlled clinical trial of dyspnea management strategies. *Chest* 107:724-729.

Satkunendrarajah, K., S.K. Karadimas, A.M. Laliberte, G. Montandon, and M.G. Fehlings. 2018. Cervical excitatory neurons sustain breathing after spinal cord injury. *Nature* 562:419-422.

Schleifer, L.M., R. Ley, and T.W. Spalding. 2002. A hyperventilation theory of job stress and musculoskeletal disorders. *American journal of industrial medicine* 41:420-432.

Seven, Y.B., and G.S. Mitchell. 2019. Mechanisms of compensatory plasticity for respiratory motor neuron death. *Respiratory physiology & neurobiology* 265:32-39.

Seven, Y.B., N.L. Nichols, M.N. Kelly, O.R. Hobson, I. Satriotomo, and G.S. Mitchell. 2018. Compensatory plasticity in diaphragm and intercostal muscle utilization in a rat model of ALS. *Experimental neurology* 299:148-156.

Seven, Y.B., A.K. Simon, E. Sajjadi, A. Zwick, I. Satriotomo, and G.S. Mitchell. 2020. Adenosine 2A receptor inhibition protects phrenic motor neurons from cell death induced by protein synthesis inhibition. *Experimental neurology* 323:113067.

Shi, Y., C. Nan, Z. Yan, L. Liu, J. Zhou, Z. Zhao, and D. Li. 2018. Synaptic plasticity of human umbilical cord mesenchymal stem cell differentiating into neuron-like cells in vitro induced by edaravone. *Stem cells international* 2018:

Shichinohe, H., S. Kuroda, H. Yasuda, T. Ishikawa, M. Iwai, M. Horiuchi, and Y. Iwasaki. 2004. Neuroprotective effects of the free radical scavenger Edaravone (MCI-186) in mice permanent focal brain ischemia. *Brain research* 1029:200-206.

Shroff, G., and R. Gupta. 2015. Human embryonic stem cells in the treatment of patients with spinal cord injury. *Annals of Neurosciences* 22:208.

Smith, J.C., A. Abdala, H. Koizumi, I.A. Rybak, and J.F. Paton. 2007. Spatial and functional architecture of the mammalian brain stem respiratory network: a

hierarchy of three oscillatory mechanisms. *Journal of neurophysiology* 98:3370-3387.

Steenland, H.W., H. Liu, S. Sood, X. Liu, and R. Horner. 2006. Respiratory activation of the genioglossus muscle involves both non-NMDA and NMDA glutamate receptors at the hypoglossal motor nucleus in vivo. *Neuroscience* 138:1407-1424.

Stone, D.J., and H. Keltz. 1963. The effect of respiratory muscle dysfunction on pulmonary function: studies in patients with spinal cord injuries. *American Review of Respiratory Disease* 88:621-629.

Strey, K.A., and T.L. Baker-Herman. 2012. Local reductions in synaptic inputs to the phrenic motor pool elicits atypical Protein Kinase C (aPKC) and Tumor Necrosis Factor alpha (TNFá) dependent inactivity-induced phrenic motor facilitation. In Wiley Online Library.

Tadjalli, A., and G.S. Mitchell. 2019. Cervical Spinal 5-HT2A and 5-HT2B receptors are both necessary for moderate acute intermittent hypoxia-induced phrenic long-term facilitation. *Journal of Applied Physiology* 127:432-443.

Tankersley, C.G., C. Haenggeli, and J.D. Rothstein. 2007. Respiratory impairment in a mouse model of amyotrophic lateral sclerosis. *Journal of applied physiology* 102:926-932.

Taoka, Y., M. Naruo, E. Koyanagi, M. Urakado, and M. Inoue. 1995. Superoxide radicals play important roles in the pathogenesis of spinal cord injury. *Spinal Cord* 33:450-453.

Tator, C.H., and M.G. Fehlings. 1991. Review of the secondary injury theory of acute spinal cord trauma with emphasis on vascular mechanisms. *Journal of neurosurgery* 75:15-26.

Teeling, J., and V. Perry. 2009. Systemic infection and inflammation in acute CNS injury and chronic neurodegeneration: underlying mechanisms. *Neuroscience* 158:1062-1073.

Terada, J., and G.S. Mitchell. 2011. Diaphragm long-term facilitation following acute intermittent hypoxia during wakefulness and sleep. *Journal of applied physiology* 110:1299-1310.

Triantafilou, M., and K. Triantafilou. 2002. Lipopolysaccharide recognition: CD14, TLRs and the LPS-activation cluster. *Trends in immunology* 23:301-304.

Trumbower, R.D., A. Jayaraman, G.S. Mitchell, and W.Z. Rymer. 2012. Exposure to acute intermittent hypoxia augments somatic motor function in humans with incomplete spinal cord injury. *Neurorehabilitation and neural repair* 26:163-172.

Tu, Z., Y. Li, Y. Dai, L. Li, G. Lv, I. Chen, and B. Wang. 2017. MiR-140/BDNF axis regulates normal human astrocyte proliferation and LPS-induced IL-6 and TNF-α secretion. *Biomedicine & Pharmacotherapy* 91:899-905.

Uno, M., K.T. Kitazato, A. Suzue, K. Matsuzaki, M. Harada, H. Itabe, and S. Nagahiro. 2005. Inhibition of brain damage by edaravone, a free radical scavenger, can be monitored by plasma biomarkers that detect oxidative and astrocyte damage in patients with acute cerebral infarction. *Free Radical Biology and Medicine* 39:1109-1116.

Vinit, S., M.R. Lovett-Barr, and G.S. Mitchell. 2009. Intermittent hypoxia induces functional recovery following cervical spinal injury. *Respiratory physiology & neurobiology* 169:210-217.

Vinit, S., J.A. Windelborn, and G.S. Mitchell. 2011. Lipopolysaccharide attenuates phrenic long-term facilitation following acute intermittent hypoxia. *Respiratory physiology & neurobiology* 176:130-135.

Vivier, E., A. Roussey, F. Doroszewski, S. Rosselli, C. Pommier, G. Carteaux, and A. Mekontso Dessap. 2019. Atrophy of diaphragm and pectoral muscles in critically ill patients. *Anesthesiology* 131:569-579.

Vucic, S., and M.C. Kiernan. 2009. Pathophysiology of neurodegeneration in familial amyotrophic lateral sclerosis. *Current molecular medicine* 9:255-272.

Walker, J.K., and D.B. Jennings. 1996. Ventilatory effects of angiotensin and vasopressin in conscious rats. *Canadian journal of physiology and pharmacology* 74:1258-1264.

Warren, P.M., C. Campanaro, F.J. Jacono, and W.J. Alilain. 2018. Mid-cervical spinal cord contusion causes robust deficits in respiratory parameters and pattern variability. *Experimental neurology* 306:122-131.

Watson, C., G. Paxinos, and G. Kayalioglu. 2009. The spinal cord: a Christopher and Dana Reeve Foundation text and atlas. Academic press,

Waypa, G.B., K.A. Smith, and P.T. Schumacker. 2016. O2 sensing, mitochondria and ROS signaling: the fog is lifting. *Molecular aspects of medicine* 47:76-89.

Weir, E.K., J. López-Barneo, K.J. Buckler, and S.L. Archer. 2005. Acute oxygen-sensing mechanisms. *New England Journal of Medicine* 353:2042-2055.

Wen, M.-H., and K.-Z. Lee. 2018. Diaphragm and intercostal muscle activity after mid-cervical spinal cord contusion in the rat. *Journal of neurotrauma* 35:533-547.

Wen, M.-H., M.-J. Wu, S. Vinit, and K.-Z. Lee. 2019. Modulation of serotonin and adenosine 2A receptors on intermittent hypoxia-induced respiratory recovery following mid-cervical contusion in the rat. *Journal of neurotrauma* 36:2991-3004.

Wilkerson, J.E., and G.S. Mitchell. 2009. Daily intermittent hypoxia augments spinal BDNF levels, ERK phosphorylation and respiratory long-term facilitation. *Experimental neurology* 217:116-123.

Wilkerson, J.E., I. Satriotomo, T.L. Baker-Herman, J.J. Watters, and G.S. Mitchell. 2008. Okadaic acid-sensitive protein phosphatases constrain phrenic long-term facilitation after sustained hypoxia. *Journal of Neuroscience* 28:2949-2958.

Williamson, T.L., and D.W. Cleveland. 1999. Slowing of axonal transport is a very early event in the toxicity of ALS–linked SOD1 mutants to motor neurons. *Nature neuroscience* 2:50-56.

Wong, P.C., H. Cai, D.R. Borchelt, and D.L. Price. 2002. Genetically engineered mouse models of neurodegenerative diseases. *Nature neuroscience* 5:633.

Xing, Y., R. Wang, D. Chen, J. Mao, R. Shi, Z. Wu, J. Kang, W. Tian, and C. Zhang. 2015. COX2 is involved in hypoxia-induced TNF-α expression in osteoblast. *Scientific reports* 5:1-7.

Yao, L., E.M. Kan, J. Lu, A. Hao, S.T. Dheen, C. Kaur, and E.-A. Ling. 2013. Toll-like receptor 4 mediates microglial activation and production of inflammatory mediators in neonatal rat brain following hypoxia: role of TLR4 in hypoxic microglia. *Journal of neuroinflammation* 10:1-21.

Yin, H.Z., C.-I. Hsu, S. Yu, S.D. Rao, L.S. Sorkin, and J.H. Weiss. 2012. TNF-α triggers rapid membrane insertion of Ca2+ permeable AMPA receptors into adult motor

neurons and enhances their susceptibility to slow excitotoxic injury. *Experimental neurology* 238:93-102.

Yoshino, H., and A. Kimura. 2006. Investigation of the therapeutic effects of edaravone, a free radical scavenger, on amyotrophic lateral sclerosis (Phase II study). *Amyotrophic Lateral Sclerosis* 7:247-251.

Zabka, A., M. Behan, and G. Mitchell. 2001a. Long term facilitation of respiratory motor output decreases with age in male rats. *The Journal of physiology* 531:509-514.

Zabka, A., M. Behan, and G. Mitchell. 2001b. Selected contribution: Time-dependent hypoxic respiratory responses in female rats are influenced by age and by the estrus cycle. *Journal of Applied Physiology* 91:2831-2838.

Zabka, A., G. Mitchell, and M. Behan. 2006. Conversion from testosterone to oestradiol is required to modulate respiratory long-term facilitation in male rats. *The Journal of physiology* 576:903-912.

Zannad, F., A.A. Garcia, S.D. Anker, P.W. Armstrong, G. Calvo, J.G. Cleland, J.N. Cohn, K. Dickstein, M.J. Domanski, and I. Ekman. 2013. Clinical outcome endpoints in heart failure trials: a European Society of Cardiology Heart Failure Association consensus document. *European journal of heart failure* 15:1082-1094.

Zetterström, P., H.G. Stewart, D. Bergemalm, P.A. Jonsson, K.S. Graffmo, P.M. Andersen, T. Brännström, M. Oliveberg, and S.L. Marklund. 2007. Soluble misfolded subfractions of mutant superoxide dismutase-1s are enriched in spinal cords throughout life in murine ALS models. *Proceedings of the National Academy of Sciences* 104:14157-14162.

Zhang, H.L., F. Pan, D. Hong, S.M. Shenoy, R.H. Singer, and G.J. Bassell. 2003. Active transport of the survival motor neuron protein and the role of exon-7 in cytoplasmic localization. *Journal of Neuroscience* 23:6627-6637.

Zholudeva, L.V., J.S. Karliner, K.J. Dougherty, and M.A. Lane. 2017. Anatomical recruitment of spinal V2a interneurons into phrenic motor circuitry after high cervical spinal cord injury. *Journal of neurotrauma* 34:3058-3065.

Zimmer, M.B., K. Nantwi, and H.G. Goshgarian. 2007. Effect of spinal cord injury on the respiratory system: basic research and current clinical treatment options. *The journal of spinal cord medicine* 30:319-330.

Zimmermann, G., and R. Taussig. 1996. Protein kinase C alters the responsiveness of adenylyl cyclases to G protein α and βγ subunits. *Journal of Biological Chemistry* 271:27161-27166.

VITA

Lauren F. Borkowski, the daughter of Timothy Borkowski and Brenda Kirby, was born in Minneapolis, MN on May 13, 1992. She completed her Bachelor of Arts in Biology in 2014 at Saint Mary's University of Minnesota in Winona, MN, and conducted undergraduate research under Dr. Randy Krainock. Following her undergraduate studies she pursued and gained a Master of Science in Biology at Minnesota State University-Mankato in 2016 in Mankato, MN, and conducted research under Dr. Penny Knoblich. She joined the Biomedical Sciences Department in 2016 and has performed her Ph.D. training in the laboratory of Dr. Nicole L. Nichols.